Advances in Experimental Medicine and Biology 966
Protein Reviews

M. Zouhair Atassi *Editor*

Protein Reviews

Volume 18

Springer

Advances in Experimental Medicine and Biology

Protein Reviews

Volume 966

Series editor
M. Zouhair Atassi

More information about this series at http://www.springer.com/series/14330

M. Zouhair Atassi
Editor

Protein Reviews

Volume 18

Springer

Editor
M. Zouhair Atassi
Biochem and Mol Biol
Baylor College of Medicine
Houston, TX, USA

ISSN 0065-2598 ISSN 2214-8019 (electronic)
Advances in Experimental Medicine and Biology
ISSN 2520-1891 ISSN 2520-1905 (electronic)
Protein Reviews
ISBN 978-981-10-6921-5 ISBN 978-981-10-6922-2 (eBook)
https://doi.org/10.1007/978-981-10-6922-2

Library of Congress Control Number: 2017938742

Printed on acid-free paper

This Springer imprint is published by Springer Nature
The registered company is Springer Nature Singapore Pte Ltd.
The registered company address is: 152 Beach Road, #21-01/04 Gateway East, Singapore 189721, Singapore

Preface

Protein Reviews is a book series which has been published by Springer since 2005. It has published 17 printed volumes to date (to see previous volumes please go to http://www.springer.com/series/6876). To speed up the publication process and enhance accessibility, all articles will appear online before they are published in a printed book. The book series appears as a subseries of Advances in Experimental Medicine and Biology (http://www.springer.com/series/14330). They are published in volumes each of which will focus on a given theme or volumes that contain reviews on an assortment of topics, in order to stay up-to-date and to publish timely reviews in an efficient manner.

The aim of the *Protein Reviews* is to serve as a publication vehicle for reviews that focus on crucial contemporary and vital aspects of protein structure, function, evolution and genetics. Publications will be selected based on their importance to the understanding of biological systems, their relevance to the unravelling of issues associated with health and disease or their impact on scientific or technological advances and developments. Proteins linked to diseases or to the appearance and progress of diseases will obviously provide essential topics that may be covered in this series. Moreover, proteins that are, or can be, used as potential biomarkers or as candidates for treatment and/or for the design of distinctive, new therapeutics will receive high attention in this book series.

The issues may include biochemistry, biophysics, immunology, structural and molecular biology, genetics, molecular and cellular mechanisms of action, clinical studies and new pioneering therapies. A given volume may be focused on a particular theme, or may contain a selected assortment of different current topics.

The authors of the articles are selected from leading basic or medical scientists in academic or industrial organizations. The invited authors are nominated by the editorial board or by experts in the scientific community. However, interested individuals may suggest a topic for review and/or may propose a person to review a current important topic. Colleagues interested in writing a review or in guest-editing a special thematic issue are encouraged to submit their proposals and list of authors of the suggested chapter/topics to the Editor before submitting a manuscript.

The manuscripts are reviewed and evaluated in the usual manner by experts in the field. The articles will be published online no later than 6 weeks after editorial review and acceptance.

It should be emphasized that *Protein Reviews* will publish all accepted review articles online before they appear in print. And there will be no page or color charges and no page or color image limitations.

The chapters in this volume are authored by experts in the field. They deal with aspects of structure and/or biological activity of the following selected systems: Review of current research on the mechanism of channel gating and regulation of the activity of calcium-activated chloride channel ANO1, structure and function of the two-component cytotoxins of *Staphylococcus aureus*, membrane fusion and infection involving the influenza virus hemagglutinin, the impact of arrhythmogenic mutations through the structural determination of the L-type voltage-gated calcium channel, discussion of some open questions pertaining to histone post-translational modifications and nucleosome organization in transcriptional regulation. Regulation of the extracellular SERPINA5 (protein C inhibitor) penetration through cellular membranes, coding of Class I and II aminoacyl-tRNA synthetases, regulation of nephrin phosphorylation in diabetes and chronic kidney injury, the structure-forming juncture in oxidative protein folding and the events in the ER, the polyspecificity of anti-lipid antibodies and its relevance to the development of autoimmunity. The volume is intended for research scientists, clinicians, physicians and graduate students in the fields of biochemistry, cell biology, molecular biology, immunology and genetics.

I hope that this volume of *Protein Reviews* will continue to serve the scientific community as a valuable vehicle for dissemination of vital and essential contemporary discoveries on protein molecules and their immensely versatile biological activities.

M. Zouhair Atassi
Editor-in-Chief

Contents

Adv Exp Med Biol - Protein Reviews (2017) 2:1–14
DOI 10.1007/5584_2016_201

Published online: 15 March 2017

The Mechanistic Role of the Calcium-Activated Chloride Channel ANO1 in Tumor Growth and Signaling

Anke Bill and Larry Alex Gaither

Abstract

Multiple studies have described the high expression and amplification of Anoctamin 1 (ANO1) in various cancers, including, but not limited to breast cancer, head and neck cancer, gastrointestinal stromal tumors and glioblastoma. ANO1 has been demonstrated to be critical for tumor growth in breast and head and neck cancers through its regulation of EGFR signaling and pathway modulators like MAPK and protein kinase B. However, the discovery of ANO1 as a calcium activated chloride channel came as a surprise to the field and has given rise to many questions. How does a chloride channel promote oncogenesis? Is the chloride channel function of ANO1 important for its role in cancer? Does ANO1 exhibits chloride-independent functions in cancer cells? This review summarizes the current understanding of ANO1's function in cancer, provides a synopsis of the findings addressing the open questions in the field and gives an outlook on the promising future of ANO1 as a potential therapeutic target for the treatment of various cancers.

Keywords

Anoctamin 1 • High-Throughput Mutagenesis • Chloride Channel • Variomics • Cancer

List of Abbreviations

AKT	protein kinase B
ANO1	Anoctamin 1
CaCC	calcium activated chloride channel
CaCC-inh	calcium activated chloride channel inhibitor
CAMK	calmodulin dependent kinase

Statement: This manuscript has not been published and has not been submitted for publication elsewhere. All authors agree to the submission to the journal.

A. Bill and L. Alex Gaither (✉)
Novartis Institutes for Biomedical Research, Cambridge, MA 02139, USA
e-mail: alex.gaither@novartis.com

EGFR	epidermal growth factor receptor
ESCC	esophageal squamous cell carcinoma
HNSCC	head and neck squamous cell carcinoma
MAPK	mitogen-activated kinase
SCC	squamous cell carcinoma

The concept of oncogenes as drivers of tumorigenesis is well accepted. Thinking about genes that promote oncogenic pathways and directly or indirectly promote cancer proliferation or progression, admittedly, ion channels are usually not the first example that comes to one's mind. However, already decades ago, multiple studies were published describing a correlation between the expression of ion channels and tumorigenesis. Granted, there have been little insights in the possible mechanism of actions explaining the role of ion channels in cancer, but the recent increase in publications in this field demonstrates a promising new development in understanding the underlying mechanism. One of those examples is anoctamin 1 (ANO1).

1 Discovery of ANO1

In the early 2000s several groups described ANO1 to be overexpressed in cancer. Without knowing the molecular identity of this highly expressed gene, these observations resulted in various alternative names for ANO1: TAOS2: tumor amplified and overexpressed sequence 2 (Huang et al. 2006), DOG1: discovered on gastrointestinal stromal tumors protein 1 (West et al. 2004) and ORAOV2: oral cancer overexpressed protein 2 (Katoh and Katoh 2004) which were subsequently summarized by naming the protein TMEM16A (transmembrane protein 16A). It was only in 2008, when three independent laboratories identified ANO1 as a calcium activated chloride channel (CaCC) (Caputo et al. 2008; Duran et al. 2010; Schroeder et al. 2008; Yang et al. 2008). All three studies verified that heterologous expression of ANO1 was sufficient to generate chloride currents with the classical properties of CaCCs and solved the almost 20 year old enigma of the molecular identity of calcium activated calcium channels. With it also came the renaming of TMEM16A to ANO1 (anoctamin 1) - anion channel with eight (octa) putative transmembrane domains – which has been defined as the official gene nomenclature by the HUGA Gene Nomenclature Committee (Yang et al. 2008). The family of anoctamins comprises 10 members. However, besides ANO1 only ANO2 has been demonstrated to function as a CaCC, while the other family members exhibit diverse functions such as mediating the exchange of phospholipids between the inner and outer leaflet of the plasma membrane or allowing the influx of calcium as a nonselective cation channel. More information about the diverse functions of anoctamins can be found in these recent reviews (Kunzelmann 2015; Picollo et al. 2015).

We now know that ANO1 is widely expressed in secretory epithelia including salivary gland, pancreas, gastrointestinal tract, mammary gland, airway epithelium, smooth muscles and sensory neurons (Gomez-Pinilla et al. 2009; Huang et al. 2012, 2009; Hwang et al. 2009; Manoury et al. 2010; Cho et al. 2012). ANO1 mediates transepithelial ion transport and exhibits an important function in regulating airway fluid secretion, gut motility, secretory functions of exocrine glands, renal function, (vascular) smooth muscle contraction and nociception (Hwang et al. 2009; Cho et al. 2012; Faria et al. 2014). But how does the discovery of ANO1 as a calcium activated chloride channel explain its overexpression in cancer?

2 ANO1 in Cancer

ANO1 is amplified and highly expressed in a variety of carcinomas including breast cancer, prostate carcinoma, glioblastoma, GIST (gastrointestinal stromal tumor), ESCC (esophageal squamous cell carcinoma) and HNSCC (head and neck squamous cell carcinoma) (West et al. 2004; Ayoub et al. 2010; Berglund et al. 2014; Britschgi et al. 2013; Duvvuri et al. 2012; Liu et al. 2012, 2014) (Fig. 1). The gene coding for ANO1 maps to a region on chromosome

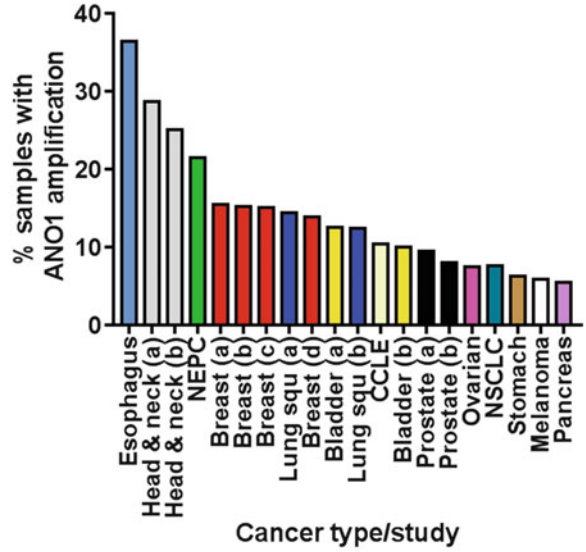

Fig. 1 ANO1 is amplified in cancer. The diagram depicts the percentage of samples found to have amplification of ANO1. All studies that identified more than 5% of samples with amplification of ANO1 and more than 100 analyzed samples are shown (data source: cBioPortal (Gao et al. 2013; Cerami et al. 2012), October 2016). The results shown here are in whole or part based upon data generated by the TCGA Research Network: http://cancergenome.nih.gov/.Study references: Esophageal Carcinoma (TCGA), Head & neck (*a*) Squamous Cell Carcinoma (Cancer Genome Atlas Network 2015), Head & neck (*b*) Squamous Cell Carcinoma (TCGA), NEPC Neuroendocrine Prostate cancer (Beltran et al. 2016), Breast (*a*) Invasive Carcinoma (TCGA), Breast (*b*) Invasive Carcinoma (Pereira et al. 2016), Breast (*c*) Invasive Carcinoma (Ciriello et al. 2015), Lung Squamous Cell Carcinoma (*a*) (TCGA), Breast (*d*) Invasive Carcinoma (Cancer Genome Atlas Network 2012), Bladder (*a*) Urothelial Carcinoma (Cancer Genome Atlas Research Network 2014), Lung Squamous Cell Carcinoma (*b*) (Cancer Genome Atlas Research Network 2012), CCLE (Cancer Cell Line Encyclopedia (Barretina et al. 2012)), Bladder (*b*) Urothelial Carcinoma (TCGA), Prostate (*a*) Adenocarcinoma (Kumar et al. 2016), Prostate (*b*) Metastatic prostate cancer (Robinson et al. 2015), Ovarian Serious Cystadenocarcinoma (TCGA), NSCLC Non-small cell lung cancer (Campbell et al. 2016), Stomach Adenocarcinoma (TCGA), Skin Cutaneous Melanoma (TCGA), Pancreatic cancer (Witkiewicz et al. 2015)

11 (11q13) known to be frequently amplified in cancer. Its genomic proximity to other known oncogenes included in the 11q13 amplicon (like CCND1, FADD or FGF19) had stamped amplification of ANO1 as a "passenger event" for a long time rather than being considered as an independent oncogenic factor contributing to tumorigenesis. Only recent studies have shed new light on the role of ANO1 in tumorigenesis and have found ANO1 to be a critical survival factor in these cells. Although the detailed mechanism is still unclear, several lines of evidence support an independent oncogenic function of ANO1 in human cancer: Firstly, RNAi-mediated knockdown of ANO1 is sufficient to reduce cell proliferation and to induce apoptosis in multiple cancer cell line models and human xenografts studies in mice (West et al. 2004; Ayoub et al. 2010; Berglund et al. 2014; Britschgi et al. 2013; Duvvuri et al. 2012; Liu et al. 2012, 2014; Jia et al. 2015). Secondly, overexpression of ANO1 in cells lacking amplification of 11q13 was sufficient to increase proliferation and anchorage-dependent growth, a hallmark of highly tumorigenic cells (Britschgi et al. 2013; Duvvuri et al. 2012). This finding was recently corroborated by another study showing that ANO1 plays a critical role in benign prostate hyperplasia,

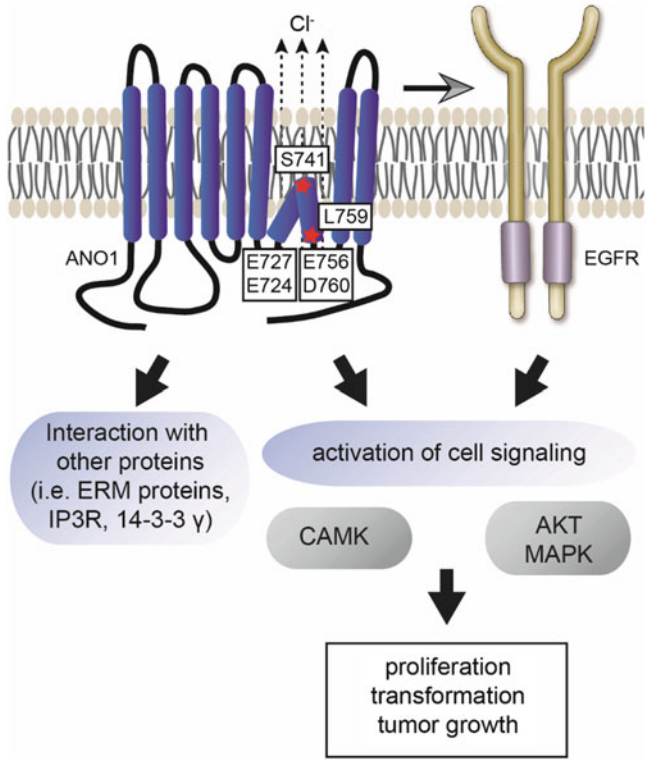

Fig. 2 ANO1's role in promoting tumorigenesis. ANO1 has been shown to interact with epidermal growth factor receptor (EGFR) in breast cancer and head and neck cancer and to promote EGFR activation and signaling (MAPK, AKT, CAMK). Furthermore, ANO1 was demonstrated to interact with the ezrin-radixin-moesin (ERM) network, inositol 1,4,5-trisphosphate receptor 1 (IP3R) and 14-3-3 ϒ. Recently discovered mutants of ANO1 provide novel tools to study ANO1's function in cancer. The proposed position of the calcium binding site and other functionally critical positions are indicated by the amino acid in boxes (numbering for ANO1-abc). The location of residues S741 (renders ANO1 constitutively active when mutated to threonine) and residue L759 (renders ANO1 inactive when mutated to glutamine) are indicated by red stars

demonstrating that expression of ANO1 alone is sufficient to induce cell proliferation in benign cells (Cha et al. 2015; Duvvuri 2015). Thirdly, ANO1 was found to be overexpressed in a subclass of tumors in the absence of amplification of other 11q13-genes like CCND1, demonstrating ANO1 overexpression to be sufficient as an oncogenic driver *in vivo* in the absence of 11q13-amplification (Huang et al. 2006). And lastly, expression of ANO1 correlates with poor prognosis in HNSCC, ESCC, gastric cancer and breast cancer (Ayoub et al. 2010; Britschgi et al. 2013; Duvvuri et al. 2012; Ruiz et al. 2012; Reddy et al. 2016; Dixit et al. 2015; Liu et al. 2015). These data suggest that ANO1 is sufficient to promote tumorigenesis. In addition to its growth promoting effect, ANO1 has been implicated in metastasis and was shown to act as a switch between the growth and metastatic stage of squamous cell carcinoma of the head and neck (SCCHN) (Shiwarski et al. 2014). But what do we know about the mechanism by which ANO1 promotes oncogenesis and regulates metastasis?

3 What Do We Know About the Underlying Mechanisms of ANO1's Role in Promoting Oncogenesis?

Recent studies have provided more insights into ANO1's role in oncogenesis (Fig. 2). Knockdown and overexpression of ANO1 in breast cancer, colorectal cancer, SCCHN and HNSCC has been shown to correlate with the inhibition or activation, respectively, of mitogen-activated kinase (MAPK) and protein kinase B (AKT) signaling, two major signaling pathways regulating cell proliferation (Britschgi et al. 2013; Duvvuri et al. 2012; Sui et al. 2014). Similar results were observed after knockdown of ANO1 in rat prostate *in vivo* (Cha et al. 2015). One mechanism for the observed regulation of the MAPK/AKT-signaling pathways might be provided by a functional link between ANO1 and EGFR. ANO1 knockdown has been reported to inhibit the activation of epidermal growth factor receptor (EGFR) (Britschgi et al. 2013). Using unbiased proteomic studies, ANO1 was found to interact with EGFR in HNSCC cells (Bill et al. 2015a). Overexpression studies with structural mutants of EGFR and ANO1 identified the trans/juxta membrane domain of EGFR to be critical for the interaction with ANO1. Interestingly, it was found that ANO1 and EGFR affected each other's expression level, suggesting a functional and regulatory link between ANO1 and EGFR. Co-inhibition of EGFR and ANO1 had an additive effect on HNSCC cell proliferation and HNSCC cell lines with amplification and high expression of ANO1 showed enhanced sensitivity to EGFR-inhibitors, suggesting that co-targeting of ANO1 and EGFR could enhance the clinical efficacy of EGFR-targeted therapy in HNSCC (Bill et al. 2015a). Taken together, these data demonstrate that ANO1 and EGFR form a functional complex and jointly regulate HNSCC cell proliferation. Similar results were found in breast cancer cells. Knockdown of ANO1 reduced secretion of EGFR ligands (EGF and TGF-alpha) in breast cancer cell lines and reduced EGFR phosphorylation and cell proliferation. Supplementation of EGF to the cells after inhibition of ANO1 was sufficient to restore EGFR phosphorylation and to partially rescue cell proliferation (Britschgi et al. 2013), providing further evidence that ANO1 is functionally linked to the EGFR-pathway.

Another study identified ANO1 to interact with the ezrin-radixin-moesin (ERM) network as well as the SNARE protein complex (Perez-Cornejo et al. 2012). ERM proteins connect transmembrane proteins and the cytoskeleton and have a crucial role in regulating signal transduction pathways, cytoskeletal organization, cell division, migration and invasion (Perez-Cornejo et al. 2012; Fehon et al. 2010). ERM can be activated by many ligands including EGF and once activated act as a scaffolding protein to facilitate signal transduction of membrane proteins and hence promoting cancer cell migration/invasion (Clucas and Valderrama 2014; Orr Gandy et al. 2013). It is possible that ANO1 interacts with EGFR and recruits ERM proteins which subsequently facilitate EGFR signaling and activation of the MAPK/AKT-pathway. Future studies are needed to improve our understanding of the molecular mechanisms underlying ANO1's function in these fundamental cellular signaling pathways.

A recent study discovered that 14–3-3 ϒ binds to the N-terminus of ANO1 and facilitates anterograde trafficking and enhances ANO1 cell surface expression in U251 glioblastoma cells (Lee et al. 2016). There is a conserved binding motif within the N-terminus of ANO1 requiring a phosphorylation site at Thr9. This site not only facilitated 14–3-3 ϒ binding and cell membrane localization, but also seemed to be required for signaling and functional activity of ANO1 in U251 cells. Both migration and invasion were adversely affected when 14–3-3 ϒ and ANO1 were knocked down, suggesting that both are necessary and sufficient for the activity of the ANO1/14–3-3 ϒ complex on the membrane. It is likely that the active complex mediates additional interactions such as EGFR to drive MAPK signaling and proliferation. The kinase for the

Thr9 site has yet to be discovered but this kinase could be a key regulator for ANO1 activity and localization in glioblastoma.

In addition to regulating cell proliferation, ANO1 has been shown to affect the motility of human cancer cells. High expression of ANO1 in HNSCC, ESCC and prostate cancer correlates with a higher risk of distant metastasis and a shorter survival of these patients (Ayoub et al. 2010; Liu et al. 2012; Ruiz et al. 2012; Shi et al. 2013). Although there is significant evidence for a role of ANO1 in cell migration, *in vitro* studies exploring the underlying mechanisms have revealed ambiguous results, pointing to a cell-specific mechanism of action. Transient knockdown of ANO1 or small molecule mediated inhibition of ANO1-dependent chloride currents in HNSCC cell lines with high ANO1 expression inhibited cell migration (Ruiz et al. 2012; Li et al. 2013). Overexpression of ANO1 in HNSCC cells with low ANO1 expression levels stimulated cell motility and migration (Ayoub et al. 2010), but had no effect in human embryonal kidney cells (HEK293 cells) (Habela et al. 2009), suggesting that a specific cell background could be essential for ANO1's role in cancer. A recent study focusing on investigating the effect of stable knockdown or inhibition of ANO1 identified ANO1 as a switch between the "grow-and-go" phenotype of human HNSCC cells (Shiwarski et al. 2014). The "grow" stage is characterized by high expression of ANO1 and a high proliferation rate of the cells. Epigenetic events leading to the hypermethylation of the promotor for ANO1 result in a downregulation of ANO1 expression and an increase in cell motility ("go" stage). In this study, downregulation of ANO1 expression correlated with an increase in migration and the formation of metastasis in mouse models, as well as in the transition of cells from the epithelial to a more mesenchymal stage. By examining matched tumor and metastases samples from HNSCC patients the authors demonstrated a reduced expression of ANO1 in distant metastases ("go" stage) as compared to the primary tumor ("grow" stage) (Shiwarski et al. 2014). Mechanistically, Ser970 in the C-terminus of ANO1 was found to be critical for both, interaction with Radixin and ANO1's role in metastasis, hence suggesting a mechanism in which ANO1 might affect cell motility by inducing changes in the actin cytoskeleton. Taken together, these results demonstrate a significant role of ANO1 in regulating cell proliferation and motility, two of the hallmarks of human cancers (Hanahan and Weinberg 2011). Does the role of ANO1 in cancer involve its chloride channel activity?

4 Does the Role of ANO1 in Cancer Involve Its Chloride Channel Activity?

Only little is known about the mechanisms underlying ANO1's role in promoting proliferation, with one of the main questions in the field, whether ANO1's role in cancer is dependent on its function as a chloride channel or whether ANO1 exhibits a chloride conductance independent function. Besides ANO1, other chloride channels like cystic fibrosis transmembrane conductance regulator (CFTR) and intracellular chloride channel (CLICs) are thought to be involved in cancer and changes in the intracellular chloride concentration have been implicated in regulating cell cycle progression and proliferation (Shiozaki et al. 2011; Hiraoka et al. 2010; Miyazaki et al. 2008; Peretti et al. 2015; Hou et al. 2016). Interestingly, ANO1 is the only anoctamin that has been shown to play a critical role in the initiation and progression of cancer (Galindo and Vacquier 2005), suggesting that ANO1 harbors a specific function that was lost in the other family members. This observation is especially intriguing since the structural regions thought to be important for the conductance of chloride are highly conserved between ANO1 and ANO2 (Picollo et al. 2015; Pedemonte and Galietta 2014), hence prompting the hypothesis that the chloride channel activity is not required for ANO1's role in promoting cancer. ANO1 has been shown to regulate mitogen-activated kinase (MAPK) and protein kinase B (AKT) signaling and to promote tumorigenesis by activating epidermal growth factor receptor (EGFR) and

calmodulin dependent kinase (CAMK)-signaling (Britschgi et al. 2013; Duvvuri et al. 2012). In addition, ANO1 has been found in dorsal root ganglia to be in a complex with the inositol 1,4,5-trisphosphate receptor 1 and to be tethered to juxtamembrane regions of the ER, suggesting a functional coupling to local calcium stores (Jin et al. 2013). It could be that ANO1 exhibits its role in different cells by building a complex with other proteins and these functional interactions result in a calcium/chloride signaling complex that drives cellular proliferation. What is the key data to support that ANO1 chloride channel activity drives proliferation in tumor cells?

A recent study from our laboratory suggests that inhibiting ANO1-mediated chloride currents is not sufficient to inhibit cell proliferation in HNSCC and ESCC cells (Bill et al. 2014). Side by side comparison of T16Ainh-A01 and CaCCinh-A01, two inhibitors of ANO1 with similar potency for inhibiting ANO1 mediated calcium activated chloride currents (CaCC) in cells, demonstrated a lack of effect of T16Ainh-A01 on the proliferation of multiple cancer cell lines, whereas CaCCinh-A01 showed a concentration dependent inhibition of cell proliferation specific to ANO1-expressing cell lines (Bill et al. 2014). We uncovered a novel mechanism of action for CaCCinh-A01: the facilitation of endoplasmatic reticulum-associated, proteasome dependent degradation of ANO1. Treatment of ANO1-expressing cell lines with CaCCinh-A01 resulted in a decrease of ANO1 protein levels which correlated with the inhibition of cell proliferation. Removal (wash out) of CaCCinh-A01 from the cells resulted in the restoration of ANO1 protein levels and the recovery of cell proliferation (Bill et al. 2014). These results indicate that inhibition of ANO1-dependent chloride currents is not sufficient to inhibit ANO1-dependent cell proliferation. Instead our data points to a mechanism where the ANO1 complex, associated with EGFR, is the complex driving MAPK signaling and cell proliferation and underline the potential of small-molecule induced protein degradation as a new targeting approach for the therapy of ANO1-dependent cancers. To prove this hypothesis and to find additional small molecules that can degrade ANO1, screening efforts will be needed that monitor ANO1 protein levels instead of only measuring ANO1 activity. Alternatively, targeted protein degradation using a bifunctional proteolysis-targeting chimera (PROTAC) consisting of an ANO1-binding molecule coupled to a degradation inducing moiety could present a promising strategy to target ANO1 in cancer. Several small molecule inhibitors for ANO1 activity have been described, most of which lack specificity and show only weak potency (Bill et al. 2014). Recently, two molecules, MONNA and Ani9, with improved potency and specificity for ANO1 over other anoctamin family members have been reported (Seo et al. 2016; Oh et al. 2013). Although their direct binding to ANO1 has not been shown yet, these molecules could serve as a starting point for the development of ANO1-specific tools and to further investigate the potential of targeted degradation of the ANO1 protein as a therapeutic strategy to inhibit growth of ANO1 dependent tumors.

The observation that ANO1's chloride channel activity is not required and that instead its scaffolding function is playing a key role in promoting tumor growth, suggests that it could be a mechanism for overexpressed membrane channels to serve as templates for oncogenic signaling molecules. It has been widely observed that channels are a class of proteins commonly overexpressed across cancers, but their role in tumor growth is not always clear. Similar to ANO1, large multiple span transmembrane proteins can become overexpressed in the context of constitutively active oncogenic signaling pathways, either directly due to hyperactive transcription factors or indirectly when located in close proximity to an amplified region of the genome. It is tempting to speculate that amplified regions of the genome have many passenger genes that are overexpressed because they are near an oncogene not because they are oncogenes themselves. But during the transformation process the passenger genes induce an environment that the cells adapt to and eventually become physiologically addicted to. In the case of ANO1, its chloride channel activity is not driving

cell growth but the complex associated with the protein is the growth promoting pathway EGFR (Bill et al. 2015a, 2014). It might be the multiple membrane domains of ANO1 serve as a multi-functional template for EGFR and co-activating proteins to bind and become activated by proximity. Key technologies such as RIME and IP-Mass spec will help aid researchers to more accurately identify and validate the interaction partners of large multipass transmembrane proteins that play both direct and indirect roles in oncogenesis.

5 A Random Mutagenesis-Based Variomics Screen Provides Insights in the Structural and Functional Requirements of ANO1 in Cancer

If chloride channel activity is not relevant, how can we learn more about what defines ANO1's role in cancer? Could a variomics analysis of ANO1 identify functionally relevant mutants in cancer? The eight-transmembrane structure of ANO1 evades classical biochemical experimentation and the little mechanistic insights into the requirements for ANO1's function originated from studies using broad chloride channel inhibitors or limited targeted mutagenesis approaches. Only very recently functional genetic tools have become available to study ANO1 biology and its role in cancer. Using a high-throughput, random mutagenesis based variomics screen, a library of ~6000 ANO1 mutant library was generated and functionally characterized. Novel mutations were identified that affected channel activity, intracellular trafficking or localization of ANO1 (Bill et al. 2015b). Mutations such as S741T increased ANO1 calcium sensitivity and rendered ANO1 calcium gating voltage-independent, whereas mutants like L759Q diminished ANO1-dependent chloride conductance without affecting ANO1's expression level or localization on the membrane. This data presented the first, unbiased and comprehensive study of the structure-function relationship of ANO1. One of the key findings is that the S741T mutation could be functional at very low intracellular calcium levels suggesting that ANO1 has the capacity to function biochemically in the absence of high calcium in the cytoplasm. S741T increased ANO1 calcium-sensitivity and rendered ANO1 voltage independent. Residues Glu-724/727 and Glu-756/Asp-760 have been proposed as the calcium-binding sites of ANO1 (Han et al. 2015; Lee et al. 2015; Peters et al. 2015), suggesting a model in which calcium is sandwiched between those residues, creating a loop between amino acids 728 and 752 that enters the membrane. Strikingly, the majority of the constitutively active mutants mapped to the predicted re-entrant loop, with Ser-741 mapping half-way between the two proposed calcium-binding sites. This finding proposes a model, in which calcium binding to residues Glu- 756/Asp-760 and Glu-727/Glu-724 causes a conformational change in the loop domain that results in the activation of the channel and in which the identified constitutively active mutants of ANO1, mapping in the loop region, all on top S741T, facilitate the calcium-induced conformational changes and thus the activation of the channel at low calcium concentrations. Characterization of the electrophysiological properties of ANO1-S741T showed that the mutation resulted in an uncoupling of the characteristic voltage and calcium dependence of ANO1, with calcium inducing channel activation with the same potency and cooperativity across the tested voltage range, thus transforming the channel from a calcium/voltage-gated channel to a ligand-gated channel. Moreover, S741T facilitated the voltage-independent step that translates the calcium binding into channel opening and increased the open probability of the channel by decreasing its deactivation time. It could be that in a tumor cell setting ANO1 can function in the absence of calcium to bind an EGFR complex and drive MAPK signaling, with or without chloride channel activity. Both, constitutively active ANO1 mutant S741T and inactive mutant L759Q, were shown to interact with EGFR, demonstrating that the interaction of EGFR and ANO1 is not dependent on the activity of ANO1

(Bill et al. 2015a). The collective data suggest that the ANO1 EGFR complex is more important than calcium or chloride levels to drive proliferation. The discovery of both, a set of constitutively active and inactive mutants will aid in better understanding how EGFR is regulated by ANO1 and its binding partners at the membrane.

Another important feature of the variomics library is the ability to screen for mutants that could be involved in compound binding to ANO1. In the absence of a crystal structure, it is difficult to clearly determine how small molecule compounds or antibodies interact with ANO1. But the variomics library provides a functional screening system to measure chloride channel activity of mutants in the presence of ANO1 inhibitors. Such a compound screen was run using the ANO1 inhibitor CaCCinh-A01 and the ANO1 mutated cDNA library and chloride channel activity was monitored for each mutant in the presence and absence of the inhibitor (Bill et al. 2015b). It was found that CaCCinh-A01 preferentially binds to the inactive form of the channel and that a single point mutation (S741T) could decrease sensitivity to CaCCinh-A01, likely by decreasing the fraction of inactive channels. Interestingly, the same mutant was still able to active EGFR signaling in cells similar to the wild type channel, further corroborating the hypothesis that modulation of chloride channel activity is not sufficient for ANO1's role in cancer (Bill et al. 2015a). Although modulators of chloride channel activity might not be sufficient for inhibiting tumor growth, a better understanding of the mechanism of action of ANO1 inhibitors can help to learn more about the requirements of channel activation which could be built upon to identify the residues essential for EGFR binding and signaling.

6 A Promising Future Ahead

ANO1 is emerging as an interesting therapeutic target and putative oncogene in cancer but many questions remain about its mechanism of action driving proliferation across tumor types. Chloride channels as a class of transporters have already been implicated in many cancer types over the years. CLCA1, CLCA2, CLCA4 are known to be downregulated in colon cancer but CLIC1 is upregulated in gastric cancer and CLIC3 is overexpressed in pancreatic cancer (Huber 2013; Lang and Stournaras 2014). Emerging data suggested a role of cystic fibrosis transmembrane conductance regulator (CFTR) in gastrointestinal cancers (Hou et al. 2016). Although the role of a chloride channel has been thought to maintain cell volume and ion secretion, it appears in cancer chloride channels may play more complex roles in multi-subunit protein complexes that signal through oncogenic pathways. The activity of chloride channels to regulate cell volume clearly effects migration and invasion of cells on plastic, but the question remains if this is a similar phenotype *in vivo*. An intriguing hypothesis would suggest the *in vitro* phenotypes of ANO1 will translate into *in vivo* studies, but these studies have yet to be completed. The in vivo studies of ANO1 are an area that is greatly understudied and there is a need to develop a model to test ANO1 *in vivo*. Because ANO1 is expressed in many tissues in the body, the modulation of this channel in a whole animal may reveal mechanisms previously unseen in the cell based work completed to date. In particular for the therapeutic intervention of ANO1 it will be critical to determine if a small molecule will be tolerated in a whole animal and if an appropriate therapeutic index can be achieved.

If ANO1 inhibition can be tolerated in an animal, it will open the door for numerous combination ideas to treat several tumor types. Since ANO1 has been shown to be a driver for proliferation in HNSCC, breast cancer and glioblastoma, it is logical to imagine taking a combination approach to each of these tumor types with a standard of care and an ANO1 inhibitor. Both CDK4 and EGFR inhibitors that are currently used could be new combination partners for ANO1 positive refractory population of patients. Similarly, for subsets of breast cancer with ANO1 expression, patients could be treated with a combination of HER2 targeted agents and ANO1 inhibitors in primary or refractory disease.

GIST is a tumor type where ANO1 is highly expressed but its effect on proliferation is not clearly defined (West et al. 2004; Berglund et al. 2014; Liegl et al. 2009). In particular the cKIT negative GIST that expresses ANO1 could be a Gleevec resistant population that could benefit from an ANO1 inhibitor. There is a need to define ANO1s role in GIST using both cKIT positive and cKIT negative cell lines and xenografts.

In addition to cancer, ANO1 has been discussed as a chloride channel that could be activated in cystic fibrosis to compensate for the loss of CFTR function. Although a discussion around mechanisms of agonizing ANO1 is beyond the scope of this review, we wanted to point out this literature in the context of better understanding ANO1 in different disease states and cellular milieu. We and others have proposed that ANO1 in a tumor environment will be in a different protein complex than ANO1 in a normal physiological environment. As ANO1 is expressed in numerous tissues in the body, it would be expected that in different tissues ANO1 would have distinct interaction partners that drive both channel gating and intracellular signaling. It will be critical to study ANO1 across tissue types to better understand how and when ANO1 is able to interact with growth promoting pathways such as EGFR. It's possible that ANO1 is able to regulate multiple signaling pathways either directly through protein protein interactions or indirectly through modulation of chloride or membrane potential. As this is still a nascent field, it will be exciting to see the field evolve as new data emerges in the future.

It is an exciting time to study chloride channels and cancer since ANO1 is leading the field in new mechanistic insights of transporters in cancer. It is hard to predict what new discoveries lay ahead, but it is clear that ANO1 biology in cancer is an up and coming field of study that will lead to new insights around how ion flux, plasma membrane complexes, and transport biology regulate tumor growth. Since ANO1 is a "druggable" protein it provides the hope that someday a therapeutic modality that is safe in humans could benefit patients with cancer or other ANO1 dysregulated diseases. It's not yet clear if ANO1 inhibition alone will be sufficient to induce tumor regression in man, but ANO1 might be an ideal combination treatment with other known anti-cancer therapies. For head and neck cancers, using EGFR inhibitors or blocking antibodies have proven to be effective treatments but resistance is common and in some cases the primary disease is so advanced and refractory to EGFR blockade. For both primary and advanced disease where 11q13 is amplified, ANO1 could be a second target to inhibit and increase the efficacy and durability of EGFR inhibitors. As ANO1 inhibitors evolve and progress into animal studies it will be only a matter of time before the hypothesis that ANO1 is a viable therapeutic target will be tested. It is our hope in the next 3–5 years ANO1 therapies, for cancer and other diseases, become a reality and are able to help patients going forward in the future.

Conflict of Interest All authors are employees of Novartis Institutes for BioMedical Research.

Ethical Approval This article does not contain any studies with human participants or animals performed by any of the authors.

References

Ayoub C, Wasylyk C, Li Y, Thomas E, Marisa L, Robe A, Roux M, Abecassis J, de RA, Wasylyk B (2010) ANO1 amplification and expression in HNSCC with a high propensity for future distant metastasis and its functions in HNSCC cell lines. Br J Cancer 103 (5):715–726

Barretina J, Caponigro G, Stransky N, Venkatesan K, Margolin AA, Kim S, Wilson CJ, Lehar J, Kryukov GV, Sonkin D, Reddy A, Liu M, Murray L, Berger MF, Monahan JE, Morais P, Meltzer J, Korejwa A, Jane-Valbuena J, Mapa FA, Thibault J, Bric-Furlong-E, Raman P, Shipway A, Engels IH, Cheng J, Yu GK, Yu J, Aspesi P Jr, de Silva M, Jagtap K, Jones MD, Wang L, Hatton C, Palescandolo E, Gupta S, Mahan S, Sougnez C, Onofrio RC, Liefeld T, MacConaill L, Winckler W, Reich M, Li N, Mesirov JP, Gabriel SB, Getz G, Ardlie K, Chan V, Myer VE, Weber BL, Porter J, Warmuth M, Finan P, Harris JL, Meyerson M, Golub TR, Morrissey MP, Sellers WR, Schlegel R, Garraway LA (2012) The cancer cell line encyclopedia enables predictive modelling of

anticancer drug sensitivity. Nature 483 (7391):603–607. doi:10.1038/nature11003

Beltran H, Prandi D, Mosquera JM, Benelli M, Puca L, Cyrta J, Marotz C, Giannopoulou E, Chakravarthi BV, Varambally S, Tomlins SA, Nanus DM, Tagawa ST, Van Allen EM, Elemento O, Sboner A, Garraway LA, Rubin MA, Demichelis F (2016) Divergent clonal evolution of castration-resistant neuroendocrine prostate cancer. Nat Med 22(3):298–305. doi:10.1038/nm.4045

Berglund E, Akcakaya P, Berglund D, Karlsson F, Vukojevic V, Lee L, Bogdanovic D, Lui WO, Larsson C, Zedenius J, Frobom R, Branstrom R (2014) Functional role of the Ca-activated Cl channel DOG1/TMEM16A in gastrointestinal stromal tumor cells. Exp Cell Res 326(2):315–325. doi:10.1016/j.yexcr.2014.05.003

Bill A, Hall ML, Borawski J, Hodgson C, Jenkins J, Piechon P, Popa O, Rothwell C, Tranter P, Tria S, Wagner T, Whitehead L, Gaither LA (2014) Small molecule facilitated degradation of ANO1 – a new targeting approach for anticancer therapeutics. J Biol Chem 289(16):11029–11041. doi:10.1074/jbc.M114.549188

Bill A, Gutierrez A, Kulkarni S, Kemp C, Bonenfant D, Voshol H, Duvvuri U, Gaither LA (2015a) ANO1 interacts with EGFR and correlates with sensitivity to EGFR-targeting therapy in head and neck cancer. Oncotarget 6(11):9173–9188. doi:10.18632/oncotarget.3277

Bill A, Popa MO, van Diepen MT, Gutierrez A, Lilley S, Velkova M, Acheson K, Choudhury H, Renaud NA, Auld DS, Gosling M, Groot-Kormelink PJ, Gaither LA (2015b) Variomics screen identifies the re-entrant loop of the calcium-activated chloride channel ANO1 that facilitates channel activation. J Biol Chem 290 (2):889–903. doi:10.1074/jbc.M114.618140

Britschgi A, Bill A, Brinkhaus H, Rothwell C, Clay I, Duss S, Rebhan M, Raman P, Guy CT, Wetzel K, George E, Popa MO, Lilley S, Choudhury H, Gosling M, Wang L, Fitzgerald S, Borawski J, Baffoe J, Labow M, Gaither LA, Bentires-Alj M (2013) Calcium-activated chloride channel ANO1 promotes breast cancer progression by activating EGFR and CAMK signaling. Proc Natl Acad Sci U S A 110(11):E1026–E1034

Campbell JD, Alexandrov A, Kim J, Wala J, Berger AH, Pedamallu CS, Shukla SA, Guo G, Brooks AN, Murray BA, Imielinski M, Hu X, Ling S, Akbani R, Rosenberg M, Cibulskis C, Ramachandran A, Collisson EA, Kwiatkowski DJ, Lawrence MS, Weinstein JN, Verhaak RG, Wu CJ, Hammerman PS, Cherniack AD, Getz G, Cancer Genome Atlas Research Network, Artyomov MN, Schreiber R, Govindan R, Meyerson M (2016) Distinct patterns of somatic genome alterations in lung adenocarcinomas and squamous cell carcinomas. Nat Genet 48 (6):607-616. doi:10.1038/ng.3564

Cancer Genome Atlas Network (2012) Comprehensive molecular portraits of human breast tumours. Nature 490(7418):61–70. doi:10.1038/nature11412

Cancer Genome Atlas Network (2015) Comprehensive genomic characterization of head and neck squamous cell carcinomas. Nature 517(7536):576–582. doi:10.1038/nature14129

Cancer Genome Atlas Research Network (2012) Comprehensive genomic characterization of squamous cell lung cancers. Nature 489(7417):519–525. doi:10.1038/nature11404

Cancer Genome Atlas Research Network (2014) Comprehensive molecular characterization of urothelial bladder carcinoma. Nature 507(7492):315–322. doi:10.1038/nature12965

Caputo A, Caci E, Ferrera L, Pedemonte N, Barsanti C, Sondo E, Pfeffer U, Ravazzolo R, Zegarra-Moran O, Galietta LJ (2008) TMEM16A, a membrane protein associated with calcium-dependent chloride channel activity. Science 322(5901):590–594

Cerami E, Gao J, Dogrusoz U, Gross BE, Sumer SO, Aksoy BA, Jacobsen A, Byrne CJ, Heuer ML, Larsson E, Antipin Y, Reva B, Goldberg AP, Sander C, Schultz N (2012) The cBio cancer genomics portal: an open platform for exploring multidimensional cancer genomics data. Cancer Discov 2 (5):401–404. doi:10.1158/2159-8290.CD-12-0095

Cha JY, Wee J, Jung J, Jang Y, Lee B, Hong GS, Chang BC, Choi YL, Shin YK, Min HY, Lee HY, Na TY, Lee MO, Oh U (2015) Anoctamin 1 (TMEM16A) is essential for testosterone-induced prostate hyperplasia. Proc Natl Acad Sci U S A 112(31):9722–9727. doi:10.1073/pnas.1423827112

Cho H, Yang YD, Lee J, Lee B, Kim T, Jang Y, Back SK, Na HS, Harfe BD, Wang F, Raouf R, Wood JN, Oh U (2012) The calcium-activated chloride channel anoctamin 1 acts as a heat sensor in nociceptive neurons. Nat Neurosci 15(7):1015–1021

Ciriello G, Gatza ML, Beck AH, Wilkerson MD, Rhie SK, Pastore A, Zhang H, McLellan M, Yau C, Kandoth C, Bowlby R, Shen H, Hayat S, Fieldhouse R, Lester SC, Tse GM, Factor RE, Collins LC, Allison KH, Chen YY, Jensen K, Johnson NB, Oesterreich S, Mills GB, Cherniack AD, Robertson G, Benz C, Sander C, Laird PW, Hoadley KA, King TA, Network TR, Perou CM (2015) Comprehensive molecular portraits of invasive lobular breast cancer. Cell 163(2):506–519. doi:10.1016/j.cell.2015.09.033

Clucas J, Valderrama F (2014) ERM proteins in cancer progression. J Cell Sci 127(Pt 2):267–275. doi:10.1242/jcs.133108

Dixit R, Kemp C, Kulich S, Seethala R, Chiosea S, Ling S, Ha PK, Duvvuri U (2015) TMEM16A/ANO1 is differentially expressed in HPV-negative versus HPV-positive head and neck squamous cell carcinoma through promoter methylation. Sci Rep 5:16657. doi:10.1038/srep16657

Duran C, Thompson CH, Xiao Q, Hartzell HC (2010) Chloride channels: often enigmatic, rarely predictable. Annu Rev Physiol 72:95–121

Duvvuri U (2015) ANO1 plays a critical role in prostatic hyperplasia. Proc Natl Acad Sci U S A 112 (31):9506–9507. doi:10.1073/pnas.1512075112

Duvvuri U, Shiwarski DJ, Xiao D, Bertrand C, Huang X, Edinger RS, Rock J, Harfe BD, Henson BJ, Kunzelmann K, Schreiber R, Seethala RR, Egloff AM, Chen X, Lui VW, Grandis JR, Gollin SM (2012) TMEM16A, induces MAPK and contributes directly to tumorigenesis and cancer progression. Cancer Res 72(13):3270–3281

Faria D, Rock JR, Romao AM, Schweda F, Bandulik S, Witzgall R, Schlatter E, Heitzmann D, Pavenstadt H, Herrmann E, Kunzelmann K, Schreiber R (2014) The calcium-activated chloride channel Anoctamin 1 contributes to the regulation of renal function. Kidney Int 85(6):1369–1381. doi:10.1038/ki.2013.535

Fehon RG, McClatchey AI, Bretscher A (2010) Organizing the cell cortex: the role of ERM proteins. Nat Rev Mol Cell Biol 11(4):276–287. doi:10.1038/nrm2866

Galindo BE, Vacquier VD (2005) Phylogeny of the TMEM16 protein family: some members are overexpressed in cancer. Int J Mol Med 16 (5):919–924

Gao J, Aksoy BA, Dogrusoz U, Dresdner G, Gross B, Sumer SO, Sun Y, Jacobsen A, Sinha R, Larsson E, Cerami E, Sander C, Schultz N (2013) Integrative analysis of complex cancer genomics and clinical profiles using the cBioPortal. Sci Signal 6(269):pl1. doi:10.1126/scisignal.2004088

Gomez-Pinilla PJ, Gibbons SJ, Bardsley MR, Lorincz A, Pozo MJ, Pasricha PJ, van de Rijn M, West RB, Sarr MG, Kendrick ML, Cima RR, Dozois EJ, Larson DW, Ordog T, Farrugia G (2009) Ano1 is a selective marker of interstitial cells of Cajal in the human and mouse gastrointestinal tract. Am J Physiol Gastrointest Liver Physiol 296(6):G1370–G1381

Habela CW, Ernest NJ, Swindall AF, Sontheimer H (2009) Chloride accumulation drives volume dynamics underlying cell proliferation and migration. J Neurophysiol 101(2):750–757. doi:10.1152/jn.90840.2008

Han Y, Zhang S, Ren S, Chen Y, Yuan H, Chai R, Yu H, Zhang H, Zhan Y, An H (2015) Two Ca-binding sites cooperatively couple together in TMEM16A channel. J Membr Biol. doi:10.1007/s00232-015-9846-1

Hanahan D, Weinberg RA (2011) Hallmarks of cancer: the next generation. Cell 144(5):646–674

Hiraoka K, Miyazaki H, Niisato N, Iwasaki Y, Kawauchi A, Miki T, Marunaka Y (2010) Chloride ion modulates cell proliferation of human androgen-independent prostatic cancer cell. Cell Physiol Biochem 25(4–5):379–388. doi:10.1159/000303042

Hou Y, Guan X, Yang Z, Li C (2016) Emerging role of cystic fibrosis transmembrane conductance regulator – an epithelial chloride channel in gastrointestinal cancers. World J Gastrointest Oncol 8(3):282–288. doi:10.4251/wjgo.v8.i3.282

Huang X, Godfrey TE, Gooding WE, McCarty KS Jr, Gollin SM (2006) Comprehensive genome and transcriptome analysis of the 11q13 amplicon in human oral cancer and synteny to the 7F5 amplicon in murine oral carcinoma. Genes Chromosom Cancer 45(11):1058–1069

Huang F, Rock JR, Harfe BD, Cheng T, Huang X, Jan YN, Jan LY (2009) Studies on expression and function of the TMEM16A calcium-activated chloride channel. Proc Natl Acad Sci U S A 106(50):21413–21418

Huang F, Zhang H, Wu M, Yang H, Kudo M, Peters CJ, Woodruff PG, Solberg OD, Donne ML, Huang X, Sheppard D, Fahy JV, Wolters PJ, Hogan BL, Finkbeiner WE, Li M, Jan YN, Jan LY, Rock JR (2012) Calcium-activated chloride channel TMEM16A modulates mucin secretion and airway smooth muscle contraction. Proc Natl Acad Sci U S A 109(40):16354–16359

Huber SM (2013) Oncochannels. Cell Calcium 53 (4):241–255

Hwang SJ, Blair PJ, Britton FC, O'Driscoll KE, Hennig G, Bayguinov YR, Rock JR, Harfe BD, Sanders KM, Ward SM (2009) Expression of anoctamin 1/TMEM16A by interstitial cells of Cajal is fundamental for slow wave activity in gastrointestinal muscles. J Physiol 587(Pt 20):4887–4904

Jia L, Liu W, Guan L, Lu M, Wang K (2015) Inhibition of calcium-activated chloride channel ANO1/TMEM16A suppresses tumor growth and invasion in human lung cancer. PLoS One 10(8):e0136584. doi:10.1371/journal.pone.0136584

Jin X, Shah S, Liu Y, Zhang H, Lees M, Fu Z, Lippiat JD, Beech DJ, Sivaprasadarao A, Baldwin SA, Gamper N (2013) Activation of the Cl- channel ANO1 by localized calcium signals in nociceptive sensory neurons requires coupling with the IP3 receptor. Sci Signal 6(290):ra73

Katoh M, Katoh M (2004) Identification and characterization of TMEM16E and TMEM16F genes in silico. Int J Oncol 24(5):1345–1349

Kumar A, Coleman I, Morrissey C, Zhang X, True LD, Gulati R, Etzioni R, Bolouri H, Montgomery B, White T, Lucas JM, Brown LG, Dumpit RF, DeSarkar N, Higano C, Yu EY, Coleman R, Schultz N, Fang M, Lange PH, Shendure J, Vessella RL, Nelson PS (2016) Substantial interindividual and limited intraindividual genomic diversity among tumors from men with metastatic prostate cancer. Nat Med 22(4):369–378. doi:10.1038/nm.4053

Kunzelmann K (2015) TMEM16, LRRC8A, bestrophin: chloride channels controlled by Ca(2+) and cell volume. Trends Biochem Sci 40(9):535–543. doi:10.1016/j.tibs.2015.07.005

Lang F, Stournaras C (2014) Ion channels in cancer: future perspectives and clinical potential. Philos Trans R Soc B Biol Sci 369(1638). doi:10.1098/rstb.2013.0108

Lee J, Jung J, Tak MH, Wee J, Lee B, Jang Y, Chun H, Yang DJ, Yang YD, Park SH, Han BW, Hyun S, Yu J, Cho H, Hartzell HC, Oh U (2015) Two helices in the third intracellular loop determine anoctamin 1 (TMEM16A) activation by calcium. Pflugers Arch 467(8):1677–1687. doi:10.1007/s00424-014-1603-2

Lee YS, Lee JK, Bae Y, Lee BS, Kim E, Cho CH, Ryoo K, Yoo J, Kim CH, Yi GS, Lee SG, Lee CJ, Kang SS, Hwang EM, Park JY (2016) Suppression of 14-3-3gamma-mediated surface expression of ANO1 inhibits cancer progression of glioblastoma cells. Sci Rep 6:26413. doi:10.1038/srep26413

Li Y, Zhang J, Hong S (2013) ANO1 as a marker of oral squamous cell carcinoma and silencing ANO1 suppresses migration of human scc-25 cells. Med Oral Patol Oral Cir Bucal 19(4):e313–e319

Liegl B, Hornick JL, Corless CL, Fletcher CD (2009) Monoclonal antibody DOG1.1 shows higher sensitivity than KIT in the diagnosis of gastrointestinal stromal tumors, including unusual subtypes. Am J Surg Pathol 33(3):437–446

Liu W, Lu M, Liu B, Huang Y, Wang K (2012) Inhibition of Ca(2+)-activated Cl(−) channel ANO1/TMEM16A expression suppresses tumor growth and invasiveness in human prostate carcinoma. Cancer Lett 326:41–51

Liu J, Liu Y, Ren Y, Kang L, Zhang L (2014) Transmembrane protein with unknown function 16A overexpression promotes glioma formation through the nuclear factorkappaB signaling pathway. Mol Med Rep 9(3):1068–1074. doi:10.3892/mmr.2014.1888

Liu F, Cao QH, Lu DJ, Luo B, Lu XF, Luo RC, Wang XG (2015) TMEM16A overexpression contributes to tumor invasion and poor prognosis of human gastric cancer through TGF-beta signaling. Oncotarget 6 (13):11585–11599. doi:10.18632/oncotarget.3412

Manoury B, Tamuleviciute A, Tammaro P (2010) TMEM16A/anoctamin 1 protein mediates calcium-activated chloride currents in pulmonary arterial smooth muscle cells. J Physiol 588(Pt 13):2305–2314

Miyazaki H, Shiozaki A, Niisato N, Ohsawa R, Itoi H, Ueda Y, Otsuji E, Yamagishi H, Iwasaki Y, Nakano T, Nakahari T, Marunaka Y (2008) Chloride ions control the G1/S cell-cycle checkpoint by regulating the expression of p21 through a p53-independent pathway in human gastric cancer cells. Biochem Biophys Res Commun 366(2):506–512. doi:10.1016/j.bbrc.2007.11.144

Oh SJ, Hwang SJ, Jung J, Yu K, Kim J, Choi JY, Hartzell HC, Roh EJ, Lee CJ (2013) MONNA, a potent and selective blocker for transmembrane protein with unknown function 16/anoctamin-1. Mol Pharmacol 84(5):726–735. doi:10.1124/mol.113.087502

Orr Gandy KA, Adada M, Canals D, Carroll B, Roddy P, Hannun YA, Obeid LM (2013) Epidermal growth factor-induced cellular invasion requires sphingosine-1-phosphate/sphingosine-1-phosphate 2 -receptor-mediated ezrin activation. FASEB J 27 (8):3155–3166. doi:10.1096/fj.13-228460

Pedemonte N, Galietta LJ (2014) Structure and function of TMEM16 proteins (Anoctamins). Physiol Rev 94 (2):419–459. doi:10.1152/physrev.00039.2011

Pereira B, Chin SF, Rueda OM, Vollan HK, Provenzano E, Bardwell HA, Pugh M, Jones L, Russell R, Sammut SJ, Tsui DW, Liu B, Dawson SJ, Abraham J, Northen H, Peden JF, Mukherjee A, Turashvili G, Green AR, McKinney S, Oloumi A, Shah S, Rosenfeld N, Murphy L, Bentley DR, Ellis IO, Purushotham A, Pinder SE, Borresen-Dale AL, Earl HM, Pharoah PD, Ross MT, Aparicio S, Caldas C (2016) The somatic mutation profiles of 2,433 breast cancers refines their genomic and transcriptomic landscapes. Nat Commun 7:11479. doi:10.1038/ncomms11479

Peretti M, Angelini M, Savalli N, Florio T, Yuspa SH, Mazzanti M (2015) Chloride channels in cancer: focus on chloride intracellular channel 1 and 4 (CLIC1 AND CLIC4) proteins in tumor development and as novel therapeutic targets. Biochim Biophys Acta 1848(10 Pt B):2523–2531. doi:10.1016/j.bbamem.2014.12.012

Perez-Cornejo P, Gokhale A, Duran C, Cui Y, Xiao Q, Hartzell HC, Faundez V (2012) Anoctamin 1 (Tmem16A) Ca2+−activated chloride channel stoichiometrically interacts with an ezrin-radixin-moesin network. Proc Natl Acad Sci U S A 109 (26):10376–10381

Peters CJ, Yu H, Tien J, Jan YN, Li M, Jan LY (2015) Four basic residues critical for the ion selectivity and pore blocker sensitivity of TMEM16A calcium-activated chloride channels. Proc Natl Acad Sci U S A 112(11):3547–3552. doi:10.1073/pnas.1502291112

Picollo A, Malvezzi M, Accardi A (2015) TMEM16 proteins: unknown structure and confusing functions. J Mol Biol 427(1):94–105. doi:10.1016/j.jmb.2014.09.028

Reddy RB, Bhat AR, James BL, Govindan SV, Mathew R, Dr R, Hedne N, Illiayaraja J, Kekatpure V, Khora SS, Hicks W, Tata P, Kuriakose MA, Suresh A (2016) Meta-analyses of microarray datasets identifies ANO1 and FADD as prognostic markers of head and neck cancer. PLoS One 11(1): e0147409. doi:10.1371/journal.pone.0147409

Robinson D, Van Allen EM, Wu YM, Schultz N, Lonigro RJ, Mosquera JM, Montgomery B, Taplin ME, Pritchard CC, Attard G, Beltran H, Abida W, Bradley RK, Vinson J, Cao X, Vats P, Kunju LP, Hussain M, Feng FY, Tomlins SA, Cooney KA, Smith DC, Brennan C, Siddiqui J, Mehra R, Chen Y, Rathkopf DE, Morris MJ, Solomon SB, Durack JC, Reuter VE, Gopalan A, Gao J, Loda M, Lis RT, Bowden M, Balk SP, Gaviola G, Sougnez C, Gupta M, Yu EY, Mostaghel EA, Cheng HH, Mulcahy H, True LD, Plymate SR, Dvinge H, Ferraldeschi R, Flohr P, Miranda S, Zafeiriou Z, Tunariu N, Mateo J, Perez-Lopez R, Demichelis F, Robinson BD, Schiffman M, Nanus DM, Tagawa ST, Sigaras A, Eng KW, Elemento O, Sboner A, Heath EI, Scher HI, Pienta KJ, Kantoff P, de Bono JS, Rubin MA, Nelson PS,

Garraway LA, Sawyers CL, Chinnaiyan AM (2015) Integrative clinical genomics of advanced prostate cancer. Cell 161(5):1215–1228. doi:10.1016/j.cell.2015.05.001

Ruiz C, Martins JR, Rudin F, Schneider S, Dietsche T, Fischer CA, Tornillo L, Terracciano LM, Schreiber R, Bubendorf L, Kunzelmann K (2012) Enhanced expression of ANO1 in head and neck squamous cell carcinoma causes cell migration and correlates with poor prognosis. PLoS One 7(8):e43265

Schroeder BC, Cheng T, Jan YN, Jan LY (2008) Expression cloning of TMEM16A as a calcium-activated chloride channel subunit. Cell 134(6):1019–1029

Seo Y, Lee HK, Park J, Jeon DK, Jo S, Jo M, Namkung W (2016) Ani9, a novel potent small-molecule ANO1 inhibitor with negligible effect on ANO2. PLoS One 11(5):e0155771. doi:10.1371/journal.pone.0155771

Shi ZZ, Shang L, Jiang YY, Hao JJ, Zhang Y, Zhang TT, Lin DC, Liu SG, Wang BS, Gong T, Zhan QM, Wang MR (2013) Consistent and differential genetic aberrations between esophageal dysplasia and squamous cell carcinoma detected by array comparative genomic hybridization. Clin Cancer Res 19(21):5867–5878

Shiozaki A, Otsuji E, Marunaka Y (2011) Intracellular chloride regulates the G(1)/S cell cycle progression in gastric cancer cells. World J Gastrointest Oncol 3(8):119–122. doi:10.4251/wjgo.v3.i8.119

Shiwarski DJ, Shao C, Bill A, Kim J, Xiao D, Bertrand C, Seethala RR, Sano D, Myers JN, Ha PK, Grandis JR, Gaither LA, Puthenveedu MA, Duvvuri U (2014) To "Grow" or "Go": TMEM16A expression as a switch between tumor growth and metastasis in SCCHN. Clin Cancer Res 20(17):4673–4688. doi:10.1158/1078-0432.CCR-14-0363

Sui Y, Sun M, Wu F, Yang L, Di W, Zhang G, Zhong L, Ma Z, Zheng J, Fang X, Ma T (2014) Inhibition of TMEM16A expression suppresses growth and invasion in human colorectal cancer cells. PLoS One 9(12):e115443. doi:10.1371/journal.pone.0115443

West RB, Corless CL, Chen X, Rubin BP, Subramanian S, Montgomery K, Zhu S, Ball CA, Nielsen TO, Patel R, Goldblum JR, Brown PO, Heinrich MC, van de Rijn M (2004) The novel marker, DOG1, is expressed ubiquitously in gastrointestinal stromal tumors irrespective of KIT or PDGFRA mutation status. Am J Pathol 165(1):107–113

Witkiewicz AK, McMillan EA, Balaji U, Baek G, Lin WC, Mansour J, Mollaee M, Wagner KU, Koduru P, Yopp A, Choti MA, Yeo CJ, McCue P, White MA, Knudsen ES (2015) Whole-exome sequencing of pancreatic cancer defines genetic diversity and therapeutic targets. Nat Commun 6:6744. doi:10.1038/ncomms7744

Yang YD, Cho H, Koo JY, Tak MH, Cho Y, Shim WS, Park SP, Lee J, Lee B, Kim BM, Raouf R, Shin YK, Oh U (2008) TMEM16A confers receptor-activated calcium-dependent chloride conductance. Nature 455(7217):1210–1215

Adv Exp Med Biol - Protein Reviews (2017) 2:15–35
DOI 10.1007/5584_2016_200

Published online: 29 April 2017

Structure and Function of the Two-Component Cytotoxins of *Staphylococcus aureus* – Learnings for Designing Novel Therapeutics

Adriana Badarau, Nikolina Trstenjak, and Eszter Nagy

Abstract

Staphylococcus aureus can produce up to five different bi-component cytotoxins: two gamma-hemolysins HlgAB and HlgCB, and leukocidins SF-PV (Panton Valentine leukocidin), ED (LukED) and GH (LukGH, also called LukAB). Their major function in *S. aureus* pathogenesis is to evade innate immunity by attacking phagocytic cells and to support bacterial growth by lysing red blood cells. The five cytotoxins display different levels of amino acid sequence conservation (30–82%), but all form a remarkably similar beta-barrel type pore structure (greatly resembling the mono-component toxin alpha-hemolysin) that inserts into the target cell membrane leading to necrotic cell death. This review provides an overview of the culmination of decades of research on the structure of these toxins, their unique sequence and structural features that helps to explain the observed functional differences, such as toxin potency towards different cell types and species, receptor specificity and formation of functional non-cognate toxin pairs. The vast knowledge accumulated in this field supports novel approaches and the design of therapeutics targeting these cytotoxins to tame virulence and fight *S. aureus* infections.

Keywords

Staphylococcus aureus • Bi-component toxins • Leukocidins • Beta-barrel pore • Oligomerization

A. Badarau, N. Trstenjak, and E. Nagy (✉)
Arsanis Biosciences, Campus Vienna Biocenter,
Helmut-Qualtinger-Gasse 2, 1030 Vienna, Austria
e-mail: eszter.nagy@arsanis.com

Abbreviations

C5aR	C5a receptor
C5L2	C5a-like receptor 2
CCR2 and CCR5	C-C chemokine receptors type 2 and 5, respectively
CXCR1 and CXCR2	CXC chemokine receptors 1 and 2, respectively
DARC	Duffy antigen receptor
Hla	alpha-hemolysin
HlgAB and CB	gamma-hemolysins AB and CB
LukED and LukGH	leukocidins ED and GH
LukSF-PV	Panton-Valentine leukocidin
mAb	monoclonal antibody
MES	2-(N-morpholino) ethanesulfonic acid
MPD	2-methylpentane-2,4-diol
PC	phosphocholine
PFTs	pore forming toxins
PMNs	polymorphonuclear cell
RBCs	red blood cells
Cα rmsd	root mean square deviation of the α-carbons
ST	sequence type

1 The Bi-component Cytolysins of *S. aureus*

1.1 Background

Several pathogenic bacteria secrete pore-forming toxins (PFTs) to eliminate target cells of their hosts and thus such toxins are very important for their pathogenesis (Dal Peraro and van der Goot 2016). *S. aureus* can produce up to six different PFTs: alpha-hemolysin (Hla), two gamma-hemolysins (HlgAB and HlgCB), Panton-Valentine Leukocidin (PVL, referred to here as LukSF-PV), leukocidins ED (LukED) and GH (LukGH, also called LukAB) (Vandenesch et al. 2012). Hla is a mono-component PFT, while the other five toxins are composed of two different polypeptides (S- and F-components). The common feature of these toxins is the beta-barrel type pore structure inserted into the target cell membrane, which allows the movement of molecules smaller than 2-kDa such as K^+ and Ca^{2+} ions, leading to necrotic cell death (Menestrina 1986). Hla and the bi-component toxins share limited sequence homology, but remarkable structural homology. Determination of the heptameric pore formation by Hla greatly supported the understanding of the molecular mechanisms of octameric pore formation by the bi-component toxins (Song et al. 1996; Kaneko and Kamio 2004; Tanaka et al. 2011).

Hla has been shown to be a very important virulence factor in different types of *S. aureus* infections (Berube and Bubeck Wardenburg 2013). Hla lyses red blood cells (RBCs) in different animal species, but it is not hemolytic to human RBCs. The major human target cells are epithelial and endothelial cells, *via* recognition of ADAM10 as receptor (Berube and Bubeck Wardenburg 2013).

The bi-component toxins all target leukocytes - therefore the name leukocidins – in a redundant, but also unique manner with regards to cell type specificity, which is driven by binding to specific receptors on the surface of immune cells. Their major pathogenic effect is immune evasion by lysing phagocytic cells, mainly neutrophil granulocytes, but also monocytes and macrophages. HlgAB and LukED also potently lyse human red blood cells using receptors that are different from those expressed on phagocytes.

The contributions of the bi-component PFTs to *S. aureus* pathogenesis are not detailed here; and we refer to the several excellent reviews recently published in this field (Vandenesch et al. 2012; Spaan et al. 2014a; Alonzo and Torres 2014). Instead, we focus on the common and unique structural features of these toxins that support the understanding of their mode of action and function, and also the design of new therapeutic approaches to combat *S. aureus* infections.

Table 1 Percent sequence identity between *S. aureus* bi-component leukocidins based on sequences derived from USA300 CA-MRSA strains

	HlgC	LukS	LukE	HlgA	LukH	LukF	LukD	HlgB	LukG
HlgC		81.12	68.62	66.32	29.64	25.88	26.20	23.96	23.42
LukS	81.12		69.44	65.40	29.94	26.28	26.92	25.00	23.49
LukE	68.62	69.44		70.18	30.06	25.63	26.58	25.32	24.14
HlgA	66.32	65.40	70.18		29.55	26.18	27.13	25.87	24.38
LukH	29.64	29.94	30.06	29.55		24.93	26.10	24.63	24.93
LukF	25.88	26.28	25.63	26.18	24.93		82.06	71.52	38.78
LukD	26.20	26.92	26.58	27.13	26.10	82.06		75.17	39.10
HlgB	23.96	25.00	25.32	25.87	24.63	71.52	75.17		39.74
LukG	23.42	23.49	24.14	24.38	24.93	38.78	39.10	39.74	

1.2 Amino acid Sequence Homology, Relatedness

The two polypeptides of bi-component leukocidins are approximately 300 amino acids in length, and belong to two sequence related groups, the S- (slow) and F- (fast) components, so named based on their elution profile in ion exchange chromatography. The S-components LukS, LukE, HlgA and HlgC and the F-components LukF, LukD and HlgB share 65–81% and 75–82% amino acid sequence homology to each other, respectively. The S-component LukH and F-component LukG are more distantly related to the other S- and F-components displaying only 30 and 40% homology, respectively. The S- and F-components are 25% homologous to each other, and also to Hla (Table 1, example with a prototype USA300 CA-MRSA strain that carries genes for all five leukocidins).

1.3 Sequence Conservation

Since the completion of sequencing of the first *S. aureus* genome in 2001 (Kuroda et al. 2001), close to 7000 *S. aureus* genome sequences have become available (https://www.patricbrc.org – 6700; http://www.ncbi.nlm.nih.gov – 6900 assembled genomes). We found that genes for HlgA, HlgB, HlgC, LukG and LukH are present in the vast majority of *S. aureus* isolates for which annotated whole genome sequences are available, while genes for LukED and LukSF-PV were found in ~66 and ~20% of sequenced strains, respectively. The sequenced *S. aureus* strains available in the public databases are enriched for certain clonal types and antibiotic resistant strains (e.g. USA300 CA-MRSA and USA100 HA-MRSA) and may introduce a bias in gene prevalence for LukSF-PV and LukED compared to those represented by clinical isolates. Gene prevalence studies with different collections of human clinical isolates reported LukED prevalence between 30 or 87% (Gravet et al. 1998; Morinaga et al. 2003; von Eiff et al. 2004) with blood isolates having higher prevalence than nasal isolates (82 vs. 61%) (von Eiff et al. 2004). Even a greater difference was reported for LukSF-PV prevalence, from only 2–3% in nasal isolates (Kuehnert et al. 2006) to over 90% in skin infections and pneumonia (Lina et al. 1999; Gillet et al. 2002).

Analysis of the available genome sequences revealed a high level of amino acid conservation (>95%) for all genes, except LukGH (>82%). We found that 1–4 unique sequences represent the genes in ~95% of sequenced isolates for all leukocidins except LukGH, typically with a dominant sequence type (present in >60% of strains carrying the given leukocidin genes)

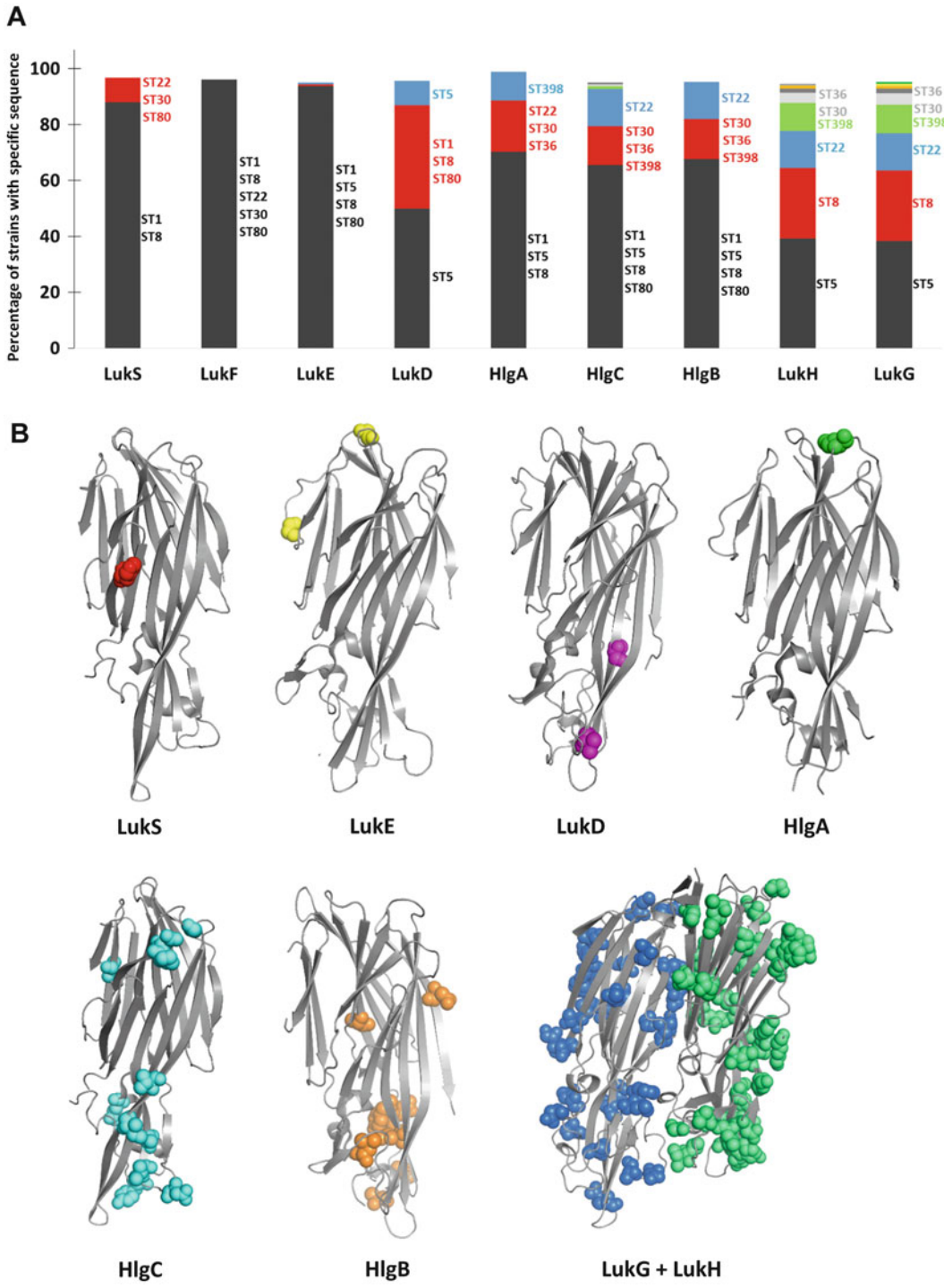

Fig. 1 Sequence conservation of bi-component toxins in *S. aureus* strains. (**a**) For each toxin, the percentage of strains that contain one unique sequence (relative to the total number of strains containing that particular toxin gene) is shown as a different color. Sequence types for the most prevalent sequences are indicated. (**b**) Non-conserved amino-acids relative to the USA300 TCH1516 sequence are shown as spheres on the toxin structures (for LukS, LukE, HlgA, LukF, LukD, HlgB and LukGH the pdb files 1T5R, 3ROH, 2QK7, 1PVL, 2Q7G, 1LKF and 5K59, respectively, were used and HlgC was modeled on the LukS structure)

(Fig. 1a). In case of LukS-PV, LukE, LukD and HlgA, these variant sequences differ from the dominant one only by one or two amino acids (Fig. 1b). HlgC and HlgB sequences are more divergent with up to 12 and 9 amino acid variability, respectively, compared to the dominant sequence type (Fig. 1b). This is quite interesting, since hlgABC are located in the same operon. This finding suggests that HlgA and HlgCB are under different selection pressure, and the changes in HlgC and HlgB, especially those in the cell binding region might be the consequence of adaptation to different host cells (human ethnicities, different animal species, e.g. live-stock). We found approximately 100 unique LukG and LukH sequences, with 6–9 different sequence types representing >95% of *S. aureus* strains (Fig. 1a). These most common sequences differ by as many as 42 amino acids, and the most different LukG and LukH sequences share only about 82% identity (changes in up to 60 amino acid positions, excluding the sequences that have deletions at C-terminus, see Sect. 2.3, Fig. 4d). In most cases, the number of amino acid changes is similar in the S- and F-component pairs within a *S. aureus* strain (for example most extensive changes in HlgC and HlgB in CC30 strains compared to ST1 & 8 strains and in LukH and LukG in CC30 sequence types relative to ST5), suggesting co-evolution/co-adaptation of sequences of the monomer pairs.

2 Three-Dimensional Structural Features

2.1 Overall Structural Features

The first crystal structure of an *S. aureus* bi-component toxin was published in 1999 for LukF-PV (PDB code 1PVL) (Pédelacq et al. 1999), showing a three-domain arrangement with predominant beta-sheet structure, which resembled that of heptameric Hla described earlier (Song et al. 1996). Based on structure comparison and sequence alignment with the other bi-component monomers, it has been postulated that LukF represents the fold of any water-soluble secreted protein in this family of transmembrane pore-forming toxins. This was later confirmed when the structures of all other S- and F-components became available (Table 2), most recently those of LukE and LukD (Nocadello et al. 2016), and monomeric alpha-hemolysin (Foletti et al. 2013; Oganesyan et al. 2014; Sugawara et al. 2015).

The bi-component leukocidins and Hla share the same fold and overall structure with three main functional domains (Fig. 2a, exemplified for LukE). The rim domain is composed of four anti-parallel beta sheets connected by flexible loops and was shown to be involved in cell binding in case of LukS, LukE and HlgB. The cap domain, composed of 11 anti-parallel beta sheets, is involved in inter-monomer interactions in the pre-pore and pore structures. The stem domain contains three anti-parallel beta-sheets, folded against the cap domain in the monomers, and undergoes a major conformational change upon pore formation, by detaching from the cap domain and assembling into a 16 anti-parallel beta-sheet barrel structure. Figures 2b, c show the structures of a representative S- and F-component, respectively, with the positions that are conserved between the different monomeric components, marked.

The exact structures uncovered the subtle differences that explain the different receptor/cell type specificity and pairing propensity. Extensive research has shown that on leukocytes the S-component binds to the cells, subsequently recruiting the F-component, but the sequence of events is less clear for erythrocytes (Nguyen et al. 2003; Yokota and Kamio 2000). Most importantly, LukGH differs from the other bi-component toxins, because it forms a stable heterodimer before contacting the target cells (Badarau et al. 2015; DuMont et al. 2014). Crystal structures of beta-barrel pore and pre-pore

Table 2 Summary of structural data for *S. aureus* bi-component toxins

Toxin	Oligomeric state	PDB code	Resolution (Å)	Region visible	Ligands	Reference
Hla	Heptamer	3ANZ	2.3	1–295	MPD, ACY[a]	Tanaka et al. (2011)
HlgA	Covalent heterodimer	2QK7	2.4	11–278	HlgB	Roblin et al. (2008)
	Octamer	4P1Y	3.0	6–280	HlgB	Yamashita et al. (2014)
	Octamer	3B07	2.5	11–280	HlgB, MPD	Yamashita et al. (2011)
HlgB	Monomer	1LKF	1.9	2–300		Olson et al. (1999)
	Monomer	2LKF	2.5	2–300		Olson et al. (1999)
	Monomer	3LKF	1.9	2–300	PC	Olson et al. (1999)
	Covalent heterodimer	2QK7	2.4	4–300	HlgA	Roblin et al. (2008)
	Octamer	4P1X	2.4	17–300	HlgC, MPD	Yamashita et al. (2014)
	Octamer	4P1Y	3.0	17–300	HlgA	Yamashita et al. (2014)
	Octamer	3B07	2.5	17–300	HlgA, MPD	Yamashita et al. (2011)
HlgC	Octamer	4P1X	2.4	12–286	HlgB	Yamashita et al. (2014)
LukS	Monomer	1T5R	2.0	3–284		Guillet et al. (2004)
LukS Y250A	Monomer	4IYA	1.6	2–284	FLC, EDO[a]	Laventie et al. (2014)
LukS T244A	Monomer	4IYC	2.8	2–284		Laventie et al. (2014)
LukS Y184A	Monomer	4IYT	2.2	3–284	MES	Laventie et al. (2014)
LukS N248A	Monomer	4IZL	2.8	2–284		Laventie et al. (2014)
LukS Y246A	Monomer	4J0O	2.5	3–284		Laventie et al. (2014)
LukF	Monomer	1PVL	2.0	1–301	MES	Pédelacq et al. (1999)
LukE	Monomer	3ROH	3.2	2–283	PGE[a]	Nocadello et al. (2016)
LukD	Monomer	4Q7G	1.7	1–300	BTB[a]	Nocadello et al. (2016)
LukGH	Heterodimer	5K59	2.8	LukG 11–305		Badarau et al. (2016)
				LukH 42–323		
	Octamer	4TW1	2.8	LukG 16–305		Badarau et al. (2015)
				LukH 35–323		

[a]*ACY* acetic acid, *FLC* citrate, *EDO* 1,2-ethanediol, *PGE* triethyleneglycol, *BTB* bis(2-hydroxyethyl)amino-tris (hydroxymethyl)methane

complexes have also been determined for HlgAB (Yamashita et al. 2011), HlgCB (Yamashita et al. 2014) and more recently for LukGH (Badarau et al. 2015); in all cases, the pore assembly is octameric, consisting of four molecules of S- and F-components located alternately in a circular pattern. Although Hla forms heptameric pores, its pore structure is very similar (Tanaka et al. 2011).

2.2 Monomer Structure

The protomers of the bi-component toxins have an ellipsoid shape and are all composed of three structural regions: the cap (or the β-sandwich), the rim (or the cell binding) and the stem (or -glycine-rich) regions as described above (Fig. 2a, exemplified for LukE). Other regions with functional relevance are the N-terminal latch and the triangle region, which undergo major changes during oligomer to pre-pore and pore transitions. Although the latch is disordered in some structures (Table 2), where visible, in the monomer it is located in the vicinity of the cap domain, as a β-strand, while in the octamer structures it unfolds and latches to the adjacent monomer. Pair-wise superimposition of the different domains of any of the protomer structures typically give root mean square deviations of the α-carbons (Cα rmsds) of <1 Å, which indicates a good overlap, despite the low sequence homology in some cases. For instance, rmsds of 0.82 and 0.89 Å were obtained for 116 and 74 Cα atoms of the cap and rim domains, respectively, for Hla and LukF (Pédelacq et al. 1999). An rmsd of 1.0 Å was calculated for 228 Cα atoms by superposing the global structures of LukS vs. LukF or LukS vs. HlgB, with a better fit between the cap than between the rim domains, and pronounced deviations in the latter corresponding to residues 60–67, 168–174, 181–191, 242–251 (LukS numbering) (Guillet et al. 2004). For the LukE vs. HlgA comparison, the global structure Cα rmsd is 0.53 Å (Fig. 3a), with greater values obtained for LukE-LukS (1.2 Å, Fig. 3b), due to a higher level of torsion of the rim domain with respect to the cap domain (Nocadello et al. 2016). The stem regions were found to be structurally similar to two toxins isolated from snake venom: erabutosin A and toxin-γ (Pédelacq et al. 1999). The β-barrel pore-forming toxins have also been found in *Clostridium perfringens* and *Bacillus cereus*, with proteins having low level of sequence similarity to the *S. aureus* pore-forming toxins (Ramaro and Sanchis 2013).

In contrast to the S-components, where most structural differences occur between the rim

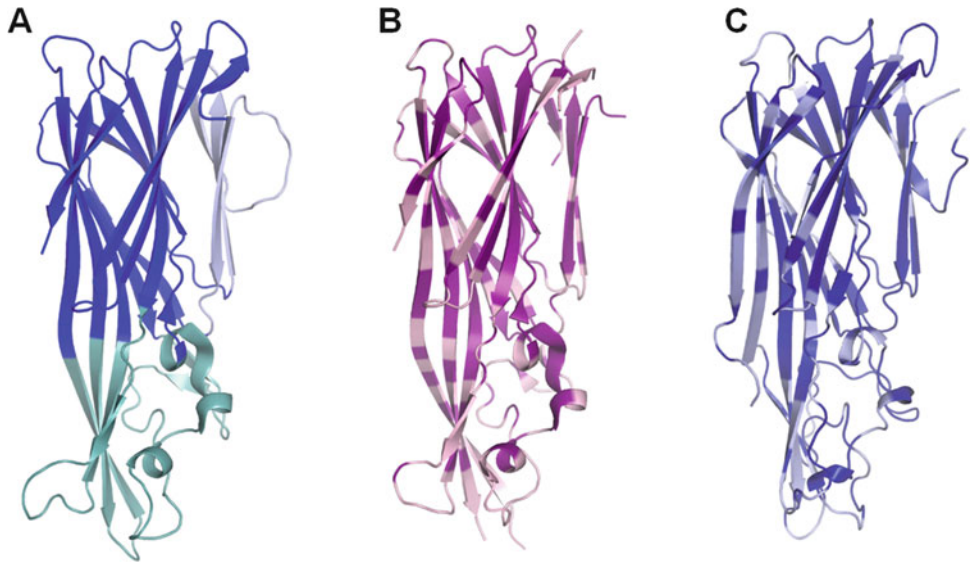

Fig. 2 Structure of monomeric *S. aureus* bi-component toxins. (**a**) Domain organization of LukE (PDB code 3ROH), with rim domain in cyan, cap domain in *dark blue* and stem in *light blue*. (**b** and **c**) Cartoon representation of LukS (*magenta*, PDB code 1T5R) and LukF (*blue*, PDB code 1PVL) with residues conserved between the S- (LukS, LukE, HlgA and HlgC) and the F- (LukF, LukD, HlgB) components in *dark colors*

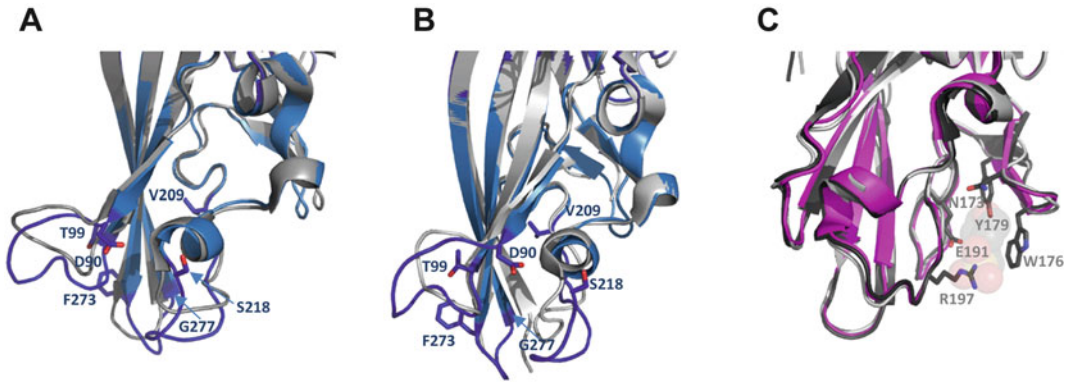

Fig. 3 Conservation of rim domain in S- and F-components. Superposition of LukE (PDB code 3ROH, *blue*) and HlgA (PDB code 2QK7, *grey*) (**a**) and of LukE (PDB code 3ROH, *blue*) and LukS (PDB code 1T5R, *grey*) (**b**) showing the rim domain as cartoon and the residues demarcating divergent loops as *sticks*. (**c**) Superposition of the F-components LukD (PDB code 4Q7G, *magenta*), HlgB (PDB code 1LKF, *light grey*), and LukF (PDB code 1PVL, *dark grey*), showing the rim domain, as cartoon, with PC binding residues as *sticks* and the MES molecule as *spheres*

domains, in the F-components the rim domains are relatively well conserved (Fig. 3c). A common feature of the F-components is the presence of a phosphocholine (PC)-binding site in the rim domain, also present in Hla, but absent in the S-components, and also in LukG and LukH. PC-binding occurs in a cleft formed by five residues (N173, W176, Y179, E191 and R197 – LukF numbering) (Fig. 3c) (Guillet et al. 2004). In the S-components this cleft is replaced by a shallow groove lined with different residues, and in LukG the pocket is occupied by the M178 side-chain.

2.3 Dimer Structure

More recently, the structure of the LukGH dimer in complex with a neutralizing antibody has been reported and shed light on the structural features that makes LukGH unique among the leukocidins (Fig. 4) (Badarau et al. 2016). Superposition of LukG with LukF (PDB code 1PVL (Pédelacq et al. 1999) Cα rmsd of 1.58 Å for 258 atoms) and LukH with LukS (PDB code 1T5R (Guillet et al. 2004) Cα rmsd of 1.37 Å for 246 atoms), shows that the highest divergence occurs in the rim regions (particularly for the LukH-LukS pair) and in the stem domain of LukG (Fig. 4a). The most striking difference is observed between the stem regions of LukG and LukF (Fig. 4b) (Cα rmsd of 10.60 Å for 33 atoms/ 9.97 Å for 32 atoms for LukG and LukF, compared e.g. to the S-components: 0.86 Å for 33 atoms for LukH and LukS) (Badarau et al. 2016). In LukF, the stem domain is folded back against the cap domain, while in LukG, it expands outside the LukG cap region to latch onto the LukH monomer. This interface is stabilized by electrostatic interactions, polar contacts and a hydrophobic core, that all favor dimerization (Badarau et al. 2016). In the rim region, the dimer is further stabilized by salt bridges between the two monomers (Badarau et al. 2015), involving residues D189, D191 and E171 from LukG and R215, R234 and R240 from LukH (Fig. 4c). These residues are conserved in the LukGH sequences, but not in the other S- and F-components (Fig. 4c). Salt bridge formation is also enabled by the rearrangement of the loops in the rim region of LukH compared to LukS (Fig. 4d) (Badarau et al. 2016). In addition, at the C-terminus, LukH has a 10 amino acid extension, which was shown to be critical for receptor binding (DuMont et al. 2014). This region is visible in the structure and consists of a flexible random coil that

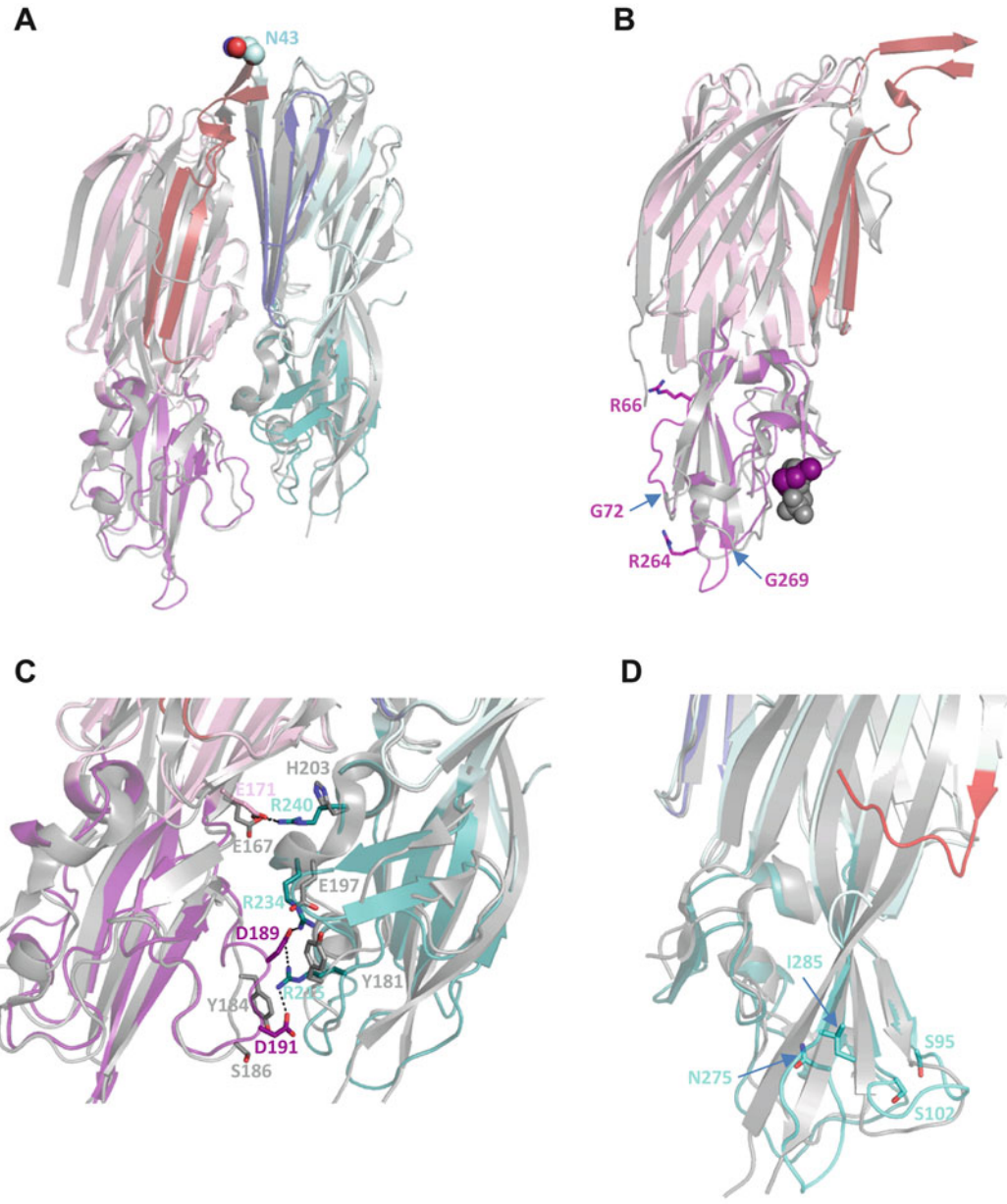

Fig. 4 Structure of the LukGH dimer. (**a**) Overlay of the LukGH dimer (PDB code 5K59, LukG cap – *pink*, rim – *purple*, stem – *brown*; LukH stem – *dark blue*, LukH cap – *light blue*, rim – *blue*) versus LukS (PDB code 1T5R) and LukF (PDB code 1PVL) monomers (*grey*), the first visible amino acid in LukH N-terminus (N43) is shown as *spheres*. (**b**) Overlay of LukG versus LukF, with residues demarcating divergent loops shown as *sticks* and MES (in LukF) and M178 (in LukG) as *spheres*. (**c**) Rim domain of LukGH, with amino acids involved in salt bridges (and corresponding amino acids in LukS and LukF) shown as *sticks*. (**d**) Overlay of LukH versus LukS, as in (a), with residues demarcating divergent loops shown as *sticks* and LukH C-terminus colored *red*

lies along the interface between the rim and the cap domain, and is surface exposed (Fig. 4d). Intriguingly, 9 unique LukH sequences (out of the ~100 identified) lack this C-terminal extension. LukH also has a 34 amino acid extension at the N-terminus, which is not visible in the structure

(Fig. 4a) and whose function is unknown. This N-terminal extension is present in all LukH sequences found in sequence databases.

Leukocidin heterodimers were also engineered based on the monomer structures and the heptamer structure of Hla. For HlgAB, one cysteine was introduced into each monomer in various positions in the oligomerization interface and the activity (Joubert et al. 2006) and X-ray and solution structures (Roblin et al. 2008) of the covalently linked heterodimers were determined. In this case, there was no advantage of the dimers over the monomers in terms of activity, presumably due to the rigid conformation of the disulfide bond. However, the genetic ligation of LukS and LukF, by placing LukS upstream of LukF, and addition of a 15 Ser/Gly spacer yielded a heterodimer with at least 50 times higher lytic activity compared to the wild-type subunits, demonstrating that dimerization is a key (rate limiting) step in the process of pore formation (Jayasinghe and Bayley 2005). This observation might explain the reason why LukGH, the most potent leukocidin against human neutrophils evolved to form a strong heterodimer before receptor interaction (Badarau et al. 2015).

2.4 Oligomer Structure

Following binding to cell membranes, the monomers assemble into octameric pores with four alternating S- and F-subunits. A similar structure was shown to be formed in solution in presence of 2-methylpentane-2,4-diol (MPD) (Yamashita et al. 2011).

The first crystal structure of a pore-like arrangement for a bi-component toxin was published in 2011 for HlgAB (Yamashita et al. 2011), 15 years after the first structure of the heptameric alpha-hemolysin was reported (Song et al. 1996). The octameric pore consists of four molecules of HlgA and HlgB, located alternately in a circular pattern, and is composed of cap, rim and stem domains with a total height and a diameter of 93 and 114 Å, respectively (Fig. 5a). The height of the aqueous part of the pore is ~70 Å, and that of the transmembrane β-barrel is ~47 Å, which would be able to span the cell lipid bilayer, which is typically 40 Å thick. The cap domain is stabilized by extensive interactions between the protomers. Two types of interfaces were identified with buried surface areas of 936 (interface 1) and 1148 (interface 2) Å. The interfaces comprise extensive interactions between the extracellular domains of the two protomers (Fig. 5b), all of the electrostatic ones, and most of the polar and non-polar interactions being conserved in the other S- and F-components, except LukGH. This explains the propensity of the two components (except for LukGH) to form non-cognate pairs with each other. The stem region also involves extensive interactions between protomers and is stabilized by 34 interprotomer hydrogen bonds.

A similar octamer was observed in the crystal structure of LukGH (Badarau et al. 2015), also with two interfaces (interface 1 and 2), stabilized by electrostatic interactions (Fig. 5c). The Cα rmsds between LukG and HlgB (chains A) and LukH and HlgA (chains B) are 1.09 and 1.11 Å, respectively, with the main differences in the loops forming the rim domain. In interface 1, the main interactions are between the cap domains, with three electrostatic interactions, two of these are also observed in HlgAB, although at somewhat different positions. In interface 2, there are four electrostatic interactions, one between the cap domains and three between the rim domains. The amino acids involved in the latter three interactions are very well conserved among the known LukGH variants, but not in the other S- and F-components (Fig. 5c). Mutagenesis studies affecting the salt bridges in the two interfaces showed that both interfaces are critical for activity, and indicated that interface 2 is involved in dimer formation, while interface 1 is responsible for oligomerization (Badarau et al. 2015).

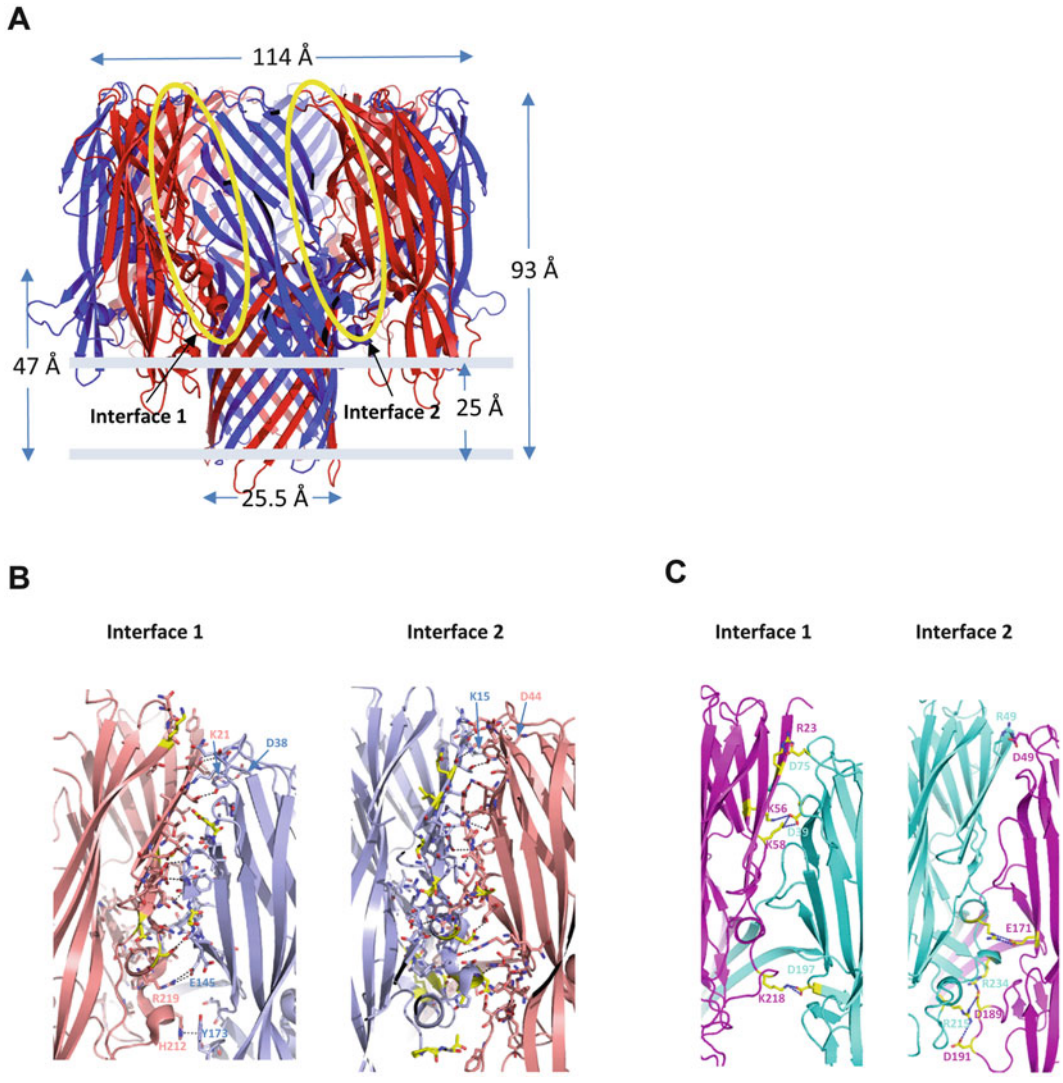

Fig. 5 Oligomer structures. (**a**) Structure of HlgAB (PDB code 3B07) octamer with HlgA in *blue* and HlgB in *red*. (**b**) The two interfaces in the HlgAB octamer (HlgA – slate, HlgB – salmon) with contact residues shown as *sticks* and electrostatic/polar interactions as *dotted lines*. The contact residues that are divergent in the other S- (HlgC, LukS, LukE) and F- (LukD, LukF) components are colored *yellow*. (**c**) The two interfaces in the LukGH octamer (PDB code 4TW1, LukG – *magenta*; LukH – *cyan*) with residues involved in electrostatic interactions shown as *sticks* and interactions marked with *dotted lines*; the residues that are divergent in all other S- and F-components are shown in *yellow*

However, crystallization of HlgCB, under similar conditions, yielded an octamer with a partly formed β-barrel transmembrane region (Yamashita et al. 2014), where the extracellular domain and the upper part of the β-barrel pore is very similar to the pore structure observed previously, while the bottom part of the stem domains corresponding to residues G120-G135 in HlgB and G143-G158 in HlgC is completely invisible in the electron density map. The same was observed with an HlgAB mutant, where W177 and R198 (two PC-binding residues) in HlgB were mutated to A; with the mutant losing both its cell binding and hemolytic activity. The authors propose that these structures correspond to pre-pore states of the toxin and postulate a

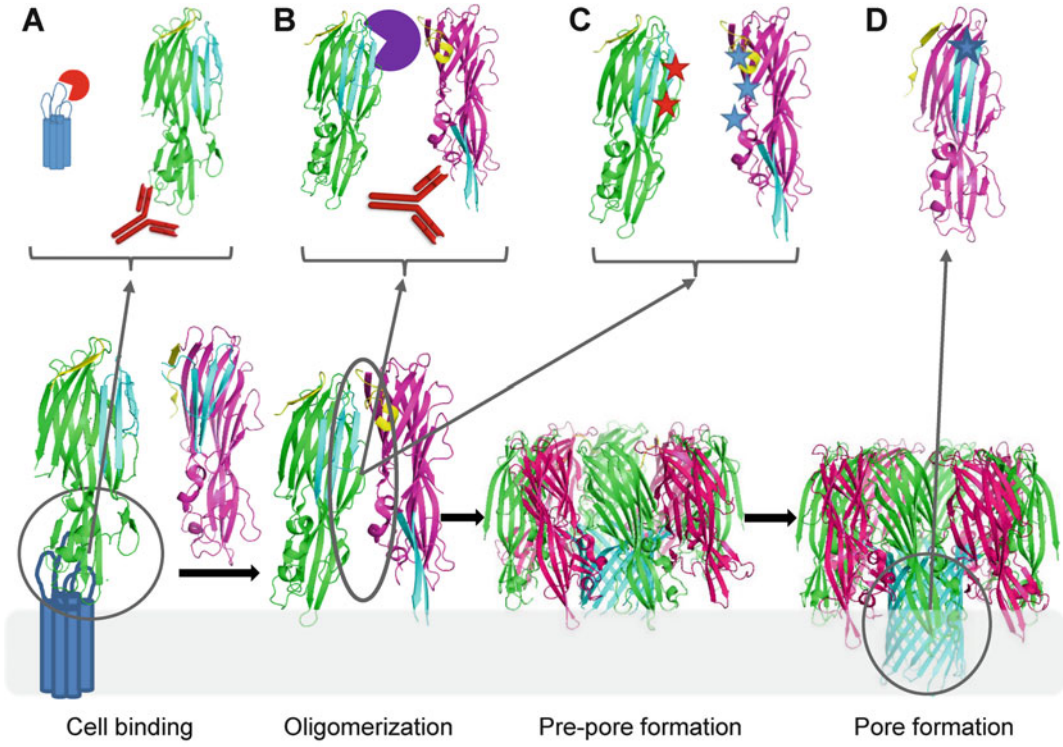

Fig. 6 Model of the proposed mechanism of pore formation and ways of intervention with novel therapeutics. S-component (LukE) is shown is *green* and F-component (LukD) in *pink* with stem domain shown in *cyan* and amino latch in *yellow*. *Lower panel*: mechanism of pore formation showing consecutive binding of the soluble monomers to the cell surface, S-component followed by F-component; dimerization of the monomers and release of the amino latch and extension of the stem from one of the monomers due to attack by amino latch; formation of the octameric pre-pore; insertion of fully formed pore with β-barrel into the membrane. *Upper panel*: toxin binding can be inhibited either by antibodies targeting the component directly interacting with the receptor or by small molecules/peptides targeting the receptor (**a**). Oligomerization can be disrupted either by antibodies or small molecules binding to the S- or F-component interface (**b**) or by engineered toxins that are unable to recruit additional toxin molecules and to form oligomers, but are maintaining binding to the receptor thus blocking the access of fully functional toxins (**c**). Pore formation can be inhibited by toxin variants that are able to bind the receptor and oligomerize, but lack a functional stem domain, and cannot form a transmembrane pore, thus trapping the receptor and the functional toxins in a pre-pore state (**d**)

mechanism of pore formation, where the β-barrel transmembrane pore is formed in two steps. The new mechanism, illustrated in Fig. 6 (lower panel), involves binding of the monomer to the cell surface, followed by dimerization, release of the amino latch, which in turn triggers the extension of the stem domain in the second monomer (which at this stage is fully unfolded). The consecutive recruitment and stem release of each of the remaining protomers, leads to the formation of the octamer pre-pore, where only the extramembrane half of the β-barrel is formed. The next step is the insertion of the transmembrane half of the β-barrel into the membrane. It is not clear what drives this final step. For HlgAB, binding to MPD (PC mimic) appears to be sufficient for pore formation, but this is not the case for HlgCB, where additional interactions with the cell membrane may be required (Yamashita et al. 2014).

A heptameric pre-pore of Hla was also recently described (Fiaschi et al. 2016). In this study, the entire stem region (T135-V175) was deleted and replaced by a short linker with the

sequence PSGS which leads to the spontaneous formation of a heptamer in solution. The heptamer obtained lacks cell binding and lytic activity against A549 cells, but induces antibodies in mice that show similar epitope coverage as those generated during *S. aureus* infection in mice or humans. This observation led to the proposal that during staphylococcal infections it is the heptamer of Hla that is mainly 'seen' by the immune system. It is not clear though whether this provides any advantage or disadvantage over induction of antibodies with the monomer used as vaccine antigen in terms of neutralization potency. It remains to be seen if the same can be concluded for the bi-component toxins.

3 Redundant and Unique Functions in Pathogenesis Determined by Structural Features

3.1 Cellular Receptors, Basis for Cell Type and Species Specificity

It is rather enigmatic why *S. aureus* employs five different bi-component toxins to evade the immune defense. The common target cells are phagocytes through the recognition of specific receptors, all playing an important role in innate immunity. LukSF-PV and HlgCB both use the complement receptors C5aR and C5L2 for cell targeting. The expression level of C5L2 is much lower than that of C5aR, which makes it likely that C5aR is the main receptor for these toxins (Laventie et al. 2014; Spaan et al. 2013, 2014b). HlgAB and LukED have three receptors, two are shared: the chemokine receptors CXCR1 and CXCR2, and in addition they bind to CCR2 and CCR5, respectively (Spaan et al. 2014b; Alonzo et al. 2013; Reyes-Robles et al. 2013). LukGH has a unique receptor, CD11b, which is the α-subunit of the complement receptor CR3 (CD11b/CD18 or Mac1) (DuMont et al. 2013).

Two bi-component leukocidins, HlgAB and LukED, are also lytic towards human RBCs that are targeted via the Duffy (DARC) receptors (Spaan et al. 2015).

Leukocidins display significant species specificity that delayed the recognition of their important roles in *S. aureus* pathogenesis. Mice, the most commonly used species for models of *S. aureus* infections, are resistant to LukSF-PV, and HlgAB, HlgCB and LukGH are very weakly cytolytic towards mouse phagocytic cells (Alonzo and Torres 2014; Löffler et al. 2010; Malachowa et al. 2012). Discovery of the identity of the cellular receptors for the five leukocidins shed light on the species and cell-type specificity. Some of the immune receptors are not expressed on mouse innate cells, and others are not sufficiently conserved to allow toxin binding. The only bi-component leukocidin with appreciable activity in mice is LukED (Alonzo et al. 2013). Since LukED and HlgAB share receptor specificity, this observation suggests that either the exact contact points between these toxins and their shared receptors are not identical or that the unique receptors (CCR2 and CCR5) are the differentiating interactions in mice (Spaan et al. 2014b). Rabbit PMNs are sensitive to the leukocidins, therefore rabbit models are much more relevant for studying of the role of the bi-component leukocidins (Malachowa et al. 2012; Diep et al. 2010, 2016).

It is widely demonstrated that the bi-component leukocidins recognize their receptors *via* the S-components. Binding affinities of the S-component toxins to their receptors are in the low nM range (Table 3). Although no structural data of complexes between the toxins and their receptors is available to date, several studies have identified residues that are important for binding (Table 3). Mutagenesis studies of LukGH identified that the 10 amino acids at the C-terminus are required for binding, and importantly substitution of a single amino acid (E323) with alanine leads to complete loss of binding and activity (DuMont et al. 2014). Alanine scanning mutagenesis of 19 residues located in the rim domain of LukS, which was previously shown to be involved in cell binding, identified a cluster of five residues (R73, Y184, T244,

Table 3 Receptor and cell binding of *S. aureus* bi-component toxins

Toxin	Receptor	Kd/EBC_{50}[a] (nM)	Cell type	Toxin region involved in binding	Reference
LukGH	MAC-1	38.4 ± 26.1	PMNs	E323	DuMont et al. (2013)
LukE	CCR5	39.6 ± 0.4	Myeloid cells		Alonzo et al. (2013)
			T lymphocytes		
LukE	CXCR1		Neutrophils, Monocytes	Q182-A196	Reyes-Robles et al. (2013)
	CXCR2				
HlgC	C5aR	5.64 ± 1.53	Neutrophils, Monocytes		Spaan et al. (2014b)
HlgA	CXCR1	5.69 ± 1.94	Neutrophils, Monocytes		Spaan et al. (2014b)
	CXCR2	27.2 ± 5.54			
	CCR2	3.51 ± 0.29			
LukS	C5aR	6.2 ± 5.1 (2.8 ± 1.2)	Neutrophils	R73, Y184, T244, H245, Y250	Laventie et al. (2014) and Spaan et al. (2013)
	C5L2	15.2 ± 6.2	Monocytes		
HlgA	DARC	29.2 ± 7.0	Human erythrocytes		Spaan et al. (2015)
HlgC	DARC	229 ± 61.9	Human erythrocytes		
LukE	DARC	56.4 ± 3.6	Human erythrocytes		
LukF	direct binding	6.2 ± 1.9	PMNs		Meyer et al. (2009)
		2.8 ± 0.8	Monocytes		
		1.2 ± 0.2	Lymphocytes		
	LukS on the membrane	10.7 ± 5.0	PMNs		
		ND	Monocytes		
		NB	Lymphocytes		
HlgB	HlgC on the membrane	0.37 ± 0.11	PMNs		
		0.11 ± 0.02	Monocytes		
		3.6 ± 1.0	Lymphocytes		
HlgB	LukS on the membrane	1.1 ± 0.2	PMNs		
		0.84 ± 0.31	Monocytes		
		NB	Lymphocytes		
HlgB	LukS on the membrane	3.4 ± 1.3	PMNs (competition w/LukF)		
LukD	LukS on the membrane	17.5 ± 1.0	PMNs (competition w/LukF)		

ND not determined, *NB* no binding
[a]EBC_{50}: half maximal effective binding concentration

H245, Y250) that are important for binding of the toxin to the C5a receptor and for biological activity (Laventie et al. 2014). Another study involving loop mutagenesis of LukE, by making LukE chimeras with various LukS loops, has mapped the CXCR1 and CXCR2 binding site on LukE to residues Q182-A196 (Reyes-Robles et al. 2013). Less is known, however, about the regions of the receptors that are involved in toxin binding. A recent study by Spaan *et al*. has shown that even toxins that target the same receptor (C5aR), i.e. LukSF and HlgCB, can have different species specificities (Spaan et al. 2014c). This observation has been nicely rationalized by constructing receptor loop chimeras of different species, revealing that different extracellular loops on the receptor are involved in binding to the different toxins. More importantly, it has been shown

that binding of the S-component to the receptor itself is not sufficient to allow pore formation, and it has been suggested that the receptors may also play roles in oligomerization and pore formation (Spaan et al. 2014c).

Before the identification of the proteinaceous receptors, there was a notion that the F-components were binding to the cells by targeting the lipid membrane via the phosphatidylcholine head-group (Potrich et al. 2009). Their weak affinity for PC was in agreement with the low binding affinity of the F-components to leukocytes in the absence of the S-components, but binding with nM affinities when the respective S-component was already bound to the cells (Table 3). Nevertheless, there are exceptions, e.g. the low level of tight binding of an F-component (LukF) to the surface of PMNs in the absence of an S-component (Meyer et al. 2009) (Table 3). The binding of HlgAB to red blood cells appears to occur differently: HlgB binds with higher affinity than HlgA, and subsequently recruits the S-component (Nguyen et al. 2003; Yokota and Kamio 2000). Removal of the PC binding site from HlgB, does not affect binding or oligomerization with HlgA on human red blood cells, but prevents formation of functional pores (Monma et al. 2004). This observation was subsequently supported by structural data (Yamashita et al. 2014). Recent data show that both LukED and HlgAB target human erythrocytes by direct binding of the S-component to the Duffy antigen receptor (DARC) present on red blood cells; and lack of activity of HlgCB correlates with lower affinity of HlgC for DARC (Table 3) (Spaan et al. 2015). It thus appears that both protein receptors and lipid head-groups are involved by the bi-component toxins on both leukocytes and erythrocytes for lytic activity.

3.2 Non-cognate Pairing: Theoretical or Physiological?

The high sequence and structural homology between gamma-hemolysins, LukED and LukSF-PV results in functional homology. The individual S- and F-components are interchangeable and able to form functional toxins. This was demonstrated by non-cognate pairing of recombinantly expressed monomers (e.g. HlgA-LukD, LukS-HlgB, etc) and detecting lytic effects towards human PMNs and RBCs (Adhikari et al. 2015; own unpublished data Rouha et al.). In addition, by using model membranes, it has been postulated that leukotoxins/gamma-hemolysin not only form equimolar pores, but also mixed pores (e.g. pores containing both S-components HlgA and HlgC), which raises the possibility that one leukocyte receptor may not be indispensable (Dalla Serra et al. 2005). LukG and LukH do not pair with any of the other S- or F-components (Badarau et al. 2015; Adhikari et al. 2015). Even if they did *in vitro*, it would not be physiologically relevant as LukG and LukH form a heterodimer, most likely immediately upon secretion by *S. aureus* since LukG and LukH co-purify from *S. aureus* culture supernatants. Whether the other S- and F-components form pairs during *S. aureus* infection is unknown. It was reported that LukSF-PV and LukED competed with each other by forming inactive non-cognate pairs when tested in assay systems where one of the two was not active (mouse PMNs, RBCs or differentiated HL-60 cells) (Yoong and Torres 2015). However, both toxins are highly potent towards human PMNs, therefore the biologic relevance of this observation is unclear.

4 Applications for Drug Development

4.1 Immune Approaches

S. aureus is an extracellular Gram positive pathogen, therefore antibodies and phagocytic cells are expected to be the main effectors of immune protection. It is paradoxical that in spite of frequent exposure to *Staphylococcus aureus*, protective immunity does not seem to develop in most humans, and many individuals experience repeated infections. This is not due to lack of

humoral response to *S. aureus* as significant fraction of serum antibodies of adults specifically react with *S. aureus* components (surface proteins, LTA, peptidoglycan). These are potential sources of opsonizing antibodies that could contribute to bacterial killing (Dryla et al. 2005). Indeed, active or passive immunization approaches, aiming to increase the levels of opsonophagocytic antibodies targeting surface antigens, all failed to show clinical efficacy.

As phagocytic cells, especially neutrophil granulocytes are the cornerstones of immune defense against extracellular bacterial pathogens, it is plausible that *S. aureus* evolved multiple mechanisms to counteract phagocytes. The most direct mechanism *S. aureus* employs is the killing of neutrophils, monocytes and macrophages by secreted toxins. The fact that *S. aureus* is capable of producing up to five potent leukocidins underlines the importance of this immune evasion mechanism. Species specificity of the leukocidins delayed the recognition of their important roles in disease pathogenesis, and it is only recently that *S. aureus* pathogenesis is considered to be driven by toxins. Ongoing clinical trials with *S. aureus* vaccines and monoclonal antibodies increasingly target toxins aiming at neutralization of toxin function. Alpha-hemolysin is known as an important virulence factor from animal models (Berube and Bubeck Wardenburg 2013), and the contribution of LukSF-PV is suggested by human epidemiological studies (increased gene prevalence in isolates causing severe pneumonia and skin infections) (Vandenesch et al. 2012). In experimental vaccines, mutated Hla (toxoid) is used, and several programs target Hla with human monoclonal antibodies for passive immunization (Rouha et al. 2015; Hua et al. 2014; Rudolf et al. 2011). LukS-PV is also considered as vaccine antigen in a combination vaccine with genetically detoxified Hla (https://clinicaltrials.gov/ct2/show/NCT01011335). Since LukS-PV is not toxic without the F-component, no mutations need to be introduced (Fig. 6a). Another vaccine approach uses both LukS and LukF subunits to broaden toxin neutralization; in this case detoxification was done by mutating amino acid residues in the inter-protomer interface to prevent oligomerization (Fig. 6a, b) (Karauzum et al. 2013).

Based on their high potency, targeting the other leukocidins that are expressed by all (gamma-hemolysins and LukGH) or the majority of *S. aureus* clinical isolates (LukED) seems to be important to avoid phagocyte killing. Due to the sequence homology among S- components (except LukH), a certain level of cross-reactive antibody response would be expected from the LukS vaccine antigen. However, there is no experimental evidence for sufficient cross-neutralization yet. Targeting all six *S. aureus* pore forming toxins individually is very challenging (if not impossible) for vaccine and antibody developers due to manufacturing and clinical development complexity and high costs. To address these challenges, our laboratory discovered a unique human monoclonal antibody with high affinity binding to Hla and three F-components (HlgB, LukF, LukD) of leukocidins resulting in potent inhibition of lysis of human cells by Hla, HlgAB, HlgCB, LukSF and LukED (Fig. 6a, b) (Rouha et al. 2015). The high affinity binding to these four toxins was very surprising as Hla shares only ~25% amino acid sequence homology with the three F-components. The antibody discovery strategy benefited from the knowledge of their structural homology and localization of conserved amino acid residues on the surface of the toxins that is a requirement for binding of cross-reactive antibodies. X-ray crystal structure analysis identified the non-linear binding epitope that encompasses the phosphocholine-binding pocket present in Hla and the three F-components (Nagy et al. 2013). Interestingly, a Hla-specific mAb (MEDI4893) that binds to the same region in Hla as the cross-reactive mAb, does not interact with any of the F-components, although based on the structural data available, the epitope overlap between the two mAbs is ~70% (Oganesyan et al. 2014; Rouha et al. 2015; Nagy et al. 2013). Since this region of the toxins is essential for pore formation, it is highly conserved and no sequence variation is observed among sequences derived

from ~7000 *S. aureus* genomes publically available. The 5th leukocidin, LukGH that seems to be the dominant leukocidin towards human phagocytes, does not contain the PC-binding pocket. Moreover, the mAb screening strategy using the toxin monomers LukG and LukH was unsuccessful, and discovering the heterodimeric complex formation in solution before target cell binding was crucial to generate LukGH neutralizing mAbs (Badarau et al. 2016). Although LukGH exists in numerous sequence variants, it was possible to identify mAbs binding and neutralizing even the most divergent LukGH forms (Badarau et al. 2016).

4.2 Inhibitors

Small molecule inhibitors that act directly by binding to the toxins, have been described for beta-barrel pore forming toxins from other organisms (Lewis et al. 2010; Wu and Guo 2010). For example, β-sitosterol, a steroid alcohol derived from plants, was able to inhibit the cytolytic activity of pneumolysin, the cholesterol dependent cytolysin of *Streptococcus pneumoniae*, and provided protection in mice models of infection (Li et al. 2015). A number of small molecule, natural compounds, were reported with inhibitory effect on Hla, and shown to interfere with Hla oligomerization (Fig. 6b). Oroxylin A (Dong et al. 2013) and baicalin (Qiu et al. 2012) show protection against Hla mediated lysis of A549 cells *in vitro* and the latter also *in vivo*, against *S. aureus* pneumonia.

More recently, following discovery of the C5aRs as LukSF-PV and HlgCB receptors, it was shown that specific C5aR1 antagonists, including CHIPS (chemotaxis inhibitory protein of *S. aureus*), C5a-mimetic peptides and two small molecule organic compounds are able to inhibit LukSF-PV, but not HlgCB, mediated pore formation (Fig. 6a) (Tawk et al. 2015). Interestingly the small molecule organic compounds were able to enhance HlgCB activity, providing further evidence that each toxin interacts differently with C5aR1 (Spaan et al. 2014c; Tawk et al. 2015).

An early report has also identified human serum vitronectin, and its fragments, as being able to specifically bind and inhibit both LukS and HlgA in red blood cell and PMN lysis, *via* formation of large molecular weight complexes (Katsumi et al. 1999).

Other approaches are based on inactive toxin variants. We have recently described LukGH variants with impaired oligomerization, obtained by replacing the residues involved in inter-monomer salt bridges with alanine (Fig. 6c) (Badarau et al. 2015); these mutants are able to bind the receptor on target cells and thus inhibit the cytolytic activity of the wild-type LukGH. Another approach of inhibiting the bi-component leukocidins, described in a recent study (Reyes-Robles et al. 2016), takes advantage of the current understanding of the mechanism of pore formation and the ability of the toxins to form cognate and non-cognate pores. Glycine rich domains in the stem region of the toxins, identified as important for toxin cytolytic activity, were deleted, and the deletion mutants were inactive, presumably due to their inability to assemble the transmembrane pore. However, the deletion mutants maintained their binding to the cellular receptors and formed oligomers with the wild-type toxins, and therefore were able to trap the active toxins in inactive pre-pore complexes (Fig. 6d). This dominant-negative approach was demonstrated both in cell based cytolytic assays and in *in vivo* models of infection (Reyes-Robles et al. 2016).

5 Concluding Remarks

Developing novel therapeutics based on empirical approaches is inefficient and less fruitful than rational design supported by structure-function analyses. The *S. aureus* pore forming toxins are particularly good examples of how knowledge accumulated during decades of research can lead to novel therapeutic approaches.

To date, active and passive immunization efforts have not been successful in human trials of *S. aureus* infections. Targeting the bi-component cytotoxins of *S. aureus* to tame

virulence and reduce pathology is a recently developed idea. There are several important aspects in this field that could be addressed using our understanding of how these toxins work at the molecular level. One of these is related to the species specificity displayed by the *S. aureus* leukocidins. Numerous experiments aimed at understanding the role of the bi-component *S. aureus* toxins have been performed in *in vivo* models where one or several of them are inactive or have very low potency (e.g. mice, rats, monkeys for LukSF-PV contribution). When animal models are not applicable, *in vitro* assays with human cells are a good alternative. However, several important aspects of the infectious disease process cannot be recapitulated without the whole organism. To understand the contribution of these toxins to human-relevant *S. aureus* diseases and predict clinical usefulness of human therapeutics, it is essential to use appropriate animal models of efficacy. Rabbits are susceptible to all leukocidins (although not with the same potencies), therefore represent a much more relevant animal model than mice to study the role of these toxins (Malachowa et al. 2012; Diep et al. 2010, 2016). Based on the vast amount of structure-function data, it is conceivable that human specific toxins can be adapted to other hosts (e.g. "murinized") if the lack of toxicity is not due to the lack of receptor expression but due to amino acid alterations at the receptor-toxin interaction site; this is the case for example for LukGH that seems to be a dominant leukocidin towards human phagocytes, but a significantly less potent toxin in animals. Its receptor, CD11b is up to 80% conserved in mice, rats and rabbits, but this is not sufficient to preserve the binding affinity required for toxin potency.

Another relevant area is blocking the bi-component toxins in a broad way that is essential to avoid the need for high complexity products. The broadly cross-reactive and cross-neutralizing human monoclonal antibody that inactivates five of the six cytolysins reported by Rouha et al. (2015) is one example of such an approach, and has already reached clinical phase testing. Passive immunization is adequate for a certain patient population (prevention of severe *S. aureus* infections in high-risk individuals or therapy in patients suffering from severe infections), but active immunization with vaccines have a broader application. Rational design of vaccine antigens based on common sequence and structural features of the cytotoxins is a reasonable approach. The discovery of novel vaccine antigens either based on mimotopes that mimic the binding epitope of antibodies with proven cross-neutralization activity or based on an artificial cytotoxin that is designed to contain the most common sequence elements, are challenging but viable options.

Other types of pluri- or omnipotent inhibitors of the cytotoxins is also a valid approach to attenuate *S. aureus* diseases. It is likely that such inhibitors would be small molecules (peptides or chemicals) and not inactive cytotoxin components, due to their high immunogenicity and expected quick inactivation by neutralizing antibodies.

Acknowledgements We thank Christine Power for the critical reading of the manuscript.

Conflict of Interest The authors declare potential conflict of interest being employees of the biotechnology company involved in this research work.

References

Adhikari RP, Kort T, Shulenin S, Kanipakala T, Ganjbaksh N, Roghmann MC, Holtsberg FW, Aman MJ (2015) Antibodies to *S. aureus* LukS-PV attenuated subunit vaccine neutralize a broad spectrum of canonical and non-canonical bicomponent leukotoxin pairs. PLoS One 10:e0137874

Alonzo F 3rd, Torres VJ (2014) The bicomponent pore-forming leucocidins of *Staphylococcus aureus*. Microbiol Mol Biol Rev 78:199–230

Alonzo F 3rd, Kozhaya L, Rawlings SA, Reyes-Robles T, DuMont AL, Myszka DG, Landau NR, Unutmaz D, Torres VJ (2013) CCR5 is a receptor for *Staphylococcus aureus* leukotoxin ED. Nature 493:51–55

Badarau A, Rouha H, Malafa S, Logan DT, Håkansson M, Stulik L, Dolezilkova I, Teubenbacher A, Gross K, Maierhofer B, Weber S, Jägerhofer M, Hoffman D, Nagy E (2015) Structure-function analysis of

heterodimer formation, oligomerization, and receptor binding of the *Staphylococcus aureus* bi-component toxin LukGH. J Biol Chem 290:142–156

Badarau A, Rouha H, Malafa S, Battles MB, Walker L, Nielson N, Dolezilkova I, Teubenbacher A, Banerjee S, Maierhofer B, Weber S, Stulik L, Logan DT, Welin M, Mirkina I, Pleban C, Zauner G, Gross K, Jägerhofer M, Magyarics Z, Nagy E (2016) Context matters: the importance of dimerization-induced conformation of the LukGH leukocidin of *Staphylococcus aureus* for the generation of neutralizing antibodies. MAbs 8:1347–1360

Berube BJ, Bubeck Wardenburg J (2013) *Staphylococcus aureus* α-toxin: nearly a century of intrigue. Toxins (Basel) 5:1140–1166

Dal Peraro M, van der Goot FG (2016) Pore-forming toxins: ancient, but never really out of fashion. Nat Rev Microbiol 14:77–92

Dalla Serra M, Coraiola M, Viero G, Comai M, Potrich C, Ferreras M, Baba-Moussa L, Colin DA, Menestrina G, Bhakdi S, Prévost G (2005) *Staphylococcus aureus* bicomponent gamma-hemolysins, HlgA, HlgB, and HlgC, can form mixed pores containing all components. J Chem Inf Model 45:1539–1545

Diep BA, Chan L, Tattevin P, Kajikawa O, Martin TR, Basuino L, Mai TT, Marbach H, Braughton KR, Whitney AR, Gardner DJ, Fan X, Tseng CW, Liu GY, Badiou C, Etienne J, Lina G, Matthay MA, DeLeo FR, Chambers HF (2010) Polymorphonuclear leukocytes mediate *Staphylococcus aureus* Panton-Valentine leukocidin-induced lung inflammation and injury. Proc Natl Acad Sci U S A 107:5587–5592

Diep BA, Le VTM, Visram ZC, Rouha H, Stulik L, Dip EC, Nagy G, Nagy E (2016) Improved protection in a rabbit model of CA-MRSA necrotizing pneumonia upon neutralization of leukocidins in addition to alpha-hemolysin. Antimicrob Agents Chemother 60:6333–6340

Dong J, Qiu J, Zhang Y, Lu C, Dai X, Wang J, Li H, Wang X, Tan W, Luo M, Niu X, Deng X (2013) Oroxylin A Inhibits hemolysis via hindering the self-assembly of α-hemolysin heptameric transmembrane pore. In: Livesay DR (ed) PLoS Comput Biol 9: e1002869

Dryla A, Prustomersky S, Gelbmann D, Hanner M, Bettinger E, Kocsis B, Kustos T, Henics T, Meinke A, Nagy E (2005) Comparison of antibody repertoires against *Staphylococcus aureus* in healthy individuals and in acutely infected patients. Clin Diagn Lab Immunol 12:387–398

DuMont AL, Yoong P, Day CJ, Alonzo F 3rd, McDonald WH, Jennings MP, Torres VJ (2013) *Staphylococcus aureus* LukAB cytotoxin kills human neutrophils by targeting the CD11b subunit of the integrin Mac-1. Proc Natl Acad Sci U S A 110:10794–10799

DuMont AL, Yoong P, Liu X, Day CJ, Chumbler NM, James DBA, Alonzo F, Bode NJ, Lacy DB, Jennings MP, Torres VJ (2014) Identification of a crucial residue required for *Staphylococcus aureus* LukAB cytotoxicity and receptor recognition. Infect Immun 82:1268–1276

Fiaschi L, Di Paolo B, Scarselli M, Pozzi C, Tomaszewski K, Galletti B, Nardi-Dei V, Arcidiacono L, Mishra RP, Mori E, Pallaoro M, Falugi F, Torre A, Fontana MR, Soriani M, Bubeck Wardenburg J, Grandi G, Rappuoli R, Ferlenghi I, Bagnoli F (2016) Auto-assembling detoxified *Staphylococcus aureus* alpha-hemolysin mimicking the wild-type cytolytic toxin. In: Burns DL (ed) Clin Vaccine Immunol 23:442–450

Foletti D, Strop P, Shaughnessy L, Hasa-Moreno A, Casas MG, Russell M, Bee C, Wu S, Pham A, Zeng Z, Pons J, Rajpal A, Shelton D (2013) Mechanism of action and in vivo efficacy of a human-derived antibody against *Staphylococcus aureus* α-hemolysin. J Mol Biol 425:1641–1654

Gillet Y, Issartel B, Vanhems P, Fournet JC, Lina G, Bes M, Vandenesch F, Piémont Y, Brousse N, Floret D, Etienne J (2002) Association between *Staphylococcus aureus* strains carrying gene for Panton-Valentine leukocidin and highly lethal necrotising pneumonia in young immunocompetent patients. Lancet 359:753–759

Gravet A, Colin DA, Keller D, Giradot R, Monteil H, Prèvost G (1998) Characterization of a novel structural member, LukE-LukD, of the bi-component staphylococcal leucotoxins family. FEBS Lett 436:202–208

Guillet V, Roblin P, Werner S, Coraiola M, Menestrina G, Monteil H, Prévost G, Mourey L (2004) Crystal structure of leucotoxin S component: new insight into the Staphylococcal beta-barrel pore-forming toxins. J Biol Chem 279:41028–41037

Hua L, Hilliard JJ, Shi Y, Tkaczyk C, Cheng LI, Yu X, Datta V, Ren S, Feng H, Zinsou R, Keller A, O'Day T, Du Q, Cheng L, Damschroder M, Robbie G, Suzich J, Stover CK, Sellman BR (2014) Assessment of an anti-alpha-toxin monoclonal antibody for prevention and treatment of *Staphylococcus aureus*-induced pneumonia. Antimicrob Agents Chemother 58:1108–1117

Jayasinghe L, Bayley H (2005) The leukocidin pore: evidence for an octamer with four LukF subunits and four LukS subunits alternating around a central axis. Protein Sci 14:2550–2561

Joubert O, Viero G, Keller D, Martinez E, Colin DA, Monteil H, Mourey L, Dalla Serra M, Prévost G (2006) Engineered covalent leucotoxin heterodimers form functional pores: insights into S–F interactions. Biochem J 396:381–389

Kaneko J, Kamio Y (2004) Bacterial two-component and hetero-heptameric pore-forming cytolytic toxins: structures, pore-forming mechanism, and organization of the genes. Biosci Biotechnol Biochem 68:981–1003

Karauzum H, Adhikari RP, Sarwar J, Devi VS, Abaandou L, Haudenschild C, Mahmoudieh M, Boroun AR, Vu H, Nguyen T, Warfield KL, Shulenin S, Aman MJ (2013) Structurally designed attenuated subunit vaccines for *S. aureus* LukS-PV

and LukF-PV confer protection in a mouse bacteremia model. PLoS One 8:e65384

Katsumi H, Tomita T, Kaneko J, Kamio Y (1999) Vitronectin and its fragments purified as serum inhibitors of *Staphylococcus aureus* gamma-hemolysin and leukocidin, and their specific binding to the hlg2 and the LukS components of the toxins. FEBS Lett 460:451–456

Kuehnert MJ, Kruszon-Moran D, Hill HA, McQuillan G, McAllister SK, Fosheim G, McDougal LK, Chaitram J, Jensen B, Fridkin SK, Killgore G, Tenover FC (2006) Prevalence of *Staphylococcus aureus* nasal colonization in the United States, 2001–2002. J Infect Dis 193:172–179

Kuroda M, Ohta T, Uchiyama I, Baba T, Yuzawa H, Kobayashi I, Cui L, Oguchi A, Aoki K, Nagai Y, Lian J, Ito T, Kanamori M, Matsumaru H, Maruyama A, Murakami H, Hosoyama A, Mizutani-Ui Y, Takahashi NK, Sawano T, Inoue R, Kaito C, Sekimizu K, Hirakawa H, Kuhara S, Goto S, Yabuzaki J, Kanehisa M, Yamashita A, Oshima K, Furuya K, Yoshino C, Shiba T, Hattori M, Ogasawara N, Hayashi H, Hiramatsu K (2001) Whole genome sequencing of meticillin-resistant *Staphylococcus aureus*. Lancet 357:1225–1240

Laventie BJ, Guérin F, Mourey L, Tawk MY, Jover E, Maveyraud L, Prévost G (2014) Residues essential for Panton-Valentine leukocidin S component binding to its cell receptor suggest both plasticity and adaptability in its interaction surface. In: Diep BA (ed) PLoS ONE 9:e92094

Lewis M, Weaver CD, McClain MS (2010) Identification of small molecule inhibitors of *Clostridium perfringens* ε-toxin cytotoxicity using a cell-based high-throughput screen. Toxins (Basel) 2:1825–1847

Li H, Zhao X, Wang J, Dong Y, Meng S, Li R, Niu X, Deng X (2015) β-sitosterol interacts with pneumolysin to prevent *Streptococcus pneumoniae* infection. Sci Rep 5:17668

Lina G, Piémont Y, Godail-Gamot F, Bes M, Peter MO, Gauduchon V, Vandenesch F, Etienne J (1999) Involvement of Panton-Valentine leukocidin-producing *Staphylococcus aureus* in primary skin infections and pneumonia. Clin Infect Dis 29:1128–1132

Löffler B, Hussain M, Grundmeier M, Brück M, Holzinger D, Varga G, Roth J, Kahl BC, Proctor RA, Peters G (2010) *Staphylococcus aureus* Panton-Valentine leukocidin is a very potent cytotoxic factor for human neutrophils. In: Cheung A (ed) PLoS Pathog 6:e1000715

Malachowa N, Kobayashi SD, Braughton KR, Whitney AR, Parnell MJ, Gardner DJ, Deleo FR (2012) *Staphylococcus aureus* leukotoxin GH promotes inflammation. J Infect Dis 206:1185–1193

Menestrina G (1986) Ionic channels formed by *Staphylococcus aureus* alpha-toxin: voltage-dependent inhibition by divalent and trivalent cations. J Membr Biol 90:177–190

Meyer F, Girardot R, Piemont Y, Prevost G, Colin DA (2009) Analysis of the specificity of Panton-Valentine leucocidin and gamma-hemolysin F component binding. Infect Immun 77:266–273

Monma N, Nguyen VT, Kaneko J, Higuchi H, Kamio Y (2004) Essential residues, W177 and R198, of LukF for phosphatidylcholine-binding and pore-formation by staphylococcal -hemolysin on human erythrocyte membranes. J Biochem 136:427–431

Morinaga N, Kaihou Y, Noda M (2003) Purification, cloning and characterization of variant luke-lukd with strong leukocidal activity of staphylococcal bi-component leukotoxin family. Microbiol Immunol 47:81–90

Nagy E, Badarau A, Rouha H, Nagy G, Mirkina I, Magyarics Z, Visram Z, Battles MB, Prinz BD, Jain TS (2013) Cross-reactive *Staphylococcus aureus* antibody. WO2013156534 A1. 24 Oct 2013

Nguyen VT, Kamio Y, Higuchi H (2003) Single-molecule imaging of cooperative assembly of γ-hemolysin on erythrocyte membranes. EMBO J 22:4968–4979

Nocadello S, Minasov G, Shuvalova L, Dubrovska I, Sabini E, Bagnoli F, Grandi G, Anderson WF (2016) Crystal structures of the components of the *Staphylococcus aureus* leukotoxin ED. Acta Cryst D Struct Biol 72:113–120

Oganesyan V, Peng L, Damschroder MM, Cheng L, Sadowska A, Tkaczyk C, Sellman BR, Wu H, Dall'Acqua WF (2014) Mechanisms of neutralization of a human anti-alpha toxin antibody. J Biol Chem 289:29874–29880

Olson R, Nariya H, Yokota K, Kamio Y, Gouaux E (1999) Crystal structure of staphylococcal LukF delineates conformational changes accompanying formation of a transmembrane channel. Nat Struct Biol 6:134–140

Pédelacq JD, Maveyraud L, Prévost G, Baba-Moussa L, González A, Courcelle E, Shepard W, Monteil H, Samama JP, Mourey L (1999) The structure of a *Staphylococcus aureus* leucocidin component (LukF-PV) reveals the fold of the water-soluble species of a family of transmembrane pore-forming toxins. Structure 7:277–287

Potrich C, Bastiani H, Colin DA, Huck S, Prévost G, Dalla Serra M (2009) The influence of membrane lipids in *Staphylococcus aureus* gamma-hemolysins pore formation. J Membr Biol 227:13–24

Qiu J, Niu X, Dong J, Wang D, Wang J, Li H, Luo M, Li S, Feng H, Deng X (2012) Baicalin protects mice from *Staphylococcus aureus* pneumonia via inhibition of the cytolytic activity of -hemolysin. J Infect Dis 206:292–301

Ramaro N, Sanchis V (2013) The pore-forming haemolysins of *Bacillus cereus*: a review. Toxins (Basel) 5:1119–1139

Reyes-Robles T, Alonzo F 3rd, Kozhaya L, Lacy DB, Unutmaz D, Torres VJ (2013) *Staphylococcus aureus* leukotoxin ED targets the chemokine receptors CXCR1 and CXCR2 to kill leukocytes and promote infection. Cell Host Microbe 14:453–459

Reyes-Robles T, Lubkin A, Alonzo F 3rd, Lacy DB, Torres VJ (2016) Exploiting dominant-negative toxins to combat *Staphylococcus aureus* pathogenesis. EMBO Rep 17:428–440

Roblin P, Guillet V, Joubert O, Keller D, Erard M, Maveyraud L, Prévost G, Mourey L (2008) A covalent S-F heterodimer of leucotoxin reveals molecular plasticity of beta-barrel pore-forming toxins. Proteins 71:485–496

Rouha H, Badarau A, Visram ZC, Battles MB, Prinz B, Magyarics Z, Nagy G, Mirkina I, Stulik L, Zerbs M, Jägerhofer M, Maierhofer B, Teubenbacher A, Dolezilkova I, Gross K, Banerjee S, Zauner G, Malafa S, Zmajkovic J, Maier S, Mabry R, Krauland E, Wittrup KD, Gerngross TU, Nagy E (2015) Five birds, one stone: neutralization of α-hemolysin and 4 bi-component leukocidins of *Staphylococcus aureus* with a single human monoclonal antibody. MAbs 7:243–254

Rudolf M, Koch H, inventors; Kenta Biotech AG, assignee (2011) Human monoclonal antibody against *Staphylococcus aureus* derived alpha-toxin and its use in treating or preventing abscess formation patent. WO2011018208. 17 Feb 2011

Song L, Hobaugh MR, Shustak C, Cheley S, Bayley H, Gouaux JE (1996) Structure of staphylococcal alpha-hemolysin, a heptameric transmembrane pore. Science 274:1859–1866

Spaan AN, Henry T, van Rooijen WJ, Perret M, Badiou C, Aerts PC, Kemmink J, de Haas CJ, van Kessel KP, Vandenesch F, Lina G, van Strijp JA (2013) The staphylococcal toxin Panton-Valentine leukocidin targets human C5a receptors. Cell Host Microbe 13:584–594

Spaan AN, Surewaard BG, Nijland R, van Strijp JA (2014a) Neutrophils versus *Staphylococcus aureus*: a biological tug of war. Annu Rev Microbiol 67:629–650

Spaan AN, Vrieling M, Wallet P, Badiou C, Reyes-Robles T, Ohneck EA, Benito Y, de Haas CJ, Day CJ, Jennings MP, Lina G, Vandenesch F, van Kessel KP, Torres VJ, van Strijp JA, Henry T (2014b) The staphylococcal toxins γ-haemolysin AB and CB differentially target phagocytes by employing specific chemokine receptors. Nat Commun 5:5438

Spaan AN, Schiepers A, de Haas CJ, van Hooijdonk DD, Badiou C, Contamin H, Vandenesch F, Lina G, Gerard NP, Gerard C, van Kessel KP, Henry T, van Strijp JA (2014c) Differential interaction of the staphylococcal toxins Panton-Valentine leukocidin and γ-hemolysin CB with human C5a receptors. J Immunol 195:1034–1043

Spaan AN, Reyes-Robles T, Badiou C, Cochet S, Boguslawski KM, Yoong P, Day CJ, de Haas CJC, van Kessel KPM, Vandenesch F, Jennings MP, Le Van Kim C, Colin Y, van Strijp JA, Henry T, Torres VJ (2015) *Staphylococcus aureus* targets the Duffy antigen receptor for chemokines (DARC) to lyse erythrocytes. Cell Host Microbe 18:363–370

Staphylococcus aureus toxoids phase 1–2 vaccine trial. https://clinicaltrials.gov/ct2/show/NCT01011335. Accessed 28 Oct 2016.

Sugawara T, Yamashita D, Kato K, Peng Z, Ueda J, Kaneko J, Kamio Y, Tanaka Y, Yao M (2015) Structural basis for pore-forming mechanism of staphylococcal alpha-hemolysin. Toxicon 108:226–231

Tanaka Y, Hirano N, Kaneko J, Kamio Y, Yao M, Tanaka I (2011) 2-Methyl-2,4-pentanediol induces spontaneous assembly of staphylococcal α-hemolysin into heptameric pore structure. Protein Sci 20:448–456

Tawk MY, Zimmermann-Meisse G, Bossu JL, Potrich C, Bourcier T, Dalla Serra M, Poulain B, Prévost G, Jover E (2015) Internalization of staphylococcal leukotoxins that bind and divert the C5a receptor is required for intracellular Ca2+ mobilization by human neutrophils. Cell Microbiol 17:1241–1257

Vandenesch F, Lina G, Henry T (2012) *Staphylococcus aureus* hemolysins, bi-component leukocidins, and cytolytic peptides: a redundant arsenal of membrane-damaging virulence factors? Front Cell Infect Microbiol 2:12

von Eiff C, Friedrich AW, Peters G, Becker K (2004) Prevalence of genes encoding for members of the staphylococcal leukotoxin family among clinical isolates of *Staphylococcus aureus*. Diagn Microbiol Infect Dis 49:157–162

Wu Q, Guo Z (2010) Glycosylphosphatidylinositols are potential targets for the development of novel inhibitors for aerolysin-type of pore-forming bacterial toxins. Med Res Rev 30:258–269

Yamashita K, Kawai Y, Tanaka Y, Hirano N, Kaneko J, Tomita N, Ohta M, Kamio Y, Yao M, Tanaka I (2011) Crystal structure of the octameric pore of staphylococcal γ-hemolysin reveals the β-barrel pore formation mechanism by two components. Proc Natl Acad Sci U S A 108:17314–17319

Yamashita D, Sugawara T, Takeshita M, Kaneko J, Kamio Y, Tanaka I, Tanaka Y, Yao M (2014) Molecular basis of transmembrane beta-barrel formation of staphylococcal pore-forming toxins. Nat Commun 5:4897

Yokota K, Kamio Y (2000) Tyrosine 72 residue at the bottom of rim domain in LukF crucial for the sequential binding of the Staphylococcal γ-Hemolysin to human erythrocytes. Biosci Biotechnol Biochem 64:2744–2747

Yoong P, Torres VJ (2015) Counter inhibition between leukotoxins attenuates *Staphylococcus aureus* virulence. Nat Commun 6:8125

Adv Exp Med Biol - Protein Reviews (2017) 2:37–54
DOI 10.1007/5584_2016_174

Published online: 14 December 2016

Membrane Fusion and Infection of the Influenza Hemagglutinin

Sean T. Smrt and Justin L. Lorieau

Abstract

The influenza virus is a major health concern associated with an estimated 5000 to 30,000 deaths every year (Reed et al. 2015) and a significant economic impact with the development of treatments, vaccinations and research (Molinari et al. 2007). The entirety of the influenza genome is comprised of only eleven coding genes. An enormous degree of variation in non-conserved regions leads to significant challenges in the development of inclusive inhibitors for treatment. The fusion peptide domain of the influenza A hemagglutinin (HA) is a promising candidate for treatment since it is one of the most highly conserved sequences in the influenza genome (Heiny et al. 2007), and it is vital to the viral life cycle. Hemagglutinin is a class I viral fusion protein that catalyzes the membrane fusion process during cellular entry and infection. Impediment of the hemagglutinin's function, either through incomplete post-translational processing (Klenk et al. 1975; Lazarowitz and Choppin 1975) or through mutations (Cross et al. 2001), leads to non-infective virus particles. This review will investigate current research on the role of hemagglutinin in the virus life cycle, its structural biology and mechanism as well as the central role of the hemagglutinin fusion peptide (HAfp) to influenza membrane fusion and infection.

Keywords

Fusion peptide • NMR • Membrane curvature • Membrane protein structure

Abbreviations

BICS	Bicelle Induced Curvature and Sorting
CD	Circular Dichroism spectroscopy

S.T. Smrt and J.L. Lorieau (✉)
Department of Chemistry, University of Illinois at Chicago, Chicago, IL 60607, USA
e-mail: justin@lorieau.com

DPC	Dodecylphosphocholine
DOPC	1,2-dioleoyl-sn-glycero-3-phosphocholine
DOPE	1,2-dioleoyl-sn-glycero-3-phosphoethanolamine
DPoPE	dipalmitoleoylphosphatidylethanolamine
DSC	Differential Scanning Calorimetry
EM	Electron Microscopy
EPR	Electron Paramagnetic Resonance
FP	Fusion Peptide
FRET	Fluorescence Resonance Energy Transfer
FTIR	Fourier Transform Infrared spectroscopy
HA	Hemagglutinin
HA0	Hemagglutinin pre-cleavage precursor
HA1	Hemagglutinin subunit 1
HA2	Hemagglutinin subunit 2
HAfp	Hemagglutinin fusion peptide domain (full-length, 23-residue form)
HAfp20	Hemagglutinin fusion peptide domain (truncated, 20-residue form)
HA-TMD	Hemagglutinin transmembrane domain
H_{II}	type II Hexagonal inverted state
MD	Molecular Dynamics simulations
NMR	Nuclear Magnetic Resonance spectroscopy
NA	Neuraminidase
NGC	Negative Gaussian Curvature
NOE	Nuclear Overhauser Effect
PI	Phosphatidylinositol
PRE	Paramagnetic Relaxation Enhancement
POPC	1-palmitoyl-2-oleoyl-sn-glycero-3-phosphocholine
POPE	1-palmitoyl-2-oleoyl-sn-glycero-3-phosphoethanolamine
POPS	1-palmitoyl-2-oleoyl-sn-glycero-3-phosphoserine
PS	Phosphatidylserine
RDC	Residual Dipolar Coupling
SM	Sphingomyelin
vRNPs	viral ribonucleoprotein complexes

The influenza virus is a major health concern associated with an estimated 5000 to 30,000 deaths every year (Reed et al. 2015) and a significant economic impact with the development of treatments, vaccinations and research (Molinari et al. 2007). The entirety of the influenza genome is comprised of only eleven coding genes. An enormous degree of variation in non-conserved regions leads to significant challenges in the development of inclusive inhibitors for treatment. The fusion peptide domain of the influenza A hemagglutinin (HA) is a promising candidate for treatment since it is one of the most highly conserved sequences in the influenza genome (Heiny et al. 2007), and it is vital to the viral life cycle. Hemagglutinin is a class I viral fusion protein that catalyzes the membrane fusion process during cellular entry and infection. Impediment of the hemagglutinin's function, either through incomplete post-translational processing (Klenk et al. 1975; Lazarowitz and Choppin 1975) or through mutations (Cross et al. 2001), leads to non-infective virus particles. This review will investigate current research on the role of hemagglutinin in the virus life cycle, its structural biology and mechanism as well as the central role of the hemagglutinin fusion peptide (HAfp) to influenza membrane fusion and infection.

Influenza is an enveloped virus with an outer membrane formed during budding and cellular egress. The envelope is composed of a different lipid composition from that of the host (Scheiffele et al. 1999), consisting largely of cholesterol, phosphatidylserine (PS) lipids and sphingolipids (Gerl et al. 2012). Domains of the apical membrane from which the virus buds share a similar lipidome distinct from the basal membrane. The viral membrane has a high density of the hemagglutinin spike glycoprotein and neuraminidase (NA), which is responsible for the release of nascent virions by cleaving the glycosidic linkage of sialic acids (Gottschalk 1957). These two proteins protrude outward and are visible by electron microscopy (Fig. 1a). Viral antigenicity is determined through variation of

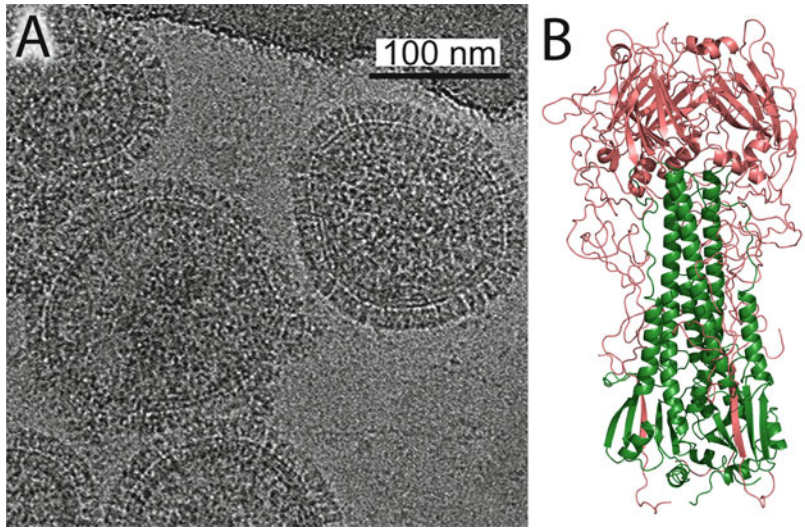

Fig. 1 (**a**) Projection image of frozen-hydrated influenza B virions generated by cryo-electron tomography and reproduced from Katz G et al. PLOS ONE (Katz et al. 2014). The HA0 and neuraminidase spikes are visible on the virion surface. (**b**) The pre-fusion hemagglutinin spike glycoprotein (HA0) homotrimer structure (PDB:2HMG). The HA1 (*pink*) and HA2 (*green*) subunits are indicated

HA, NA and their receptor-binding partners. Viral subtypes are commonly abbreviated for clinical distinction and are associated to species-specific infectivity (e.g. H1N1). Despite extensive variation in the hemagglutinin's primary sequence, it maintains a similar overall structure across influenza serotypes (Munster et al. 2007).

Influenza infection is initiated through endocytosis by the host cell (Marsh 1984). Surface adhesion is achieved by cellular receptor binding of hemagglutinin to sialoglycan. Endocytosis is typically facilitated by clathrin-dependent pathways, although some studies indicate that clathrin is not strictly a requirement (Sieczkarski and Whittaker 2002). Recent research suggests that initiation of endocytosis is not automatic, but it may be mediated by variable signaling pathways (Eierhoff et al. 2010). The viral particle is then transported to an endosome, where it is temporarily segregated from the cytosolic environment. This process can be visualized by electron microscopy (Matlin et al. 1981; Morgan and Rose 1968). Acidification of the endosome to a pH 5.5 or lower triggers a conformational change in the hemagglutinin to its post-fusion structure, and it activates the membrane fusion process between viral and endosomal membranes, leading to entry of the virus Viral Contents into the cytosol (Yoshimura and Ohnishi 1984; Stegmann et al. 1986). Thereafter, the viral ribonucleoprotein complexes (vRNPs) are released for further processing. Viral proteins and vRNPs are synthesized by host components and shuttled to lipid raft domains at the budding site where nascent viral particles emerge by non-lytic fission (Nayak et al. 2004; Chazal and Gerlier 2003). Hemagglutinin is a trimer of a receptor binding subunit, HA1, and a fusion subunit, HA2, embedded in the viral membrane (Doms and Helenius 1986). The two subunits are produced from a proteolytic cleavage of the HA0 precursor (Klenk et al. 1975; Lazarowitz and Choppin 1975), which is fusion inactive. The HA0 structure (Fig. 1b) is 135Å long with a radius of 15–40Å (Wilson et al. 1981). Additional structures of the precursor HA0 (Chen et al. 1998) show a minimal rearrangement of the trimer upon cleavage, with the exception of the cleaved termini at the HA1/HA2 boundary.

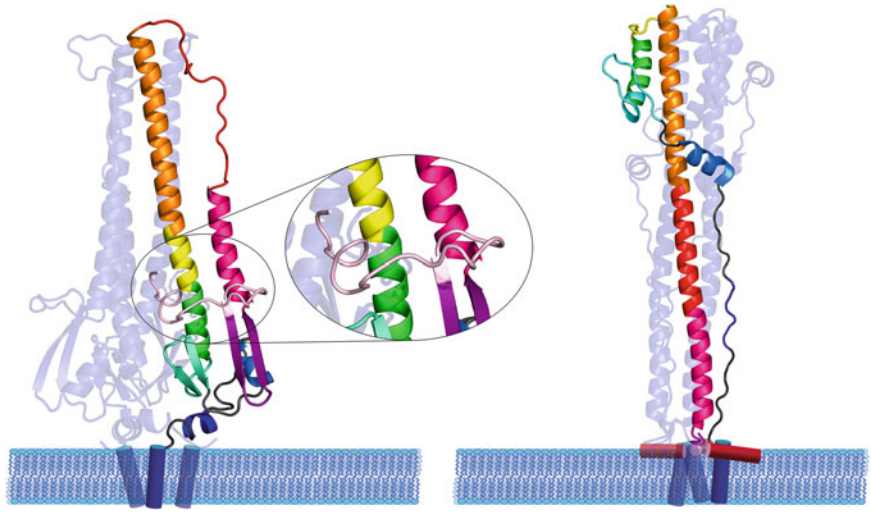

Fig. 2 The pre-fusion (*left* – PDB:2HMG) and post-fusion (*right* – PDB:1QU1) structures of cleaved HA2 trimers. A single HA2 monomer has been colored to emphasize the regions undergoing structural rearrangement upon acidification. The HAfp domain in the pre-fusion structure, before membrane integration, is unstructured and shown in *pink*. HAfp and HA-TMD were excluded from the reported post-fusion structure, and they are represented by *red* and *blue cylinders*, respectively

1 Hemagglutinin Structure

The headgroup region of the pre-fusion structure is formed by the HA1 subunit, and it consists of a mixed α/β structure and a number of unstructured loops. The pre-fusion HA2 subunit has a central α-helical stalk region (Fig. 2) that is anchored to the viral membrane by the hemagglutinin transmembrane domain (HA-TMD). Upon acidification of the endosome, HA2 undergoes a 'spring-loaded' (Carr et al. 1997) conformational change. The 'spring-loaded' conformational change is believed to facilitate the joining of viral and endosomal membranes, yet recent evidence suggests that the final post-fusion conformation is sufficient to catalyze membrane fusion (Sup Kim et al. 2011). The sequence of events in membrane fusion remains unclear, but it is known that the highly hydrophobic 23–28 N-terminal residues of the HA2 subunit, the HAfp domain, is embedded in the endosomal membrane of the host (Weber et al. 1994). In the final post-fusion state, the HAfp domain and the endosomal membrane are brought together with the HA-TMD and the viral membrane to form a fusion pore (Fig. 2). During the "spring-loaded" transition, the HA1 subunits remain covalently linked through disulfide bridges to the HA2 subunits (Wilson et al. 1981).

Upon HA0 cleavage, the HAfp domain buries in an internal pocket within the trimer (Chen et al. 1998). This relocation displaces solvent molecules in the cavity formed by ionizable residues. More recent attention has been placed on the residues lining the pocket, which are primarily conserved through all subtypes. Mutational variations in these residues have been classified into two distinct groups depending on their sequence (Russell et al. 2004; Thoennes et al. 2008). Based on mutational data, there is evidence that these residues stabilize the cleaved N-terminus and prime the system for fusion, having the effect of modulating the pH of membrane fusion.

It was recognized early on that the HAfp domain plays a central role to the hemagglutinin mechanism. It is highly sensitive to mutation such that even conservative mutations in this sequence abolish fusion activity (Cross et al. 2009). Radiolabeling experiments of hemagglutinin in small unilamellar liposomes derived

from egg lecithin demonstrated a clear interaction between the HAfp domain and vesicles (Harter et al. 1989; Brunner 1989). Early proposals postulated that this domain was simply a hydrophobic anchor for the hemagglutinin to the endosomal membrane (Ruigrok et al. 1986). Later research, however, showed that peptides synthesized from this sequence were themselves fusiogenic (Wharton et al. 1988; Lear and DeGrado 1987).

1.1 Fusion Domain

1.1.1 Structure

The purification and characterization of highly hydrophobic HAfp peptides proved difficult due to aggregation and precipitation in aqueous solution. Lear and DeGrado first investigated the synthesis of peptides with the minimum number of residues needed to replicate the HAfp domain from the HA2 N-terminus (Lear and DeGrado 1987). They found that a minimum of 20 residues (HAfp20) was needed to recover lipid-mixing fusion activity. In the following year, the Wiley group reported that a full-length HAfp sequence that extended an additional 3 conserved hydrophobic residues was significantly more fusiogenic than the truncated HAfp20 (Wharton et al. 1988; Ghosh et al. 2015). Later studies nevertheless focused on the structural biology and membrane activity of the truncated HAfp20.

Early purification techniques that included a solubilizing tail in the synthesis proved useful with HAfp20 (Smith et al. 1984; Stempfer et al. 1996). This strategy was utilized by the Tamm group with a poly-lysine host-guest tail to purify the HAfp20 peptide (Han and Tamm 2000). Using this strategy, they presented the first solution state NMR structure of HAfp20 (H3 subtype) (Han et al. 2001). The NMR experiments were conducted on a natural abundance peptide, and they utilized ^{1}H-^{1}H nuclear Overhauser effect (NOEs) distance constraints to solve the structure. The structures at pH 7.4 (PDB: 1IBN) and at pH 5 (PDB: 1IBO) were solved in dodecylphosphocholine (DPC) micelles (Fig. 3a). The high pH structure consisted of an N-terminal α-helix and a disordered C-terminal tail, which partially reconfigured to a 3_{10}-helix at lower pH. The structure determination was complemented with spin-labeled electron paramagnetic resonance (EPR) measurements to determine the insertion depth of the peptide in the membrane. The structure was reported to adopt an inverted 'V' shape, referred to as the boomerang. The fixed boomerang angle was believed to correlate with the peptide's activity in disrupting membranes (Lai et al. 2006a). The experimental constraints that define the boomerang angle are unavailable for the wildtype HAfp20 structure, but they are available for the hemifusiogenic G1S mutant structure (Fig. 3b, PDB: 1XOO) (Li et al. 2005). A small number of NOE restraints define the boomerang angle, and they represent unusually long distances (5–7.5Å) between side-chain hydrogens. These NOEs are from low-intensity peaks and are subject to greater experimental error (Liu et al. 1995). The impact of molecular dynamics and spin diffusion, particularly in the sidechains, further complicates the accurate analysis of NOEs and, consequently, the accuracy of the boomerang angle in the structure. The backbone dynamics of the wildtype HAfp20 structure was only later characterized using peptides with ^{13}C and ^{15}N isotope labels (Lorieau et al. 2013), and it was found that residues 12–20 were highly flexible, unfolded and inconsistent with a single, fixed boomerang angle.

Though the truncated HAfp20 peptide was the first structure solved, the HAfp domain extends to a longer sequence (Cross et al. 2009). The three following residues, Trp21-Tyr22-Gly23, are completely conserved and highly hydrophobic, and the full-length HAfp peptide has a significantly higher fusion activity (Wharton et al. 1988; Ghosh et al. 2015). Both tyrosine and tryptophan have been shown to anchor proteins to membrane surfaces (De Planque et al. 2003; Ridder et al. 2000), and the GXXG/GXXXG motif is commonly found in interhelical interactions of membrane proteins (Yao and Hong 2014; Senes et al. 2001; Bowie 2011).

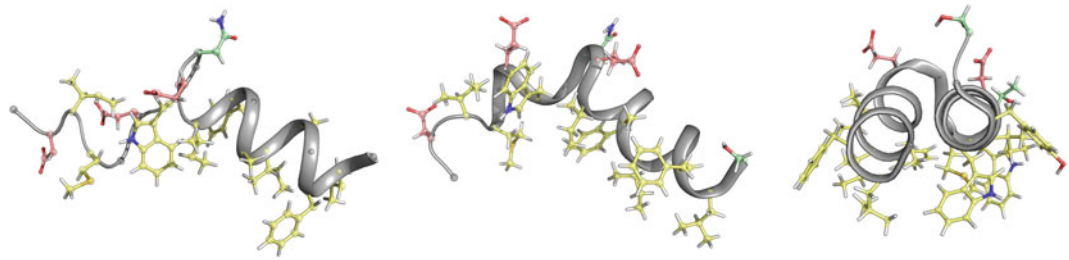

Fig. 3 NMR structures of the truncated HAfp20 for the H3 subtype at pH 7.4 (*left*, PDB: 1IBO), the HAfp20 structure at pH 5 (*middle*, PDB: 1XOO) and the full-length HAfp for the H1 subtype at pH 4 and 7 (*right*, PDB: 2KXA)

The full-length HAfp (H1 subtype) was expressed with the ^{2}H, ^{13}C and ^{15}N isotope labels needed for high-resolution NMR, and the structure was solved at pH 7.4 and 4.0 in DPC micelles using chemical shift, NOE and residual dipolar coupling (RDC) restraints (Lorieau et al. 2010). In contrast to NOEs, which contain local structural information, the RDC restraints accurately define the orientation of the α-helices in the structure (Bax and Grishaev 2005).

The full-length HAfp structure has a tight helical-hairpin structure (Fig. 3c) with a distinct fold from the truncated HAfp20. The full-length structure is highly ordered. It is stabilized by four aliphatic hydrogen bonds between the GXXG/GXXXG motifs of the two helices as well as a charge-dipole interaction between the C-terminal carbonyls and the positively charged α-amino group of Gly-1 (Lorieau et al. 2011a). The full-length helical-hairpin structure has an amphipathic profile (Worch 2013) such that the two helices lie near the plane of the membrane (Lorieau et al. 2010; Eichmann et al. 2014). Peptides that extend beyond 23 residues have the same helical-hairpin structure (Lorieau et al. 2013).

Later studies substantiated a correlation between fusion activity and the helical hairpin structure. The G8A mutation has a significantly reduced fusion activity (Han et al. 1999), and its NMR structure in micelles revealed a largely open and highly dynamic configuration (Lorieau et al. 2012). HAfp-G8A however populates the closed helical-hairpin structure with a *ca.* 15 % population, consistent with its reduced fusion activity. Likewise, the truncated HAfp20 has a reduced fusion activity, and it populates the closed helical-hairpin structure with a *ca.* 11 % population (Lorieau et al. 2013). Solid-state NMR studies confirm a conformational equilibrium between closed and semi-closed states when HAfp20 is placed in a planar membrane environment indicating that a closed/semi-closed mixture is present for both HAfp23 and the truncated HAfp20 (Ghosh et al. 2013; Sun and Weliky 2009).

At low pH, it was found that the wildtype HAfp itself transiently visits activated, open states on a microsecond timescale (Lorieau et al. 2012). Computational studies suggest that structural plasticity may be vital to fusion. It has been suggested that these transitions are coupled to membrane binding (Haria et al. 2014; Vaccaro et al. 2005). Recent experimental evidence suggests that the dynamics between closed, semi-closed and open states correlates with fusion activity (Ghosh et al. 2015). Here it was demonstrated that both HAfp20 and HAfp23 share a similar semi-closed inter-helical structure when studied in vesicles as opposed to the strict open and closed states previously seen in micelles. Since fusion assays are typically performed in vesicles, this result indicates a possible correlation between fusion activity and the overall hydrophobic surface area of HAfp conformers. Alternatively, these activated transient states may be involved in the interaction with the HA-TMD in the post-fusion structure, when these two domains are brought together during pore formation.

1.1.2 Depth and Orientation

The lipid environment plays an integral role in the functional structure of membrane proteins. The ectodomain does not directly influence membrane insertion, as it remains entirely soluble at both pH 7.4 and 5 (Harter et al. 1989; Durrer et al. 1996). This consideration further substantiated the use of water-soluble HAfp peptides as useful structural and function models for the fusion domain. The HAfp peptide with the poly-lysine tail is soluble alone in aqueous solution, and it is folded as an amphipathic helical-hairpin structure in DPC micelles. The HAfp helical-hairpin lies at the surface of DPC micelles and bicelles, as confirmed by an amphipathic hydrogen exchange rate profile and paramagnetic relaxation enhancement (PRE) measurements (Lorieau et al. 2011b). Intermolecular NOEs between the DPC detergent and the HAfp peptides also confirm a surface-lying configuration with the helical axes oriented near the plane of the membrane (Eichmann et al. 2014).

Investigations on the truncated HAfp20 support an orientation nearly parallel to the surface of a lipid layer. Ishiguro and Takahshii used FTIR to show that the HAfp20 helix aligns with a ~70° angle to the membrane director of DMPC vesicles (Ishiguro et al. 1993). Weliky et al. used solid-state NMR to measure an orientation parallel to the planar membrane in POPC:POPG lamellar membranes (Wasniewski et al. 2004). These studies were also conducted using mimetic membranes (LM3) of the host-cell with POPC, POPE, POPS, PI, SM and cholesterol. In this case, the upfield migration of the L2 and F8 ^{13}C' chemical shifts supports a reconfiguration to a β-sheet structure. This is thought to be an effect resulting from the high concentration of cholesterol (33 %) in the membrane, as seen previously (Yang et al. 2002; Zhang et al. 2003).

Acidification of HAfp20 and HAfp below the fusion active pH 5.5 appears to have no significant impact on secondary structure and orientation (Lorieau et al. 2010; Luneberg et al. 1995; Zhou et al. 2000; Macosko et al. 1997). At the fusiogenic pH, the Glu-11 residue, and in some subtypes Glu-15 and Asp-19, are protonated, allowing for deeper burial of the fusion peptide (Lorieau et al. 2011b). EPR data indicates a slight (3–6Å) increase in membrane penetration at pH 5 versus pH 7.4 (Han et al. 2001). However, detergent-protein NOEs between HAfp and DPC aliphatic protons change only slightly upon acidification and are consistent with a similar depth and orientation of membrane integration at both high and low pH.

1.2 Mechanism of Membrane Fusion

Hemagglutinin fusion is believed to proceed first by the dehydration and merging of the outer leaflets of the merging membranes, forming an hourglass-shaped fusion stalk structure, before proceeding to a hemifusion diaphragm and a fusion pore (Fig. 4). The progression of these steps can be visualized using fluorescence spectroscopy, electron microscopy or a combination of the two (Heuvingh et al. 2004; Kanaseki et al. 1997). Theoretical models place the high-energy fusion stalk and hemifusion diaphragm (Kozlov and Markin 1984; Kozlov and Markin 1983) as the kinetically prohibitive steps in the membrane fusion mechanism (Kozlovsky et al. 2002; Chernomordik and Kozlov 2008).

A sharp protrusion between the two fusing membranes bridge to form the fusion stalk, and lipids between the outer leaflets may exchange in this structure (Fig. 3a). Radial expansion of the fusion stalk generates the hemifusion diaphragm in which the trans monolayers make contact (Fig. 3b). The rim of the diaphragm forms a trilamellar structure consisting of the original membranes and the newly formed bilayer. Geometric modeling of the rim reveals a high energy barrier from an uncompensated vacuum void space formed at the membrane junction and the highly curved membrane intermediates (Siegel 1993). These energy barriers are relieved in part by reducing the membrane's bending modulus and rigidity by tilting the lipids to the curved structure (Kozlovsky and Kozlov 2002). Deviations from a circular stalk and diaphragm structure to an elliposoidal shape further alleviate

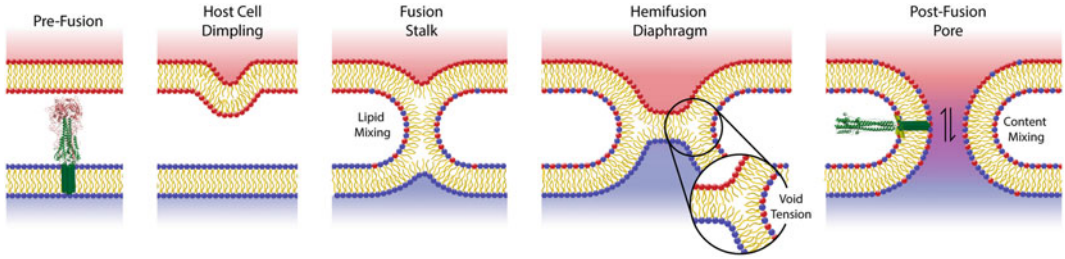

Fig. 4 A cartoon diagram outlining the putative steps of fusion in the fusion stalk mechanism. The pre-fusion hemagglutinin (PDB: 2HMG) embedded in the viral membrane (*blue*) by HA-TMD (*green* cylinders) protrudes toward the host endosomal membrane (*red*). The membranes thereafter dimple, requiring the displacement of water between membranes. The fusion stalk is formed and lipid mixing of the outer leaflets is achieved. The hemifusion diaphragm is formed as the outer leaflets form a new bilayer. This trilamellar structure forms a theoretical void between membrane monolayers. Fusion is achieved with the formation of a pore and the mixing of the contents bounded by both membranes. In the fusion pore diagram, the post-fusion HA2 structure (PDB: 1QU1) forms a 6-helix bundle-like structure, which brings the HA-TMD and HAfp domain (*green* cylinders) in tight proximity. Intermediate hemagglutinin structures between the initial pre-fusion state and the post-fusion state have not been characterized

the high energy requirements of these models (Markin and Albanesi 2002). These structures remain, nonetheless, prohibitively high in energy to form spontaneously. The HAfp domain and possibly the HA-TMD are believed to catalyze fusion by promoting curvature in these high-energy intermediates (Epand and Epand 2000; Langosch et al. 2007).

1.2.1 Membrane Fusion Measurements

Membrane fusion can be measured *in vitro* and *in vivo*. Experiments differ in concentration, lipid composition, peptide sequence, buffer conditions and many other nuanced variables. Consequently, a direct comparison between techniques is generally not possible, yet qualitative comparisons can still be achieved. Assays can monitor lipid-mixing fusion through the redistribution of lipids between outer leaflets of fusing membranes, or they can monitor content-mixing fusion and the redistribution of vesicle contents through fusion pores. Since lipid-mixing assays only monitor the interaction between the outer leaflets and the formation of fusion stalk structures, these assays are unable to monitor the formation of fusion pores. The most common *in vitro* fusion assays monitor the lipid-mixing redistribution of fluorophores between vesicle membranes (Struck et al. 1981; Hoekstra et al. 1984) or the content mixing of fluorophores between vesicle lumens (Ellens et al. 1985). Lipid-mixing fusion assays monitor the redistribution of fluorescently tagged FRET pair lipids as they are diluted from the surface of labeled vesicles by fusing with unlabeled vesicles. These vesicles can be prepared by extrusion and include a lipid donor, such as cholesteryl anthracene-9-carboxylate (CAC) or N-(lissamine rhodamine B sulphonyl)- dioleyl phosphatidylethanolamine (Rh-PE), and a lipid acceptor, such as N-4-nitrobenzo-2-oxa-1,3-diazole phosphatidylethanolamine (NBD-PE). Content mixing fusion assays monitor the redistribution of soluble probes enclosed within labeled vesicles. Vesicles containing octadecyl Rhodamine B chloride (R18) or 8-aminonapthalene-1,3,6 trisulfonic acid (ANTS) and p-xylene-bis-pyridinium bromide (DPX) can report a reduction in self-quenching, as the vesicles containing the fluorophore are diluted by the contents of unlabeled vesicles upon fusion (Hoekstra et al. 1984; Wimley et al. 1994). Depending on the experimental design, content mixing assays may fail to distinguish between content leakage or actual fusion, which can occur at much slower rates. These methods are typically applied to isolated fusion peptide domains or soluble hemaggluntinin proteins and have proven useful for comparisons of point mutations (Epand et al. 2001; Smrt et al. 2015; Stegmann et al. 1990).

In vivo assays measure the perforation of mammalian cells or cell-to-cell fusion to form cell bodies with multiple nuclei (polykaryons). CV1 cells infected with recombinant simian virus express hemagglutinin bound to the cell's surface and fuse into large polykaryons when the hemagglutinin is cleaved by trypsin and activated by a drop in pH (White et al. 1982). MDCK, 3T3 and CV1 cell lines expressing surface hemagglutinin were shown to fuse with erythrocytes (Doxsey et al. 1985; Gething et al. 1986). Polykaryons are large enough to be directly monitored microscopically, yet the qualitative nature in the characterization of polykaryons complicates the quantitative comparison of different fusion peptides.

Conductance assays measure the formation of pores directly from cells. Conductance is measured from a group of cells anchored to a bilayer surface or from individual patch-clamped cells. Initial measurements indicated a 10–50 ms time scale of pore formation in HA-transfected fibroblasts with the pore gradually widening from an initial width of ~1–2 nm (Spruce et al. 1991). HA-expressing MDCK cells fusing with a planer bilayer show a conductance "flickering" characteristic of the reversible formation of a pore (Melikyan et al. 1993a, b). This quiescent flickering can be halted or irreversibly advanced over ~20 ms to a fully formed pore with an estimated diameter up to ~475 nm. Transient pore conductance is correlated with overall HA surface density, indicating hemagglutinin mediates pore dilation kinetics (Melikyan et al. 1995).

Reversible pore formation events may be indicative of a preparatory rearrangement or HA aggregation upon acidification. Nonfunctional small pores (<10 nm wide) have been observed by quick-freezing electron microscopy of fusing virions or liposomes (Kanaseki et al. 1997). Zimmerburg et al. combined conductance measurements with lipid and content mixing assays to measure HA-expressing fibroblasts fusing with erythrocytes (Zimmerberg et al. 1994). Conductance measurements indicative of pore formation were measured before lipid mixing, within ~9.4 s from the reduction in sample pH. This was attributed to the relatively slow rate of lipid diffusion and the large lipid flux required for measurement. Surprisingly, despite the 100-fold larger diffusion constant of the aqueous dye, lipid mixing was still measured prior to content mixing. The authors attributed this observation to the formation of numerous small reversible pores that preclude the transmission of the larger dye molecules and appear to be a requirement for full pore progression. Flickering was further observed in conductance measurements of fusion events between insect Sf9 cells expressing trypsin-cleaved hemagglutinin with red blood cells (Plonsky et al. 2008). In this report, a long waiting time of ~11.3 s between the start of fusion, triggered by a reduction in pH, and pore formation was observed when compared to 0.27 s measured for the major fusion glycoprotein of baculovirus Autographa californica (GP64), which experiences no flickering events.

1.2.2 Factors That Impact Hemagglutinin and HAfp Fusion Activities

pH stability plays a major role in the fusogenicity and genetic variation of hemagglutinin (Di Lella et al. 2016) since the 'spring loaded' conformational change is triggered by pH in the late endosome. Infectivity and pathogenicity are both correlated to pH stability (Russier et al. 2016). Early studies, which included circular dichroism (CD) spectroscopy, electron microscopy (EM) and crystallography, showed a correlation between a reduction in pH and the increase in hemagglutinin α-helical content and elongation (Ruigrok et al. 1986; Tatulian et al. 1995; Skehel et al. 1982; Bullough et al. 1994). Fusion at reduced temperatures revealed pH dependent intermediate steps with a final pH independent step (Stegmann et al. 1990). The pre-fusion conformation appears to be trapped in a metastable state, which normally is activated by a reduction in pH, but can also be activated through temperature or chaotropic destabilization (Carr et al. 1997). Likewise, the fusion activity of isolated HAfp peptides show a direct correlation with pH (Wharton et al. 1988; Murata et al. 1987). At low

pH, there are conformational changes to a small population of open structures (Lorieau et al. 2012), which are postulated to be more fusiogenic (Ghosh et al. 2015).

Cholesterol has an important impact on the rigidity of membranes and their propensities to fuse. The cholesterol content of the influenza membrane is nearly twice that of the host membrane from which the virus particle forms its outer coat on egress (Gerl et al. 2012). Cholesterol accumulates in membrane regions with high curvature and modulates the physical properties of bilayers (Wang et al. 2007; Yang et al. 2016). This suggests the involvement of membrane rafts in the final stages of viral budding. However, the high composition of cholesterol in the viral membrane may stimulate membrane fusion during infection. The addition of cholesterol demonstrates a substantial increase in fusion activity (Domanska et al. 2013, 2015). Fusion measurements of HA-expressing Sf9 cells and red blood cells were performed with host cell cholesterol enrichment (Biswas et al. 2008). Cholesterol enrichment facilitates lipid mixing prior to pore formation and increased fusion pore dilation. The presence of cholesterol also increases the average trimer-to-trimer spacing in the viral membrane (Domanska et al. 2015). Cryo-EM tomography revealed the formation of lipidic junctions under conditions depleted of cholesterol (Chlanda et al. 2016). The authors suggest that these junctions are formed from liposomal rupture stabilized by HA. Cholesterol may act as a pathway switch between hemifusion stalk formation and ruptured insertion. In addition to modulating lipid dynamics, cholesterol may impact the structure of HAfp23.

In giant unilamellar vesicles, HA-TMD and hemagglutinin segregate into the liquid disordered phase (Nikolaus et al. 2010). The hydrophobic length of HA-TMD extends beyond the thickness of the surrounding membrane in both liquid ordered and disordered phases, but this mismatch was 9.5Å greater in the liquid disorded phase, where HA-TMD is localized. While the viral envelope is enriched with a higher fraction of cholesterol than the host membrane (Scheiffele et al. 1999), the phase behavior resembles a liquid disordered state (Polozov et al. 2008). It was suggested that protein-lipid interactions modulated the phase behavior for hemagglutinin recruitment. Therefore, the cooperative effects between the hemagglutinin ectodomain, HA-TMD and HAfp may be indirect. Niles and Cohen applied epifluorescence microscopy to monitor single virion fusion and reported fusion kinetics dependent on receptor binding (Niles and Cohen 1993). In the presence of receptor, fusion could be described in a Poisson dictated Markovian process. Removal of sialic acid receptors shifted fusion to a non-Markovian process. This indicates a coupling of the binding and fusion processes.

The hemagglutinin fusion activity is highly sensitive to mutations in the conserved HAfp domain. Substitutions in the HAfp domain, including the N-terminal G1E and G4E, abolished or lowered fusion activity. A comprehensive mutational study by Steinhauer et. al. combined polykaryon and hemolytic assays with R18 dequenching (Cross et al. 2001). Fusion activity was severely reduced or abolished for nearly all single-site mutations and deletions in the HAfp domain, including ΔG1, G1L, G1S, L2G, F3A, F3G, I6G and I10G. For some residues, glycine mutations that abolish fusion activity can be recovered with alanine mutations (I6A and I10A), suggesting that the side-chain volume of hydrophobic residues could impact fusiogenicity. Likewise, the length of the HAfp domain appears critical to its function, as single residue deletions (L2, G4, I6, F9, N12, E15, D19 and F24) reduce fusion activity (Langley et al. 2009). With the exception of F24, these mutations correlate directly with the full-length helical-hairpin structure: shortening one of the two helices by deleting a residue eliminates key charge-dipole or aliphatic hydrogen bond interactions, or mutations reduce fusion by introducing steric clashes (G8A) between the two helices in the structure (Han et al. 1999; Lorieau et al. 2012). The F24 mutation, however, is non-fusiogenic due to incomplete cleavage of the HA0 precursor (Langley et al. 2009).

1.2.3 Mechanism of HAfp Fusion

Numerous mechanisms have been postulated for the impact of HAfp on membranes, including the destabilization of membranes (Han et al. 2001; Lai et al. 2006b), the promotion of lipid tail protrusions (Larsson and Kasson 2013), the modulation of membrane rupture tension (Risselada et al. 2012; Longo and Waring 1997), the filling of interstitial voids in fusing membranes (Chakraborty et al. 2013) and the change in membrane curvature (Epand et al. 2001; Tenchov et al. 2013; Fuhrmans and Marrink 2012). A membrane curvature mechanism is likely a major component of the HAfp mechanism since the highly curved fusion stalk and hemifusion diaphragm structures have high energy barriers (Kozlovsky and Kozlov 2002). A surface bound HAfp20 provides a wedge shape, which was predicted to promote curvature (Luneberg et al. 1995).

Molecular simulations have proposed multiple membrane curvature mechanisms for HAfp and for amphipathic helices in general. Molecular modeling studies have identified molecular shape, electrostatics, hydrogen bonding interactions (Sodt and Pastor 2014)and insertion depth (Campelo et al. 2008) as key factors in modulating membrane curvature of amphiphiles. Most amphipathic helices induce positive curvature with convex structure, yet some amphipathic helices, L-helices, induce negative curvature (Epand et al. 1995) with concave curvature. Molecular dynamics (MD) simulations show that the truncated and partially unfolded HAfp20 induces positive curvature, which would promote pore formation in the trans leaflets of the fusing bilayers (Fuhrmans and Marrink 2012; Li et al. 2010). However, relevant structural details are not always captured in simulations, making a comparison between theory and experiment difficult. For instance, the charge state of important residues, including the positively charged Gly-1, or the flexibility of the truncated HAfp20 are not always captured in simulations.

Experimental evidence, by contrast, supports a negative curvature activity and a negative Gaussian curvature (NGC) activity with saddle-like curvature. At low peptide:lipid ratios (*ca.* 1:1000), HAfp stabilizes negative curvature (Smrt et al. 2015). Membrane curvature propensity can be measured with dipalmitoleoylphosphatidylethanolamine (DPoPE) and a differential scanning calorimetry (DSC) assay (Siegel and Epand 1997). The addition of truncated HAfp20 and full length HAfp decreases the transition temperature of DPoPE from the planar alpha lamellar (L_α) to the negatively curved type II hexagonal inverted (H_{II}) state in a pH dependent manner (Smrt et al. 2015; Epand and Epand 1994). The G1E, F3G and G4E mutants, by contrast, are unable to lower the transition temperature and induce appreciable curvature. Lipid-mixing fusion and polykaryon assays show that these mutations are compromised in their fusion activities (Sup Kim et al. 2011; Smrt et al. 2015; Gething et al. 1986). These results suggest that the fusion activity of HAfp correlates with its propensity to induce negative curvature and to stabilize fusion stalks.

At higher peptide:lipid ratios (*ca.* 1:100–1:200), HAfp20 induces cubic states in lipids (Colotto and Epand 1997). X-ray diffraction experiments show the stabilization of cubic membrane structures with NGC (Tenchov et al. 2013; Siegel and Epand 2000). Fusion stalks have a characteristic cubic structure with a high degree of negative curvature on one axis in the membrane and positive curvature along the other. Curvature effects at these high concentrations are likely relevant in the late fusion mechanism, as multiple hemagglutinins come together to form a pore. These results suggest a concentration dependent wedging and curvature mechanism.

The helical-hairpin structure of full-length HAfp further supports a curvature induction mechanism. The two helices of the helical-hairpin lie near the plane of the membrane, and the hydrophobic base of the structure has a much larger volume than the hydrophiphilic headgroup region, producing an inverted wedge shape (Lorieau et al. 2010). Inverted wedge lipids with a small head group and large hydrophobic tail, like DOPE, induce negative membrane curvature and promote lipid-mixing fusion (Haque

and Lentz 2004; Leikin et al. 1996). Likewise, HAfp induces significant negative curvature at low peptide:lipid ratios using the DSC membrane curvature assay and a bicelle induced curvature and sorting (BICS) assay using NMR (Smrt et al. 2015; Draney et al. 2014). Mutations further substantiate this mechanism, as the HAfp-F3G mutant (Cross et al. 2001) is significantly less fusiogenic and induces curvature to a much lesser extent than wildtype (Smrt et al. 2015). The HAfp-F3G mutant maintains the same backbone structure and membrane affinity as the wildtype, yet the reduction in the volume of its hydrophobic base gives this peptide a cylindrical shape. Consequently, it cannot promote negative curvature and fusion to the same extent as the wildtype.

Open and activated states of the HAfp helical-hairpin structure are also believed to promote fusion. Molecular dynamic simulations have recently suggested that flexibility (i.e. opening and closing) of HAfp20 is a key characteristic of fusion (Légaré and Lagüe 2012). HAfp in DPC micelles populates open conformations with a population of 11 $\pm$ 4 % at low pH (Lorieau et al. 2012). Recent solid-state studies have characterized a semi-closed state, which the authors suggest promotes fusion by virtue of the fact that average the hydrophobic surface area of the molecule is larger (Ghosh et al. 2015).

1.2.4 Mechanism of Hemagglutinin Fusion

The membrane density and aggregation of hemagglutinin molecules may play a significant role in the complete fusion mechanism. The HA-TMD and HAfp domains both show a tendency to aggregate and could promote hemagglutinin self-assembly (Chang et al. 2008; Cheng et al. 2003; Collu et al. 2015). At low hemagglutinin surface density, fusion is halted at the hemifusion intermediate with unrestricted lipid-mixing (Chernomordik et al. 1998). Thereafter, full fusion proceeds by increasing hemagglutinin surface density. The authors attribute this observation to a ring-like complex of HAfp molecules that impedes lipid diffusion. Fusion activation by increasing the hemagglutinin surface density was observed by other reports as well (Markovic et al. 2001). A minimum of three hemagglutinin trimers are necessary for fusion of 3T3 cells (Danieli et al. 1996). Activation of fusion, however, does not require all three hemagglutinin trimers to adopt the elongated 'post fusion' structure at low pH. A combination of stochastic fusion simulations and microfluidic fusion assays further support a minimum of 3 hemagglutinin trimers, with at least one active trimer needed for fusion (Lee et al. 2014). This suggests a passive role for the non-active trimers, which may be employed by the transmembrane domain.

Another feature of hemagglutinin aggregation is the requirement of membrane dehydration during fusion. High resolution cryo-electron tomography (cryo-ET) was used to monitor fusion of intact H3N2 virions with DOPC liposomes (Gui et al. 2016). Dimpling of the liposomal membranes towards localized clusters of hemagglutinin trimers preceded the merger of membranes. Membrane dimpling may act to reduce the energy requirements of dehydration along the membrane surface. In this same study, the observation of hemifusion intermediates was infrequent, indicating that these intermediates are short lived. By contrast, hemifusion states in eukaryotic membrane fusion systems are long lived (Hernandez et al. 2012). The elongation of hemagglutinin in the fusion-active structure may further reduce the penalty of local dehydration. Molecular models suggest that local dehydration allows individual lipid tails to exchange between membranes and initiate stalk formation (Larsson and Kasson 2013; Kasson et al. 2010; Smirnova et al. 2010).

The hemagglutinin ectodomain and transmembrane domain may play individual roles in pore formation. Fusion progression stalls at the hemifusion intermediate if the HA-TMD is replaced with a glycosylphosphatidylinositol lipid tail (Kemble et al. 1994). Truncation experiments show that fusion is arrested at the hemifusion intermediate upon removing at least 12 residues from the C-terminus of HA-TMD (Armstrong et al. 2000). Lai and Freed propose a synergetic effect on lipid ordering achieved by TMD and HAfp (Lai and Freed 2015). The

non-fusogenic G1V mutant showed no effect on lipid order, whereas the G1S and W14A mutants, which stall at hemifusion, mildly increase lipid order (Epand et al. 2001; Lai et al. 2006b). In addition, HA-TMD appears to generate ordered lipid domains, which facilitate vesicle aggregation through dehydration (Ge and Freed 2011). The ordering effect is thought to be electrostatically driven by interactions with positively charged lipids and can be abolished with the substitution of a lysine with glutamic acid. Fold-back models describe aggregated FP and TMD in a final pore forming conformation (Ivanovic et al. 2013). Alternatively, Chang Sup Kim et. al. reported pH dependent fusion and lipid mixing with complete removal of the transmembrane domain (Sup Kim et al. 2011).

1.3 Conclusions

Hemagglutinin membrane fusion and infection remain an important and poorly understood component of the influenza virus's life cycle. The characterization of hemagglutinin structures and the HAfp domain in membranes has revealed important features in the pre-fusion and post-fusion mechanism. The interaction of HAfp with membranes has further elucidated how this vital domain promotes unfavorable membrane fusion intermediates. Future work in investigating how to disrupt these structures and their function will lead to important new insights in the mechanism of protein-mediated fusion and the development of treatments for influenza and diseases with similar infection processes, like HIV and Ebola.

References

Armstrong RT, Kushnir AS, White JM (2000) The transmembrane domain of influenza hemagglutinin exhibits a stringent length requirement to support the hemifusion to fusion transition. J Cell Biol 151:425–437

Bax A, Grishaev A (2005) Weak alignment NMR: a hawk-eyed view of biomolecular structure. Curr Opin Struct Biol 15:563–570

Biswas S, Yin SR, Blank PS, Zimmerberg J (2008) Cholesterol promotes hemifusion and pore widening in membrane fusion induced by influenza hemagglutinin. J Gen Physiol 131:503–513

Bowie JU (2011) Membrane protein folding: how important are hydrogen bonds? Curr Opin Struct Biol 21:42–49

Brunner J (1989) Testing topological models for the membrane penetration of the fusion peptide of influenza virus hemagglutinin. FEBS Lett 257:369–372

Bullough PA, Hughson FM, Skehel JJ, Wiley DC (1994) Structure of influenza haemagglutinin at the pH of membrane fusion. Nature 371:37–43

Campelo F, McMahon HT, Kozlov MM (2008) The hydrophobic insertion mechanism of membrane curvature generation by proteins. Biophys J 95:2325–2339

Carr CM, Chaudhry C, Kim PS (1997) Influenza hemagglutinin is spring-loaded by a metastable native conformation. Proc Natl Acad Sci 94:14306–14313

Chakraborty H, Tarafdar PK, Klapper DG, Lentz BR (2013) Wild-type and mutant hemagglutinin fusion peptides alter bilayer structure as well as kinetics and activation thermodynamics of stalk and pore formation differently: mechanistic implications. Biophys J 105:2495–2506

Chang DK, Cheng SF, Kantchev EA, Lin CH, Liu YT (2008) Membrane interaction and structure of the transmembrane domain of influenza hemagglutinin and its fusion peptide complex. BMC Biol 6:2

Chazal N, Gerlier D (2003) Virus Entry, Assembly, Budding, and Membrane Rafts. Microbiol Mol Biol Rev 67:226–237

Chen J, Lee KH, Steinhauer DA, Stevens DJ, Skehel JJ, Wiley DC (1998) Structure of the hemagglutinin precursor cleavage site, a determinant of influenza pathogenicity and the origin of the labile conformation. Cell 95:409–417

Cheng SF, Kantchev AB, Chang DK (2003) Fluorescence evidence for a loose selfassembly of the fusion peptide of influenza virus HA2 in the lipid bilayer. Mol Membr Biol 20:345–351

Chernomordik LV, Kozlov MM (2008) Mechanics of membrane fusion. Nat Struct Mol Biol 15:675–683

Chernomordik LV, Frolov VA, Leikina E, Bronk P, Zimmerberg J (1998) The pathway of membrane fusion catalyzed by influenza hemagglutinin: restriction of lipids, hemifusion, and lipidic fusion pore formation. J Cell Biol 140:1369–1382

Chlanda P, Mekhedov E, Waters H, Schwartz CL, Fischer ER, Ryham RJ, Cohen FS, Blank PS, Zimmerberg J (2016) The hemifusion structure induced by influenza virus haemagglutinin is determined by physical properties of the target membranes. Nat Microbiol 1:16050

Collu F, Spiga E, Lorenz CD, Fraternali F (2015) Assembly of Influenza Hemagglutinin Fusion Peptides in a Phospholipid Bilayer by Coarse-grained Computer Simulations. Front Mol Biosci 2:66

Colotto A, Epand RM (1997) Structural study of the relationship between the rate of membrane fusion and the ability of the fusion peptide of influenza virus to perturb bilayers. Biochemistry 36:7644–7651

Cross KJ, Wharton SA, Skehel JJ, Wiley DC, Steinhauer DA (2001) Studies on influenza haemagglutinin fusion peptide mutants generated by reverse genetics. EMBO J 20:4432–4442

Cross KJ, Langley WA, Russell RJ, Skehel JJ, Steinhauer DA (2009) Composition and functions of the influenza fusion peptide. Protein Pept Lett 16:766–778

Danieli T, Pelletier S, Henis Y, White J (1996) Membrane fusion mediate by the influenza virus hemagglutinin requires the concerted action of at least three hemagglutinin trimers. J Cell Biol 133:559–569

De Planque MR, Bonev BB, Demmers JA, Greathouse DV, Koeppe RE, Separovic F, Watts A, Killian JA (2003) Interfacial anchor properties of tryptophan residues in transmembrane peptides can dominate over hydrophobic matching effects in peptide-lipid interactions. Biochemistry 42:5341–5348

Di Lella S, Herrmann A, Mair CM (2016) Modulation of the pH stability of influenza virus hemagglutinin: a host cell adaptation strategy. Biophys J 110:2293–2301

Domanska MK, Wrona D, Kasson PM (2013) Multiphasic effects of cholesterol on influenza fusion kinetics reflect multiple mechanistic roles. Biophys J 105:1383–1387

Domanska MK, Dunning RA, Dryden KA, Zawada KE, Yeager M, Kasson PM (2015) Hemagglutinin Spatial Distribution Shifts in Response to Cholesterol in the Influenza Viral Envelope. Biophys J 109:1917–1924

Doms RW, Helenius A (1986) Quaternary structure of influenza virus hemagglutinin after acid treatment. J Virol 60:833–839

Doxsey SJ, Sambrook J, Helenius A, White J (1985) An Efficient Method for Introducing Macromolecules into Living Cells. J Cell Biol 101:19–27

Draney AW, Smrt ST, Lorieau JL (2014) Use of isotropically tumbling bicelles to measure curvature induced by membrane components. Langmuir 30:11723–11733

Durrer P, Galli C, Hoenke S, Corti C (1996) H+-induced membrane insertion of influenza virus hemagglutinin involves the HA2 amino-terminal fusion peptide but not the coiled coil region. J Biol Chem 271:13417–13421

Eichmann C, Orts J, Tzitzilonis C, Vögeli B, Smrt S, Lorieau J, Riek R (2014) Intermolecular Detergent-Membrane Protein NOEs for the Characterization of the Dynamics of Membrane Protein-Detergent Complexes. J Phys Chem B 118:14288–14301

Eierhoff T, Hrincius ER, Rescher U, Ludwig S, Ehrhardt C (2010) The epidermal growth factor receptor (EGFR) promotes uptake of influenza A viruses (IAV) into host cells. PLoS Pathog 6(9):e1001099

Ellens H, Bentz J, Szoka FC (1985) H+- and Ca2+-induced fusion and destabilization of liposomes. Biochemistry 24:3099–3106

Epand RM, Epand RF (1994) Relationship between the infectivity of influenza virus and the ability of its fusion peptide to perturb bilayers. Biochem Biophys Res Commun 202:1420–1425

Epand RM, Epand RF (2000) Modulation of membrane curvature by peptides. Biopolymers 55:358–363

Epand R, Shai Y, Segrest JP, Anantharamaiah GM (1995) Mechanisms for the modulation of membrane bilayer properties by amphipathic helical peptides. Biopolymers 37:319–338

Epand RM, Epand RF, Martin I, Ruysschaert JM (2001) Membrane interactions of mutated forms of the influenza fusion peptide. Biochemistry 40:8800–8807

Fuhrmans M, Marrink SJ (2012) Molecular view of the role of fusion peptides in promoting positive membrane curvature. J Am Chem Soc 134:1543–1552

Ge M, Freed JH (2011) Two conserved residues are important for inducing highly ordered membrane domains by the transmembrane domain of influenza hemagglutinin. Biophys J 100:90–97

Gerl MJ, Sampaio JL, Urban S, Kalvodova L, Verbavatz JM, Binnington B, Lindemann D, Lingwood CA, Shevchenko A, Schroeder C, Simons K (2012) Quantitative analysis of the lipidomes of the influenza virus envelope and MDCK cell apical membrane. J Cell Biol 196:213–221

Gething MJ, Doms RW, York D, White J (1986) Studies on the mechanism of membrane fusion: site-specific mutagenesis of the hemagglutinin of influenza virus. J Cell Biol 102:11–23

Ghosh U, Xie L, Weliky DP (2013) Detection of closed influenza virus hemagglutinin fusion peptide structures in membranes by backbone (13)CO- (15)N rotational-echo double-resonance solidstate NMR. J Biomol NMR 55:139–146

Ghosh U, Xie L, Jia L, Liang S, Weliky DP (2015) Closed and semiclosed interhelical structures in membrane vs closed and open structures in detergent for the influenza virus hemagglutinin fusion peptide and correlation of hydrophobic surface area with fusion catalysis. J Am Chem Soc 137:7548–7551

Gottschalk A (1957) Neuraminidase: the specific enzyme of influenza virus and Vibrio cholerae. Biochim Biophys Acta 23:645–646

Gui L, Ebner JL, Mileant A, Williams JA, Lee KK (2016) Visualization and sequencing of membrane remodeling leading to influenza virus fusion. J Virol 90:6948–6962

Han X, Tamm LK (2000) A host – guest system to study structure – function relationships of membrane fusion peptides. Proc Natl Acad Sci 97:13097–13102

Han X, Steinhauer DA, Wharton SA, Tamm LK (1999) Interaction of mutant influenza virus hemagglutinin fusion peptides with lipid bilayers: probing the role of hydrophobic residue size in the central region of the fusion peptide. Biochemistry 38:15052–15059

Han X, Bushweller JH, Cafiso DS, Tamm LK (2001) Membrane structure and fusiontriggering conformational change of the fusion domain from influenza hemagglutinin. Nat Struct Biol 8:715–720

Haque M, Lentz B (2004) Roles of curvature and hydrophobic interstice energy in fusion: studies of lipid perturbant effects. Biochemistry 43:3507–3517

Haria NR, Monticelli L, Fraternali F, Lorenz CD (2014) Plasticity and conformational equilibria of influenza fusion peptides in model lipid bilayers. Biochim Biophys Acta Biomembr 1838:1169–1179

Harter C, James P, Bachi T, Semenza G, Brunner J (1989) Hydrophobic binding of the ectodomain of influenza hemagglutinin to membranes occurs through the "fusion peptide". J Biol Chem 264:6459–6464

Heiny AT, Miotto O, Srinivasan KN, Khan AM, Zhang GL, Brusic V, Tan TW, August JT (2007) Evolutionarily conserved protein sequences of influenza a viruses, avian and human, as vaccine targets. PLoS One 2(11):e1190

Hernandez JM, Stein A, Behrmann E, Riedel D, Cypionka A, Farsi Z, Walla PJ, Raunser S, Jahn R (2012) Membrane fusion intermediates via directional and full assembly of the SNARE complex. Science 336:1581–1584

Heuvingh J, Pincet F, Cribier S (2004) Hemifusion and fusion of giant vesicles induced by reduction of intermembrane distance. Eur Phys J E 14:269–276

Hoekstra D, de Boer T, Klappe K, Wilschut J (1984) Fluorescence Method for Measuring the Kinetics of Fusion. Biochemistry 23:5675–5681

Ishiguro R, Kimura N, Takahashi S (1993) Orientation of fusion-active synthetic peptides in phospholipid bilayers: determination by Fourier transform infrared spectroscopy. Biochemistry 32:9792–9797

Ivanovic T, Choi JL, Whelan SP, van Oijen AM, Harrison SC (2013) Influenza-virus membrane fusion by cooperative fold-back of stochastically induced hemagglutinin intermediates. Elife 2013:1–20

Kanaseki T, Kawasaki K, Murata M, Ikeuchi Y, Ohnishi SI (1997) Structural features of membrane fusion between influenza virus and liposome as revealed by quick-freezing electron microscopy. J Cell Biol 137:1041–1056

Kasson PM, Lindahl E, Pande VS (2010) Atomic-resolution simulations predict a transition state for vesicle fusion defined by contact of a few lipid tails. PLoS Comput Biol 6:1–11

Katz G, Benkarroum Y, Wei H, Rice WJ, Bucher D, Alimova A, Katz A, Klukowska J, Herman GT, Gottlieb P (2014) Morphology of influenza B/lee/40 determined by cryo-electron microscopy. PLoS One 9 (2):e88288

Kemble GW, Danieli T, White JM (1994) Lipid-anchored influenza hemagglutinin promotes hemifusion, not complete fusion. Cell 76:383–391

Klenk H, Rott R, Orlich M, Blödorn J (1975) Activation of influenza A viruses by trypsin treatment. Virology 68:426–439

Kozlov MM, Markin VS (1983) Possible mechanism of membrane fusion. Biofizika 28:242–247

Kozlov MM, Markin VS (1984) On the theory of membrane fusion. The adhesioncondensation mechanism. Gen Physiol Biophys 3:379–402

Kozlovsky Y, Kozlov MM (2002) Stalk model of membrane fusion: solution of energy crisis. Biophys J 82:882–895

Kozlovsky Y, Chernomordik LV, Kozlov MM (2002) Lipid intermediates in membrane fusion: formation, structure, and decay of hemifusion diaphragm. Biophys J 83:2634–2651

Lai AL, Freed JH (2015) The interaction between influenza HA fusion peptide and transmembrane domain affects membrane structure. Biophys J 109:2523–2536

Lai AL, Park H, White JM, Tamm LK (2006a) Fusion peptide of influenza hemagglutinin requires a fixed angle boomerang structure for activity. J Biol Chem 281:5760–5770

Langley WA, Thoennes S, Bradley KC, Galloway SE, Talekar GR, Cummings SF, Varecková E, Russell RJ, Steinhauer DA (2009) Single residue deletions along the length of the influenza HA fusion peptide lead to inhibition of membrane fusion function. Virology 394:321–330

Langosch D, Hofmann M, Ungermann C (2007) The role of transmembrane domains in membrane fusion. Cell Mol Life Sci 64:850–864

Larsson P, Kasson PM (2013) Lipid tail protrusion in simulations predicts fusogenic activity of influenza fusion peptide mutants and conformational models. PLoS Comput Biol 9:e1002950

Lazarowitz SG, Choppin PW (1975) Enhancement of the infectivity of influenza A and B viruses by proteolytic cleavage of the hemagglutinin polypeptide. Virology 68:440–454

Lear JD, DeGrado WF (1987) Membrane binding and conformational properties of peptides representing the NH2 terminus of influenza HA-2. J Biol Chem 262:6500–6505

Lee DW, Thapar V, Clancy P, Daniel S (2014) Stochastic fusion simulations and experiments suggest passive and active roles of hemagglutinin during membrane fusion. Biophys J 106:843–854

Légaré S, Lagüe P (2012) The influenza fusion peptide adopts a flexible flat v conformation in membranes. Biophys J 102:2270–2278

Leikin S, Kozlov MM, Fuller NL, Rand RP (1996) Measured effects of diacylglycerol on structural and elastic properties of phospholipid membranes. Biophys J 71:2623–2632

Li Y, Han X, Lai AL, Bushweller JH, Cafiso DS, Tamm LK (2005) Membrane structures of the hemifusion-inducing fusion peptide mutant G1S and the fusion-blocking mutant G1V of influenza virus hemagglutinin suggest a mechanism for pore opening in membrane fusion. J Virol 79:12065–12076

Li J, Das P, Zhou R (2010) Single mutation effects on conformational change and membrane deformation of influenza hemagglutinin fusion peptides. J Phys Chem B 114:8799–8806

Liu H, Spielmann HP, Ulyanov NB, Wemmer DE, James TL (1995) Interproton distance bounds from 2D NOE intensities: effect of experimental noise and peak integration errors. J Biomol NMR 6:390–402

Longo ML, Waring AJ, DA H (1997) Interaction of the influenza hemagglutinin fusion peptide with lipid bilayers: area expansion and permeation. Biophys J 73:1430–1439

Lorieau JL, Louis JM, Bax A (2010) The complete influenza hemagglutinin fusion domain adopts a tight helical hairpin arrangement at the lipid:water interface. Proc Natl Acad Sci U S A 107:11341–11346

Lorieau JL, Louis JM, Bax A (2011a) Helical hairpin structure of influenza hemagglutinin fusion peptide stabilized by charge− dipole interactions between the N-Terminal Amino Group and the Second. J Am Chem Soc 133:2824–2827

Lorieau JL, Louis JM, Bax A (2011b) Whole-body rocking motion of a fusion peptide in lipid bilayers from size-dispersed 15N NMR relaxation. J Am Chem Soc 133:14184–14187

Lorieau JL, Louis JM, Schwieters CD, Bax A (2012) pH-triggered, activated-state conformations of the influenza hemagglutinin fusion peptide revealed by NMR. Proc Natl Acad Sci U S A 109:19994–19999

Lorieau JL, Louis JM, Bax A (2013) The impact of influenza hemagglutinin fusion peptide length and viral subtype on its structure and dynamics. Biopolymers 99:189–195

Luneberg J, Martin I, Nussler F, Ruysschaert JM, Herrmann A (1995) Structure and topology of the influenza virus fusion peptide in lipid bilayers. J Biol Chem 270:27606–27614

Macosko JC, Kim CH, Shin YK (1997) The membrane topology of the fusion peptide region of influenza hemagglutinin determined by spin-labeling EPR. J Mol Biol 267:1139–1148

Markin VS, Albanesi JP (2002) Membrane fusion: stalk model revisited. Biophys J 82:693–712

Markovic I, Leikina E, Zhukovsky M, Zimmerberg J, Chernomordik LV (2001) Synchronized activation and refolding of influenza hemagglutinin in multimeric fusion machines. J Cell Biol 155:833–843

Marsh M (1984) The entry of enveloped viruses into cells by endocytosis. Biochem J 218:1–10

Matlin KS, Reggio H, Helenius A, Simons K (1981) Infectious Entry Pathway of Influenza-Virus in A Canine Kidney-Cell Line. J Cell Biol 91:601–613

Melikyan GB, Niles WD, Peeples ME, Cohen FS (1993a) Influenza hemagglutinin- mediated fusion pores connecting cells to planar membranes: flickering to final expansion. J Gen Physiol 102:1131–1149

Melikyan GB, Niles WD, Cohen FS (1993b) Influenza virus hemagglutinin-induced cellplanar bilayer fusion: quantitative dissection of fusion pore kinetics into stages. J Gen Physiol 102:1151–1170

Melikyan GB, Niles WD, Ratinov VA, Karhanek M, Zimmerberg J, Cohen FS (1995) Comparison of transient and successful fusion pores connecting influenza hemagglutinin expressing cells to planar membranes. J Gen Physiol 106:803–819

Molinari NA, Ortega-Sanchez IR, Messonnier ML, Thompson WW, Wortley PM, Weintraub E, Bridges CB (2007) The annual impact of seasonal influenza in the US: measuring disease burden and costs. Vaccine 25:5086–5096

Morgan C, Rose HM (1968) Structure and Development of Viruses as Observed in the Electron Microscope: VIII. Entry of Influenza Virus J Virol 2:925–936

Munster VJ, Baas C, Lexmond P, Waldenström J, Wallensten A, Fransson T, Rimmelzwaan GF, Beyer WEP, Schutten M, Olsen B, Osterhaus AD, Fouchier RA (2007) Spatial, temporal, and species variation in prevalence of influenza A viruses in wild migratory birds. PLoS Pathog 3:0630–0638

Murata M, Sugahara Y, Ohnishi S, Takahashi S (1987) pH-Dependent Membrane Fusion Activity of a Synthetic Twenty Amino Acid Peptide with the Same Sequence as That of the Hydrophobic Segment of Influenza Virus Hemagglutinin. J Biochem 102:957–962

Nayak DP, Hui EK, Barman S (2004) Assembly and budding of influenza virus. Virus Res 106:147–165

Nikolaus J, Scolari S, Bayraktarov E, Jungnick N, Engel S, Plazzo AP, Stöckl M, Volkmer R, Veit M, Herrmann A (2010) Hemagglutinin of influenza virus partitions into the nonraft domain of model membranes. Biophys J 99:489–498

Niles WD, Cohen FS (1993) Single event recording shows that docking onto receptor alters the kinetics of membrane fusion mediated by influenza hemagglutinin. Biophys J 65:171–176

Plonsky I, Kingsley DH, Rashtian A, Blank PS, Zimmerberg J (2008) Initial size and dynamics of viral fusion pores are a function of the fusion protein mediating membrane fusion. Biol Cell 100:377–386

Polozov IV, Bezrukov L, Gawrisch K, Zimmerberg J (2008) Progressive ordering with decreasing temperature of the phospholipids of influenza virus. Nat Chem Biol 4:248–255

Reed C, Chaves SS, Kirley PD, Emerson R, Aragon D, Hancock EB, Butler L, Baumbach J, Hollick G, Bennett NM, Laidler MR, Thomas A, Meltzer MI, Finelli L (2015) Estimating influenza disease burden from population-based surveillance data in the United States. PLoS One 10:1–13

Ridder AN, Morein S, Stam JG, Kühn A, De Kruijff B, Killian JA (2000) Analysis of the role of interfacial tryptophan residues in controlling the topology of membrane proteins. Biochemistry 39:6521–65286

Risselada HJ, Marelli G, Fuhrmans M et al (2012) Line-tension controlled mechanism for influenza fusion. PLoS One 7:E38302

Ruigrok RW, Wrigley NG, Calder LJ, Cusack S, Wharton SA, Brown EB, Skehel JJ (1986) Electron microscopy of the low pH structure of influenza virus haemagglutinin. EMBO J 5:41–49

Russell RJ, Gamblin SJ, Haire LF, Stevens DJ, Xiao B, Ha Y, Skehel JJ (2004) H1 and H7 influenza haemagglutinin structures extend a structural classification of haemagglutinin subtypes. Virology 325:287–296

Russier M, Yang G, Rehg JE, Wong S, Mostafa HH, Barman S, Krauss S, Webster RG, Webby RJ, Charles J (2016) Molecular requirements for a pandemic influenza virus: an acidstable hemagglutinin protein. Proc Natl Acad Sci 113:1636–1641

Scheiffele P, Rietveld A, Simons K, Wilk T (1999) Influenza viruses select ordered lipid membrane influenza viruses select ordered lipid domains during budding from the plasma membrane. J Biol Chem 274:2038–2044

Senes A, Ubarretxena-Belandia I, Engelman DM (2001) The Calpha ---H...O hydrogen bond: a determinant of stability and specificity in transmembrane helix interactions. Proc Natl Acad Sci U S A 98:9056–9061

Sieczkarski SB, Whittaker GR (2002) Influenza virus can enter and infect cells in the absence of clathrin-mediated endocytosis influenza virus can enter and infect cells in the absence of clathrin-mediated endocytosis. J Virol 76:10455–10464

Siegel D (1993) Energetics of intermediates in membrane fusion: comparison of stalk and inverted micellar intermediate mechanisms. Biophys J 65:2124–2140

Siegel D, Epand R (1997) The mechanism of lamellar-to-inverted hexagonal phase transitions in phosphatidylethanolamine: implications for membrane fusion mechanisms. Biophys J 73:3089–3111

Siegel DP, Epand RM (2000) Effect of influenza hemagglutinin fusion peptide on lamellar/inverted phase transitions in dipalmitoleoylphosphatidylethanolamine: implications for membrane fusion mechanisms. Biochim Biophys Acta 1468:87–98

Skehel JJ, Bayley PM, Brown EB, Martin SR, Waterfield MD, White JM, Wilson IA, Wiley DC (1982) Changes in the conformation of influenza virus hemagglutinin at the pH optimum of virus-mediated membrane fusion. Proc Natl Acad Sci U S A 79:968–972

Smirnova YG, Marrink SJ, Lipowsky R, Knecht V (2010) Solvent-exposed tails as prestalk transition states for membrane fusion at low hydration. J Am Chem Soc 132:6710–6718

Smith JC, Derbyshire RB, Cook E, Dunthorne L, Viney J, Brewer SJ, Sassenfeld HM, Bell LD (1984) Chemical synthesis and cloning of a poly(arginine)-coding gene fragment designed to aid polypeptide purification. Gene 32:321–327

Smrt ST, Draney AW, Lorieau JL (2015) The influenza hemagglutinin fusion domain is an amphipathic helical hairpin that functions by inducing membrane curvature. J Biol Chem 290:228–238

Sodt AJ, Pastor RW (2014) Molecular modeling of lipid membrane curvature induction by a peptide: more than simply shape. Biophys J 106:1958–1969

Spruce AE, Iwata A, Almers W (1991) The first milliseconds of the pore formed by a fusogenic viral envelope protein during membrane fusion. Proc Natl Acad Sci U S A 88:3623–3627

Stegmann T, Hoekstra D, Scherphof G, Wilschut J (1986) Fusion activity of influenza virus: a comparison between biological and artificial target membrane vesicles. J Biol Chem 261:10966–10969

Stegmann T, White JM, Helenius A (1990) Intermediates in influenza induced membrane fusion. EMBO J 9:4231–4241

Stempfer G, Höll-Neugebauer B, Kopetzki E, Rudolph R (1996) A fusion protein designed for noncovalent immobilization: stability, enzymatic activity, and use in an enzyme reactor. Nat Biotechnol 14:481–484

Struck DK, Hoekstra D, Pagano RE (1981) Use of resonance energy transfer to monitor membrane fusion. Biochemistry 20:4093–4099

Sun Y, Weliky DP (2009) 13C-13C correlation spectroscopy of membrane-associated influenza virus fusion peptide strongly supports a helix-turn-helix motif and two turn conformations. J Am Chem Soc 131:13228–13229

Sup Kim C, Epand RF, Leikina E, Epand RM, Chernomordik LV (2011) The final conformation of the complete ectodomain of the HA2 subunit of influenza hemagglutinin can by itself drive low pH-dependent fusion. J Biol Chem 286:13226–13234

Tatulian S, Hinterdorfer P, Baber G, Tamm L (1995) Influenza hemagglutinin assumes a tilted conformation during membrane fusion as determined by attenuated total reflection FTIR spectroscopy. EMBO J 14:5514–5523

Tenchov BG, MacDonald RC, Lentz BR (2013) Fusion peptides promote formation of bilayer cubic phases in lipid dispersions. An X-ray diffraction study. Biophys J 104:1029–1037

Thoennes S, Li ZN, Lee BJ, Langley WA, Skehel JJ, Russell RJ, Steinhauer DA (2008) Analysis of residues near the fusion peptide in the influenza hemagglutinin structure for roles in triggering membrane fusion. Virology 370:403–414

Vaccaro L, Cross KJ, Kleinjung J, Straus SK, Thomas DJ, Wharton SA, Skehel JJ, Fraternali F (2005) Plasticity of influenza haemagglutinin fusion peptides and their interaction with lipid bilayers. Biophys J 88:25–36

Wang W, Yang L, Huang HW (2007) Evidence of cholesterol accumulated in high curvature regions: implication to the curvature elastic energy for lipid mixtures. Biophys J 92:2819–2830

Wasniewski CM, Parkanzky PD, Bodner ML, Weliky DP (2004) Solid-state nuclear magnetic resonance studies of HIV and influenza fusion peptide orientations in membrane bilayers using stacked glass plate samples. Chem Phys Lipids 132:89–100

Weber T, Paesold G, Galli C, Mischler R, Semenza G, Brunner J (1994) Evidence for H +- induced insertion of influenza hemagglutinin HA2 N-terminal segment into viral membrane. J Biol Chem 269:18353–18358

Wharton SA, Martin SR, Ruigrok RW, Skehel JJ, Wiley DC (1988) Membrane fusion by peptide analogues of influenza virus haemagglutinin. J Gen Virol 69:1847–1857

White J, Helenius A, Gething MJ (1982) Haemagglutinin of influenza virus expressed from a cloned gene promotes membrane fusion. Nature 300:658–659

Wilson IA, Skehel JJ, Wiley DC (1981) Structure of the haemagglutinin membrane glycoprotein of influenza virus at 3 A resolution. Nature 289:366–373

Wimley WC, Selsted ME, White SH (1994) Interactions between human defensins and lipid bilayers: evidence for formation of multimeric pores. Protein Sci 3:1362–1373

Worch R (2013) The helical hairpin structure of the influenza fusion peptide can be seen on a hydrophobic moment map. FEBS Lett 587:2980–2983

Yang J, Parkanzky PD, Bodner ML, Duskin CA, Weliky DP (2002) Application of REDOR subtraction for filtered MAS observation of labeled backbone carbons of membrane-bound fusion peptides. J Magn Reson 159:101–110

Yang ST, Kreutzberger AJ, Lee J, Kiessling V, Tamm LK (2016) The role of cholesterol in membrane fusion. Chem Phys Lipids 199:136–143

Yao H, Hong M (2014) Conformation and lipid interaction of the fusion peptide of the paramyxovirus PIV5 in anionic and negative-curvature membranes from solid-state NMR. J Am Chem Soc 136:2611–2624

Yoshimura A, Ohnishi S (1984) Uncoating of influenza virus in endosomes. J Virol 51:497–504

Zhang H, Neal S, Wishart DS (2003) RefDB: a database of uniformly referenced protein chemical shifts. J Biomol NMR 25:173–195

Zhou Z, Macosko JC, Hughes DW, Sayer BG, Hawes J, Epand RM (2000) 15N NMR study of the ionization properties of the influenza virus fusion peptide in zwitterionic phospholipid dispersions. Biophys J 78:2418–2425

Zimmerberg J, Blumenthal R, Sarkar DE, Curran M, Morris SJ (1994) Restricted movement of lipid and aqueous dyes through pores formed by influenza hemagglutinin during cell fusion. J Cell Biol 127:1885–1894

Adv Exp Med Biol - Protein Reviews (2017) 2:55–64
DOI 10.1007/5584_2016_186

Published online: 18 March 2017

Inherited Ventricular Arrhythmias: The Role of the Multi-Subunit Structure of the L-Type Calcium Channel Complex

Julie Briot, Marie-Philippe Tétreault, Benoîte Bourdin, and Lucie Parent

Abstract

The normal heartbeat is conditioned by transient increases in the intracellular free Ca^{2+} concentration. Ca^{2+} influx in cardiomyocytes is regulated by the activity of the heteromeric L-type voltage-activated $Ca_V1.2$ channel. A complex network of interactions between the different proteins forming the ion channel supports the kinetics and the activation gating of the Ca^{2+} influx. Alterations in the biophysical and biochemical properties or in the biogenesis in any of these proteins can lead to serious disturbances in the cardiac rhythm. The multi-subunit nature of the channel complex is better comprehended by examining the high-resolution three-dimensional structure of the closely related $Ca_V1.1$ channel. The architectural map identifies precise interaction loci between the different subunits and paves the way for elucidating the mechanistic basis for the regulation of Ca^{2+} balance in cardiac myocytes under physiological and pathological conditions.

Keywords

Structural Biology • Cardiac Arrhythmias • Posttranslational Modifications • *CACNA2D1*

Abbreviations

3-D	Three dimensional
BrS	Brugada syndrome
CaM	Calmodulin
Cryo-EM	Cryo-electron microscopy
LQT8	Long QT syndrome 8
NavAb	Voltage-gated Na^+ channel from *Arcobacter butzleri*
QT	Time interval between the Q and the T waves on the cardiac electrocardiogram
SQTS	Short QT syndrome
VWA	Von Willebrand factor A

J. Briot, M.-P. Tétreault, B. Bourdin, and L. Parent (✉)
Département de Pharmacologie et Physiologie, Faculté de Médecine, Institut Cardiologie de Montréal, Université de Montréal, 5000 Bélanger, Montréal, QC H1T 1C8, Canada
e-mail: lucie.parent@umontreal.ca

1 Introduction

Voltage-activated Ca^{2+} channels convert electrical signals to stimulate selective Ca^{2+} influx which in turn prompts biological responses such as cardiac contraction and neurotransmitter release (Catterall 2011). There are three gene families coding for voltage-activated Ca^{2+} channels: L-type $Ca_V1.1$ – $Ca_V1.4$; Neuronal P/Q, N and R-type $Ca_V2.1$-$Ca_V2.3$; and T-type $Ca_V3.1$-$Ca_V3.3$ (Snutch and Reiner 1992). The L-type $Ca_V1.2$ is the major Ca^{2+} influx pathway in ventricular cardiomyocytes. It is a hetero-oligomer complex comprising the main transmembrane pore-forming $Ca_V\alpha1$ associated with tissue-specific $Ca_V\beta1$–4 and $Ca_V\alpha2\delta1$–4 auxiliary subunits. The full complement of subunits is required to reproduce in vitro the properties of the native channel. Deletion of the *CACNA2D1* gene decreased L-type currents and impaired myocardial contractility (Fuller-Bicer et al. 2009) and $Ca_V\alpha2\delta1$ transcripts were reduced in patients suffering from atrial (Gaborit et al. 2005) and ventricular fibrillation (Sivagangabalan et al. 2014). Due to the complex network of protein-protein interactions of $Ca_V\beta3$, $Ca_V\alpha2\delta$ and calmodulin (CAM) within the L-type $Ca_V1.2$ complex and phosphorylation by multiple kinases, the slightest modification in this delicate balance, could impact the heart rhythm (Bodi et al. 2005; Platzer et al. 2000; Mangoni et al. 2003; Dragicevic et al. 2014; Hell et al. 1993) and triggers a chain reaction ultimately causing cardiac sudden death (Borchard and Hafner 2000). Cardiac arrhythmias might originate from (1) external substances (cigarette, stress, and stimulant drugs); pathological states (thyroid disorder, diabetes); or more rarely from (2) genetic-based disorders (the long QT syndrome (LQTS) (Krause et al. 2011), the short QT syndrome (SQTS), or the Brugada syndrome (BrS)) (Burashnikov et al. 2010; Betzenhauser et al. 2015). The quest for the identification of the structural determinants of Ca^{2+} channels started with the purification and cloning of $Ca_V1.1$ from the skeletal muscle (Takahashi et al. 1987; Sharp and Campbell 1989) and has reached a pinnacle with the elucidation of its three-dimensional (3-D) structure at a resolution of 4.2 Å and 3.6 Å (Wu et al. 2015; Wu et al. 2016). This short review brushes up an overview of the structural characterization of the multi-subunit complex referred to as the L-type $Ca_V1.2$ channel with a special emphasis on $Ca_V\alpha2\delta1$ to establish the contribution of this channel to cardiac sudden death.

2 Molecular Makeup of the L-Type $Ca_V1.2$ Channel

The L-type Ca^{2+} channel was first purified from rat brain membranes (Curtis and Catterall 1983) and rabbit skeletal muscle transverse tubules (Curtis and Catterall 1984) using radiolabeled ligands. This pioneering work led to the biochemical determination of four distinct subunits at 175 kDa, 170 kDa, 52 kDa, and 32 kDa (Borsotto et al. 1985; Leung et al. 1987; Sharp and Campbell 1989; Sharp et al. 1987) followed by the cloning and sequencing of the cDNAs encoding $Ca_V\alpha1$ and the ancillary subunits (Tanabe et al. 1987). $Ca_V\alpha1$ is a single polypeptide chain composed of $\approx$ 2000 amino acids organized in four homologous repeats (I, II, III and IV) of six transmembrane segments (Takahashi et al. 1987). The first 3-D structures of $Ca_V\alpha1$ were obtained through the crystallization of a bacterial homologue, the homotetrameric Na_VAb-derived Ca_VAb protein (Tang et al. 2014, 2016; Catterall and Zheng 2015). The crystal structure of the subunit-less Ca_VAb provided the first high-resolution depiction of multi-ion permeation, highlighted the electrostatic interactions between hydrated Ca^{2+} ions and the carboxylate side-chains of the aspartate residues (Parent and Gopalakrishnan 1995) and confirmed that $Ca_V\alpha1$ and $K_V1.2$ share a similar fold (Long et al. 2005).

Protein interactions within the L-type channel were teased out from the co-purification of auxiliary subunits and intracellular fragments of mammalian $Ca_V\alpha1$. At least three high-

resolution X-ray structures (resolution < 2 Å) of $Ca_V\beta$ in complex with its intracellular high-affinity binding site on $Ca_V\alpha1$ were reported (Buraei and Yang 2013). $Ca_V\beta$ subunits are organized around a guanylate kinase domain connected by a HOOK region to the src-homology 3 domain. $Ca_V\beta$ modulates channel kinetics (Berrou et al. 2002, 2005; Dafi et al. 2004; Raybaud et al. 2006) and increases total and cell surface protein expression of $Ca_V1.2$ (Bourdin et al. 2010; Shakeri et al. 2012) through binding to a single site anchored around the conserved tryptophan residue located in the first intracellular linker of $Ca_V\alpha1$ (Van Petegem et al. 2008).

CaM mediates a crucial negative feedback mechanism referred to as Ca^{2+}-dependent inactivation whereby incoming Ca^{2+} decreases ion fluxes. High-resolution structural data highlighted the role of van der Waals interactions between Ca^{2+}-free CaM and the isoleucine-glutamine "IQ" domain located in the C-terminus of $Ca_V\alpha1$ (Kim et al. 2008; Van Petegem et al. 2005; Halling et al. 2009). The α-helix formed by the "IQ" domain is surrounded by Ca^{2+}/CaM that bind to aromatic residues on opposite faces of the IQ α-helix. Ca^{2+}/CaM was also found to bind to the pre-IQ region suggesting that additional binding sites might confer different modes of channel regulation (Minor and Findeisen 2010).

$Ca_V\alpha2\delta1$ improves peak current density by promoting channel activation with smaller depolarization (Bourdin et al. 2015; Tetreault et al. 2016). $Ca_V\alpha2\delta1$ is characterized by numerous post-translational modifications (Tetreault et al. 2016; Jay et al. 1991; Andrade et al. 2007; Davies et al. 2010). In particular, complex Asn-linked glycans confer a great degree of conformational freedom to the protein, while at the same time shielding polar residues required for intermolecular crystal contact formation (Deller et al. 2016) and as a result, $Ca_V\alpha2\delta1$ is a poor candidate for crystallization studies.

3 Genetic Mutations of the $Ca_V1.2$ Channel Associated with Ventricular Arrhythmias

The kinetics of activation of L-type $Ca_V1.2$ channel are determined by its primary structure and its network of interactions with auxiliary subunits. Alterations in the primary structure of any of the proteins forming the channel through congenital mutations could impact the delicate balance between the "off" and "on" state of the $Ca_V1.2$ channel and significantly impair the heart normal rhythm ultimately leading to lethal ventricular tachyarrythmias (Napolitano and Antzelevitch 2011; Scoote and Williams 2004). Genetic variants of the $Ca_V1.2$ channel are associated with electric abnormalities causing a variety of clinical phenotypes from the Brugada-like syndromes to the Timothy (LQT8) syndrome. LQT8 is a monogenic channelopathy resulting from de novo missense mutations in the *CACNA1C* gene for all 17 reported cases. It is characterized by extreme QT-prolongation (Splawski et al. 2004, 2005; Gillis et al. 2012) causing delayed afterdepolarizations (Splawski et al. 2004) and severe ventricular tachycardia. The initial cardiac rhythm disturbances often occur early in life with clear clinical symptoms such as fetal bradycardia and marked QT prolongation ranging from 470 to 700 ms at rest as compared with a normal QT ≈ 420–440 ms. Prognosis is poor with lethal arrhythmia being the primary cause of death (>75%) during infancy (Gillis et al. 2012). The relationship between genotype and phenotype was easily established in recombinant systems and in induced pluripotent stem cells. Gain-of-function mutations G406R and G402S severely delayed Ca^{2+}-dependent inactivation kinetics (Raybaud et al. 2006; Depil et al. 2011) thereby increasing Ca^{2+} influx during each heartbeat (Yazawa et al. 2011). Likewise, single mutations within CaM have also been associated with an increased

repolarization interval causing significant arrhythmias (Limpitikul et al. 2014; Kryshtal et al. 2015). LQTS-CaM mutants (D96V, D130G, and F142 L) induced action-potential prolongation by specifically suppressing Ca^{2+}-dependent inactivation of the L-type $Ca_V1.2$ channel, suggesting that the biophysical properties of the L-type $Ca_V1.2$ channels are crucial in determining the electrical profile of cardiomyocytes.

At the other end of the spectrum, missense mutations of the L-type $Ca_V1.2$ channels were also identified in cohorts diagnosed with Brugada-like syndrome (BrS) and short repolarization intervals. In most cases mutations in $Ca_V1.2$ proteins give rise to BrS associated with short QT intervals (QTc $\leq$ 360 ms) (Burashnikov et al. 2010; Antzelevitch et al. 2007; Templin et al. 2011). Up to 20% of the BrS and BrS + SQTS probands display mutations in $Ca_V\alpha1$, $Ca_V\beta2$, or $Ca_V\alpha2\delta1$ subunits (Burashnikov et al. 2010; Napolitano and Antzelevitch 2011). Some recombinant studies showed that mutations A39V and G490R in $Ca_V1.2$ impair the trafficking of $Ca_V1.2$ (Antzelevitch et al. 2007; Templin et al. 2011) although other groups differed (Bourdin et al. 2010; Simms and Zamponi 2012). Loss-of-function variante T11I and S481L in the $Ca_V\beta2a$ protein were found to accelerate the inactivation kinetics and decrease the cell surface expression of the ion channel but the mechanism responsible for these effects remains to be identified (Antzelevitch et al. 2007; Cordeiro et al. 2009). Most reported mutations are located outside the "guanylate kinase" domain, the region supporting protein-protein interaction, suggesting an indirect modulation of channel function.

Single missense mutations and/or genetic variants of *CACNA2D1* are contributing to cardiac arrhythmias associated with a short repolarization interval (Burashnikov et al. 2010; Templin et al. 2011). Heterologous expression studies have shown that the "loss-of-function" mutations studied in isolation had only a minor impact, if any, on the protein expression of $Ca_V\alpha2\delta1$ or on channel function (Bourdin et al. 2015; Templin et al. 2011). This raises the limitations of studying genotype–phenotype relationships carried in the presence of genetically altered ion channels overexpressed in recombinant systems. Important factors that modulate ion channel expression, subcellular localization, and function, such as the relative expression of the native $Ca_V\beta$ subunits, transcription factors, microRNAs, and epigenetic profile, may differ between model cells and mature cardiomyocytes. Nonetheless, combining two of these silent variants ($Ca_V\alpha2\delta1$ D550Y/Q917H) significantly decreased L-type $Ca_V1.2$ currents and this effect appeared to be mediated through a decrease in the cell surface expression of $Ca_V\alpha2\delta1$ (Bourdin et al. 2015; Savalli et al. 2016). Silent polymorphisms in *CACNA2D1* could thus together contribute to create a arrhythmogenic substrate by impairing $Ca_V1.2$ currents.

Since the $Ca_V1.2$ channel properties are ultimately determined by the complex set of interactions between a host of subunits, one needs to consider the structural impact of various silent variants identified in the auxiliary subunits of the $Ca_V1.2$ channel. Insights into the protein interaction loci require the 3-D structure of native heteromeric complexes that can be manipulated through in silico modeling and molecular replacement. The first milestone was recently reached by the purification of the related $Ca_V1.1$ channel and structure determination by cryo-electron microscopy (cryo-EM).

4 High-Resolution Structure of L-Type Ca^{2+} Channels

As a result of formidable technical advances in image processing and direct electron detectors (Doerr 2015), the skeletal L-type $Ca_V1.1$ complex was recently solved by single particle cryo-

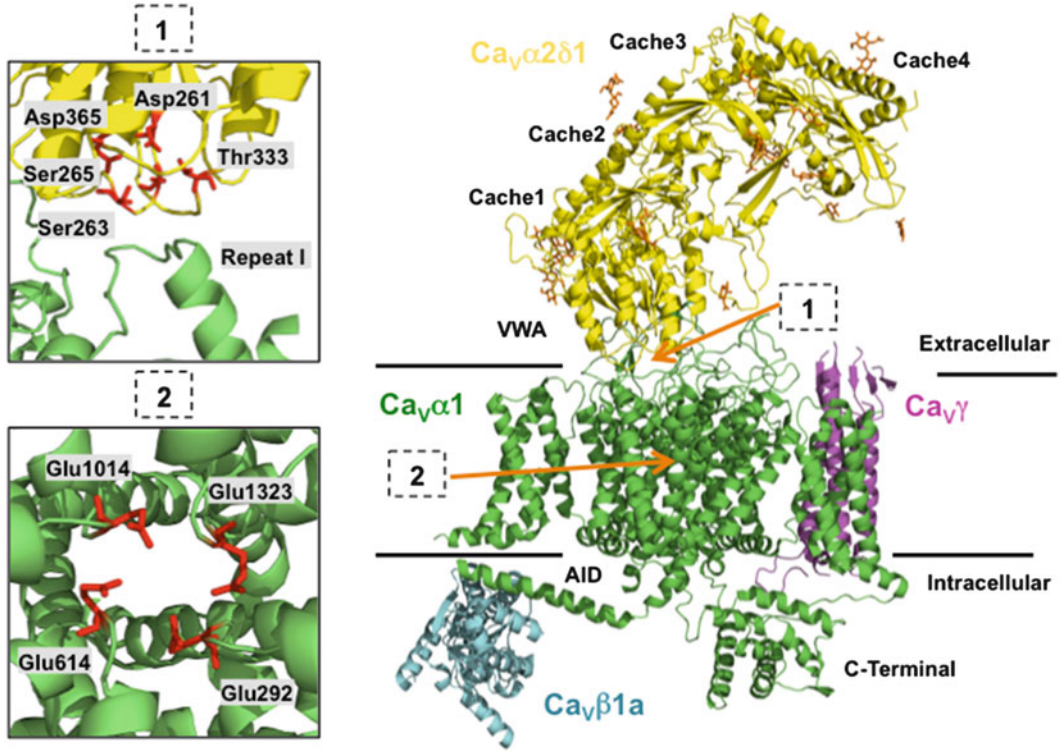

Fig. 1 Membrane topology of the skeletal $Ca_V1.1$ protein complex from the cryo-EM structure (PDB code 5GJV). $Ca_V\alpha1$ (in *green*) is composed of 24 transmembrane helices organized in four homologous repeats (I–IV) around a central pore. $Ca_V\beta1a$ (in *blue*) binds to the intracellular domain between Repeats I and II of $Ca_V\alpha1$. The VWA domain of the extracellular $Ca_V\alpha2\delta1$ (in *yellow)* is topping $Ca_V\alpha1$. Asn-linked glycans are in *orange*. The $Ca_V\gamma$ subunit (*purple*) is not found in the L-type $Ca_V1.2$ channel. *Inset* (1): four polar residues of $Ca_V\alpha2\delta1$ are potentially interfacing with repeat I of $Ca_V\alpha1$. *Inset* (2): the selectivity locus formed by the projection of glutamate residues in the pore domain of $Ca_V\alpha1$. Cartoons were produced with PyMOL (Molecular Graphics System, Version 1.8 Schrödinger, LLC)

EM at a resolution of 4.2 Å (Wu et al. 2015) and 3.6 Å (Wu et al. 2016). Cryo-EM is best suited to study large macro-molecular complexes as it entails a flash-freezing process that minimizes disruptions in intermolecular interactions. $Ca_V\beta1$ was expressed and purified as a GST-fusion protein which was then used to pull down the ion channel complex ($Ca_V\alpha1$, $Ca_V\gamma1$, and $Ca_V\alpha2\delta1$) (Wu et al. 2015, 2016) (Fig. 1). As shown with Ca_VAb, the selectivity filter is pictured with the four glutamate residues forming critical high-affinity binding locus that confers robust Ca^{2+} selectivity (Parent and Gopalakrishnan 1995). Hydrophobic residues face each other at the channel intracellular cavity with an inner pore radius of ≈ 0.66 Å suggesting that the channel was captured in its closed state. The electronic density map declines significantly for the flexible intracellular linkers but the 3-D structure is compatible with a single high-affinity binding site for $Ca_V\beta$ on $Ca_V\alpha1$.

One of the greatest scientific achievements in the cryo-EM models remains the elucidation of the 3-D structure of $Ca_V\alpha2\delta1$. By homology with the structure of the rabbit isoform, the human $Ca_V\alpha2\delta1$ is built from five structural domains: Cache1, von willebrand factor A (VWA), Cache2, Cache3, and Cache4 (Briot et al. 2016)

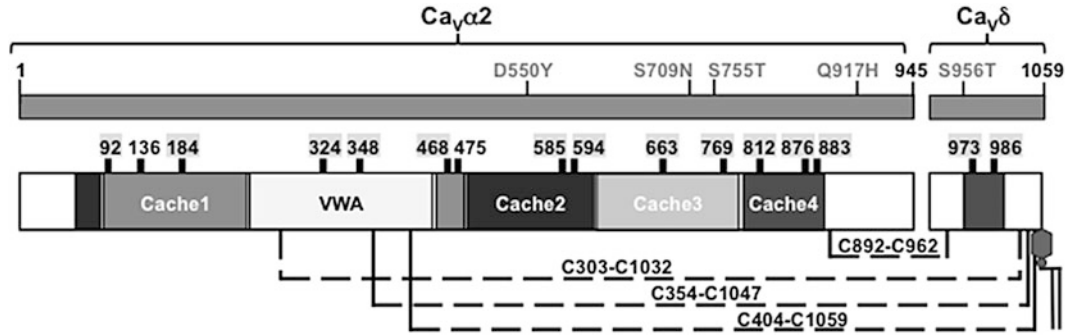

Fig. 2 Structural organization of the human Ca$_V$α2δ1 (NM_000722.3). The five domains Cache1, VWA, Cache2, Cache3, and Cache4 are shown in different shades of grey. The numbers in *black* on the *top rectangle* indicate the amino acid boundaries for the human isoform 1 of Ca$_V$α2 and Ca$_V$δ. The exact residue numbering varies between species due to slight differences in their primary structures. The five mutations of Ca$_V$α2δ1 associated with cardiac arrhythmias are shown in pale grey. The 14 Asn-glycosylation sites identified in the cryo-EM structure are shaded and positioned directly above the domains. The two other Asn-glycosylation sites that were not identified are not shaded. The four intermolecular disulfide bonds between Ca$_V$α2 and Ca$_V$δ1 are shown above the *dotted lines*. The glycosyl-phosphatidyl-inositol anchor is located at cysteine 1059 which is equivalent to the last cysteine residue 1074 solved in the cryo-EM structure of the rabbit isoform

(Fig. 2). Ca$_V$α2δ1 is entirely extracellular and is held in the membrane through a glycosyl-phosphatidyl-inositol anchor at cysteine 1074. The Cache domains are deployed away from the membrane and are formed by 3 α-helices intertwined with 5 anti-parallel β-sheets. The 6 -α-helices of the VWA domain are organized along 6 anti-parallel β-sheets. The 3 β-sheets from Ca$_V$δ are folded back beneath the Cache4 domain at more than 90 Å from the plasma membrane. Of the 16 potential sites, 14 glycosylation sites were identified in the structure. Only 5 of these sites are facing the extracellular medium (Asn94, Asn186, Asn470, Asn615, and Asn827). The glycans at Asn678 appear to bridge the Cache3 and the Cache2 domains suggesting they could contribute to protein folding. Disruption of this site in the rat isoform significantly decreased protein stability (Tetreault et al. 2016). The six novel disulfide bridges (C305–C1047, C356–C1062, C406–C1074, C907–C977, C999–C1029, and C1002–C1027 in the rabbit isoform) differ significantly from the residues previously identified in the rat isoform through mutational analysis (Calderon-Rivera et al. 2012). Additionally, the cryo-EM structure shows multiple contact areas between the Cache1, VWA and Cache2 domains of Ca$_V$α2δ1 and the extracellular loops of repeat I and III of Ca$_V$α1. It can be speculated that the arrhythmogenic mutations of Ca$_V$α2δ1 either directly alter protein trafficking and cell surface expression or indirectly modify the protein interface it shares with Ca$_V$α1. The latter will be better pursued using structural biology methods.

5 Perspectives

The L-type Ca$_V$1.2 channel uniquely controls Ca^{2+} influx and contributes to cardiac rhythmicity (Bodi et al. 2005). Genetic mutations in the proteins forming the Ca$_V$1.2 complex have been associated with alterations in the repolarization interval that ultimately lead to sudden cardiac death (Burashnikov et al. 2010). The molecular basis for these clinical manifestations is still being studied (Bourdin et al. 2015; Antzelevitch et al. 2007). The 3-D structure of the related Ca$_V$1.1 channel complex, solved by cryo-EM (Wu et al. 2016), is improving significantly our understanding of the

protein interaction network. This is especially important for the integrin-like $Ca_V\alpha2\delta1$ subunit that appears to display a unique 3-D structure. This discovery will provide a mechanistic basis to understand the contribution of $Ca_V\alpha2\delta1$ to cardiac dysfunctions and will open the door for the development of new drugs aimed at regulating the cell surface expression of the $Ca_V1.2$ channel complex.

Acknowledgments This work was supported by a grant from the Natural Sciences and Engineering Research Council of Canada to LP

Conflict of Interest The authors declare that they have no conflict of interest

Ethical Approval This article does not contain any studies with human participants or animals performed by any of the authors

Disclosures NONE

References

Andrade A, Sandoval A, Oviedo N, De Waard M, Elias D, Felix R (2007) Proteolytic cleavage of the voltage-gated Ca^{2+} channel alpha2delta subunit: structural and functional features. Eur J Neurosci 25(6):1705–1710. doi:10.1111/j.1460-9568.2007.05454.x

Antzelevitch C, Pollevick GD, Cordeiro JM, Casis O, Sanguinetti MC, Aizawa Y, Guerchicoff A, Pfeiffer R, Oliva A, Wollnik B, Gelber P, Bonaros EP Jr, Burashnikov E, Wu Y, Sargent JD, Schickel S, Oberheiden R, Bhatia A, Hsu LF, Haissaguerre M, Schimpf R, Borggrefe M, Wolpert C (2007) Loss-of-function mutations in the cardiac calcium channel underlie a new clinical entity characterized by ST-segment elevation, short QT intervals, and sudden cardiac death. Circulation 115(4):442–449. doi:10.1161/CIRCULATIONAHA.106.668392

Berrou L, Klein H, Bernatchez G, Parent L (2002) A specific tryptophan in the I-II linker is a key determinant of beta-subunit binding and modulation in $Ca_V2.3$ calcium channels. Biophys J 83(3):1429–1442. doi:10.1016/S0006-3495(02)73914-3

Berrou L, Dodier Y, Raybaud A, Tousignant A, Dafi O, Pelletier JN, Parent L (2005) The C-terminal residues in the alpha-interacting domain (AID) helix anchor Ca_V beta subunit interaction and modulation of $Ca_V2.3$ channels. J Biol Chem 280(1):494–505. doi:10.1074/jbc.M410859200

Betzenhauser MJ, Pitt GS, Antzelevitch C (2015) Calcium channel mutations in cardiac arrhythmia syndromes. Curr Mol Pharmacol 8(2):133–142

Bodi I, Mikala G, Koch SE, Akhter SA, Schwartz A (2005) The L-type calcium channel in the heart: the beat goes on. J Clin Invest 115(12):3306–3317. doi:10.1172/JCI27167

Borchard U, Hafner D (2000) Ion channels and arrhythmias. Zeitschrift fur Kardiologie 89(Suppl 3):6–12

Borsotto M, Barhanin J, Fosset M, Lazdunski M (1985) The 1,4-dihydropyridine receptor associated with the skeletal muscle voltage-dependent Ca^{2+} channel. Purification and subunit composition. J Biol Chem 260(26):14255–14263

Bourdin B, Marger F, Wall-Lacelle S, Schneider T, Klein H, Sauve R, Parent L (2010) Molecular determinants of the Ca_Vbeta-induced plasma membrane targeting of the $Ca_V1.2$ channel. J Biol Chem 285(30):22853–22863. doi:10.1074/jbc.M110.111062

Bourdin B, Shakeri B, Tetreault MP, Sauve R, Lesage S, Parent L (2015) Functional characterization of Ca_Valpha2delta mutations associated with sudden cardiac death. J Biol Chem 290(5):2854–2869. doi:10.1074/jbc.M114.597930

Briot J, D'Avanzo N, Sygusch J, Parent L (2016) Three-dimensional architecture of the L-type calcium channel: structural insights into the $Ca_V\alpha2\delta1$ auxiliary protein. Biochem Mol Biol J 2(3). doi:10.21767/2471-8084.100025

Buraei Z, Yang J (2013) Structure and function of the beta subunit of voltage-gated Ca^{2+} channels. Biochim Biophys Acta 1828(7):1530–1540. doi:10.1016/j.bbamem.2012.08.028

Burashnikov E, Pfeiffer R, Barajas-Martinez H, Delpon E, Hu D, Desai M, Borggrefe M, Haissaguerre M, Kanter R, Pollevick GD, Guerchicoff A, Laino R, Marieb M, Nademanee K, Nam GB, Robles R, Schimpf R, Stapleton DD, Viskin S, Winters S, Wolpert C, Zimmern S, Veltmann C, Antzelevitch C (2010) Mutations in the cardiac L-type calcium channel associated with inherited J-wave syndromes and sudden cardiac death. Heart Rhythm 7(12):1872–1882. doi:10.1016/j.hrthm.2010.08.026

Calderon-Rivera A, Andrade A, Hernandez-Hernandez O, Gonzalez-Ramirez R, Sandoval A, Rivera M, Gomora JC, Felix R (2012) Identification of a disulfide bridge essential for structure and function of the voltage-gated Ca^{2+} channel alpha2delta-1 auxiliary subunit. Cell Calcium 51(1):22–30. doi:10.1016/j.ceca.2011.10.002

Catterall WA (2011) Voltage-gated calcium channels. Cold Spring Harb Perspect Biol 3(8):a003947. doi:10.1101/cshperspect.a003947

Catterall WA, Zheng N (2015) Deciphering voltage-gated Na^+ and Ca^{2+} channels by studying prokaryotic ancestors. Trends Biochem Sci 40(9):526–534. doi:10.1016/j.tibs.2015.07.002

Cordeiro JM, Marieb M, Pfeiffer R, Calloe K, Burashnikov E, Antzelevitch C (2009) Accelerated inactivation of the L-type calcium current due to a mutation in CACNB2b underlies Brugada syndrome. J Mol Cell Cardiol 46(5):695–703

Curtis BM, Catterall WA (1983) Solubilization of the calcium antagonist receptor from rat brain. J Biol Chem 258(12):7280–7283

Curtis BM, Catterall WA (1984) Purification of the calcium antagonist receptor of the voltage-sensitive calcium channel from skeletal muscle transverse tubules. Biochemistry 23(10):2113–2118

Dafi O, Berrou L, Dodier Y, Raybaud A, Sauve R, Parent L (2004) Negatively charged residues in the N-terminal of the AID helix confer slow voltage dependent inactivation gating to $Ca_V1.2$. Biophys J 87(5):3181–3192. doi:10.1529/biophysj.104.045559

Davies A, Kadurin I, Alvarez-Laviada A, Douglas L, Nieto-Rostro M, Bauer CS, Pratt WS, Dolphin AC (2010) The alpha2delta subunits of voltage-gated calcium channels form GPI-anchored proteins, a post-translational modification essential for function. Proc Natl Acad Sci U S A 107(4):1654–1659. doi:10.1073/pnas.0908735107

Deller MC, Kong L, Rupp B (2016) Protein stability: a crystallographer's perspective. Acta Crystallogr Sect F Struct Biol Commun 72(Pt 2):72–95. doi:10.1107/S2053230X15024619

Depil K, Beyl S, Stary-Weinzinger A, Hohaus A, Timin E, Hering S (2011) Timothy mutation disrupts the link between activation and inactivation in $Ca_V1.2$ protein. J Biol Chem 286(36):31557–31564. doi:10.1074/jbc.M111.255273

Doerr A (2015) Cryo-Em goes high-resolution. Nat Methods 12(7):598–599

Dragicevic E, Poetschke C, Duda J, Schlaudraff F, Lammel S, Schiemann J, Fauler M, Hetzel A, Watanabe M, Lujan R, Malenka RC, Striessnig J, Liss B (2014) Cav1.3 channels control D2-autoreceptor responses via NCS-1 in substantia nigra dopamine neurons. Brain 137(Pt 8):2287–2302. doi:10.1093/brain/awu131

Fuller-Bicer GA, Varadi G, Koch SE, Ishii M, Bodi I, Kadeer N, Muth JN, Mikala G, Petrashevskaya NN, Jordan MA, Zhang SP, Qin N, Flores CM, Isaacsohn I, Varadi M, Mori Y, Jones WK, Schwartz A (2009) Targeted disruption of the voltage-dependent calcium channel alpha2/delta-1-subunit. Am J Phys Heart Circ Phys 297(1):H117–H124. doi:10.1152/ajpheart.00122.2009

Gaborit N, Steenman M, Lamirault G, Le Meur N, Le Bouter S, Lande G, Leger J, Charpentier F, Christ T, Dobrev D, Escande D, Nattel S, Demolombe S (2005) Human atrial ion channel and transporter subunit gene-expression remodeling associated with valvular heart disease and atrial fibrillation. Circulation 112 (4):471–481. doi:10.1161/CIRCULATIONAHA.104.506857

Gillis J, Burashnikov E, Antzelevitch C, Blaser S, Gross G, Turner L, Babul-Hirji R, Chitayat D (2012) Long QT, syndactyly, joint contractures, stroke and novel CACNA1C mutation: expanding the spectrum of Timothy syndrome. Am J Med Genet A 158A(1):182–187. doi:10.1002/ajmg.a.34355

Halling DB, Georgiou DK, Black DJ, Yang GJ, Fallon JL, Quiocho FA, Pedersen SE, Hamilton SL (2009) Determinants in Ca_V1 channels that regulate the Ca^{2+} sensitivity of bound calmodulin. J Biol Chem 284(30):20041–20051. doi:10.1074/jbc.M109.013326

Hell JW, Westenbroek RE, Warner C, Ahlijanian MK, Prystay W, Gilbert MM, Snutch TP, Catterall WA (1993) Identification and differential subcellular localization of the neuronal class C and class D L-type calcium channel alpha 1 subunits. J Cell Biol 123(4):949–962

Jay SD, Sharp AH, Kahl SD, Vedvick TS, Harpold MM, Campbell KP (1991) Structural characterization of the dihydropyridine-sensitive calcium-channel Alpha-2-subunit and the associated delta-peptides. J Biol Chem 266(5):3287–3293

Kim EY, Rumpf CH, Fujiwara Y, Cooley ES, Van Petegem F, Minor DL Jr (2008) Structures of Ca_V2 Ca^{2+}/CaM-IQ domain complexes reveal binding modes that underlie calcium-dependent inactivation and facilitation. Structure 16(10):1455–1467. doi:10.1016/j.str.2008.07.010

Krause U, Gravenhorst V, Kriebel T, Ruschewski W, Paul T (2011) A rare association of long QT syndrome and syndactyly: Timothy syndrome (LQT 8). Clin Res Cardiol 100(12):1123–1127. doi:10.1007/s00392-011-0358-4

Kryshtal DO, Hwang HS, Johnson CN, Chazin WJ, George AL, Knollmann BC (2015) Divergent regulation of cardiomyocyte Cav1.2 currents by calmodulin mutants associated with human sudden death syndromes. Biophys J 108(2):580A

Leung AT, Imagawa T, Campbell KP (1987) Structural characterization of the 1,4-dihydropyridine receptor of the voltage-dependent Ca^{2+} channel from rabbit skeletal muscle. Evidence for two distinct high molecular weight subunits. J Biol Chem 262(17):7943–7946

Limpitikul WB, Dick IE, Joshi-Mukherjee R, Overgaard MT, George AL Jr, Yue DT (2014) Calmodulin mutations associated with long QT syndrome prevent inactivation of cardiac L-type Ca^{2+} currents and promote proarrhythmic behavior in ventricular myocytes. J Mol Cell Cardiol 74:115–124. doi:10.1016/j.yjmcc.2014.04.022

Long SB, Campbell EB, MacKinnon R (2005) Crystal structure of a mammalian voltage-dependent Shaker family K^+ channel. Science 309(5736):897–903. doi:10.1126/science.1116269

Mangoni ME, Couette B, Bourinet E, Platzer J, Reimer D, Striessnig J, Nargeot J (2003) Functional role of L-type Cav1.3 Ca^{2+} channels in cardiac pacemaker activity. Proc Natl Acad Sci U S A 100(9):5543–5548. doi:10.1073/pnas.0935295100

Minor DL Jr, Findeisen F (2010) Progress in the structural understanding of voltage-gated calcium channel (CaV) function and modulation. Channels 4(6):459–474. doi:10.4161/chan.4.6.12867

Napolitano C, Antzelevitch C (2011) Phenotypical manifestations of mutations in the genes encoding subunits of the cardiac voltage-dependent L-type calcium channel. Circ Res 108(5):607–618. doi:10.1161/CIRCRESAHA.110.224279

Parent L, Gopalakrishnan M (1995) Glutamate substitution in repeat IV alters divalent and monovalent cation permeation in the heart Ca^{2+} channel. Biophys J 69 (5):1801–1813. doi:10.1016/S0006-3495(95)80050-0

Platzer J, Engel J, Schrott-Fischer A, Stephan K, Bova S, Chen H, Zheng H, Striessnig J (2000) Congenital deafness and sinoatrial node dysfunction in mice lacking class D L-type Ca^{2+} channels. Cell 102 (1):89–97

Raybaud A, Dodier Y, Bissonnette P, Simoes M, Bichet DG, Sauve R, Parent L (2006) The role of the GX9GX3G motif in the gating of high voltage-activated Ca^{2+} channels. J Biol Chem 281(51):39424–39436. doi:10.1074/jbc.M607405200

Savalli N, Pantazis A, Sigg D, Weiss JN, Neely A, Olcese R (2016) The alpha2delta-1 subunit remodels CaV1.2 voltage sensors and allows Ca^{2+} influx at physiological membrane potentials. J Gen Physiol 148(2):147–159. doi:10.1085/jgp.201611586

Scoote M, Williams AJ (2004) Myocardial calcium signalling and arrhythmia pathogenesis. Biochem Biophys Res Commun 322(4):1286–1309. doi:10.1016/j.bbrc.2004.08.034

Shakeri B, Bourdin B, Demers-Giroux PO, Sauve R, Parent L (2012) A quartet of leucine residues in the guanylate kinase domain of Ca_Vbeta determines the plasma membrane density of the Ca_V2.3 channel. J Biol Chem 287(39):32835–32847. doi:10.1074/jbc.M112.387233

Sharp AH, Campbell KP (1989) Characterization of the 1,4-dihydropyridine receptor using subunit-specific polyclonal antibodies – evidence for a 32,000-Da-subunit. J Biol Chem 264(5):2816–2825

Sharp AH, Imagawa T, Leung AT, Campbell KP (1987) Identification and characterization of the dihydropyridine-binding subunit of the skeletal muscle dihydropyridine receptor. J Biol Chem 262(25):12309–12315

Simms BA, Zamponi GW (2012) The Brugada syndrome mutation A39V does not affect surface expression of neuronal rat Cav1.2 channels. Mol Brain 5:9. doi:10.1186/1756-6606-5-9

Sivagangabalan G, Nazzari H, Bignolais O, Maguy A, Naud P, Farid T, Masse S, Gaborit N, Varro A, Nair K, Backx P, Vigmond E, Nattel S, Demolombe S, Nanthakumar K (2014) Regional ion channel gene expression heterogeneity and ventricular fibrillation dynamics in human hearts. PLoS One 9(1): e82179. doi:10.1371/journal.pone.0082179

Snutch TP, Reiner PB (1992) Ca^{2+} channels: diversity of form and function. Curr Opin Neurobiol 2(3):247–253

Splawski I, Timothy KW, Sharpe LM, Decher N, Kumar P, Bloise R, Napolitano C, Schwartz PJ, Joseph RM, Condouris K, Tager-Flusberg H, Priori SG, Sanguinetti MC, Keating MT (2004) Ca_V1.2 calcium channel dysfunction causes a multisystem disorder including arrhythmia and autism. Cell 119(1):19–31. doi:10.1016/j.cell.2004.09.011

Splawski I, Timothy KW, Decher N, Kumar P, Sachse FB, Beggs AH, Sanguinetti MC, Keating MT (2005) Severe arrhythmia disorder caused by cardiac L-type calcium channel mutations. Proc Natl Acad Sci U S A 102(23):8089–8096. doi:10.1073/pnas.0502506102. discussion 8086–8088.

Takahashi M, Seagar MJ, Jones JF, Reber BFX, Catterall WA (1987) Subunit Structure of Dihydropyridine-Sensitive Calcium Channels from Skeletal-Muscle. Proc Natl Acad Sci U S A 84(15):5478–5482. doi:10.1073/Pnas.84.15.5478

Tanabe T, Takeshima H, Mikami A, Flockerzi V, Takahashi H, Kangawa K, Kojima M, Matsuo H, Hirose T, Numa S (1987) Primary structure of the receptor for calcium channel blockers from skeletal muscle. Nature 328(6128):313–318. doi:10.1038/328313a0

Tang L, Gamal El-Din TM, Payandeh J, Martinez GQ, Heard TM, Scheuer T, Zheng N, Catterall WA (2014) Structural basis for Ca^{2+} selectivity of a voltage-gated calcium channel. Nature 505(7481):56–61. doi:10.1038/nature12775

Tang L, El-Din TM, Swanson TM, Pryde DC, Scheuer T, Zheng N, Catterall WA (2016) Structural basis for inhibition of a voltage-gated Ca^{2+} channel by Ca^{2+} antagonist drugs. Nature. doi:10.1038/nature19102

Templin C, Ghadri JR, Rougier JS, Baumer A, Kaplan V, Albesa M, Sticht H, Rauch A, Puleo C, Hu D, Barajas-Martinez H, Antzelevitch C, Luscher TF, Abriel H, Duru F (2011) Identification of a novel loss-of-function calcium channel gene mutation in short QT syndrome (SQTS6). Eur Heart J 32(9):1077–1088. doi:10.1093/eurheartj/ehr076

Tetreault MP, Bourdin B, Briot J, Segura E, Lesage S, Fiset C, Parent L (2016) Identification of glycosylation sites essential for surface expression of the Ca_Valpha2delta1 subunit and modulation of the cardiac Ca_V1.2 channel activity. J Biol Chem 291(9):4826–4843. doi:10.1074/jbc.M115.692178

Van Petegem F, Chatelain FC, Minor DL (2005) Insights into voltage-gated calcium channel regulation from the structure of the Ca_V1.2 IQ domain-Ca^{2+}/calmodulin complex. Nat Struct Mol Biol 12(12):1108–1115. doi:10.1038/nsmb1027

Van Petegem F, Duderstadt KE, Clark KA, Wang M, Minor DL Jr (2008) Alanine-scanning mutagenesis defines a conserved energetic hotspot in the Ca_Valpha1 AID-Ca_Vbeta interaction site that is critical for channel modulation. Structure 16(2):280–294. doi:10.1016/j.str.2007.11.010

Wu J, Yan Z, Li Z, Yan C, Lu S, Dong M, Yan N (2015) Structure of the voltage-gated calcium channel Cav1.1 complex. Science 350(6267):aad2395. doi:10.1126/science.aad2395

Wu J, Yan Z, Li Z, Qian X, Lu S, Dong M, Zhou Q, Yan N (2016) Structure of the voltage-gated calcium channel Cav1.1 at 3.6 a resolution. Nature. doi:10.1038/nature19321

Yazawa M, Hsueh B, Jia X, Pasca AM, Bernstein JA, Hallmayer J, Dolmetsch RE (2011) Using induced pluripotent stem cells to investigate cardiac phenotypes in Timothy syndrome. Nature 471(7337):230–234. doi:10.1038/nature09855

Adv Exp Med Biol - Protein Reviews (2017) 2:65–92
DOI 10.1007/5584_2017_58

Published online: 22 June 2017

Histone Post-Translational Modifications and Nucleosome Organisation in Transcriptional Regulation: Some Open Questions

Josefa Castillo, Gerardo López-Rodas, and Luis Franco

Abstract

The organisation of chromatin is first discussed to conclude that nucleosomes play both structural and transcription-regulatory roles. The presence of nucleosomes makes difficult the access of transcriptional factors to their target sequences and the action of RNA polymerases. The histone post-translational modifications and nucleosome remodelling are first discussed, from a historical point of view, as mechanisms to remove the obstacles imposed by chromatin structure to transcription. Instead of reviewing the state of the art of the whole field, this review is centred on some open questions. First, some "non-classical" histone modifications, such as short-chain acylations other than acetylation, are considered to conclude that their relationship with the concentration of metabolic intermediaries might make of them a sensor of the physiological state of the cells. Then attention is paid to the interest of studying chromatin organisation and epigenetic marks at a single nucleosome level as a complement to genome-wide approaches. Finally, as a consequence of the above questions, the review focuses on the presence of multiple histone post-translational modifications on a single nucleosome. The methods to detect them and their meaning, with special emphasis on bivalent marks, are discussed.

Keywords

Chromatin • Nucleosome • Epigenetics • Histone post-translational modifications • Metabolism and histone modifications

J. Castillo, G. López-Rodas, and L. Franco (✉)
Department of Biochemistry and Molecular Biology and Institute of Health Research INCLIVA, University of Valencia, Valencia, Spain
e-mail: luis.franco@uv.es

Abbreviations

BRD	bromodomain
ChIP	chromatin immunoprecipitation

HAT	histone acetyltransferase
HDAC	histone deacetylase
HP1	heterochromatin protein 1
MNP	micrococcal nuclease protection
NFR	nucleosome-free region
PCR	polymerase chain reaction
PHD	plant homeodomain
PTM	post-translational modification
RT-qPCR	real time quantitative PCR
TG	transglutaminase
TPA	12-*O*-tetradecanoylphorbol-13-acetate
TSS	Transcription start site
YEATS	YNL107w, ENL, AF-9, and TFIIF small subunit
ZMYND8	zinc finger MYND (Myeloid, Nervy and DEAF-1)-type containing 8

1 Introduction

Eukaryotic nuclear DNA is not naked, but organized in chromatin, a complex in which histones and non-histone proteins, as well as some RNA molecules, are packed with DNA in nuclei. A somatic human cell, for instance, contains almost 2 m DNA within a nucleus of around 10 μm diameter at the most. It seems evident that this enormous compaction is an obstacle that the nuclear machinery has to surmount to play all the functions required for cell survival: replication, transcription, reparation and recombination of DNA. The present review deals with the mechanisms involved in allowing eukaryotic transcription to occur within the frame of a chromatin context. It will be centred in mammalian genes transcribed by RNA polymerase II and, rather than being a comprehensive review, particular attention will be paid to some open questions. It should be emphasized from the very beginning that, in spite of the above statement on the obstacles that chromatin structure raises to the action of RNA polymerases, chromatin plays a dualistic regulatory role. Its organisation may either repress or allow transcription often in a reversible way and, therefore, chromatin has to be considered as a highly dynamic regulatory complex. The present article starts by a brief account on how the chromatin structure interferes with the action of RNA pol II and how the difficulties are surmounted. These questions are presented from a historical perspective and then we focus on some issues that are attracting a deep attention.

2 The Landscape of Eukaryotic Transcription

The study of eukaryotic transcription would be senseless without considering the landscape in which it occurs, the chromatin. Histones are the main protein counterpart of DNA in chromatin, from both a quantitative and a functional point of view. A histone octamer made by two copies of each inner histones, namely H2A, H2B, H3 and H4, forms a tripartite structure (Arents et al. 1991), around which 147 bp of DNA were subsequently docked into 1.75 left-handed superhelical turns to yield the first atomic-level model of the nucleosome core, the structural unit of chromatin (Arents and Moudrianakis 1993). The co-crystal structure of the nucleosome core particle was subsequently solved (Luger et al. 1997). The results of this newer study contributed the following significant new specific information about nucleosome organisation. A variable length of linker DNA connects successive nucleosome cores. H1 (H5 in some cells), a fifth histone molecule, interacts with 20 bp of linker DNA at the entrance and exit of some nucleosome cores to form the chromatosome (Simpson 1978). While the structure of the nucleosome core crystals are known to a great detail, for the chromatosome, which has not been crystallized to date, only models for its structure have been described. A short but comprehensive review on nucleosome structure, including some chromatosome models, has been recently published and the interested reader is referred to it for details (Cutter and Hayes 2015).

The presence of nucleosomes gives to the chromatin fibres, when observed through the

electron microscope at low ionic strength, the classical appearance of "beads on a string". This aligned arrangement of nucleosomes constitutes the first level of chromatin structure. Increasing ionic strength results in the folding of chromatin, which acquires the appearance of a 30 nm fibre (van Holde 1989), often referred to as the secondary level of chromatin structure (Sajan and Hawkins 2012). Starting with the solenoidal model of Finch and Klug (Finch and Klug 1976), several possibilities have been proposed for the structure of this fibre, but the actual existence of the 30 nm *in vivo* remains a controversial issue. It has been suggested that, while 30 nm fibres may occur in the diluted chromatin solutions required for experimental analyses, the highly compacted chromatin within the nuclei adopts a disordered and interdigitated state (Eltsov et al. 2008). This and other experimental results have made the very existence of the 30 nm fibre *in vivo* a somewhat contested question (Grigoryev and Woodcock 2012; Li and Zhu 2015) and pose some doubts as to the actual interest of a debate on the structure of chromatin in diluted solutions, which would be mainly of academic interest. At any rate, the N-terminal tails of histones play a fundamental role in maintaining the internucleosomal interactions that stabilize the secondary structure of chromatin. When the nucleosome structure was described at 2.8 Å resolution, Richmond and his colleagues noticed that the 16–25 segment of the H4 tail, which contains a succession of basic amino acid residues, binds to the flat face of a neighbour nucleosome core in the crystal lattice. The binding is facilitated by the presence of a cluster of acidic amino acids in the H2A/H2B dimer surface, and the authors advanced that these interactions might take place in nuclei to stabilize chromatin superstructure (Luger et al. 1997). Some years later, an elegant piece of work from the same group showed that deletion of the H4 N-terminus dramatically destabilizes the folding of nucleosome arrays and they were able to identify residues 14–19 as responsible for acquisition of superstructure (Dorigo et al. 2003).

Due to the above reasons, the *in situ* structural organisation of chromatin within the nucleus is attracting more attention. It was early assumed that the 30 nm fibre –or their alternative secondary structures– is progressively folded to yield more compact structures (for a review, see (Maeshima et al. 2014)). It has been proposed that the different chromatin domains are organised in loops, often referred to as the tertiary level of compaction, but these loops do not represent a unique possibility for this structural level, because interdigitating layers of irregularly oriented nucleosomes have also been proposed to occur in interphase nuclei (Sajan and Hawkins 2012).

Curiously enough, the use of several electron microscopy techniques applied to the study of metaphasic chromosomes, which represent the state of highest compaction of chromatin, has prompted Daban and his colleagues to propose the "thin-plate" model. Layers of planar chromatin are organised perpendicular to the chromosome axis and nucleosomes would be irregularly disposed within these plates (Gállego et al. 2009; Daban 2015). If interdigitating layers of nucleosomes actually exist in interphase chromatin, the transition to metaphasic chromosomes would be easily explained.

It is within this complex landscape that eukaryotic transcription occurs. To do this, RNA polymerase has to bind DNA at the transcription start site (TSS) to form the pre-initiation complex together with the basal transcriptional factors. Then, to start transcription, RNA pol II has to unwind the DNA double helix and to process along the template chain. The presence of nucleosomes obstructs all these steps, and the binding of transcriptional factors to DNA, which often circularly embrace the double helix contour, also may be hindered by the presence of a nucleosome. Nevertheless, in many instances, nucleosomes are placed on the TSS or cover the *cis* regulatory sites, and the gene bodies always display a nucleosomal organisation. For transcription to occur it is, then, necessary that the nucleosomes be eliminated, displaced or structurally reorganised. This is achieved through two interconnected processes: epigenetic modifications and nucleosome remodelling.

3 Removing the Obstacles

The post-translational modification (PTM) of histones was first described more than 50 years ago in the seminal paper by Allfrey et al. (Allfrey et al. 1964). The authors described the acetylation and the methylation of the amino groups of the lysine side chains. They remarked that, as the acetamide group generated by lysine acetylation is not charged, this modification would loosen the interactions between histones and DNA. Histones were considered as repressors of transcription, and so it was assumed that their acetylation may result in a transcriptional activation. On the contrary, histone methylation does not modify the charge of lysyl residues and the relevance of this modification was passed over at the moment. The interest in histone acetylation as a possible activator of transcription led researchers to discover the fundamentals of histone acetylation. The acetyl group is transferred from acetyl-CoA to histones in a reaction catalysed by histone acetyltransferases (HATs) and hydrolytically removed by the histone deacetylases (HDACs). Nevertheless, research on histone acetylation experienced an impasse until 1988, when Peter Loidl proposed a signalling role for this PTM. The author emphasized that the specific acetylation of some residues may represent "*a distinct signal for induction or maintenance of certain structural features of chromatin*". Of course, not all the combinations of acetylated lysines ought to be meaningful, but some examples were provided by the author in support of the model, assuming that site specificity of histone acetylation would drive chromatin to transcription, replication or differentiation (Loidl 1988).

The Loidl's model implied that the enzymes involved in histone acetylation and deacetylation should be multiple, histone- and site-specific. The multiplicity of HATs was first described in our laboratory, working with the yeast *Saccharomyces cerevisiae*. We found at least three, chromatographically resolved, nuclear HATs, which displayed different histone specificity (López-Rodas et al. 1989, 1991a) and these results were soon extended to other organisms (López-Rodas et al. 1991b; Georgieva et al. 1991). HDACs also proved to display a limited multiplicity, associated with histone specificity (Sendra et al. 1988, 1991). It was also soon checked that HATs were not only histone-specific, but also site-specific. These and other findings aroused a great interest in cloning nuclear HAT genes, a goal which was first achieved in David Allis' laboratory working with the ciliate *Tetrahymena thermophila*. The results were of exceptional interest, because the cloned gene was homologous to yeast *Gcn5*, which codes for a protein known as a transcriptional activator (Brownell et al. 1996), thus establishing a direct link between histone acetylation and transcriptional activation.

Almost contemporarily to the cloning of the *Tetrahymena* HAT, the cloning of a human HDAC was also reported (Taunton et al. 1996), and since this pioneering work many HAT and HDAC genes from a wide variety of eukaryotes were cloned and characterized. Nuclear HATs may be grouped into five families, based on sequence similarity (for a recent review, see (Wapenaar and Dekker 2016)), while the 18 HDACs described to date are grouped in 4 classes, one of them, class 2, comprising two subclasses (Haery et al. 2015). The seven members of class 3 are called sirtuins, after the first one characterized coded by the yeast *Sir2* (silent mating-type information regulation 2) gene (Rine and Herskowitz 1987).

HDACs and HATs are involved in a complex network of interactions with many other cellular components. It is not the purpose of the present paper to analyze in detail the nature and properties of the HAT and HDAC complexes, and the reader may find useful data in some recent reviews (Haery et al. 2015; Wang and Dent 2014; Yang 2015; Su et al. 2016a). Both, HATs and HDACs, possess functional domains that enable them to interact with many other regulatory proteins, so the possibility exists that the components of the complexes change from cell to cell and from one physiological situation to another.

Histone methylation attracted at first less attention. This PTM, which occurs at the side chains of lysine and arginine, does not eliminate the positive charge of these residues and it was, therefore, supposed that it did not modify the histone-DNA interactions. Moreover, the enzymes involved in this histone modification, especially those catalysing removal of methyl groups, proved to be refractory to research. The landscape of histone methylation changed around the end of the last century, mainly due to the work in Allis' laboratory (Strahl et al. 1999, 2001). The ε-amino group of lysines may be mono- di- or trimethylated, whereas the guanidinium group of arginines can be mono- and dimethylated *in vivo*. In the last instance, methyl groups may be added symmetrically (*i.e.*, in each of the nitrogen atoms) or asymmetrically (both methyl groups in the same nitrogen). The reaction of methylation is catalysed by protein methyltransferases or histone methyltransferases and uses S-adenosylmethionine as methyl donor.

While histone acetylation was, and still is, associated with transcriptional activation, histone methylation may play activating or repressing roles depending upon the histone and residue modified as first shown by Noma et al. (2001), working with the pericentromeric loci in the yeast *Saccharomyces cerevisiae*. The subsequent discovery of histone demethylases (Shi et al. 2004) definitively raised the interest on this histone modification. There are two classes of lysine demethylases, the FAD-dependent enzymes, to which the first histone demethylase belongs, and the Jumonji-type family. The catalytic mechanism of the latter enzymes requires a 2-oxoglutarate dependent oxidation of methyllysines (for a recent review, see (Nowak et al. 2016)).

Some of these facts, together with knowledge that histones, like many other proteins, may be reversibly phosphorylated at serine or threonine residues, induced Strahl and Allis, extending the Loidl's signalling hypothesis (Loidl 1988), to propose that "*multiple histone modifications, acting in a combinatorial or sequential fashion on one or multiple histone tails, specify unique downstream functions*" (Strahl and Allis 2000). This proposal was designated by the authors as the "histone code hypothesis" and, albeit it cannot be understand in a univocal way (Rando 2012) and PTMs of histones seem to operate in a much complex way than first envisaged (Rothbart and Strahl 2014), it had the undeniable merit of raising the interest on histone modifications to the level in which now stands. Some of the histone PTMs have been shown to be heritable, at least through mitotic division, and in this way they fulfil the criteria to be considered, together with DNA methylation at cytosine rings, as epigenetic modifications. In fact, nowadays the adjective epigenetic refers to those mitotically and/or meiotically heritable phenotypic traits that result from changes in gene expression without alterations in the DNA sequence (Berger et al. 2009; Rodríguez-Paredes and Esteller 2011).

Taking into account that there are two copies of each histone in a nucleosome, the PTMs may be symmetrical or asymmetrical. In the former case, both copies of the histone harbour the same modification; in the latter, either one copy is modified and the other is not, or each histone molecule has a different PTM. We will deal with this question later.

For PTMs of histones to play a regulatory role, they have to be reversible. To use a terminology that has gained relevance, mechanisms must exist not only to "*write*", but also to "*erase*" them. Of course, the reversibility of histone PTMs may also result from histone turnover, although this process would be more time-consuming than an enzyme-catalysed removal of the epigenetic mark. But, obviously, writing and erasing do not suffice if histone PTMs have to play a signalling role. Strahl and Allis named one of the headings of their paper as "*How is the histone code read?*", the subsequent one being "*Who reads the code?*" (Strahl and Allis 2000). A great progress has been made in identifying the "*readers*", protein molecules carrying one or several domains capable of specifically interacting with a given epigenetic mark or with a combination of marks. Plant homeodomains (PHD) and ATRX-DNMT3-DNMT3L domains

interact with unmodified lysine residues. Bromodomains (BRD) are the classical readers of acetylated lysines and the YNL107w, ENL, AF-9, and TFIIF small subunit (YEATS) domains also have recently proven to play this role. Ankyrin repeats, chromodomains, PHDs, bromo-adjacent homology domains, malignant brain tumour domains, ZF-CW, Pro-Trp-Trp-Pro (PWWP) domains, ATRX-DNMT3-DNMT3L domains and Tudor domains, recognize methylated lysines, the latter two being also able to interact with methylated arginine, together with triptophan-aspartic acid repeats, which also read both, methylated and unmodified lysine side chains (Rothbart and Strahl 2014; Su and Denu 2016). It has been recently proposed that some readers, for instance the heterochromatin proteins HP1-α, HP1-β and M-phase phosphoprotein 8, which contain a chromodomain, the histone lysine methyltransferase WHSC1L1, in which a PWWP domain is present, and the Tudor-containing proteins PHF19 and 53BP1 may be phosphorylated at a tyrosyl residue and that this modification alters or even suppress their capacity to recognise methylated histone residues (Irving-Hooper and Binda 2015). In this way, a possibility to regulate recognition of histone PTMs by the corresponding readers has been opened, and this offers more and more versatility to the histone code.

As mentioned above, histone acetylation is usually associated with transcriptionally active chromatin. When this PTM occurs in the N-terminal tails of histones, the neutralization of their positive charges results in loosening the internucleosomal interactions that stabilize higher order structures. Of course, this facilitates transcription, but the presence of nucleosomes may still represent an obstacle for the accession of the transcriptional machinery and transcriptional factors to DNA.

For many years this question was the most serious challenge the chromatin researchers have to face, but it began to be solved by the end of the last century, by a series of initially non-connected experiments, which ended in the discovery of the yeast SWI/SNF remodelling complex. One of the components of this complex, namely Swi2p/Snf2p is an ATPase stimulated by DNA (Laurent et al. 1993) and hydrolysis of ATP provides the energy required to alter the stable structure of nucleosomes. In the subsequent years, more remodelling complexes were described. All of them are formed by an ATPase molecule, accompanied by several regulatory proteins, and they are grouped into four families according to the nature of the ATPase molecule: SWI/SNF, ISWI (imitation of SWI), CHD (chromodomain helicase DNA-binding) and INO80, which have been found in almost all eukaryotes examined to date (for a recent review, see (Längst and Manelyte 2015)). Remodellers may promote the sliding of the histone octamer along the DNA, the loosening of the histone-DNA contacts, the eviction of H2A-H2B dimers or the eviction of the whole octamer. These events make accessible the DNA sequences to transcriptional factors, to RNA pol II and associated factors, to mediator complexes or to any other DNA-interacting molecule required for regulated transcription.

Either the ATPase molecules or their regulatory partners in remodelling complexes possess epigenetic reader domains, as well as domains capable of interacting with whole nucleosomes or naked DNA. In this way, the remodellers may act in combination with epigenetic modifiers to direct their action to specific nucleosomes. On these grounds, it can be understood how the position occupied by a given nucleosome contributes decisively to the regulation of transcription. A nucleosome may be positioned in such a way that hinders transcription, but after the coordinate action of epigenetic modifiers and remodellers the obstacle may be removed. Conversely, these coordinate actions may be used to repress transcription, so remodelling machines are often necessary for both, activation and repression of genes.

It is within this frame of chromatin structure, epigenetic modifications and nucleosome remodelling that eukaryotic transcription occurs. Much has been done in the last decades to unravel these complex relationships, but in spite of all those efforts, much more is still to solve.

The following sections deal with some of these questions.

4 Are all the Histone Post-Translational Modifications Meaningful?

4.1 Histone PTMs: Much More Than Acetylation, Methylation and Phosphorylation

If any database is searched for histone PTMs, most of the results retrieved will deal with methylation and acetylation at their N-termini, followed by those describing phosphorylation of serine and threonine side chains. Nevertheless, many other histone PTMs have been described. For instance, histones can be ubiquitinated, sumoylated, ADP-ribosylated, citrullinated and glycosylated and a reasonably high number of articles may be found on these items. These PTMs have been dealt with, especially from the point of view of the complex relationships among the different epigenetic marks, in several recent and excellent reviews (see, for instance, (Rothbart and Strahl 2014; Su and Denu 2016; Lawrence et al. 2016; Noh et al. 2016)) and they will not be further commented here. Reports on other PTMs, such as proline isomerisation, formylation, butyrylation, malonylation, succinylation, glutathionylation, glutarylation, 2-hydroxyisobutyrylation, tyrosine hydroxylation and histidine phosphorylation are found in literature to a lesser degree. Novel PTMs or novel sites for classical modifications are being continuously described, especially through mass spectrometry (MS) methods.

Tan et al., by means of an integrated, mass spectrometry-based proteomics approach, reported in 2011 the occurrence of 67 previously non-described modifications. Most of them corresponded to novel sites for "old" modifications, several of them occurring within the inner residues of the histone octamer, but a novel modification, namely crotonylation of lysine residues (Tan et al. 2011) was described. A question immediately arises in view of this great wealth of histone PTMs: are all of them functionally meaningful? We will try to provide an answer for some of these PTMs in the following paragraphs. In so doing, it is necessary to keep in mind that for a PTM to be functionally significant, apart from writers of this modification, the existence of erasers and of readers would be convenient if that PTM plays a regulatory, reversible role. By saying "convenient" we mean that the existence of erasers may be circumvented by the passive removing of the modification by histone turnover and the existence of readers is not necessary if a given PTM interferes with the acquisition of another mark with a different function (Schmitges et al. 2011).

All five histones are formylated at some of their lysyl residues, but this modification results from a non-enzymatic reaction after damage of DNA (Jiang et al. 2007) and, although the possibility that an enzyme-driven formylation using formyl-tetrahydrofolate cannot be discarded (Lin et al. 2012), the hypothetical enzyme involved has not been identified. Due to the absence of definite writers, erasers and readers, and of a clear role for histone formylation, this PTM will not be further considered in the present review.

Aminylation also represents a controversial histone PTM. That neologism defines the covalent binding of primary amines to protein glutaminyl residues by the reaction catalysed by transglutaminases (TGs) (Lai et al. 2016), an acyl transfer reaction in which the γ-carboxamide group of a glutamine residue in a protein acts as acyl donor and several primary amines may act as acceptors. The side chain of glutamine results linked to the amine through a secondary amide bond, with the release of ammonia. Tissue transglutaminase (TG2), the most abundant animal TG, is present in various subcellular locations, including nuclei (for a review, see (Kuo et al. 2011)), and all four core histones are excellent glutaminyl substrates for TG2 *in vitro* and 9 out of their 18 glutamines incorporate polyamines. When nucleosomes were used as substrates, only two glutamines from the N-terminus of H3 and one of H2B are modified (Ballestar et al. 1996).

Several attempts to detect whether incorporation of polyamines to histones take place *in vivo* have been done and a model in which polyamination of H3 leads to chromatin compaction by increasing the positive charge of the histone tail (McConoughey et al. 2010; Basso and Ratan 2013) has been proposed. Nevertheless, the actual existence of polyaminated H3 *in vivo* has not yet been demonstrated, nor has the existence of a proper eraser, catalysing an ammoniolytic reaction to restore the glutaminyl residue of the histones. Probably, aminylation cannot be yet included among the *bona fide* histone functional PTMs.

4.2 Short-Chain Acylations Other Than Acetylation

Histone crotonylation affects lysines in all the four inner histones and linker histone H1. There are 21 crotonylation sites in human inner histones (Tan et al. 2011), most of them residing in the N- or C-termini of the histones that project out of the globular region of the histone octamer. Genome-wide studies also allowed Tan et al. to conclude that crotonylation mainly takes place at both sides of the TSS in active genes (Tan et al. 2011) and similar results were obtained by Sabari et al. when studying the localization of H3K18Cr (Sabari et al. 2015).

The p300 HAT catalyses the crotonylation *in vitro* of both H3 and H4 using crotonyl-CoA as acyl donor and genome-wide approaches show that peaks of H3K18Cr map together with p300, so it is probable that the enzyme be also responsible for *in vivo* crotonylation. p300, then, is able to transfer either acetyl or crotonyl groups to histones, the choice between them depending on the relative concentration of both acyl donors (Sabari et al. 2015). Therefore, this histone PTM is related to the metabolic state of the cell, a question that will be dealt with later.

Sirtuins 1, 2 and 3 are able to remove crotonyl marks from histone peptides *in vitro*, and there are some indications that Sirt3 may be able to do so *in vivo*, because knocking down the *SIRT3* gene in HeLa cells results in the increase of global crotonylated histones and of H3K4Cr (Bao et al. 2014). Moreover, ChIP analyses with a pan anti-KCr antibody in some selected genes, which had been reported to be enriched in Sirt3 in U2OS cells (Iwahara et al. 2012), showed that the level of crotonylated histones increases near their TSSs (Bao et al. 2014).

Human Taf1, which contains two bromodomains, is able to interact with peptides containing crotonyllysine through its second bromodomain (Flynn et al. 2015). In a recent review, Su and Denu remarked that it will be interesting to examine whether the YEATS domain also has the structural plasticity to accommodate longer chain acyl groups (Su and Denu 2016). Recently, this question was positively answered by three independent groups of workers (Andrews et al. 2016; Li et al. 2016; Zhao et al. 2016). Kutateladze and her colleagues have shown that Taf14, one on the components of the yeast transcription factors TFIID and TFIIF that contains a YEATS domain, is the sole H3K9Cr reader in the yeast *Saccharomyces cerevisiae* and that their binding affinity ($K_d = 9.5$ μM) is in the usual range of epigenetic readers (Andrews et al. 2016).

Similar results have been almost simultaneously reported for human AF9 (Li et al. 2016) and YEATS2 a subunit of the HAT ADA Two A-Containing (ATAC) complex (Zhao et al. 2016). AF9 recognizes crotonyllysine with high affinity. The dissociation constant for the crotonylated H3 peptides ranges between 2.1 and 5.7 μM, depending on the particular lysine modified (9 or 18) and the affinity towards the equivalent, acetylated peptides is 2–3 times lower. Other longer acyl derivatives, such as propionyl or butyryl peptides are also recognized by AF9, but the affinity is reduced due to steric constraints. YEATS2 shows a preference for crotonylation in H3K27. The crotonyl-reading activity of AF9 is not limited to crotonylated peptides, because it can also recognize this PTM in nucleosomes, in preference to acetylated nucleosomes. This may explain why AF9 co-localizes with H3K18Cr at actively transcribing loci. Moreover, a YEATS domain-dependent correlation exists between the presence of AF9

and transcription as the mutation F59A, which reduces the affinity of AF9 for crotonyllysine, does not result in gene activation (Li et al. 2016).

Lysine propionylation and butyrylation were first described in 2007 by means of a proteomic approach (Chen et al. 2007), whereas succinylation and malonylation were detected in 2012 by immunological methods and confirmed by MS analyses (Xie et al. 2012). All these four acylations use the corresponding acyl-CoA derivatives, which are important metabolites. Malonylation is the less frequent of these histone PTMs having only been reported to occur in human H2BK116 (Xie et al. 2012), whereas the other three acylations are more widespread among the lysyl residues of the four inner histones (Chen et al. 2007; Xie et al. 2012; Liu et al. 2009; Xu et al. 2014a, b; Goudarzi et al. 2016).

Although these acylations of histones have been studied in some detail in the last years, there are still many unanswered questions. First, only a few data, and often controversial, exist on the nature of the writers of these PTMs. It was first reported that, in contrast to other enzymes tested, such as Tip60, MOF and PCAF, acetyltransferases p300/CBP were able to transfer propionyl groups from its coenzyme A derivative to H4 (Chen et al. 2007) and H3 (Liu et al. 2009) histones *in vitro*. These acetyltransferases also catalyse the *in vitro* butyrylation of histones (Chen et al. 2007) and the reaction also takes place when histone octamers or chromatin templates are used as substrates (Goudarzi et al. 2016). p300/CBP have also been shown to catalyse propionylation of some non-histone proteins *in vivo*, but transfection of human cells with genes encoding MOF, PCAF, Tip60, and HBO1 deacetylases does not enhance the propionylation of proteins (Cheng et al. 2009), a result in accordance with the data of Liu et al. (2009), but conflicting with the results of Leemhuis et al., who found that PCAF may propionylate H3 peptides *in vitro* (Leemhuis et al. 2008). MYST, another HAT belonging to the same family as MOF and Tip60, is able to bind propionyl-CoA and Denu and his colleagues found after a detailed kinetic analysis that, although the K_m is higher than for acetyl-CoA, the k_{cat} is similar for both acyl donors (Berndsen et al. 2007).

Regarding the nature of the writers of succinylation and malonylation of histones, no conclusive data have been yet obtained and, therefore, more research is needed to identify the enzymes responsible for introducing all these histone PTMs.

On the contrary, many reports on the nature of acyl-histone mark erasers have been published. In 2009, Zhang et al. reported that propionylation and butyrylation of yeast histones was enhanced by trichostatin A and sodium butyrate (Zhang et al. 2009). Suberoylanilide hydroxamic acid also enhances butyrylation in neuroblastome (Xu et al. 2014b). These compounds are inhibitors of HDACs from class I and/or II, so these results suggest that these deacetylases may be involved in removing propionyl or butyryl groups from histones.

Nevertheless, sirtuins are the best characterized enzymes catalysing the removal of non-acetyl acyl groups in proteins. It is known since almost 10 years ago that these NAD^+-dependent enzymes may depropionylate bacterial proteins (Garrity et al. 2007) and soon afterwards it was shown that they were also able to remove the propionyl group from an H3 peptide containing modified lysine 23 (Liu et al. 2009). The first evidence for the *in vivo* depropionylating activity of a specific mammalian sirtuin, namely SIRT1, was obtained with non-histone proteins (Cheng et al. 2009), but the most relevant data on the role of sirtuins were obtained in 2011, when it was, almost simultaneously, described that SIRT5 is a demalonylase of non-histone proteins (Peng et al. 2011) and that it has demalonylase and desuccinylase activity towards histone peptides *in vitro* (Du et al. 2011). These authors also suggested that the enzyme may desuccinylate proteins in *vivo*. Based on a 3D structural comparison of human SIRT5, which has a low deacetylating activity, and its orthologous Sir2Tm from *Thermatoga maritima*, which is a potent protein deacetylase, Du et al. reasoned that a peptide containing a lysine acyl derivative carrying an extra carboxyl group

would be a substrate of SIRT5 better than an acetyl peptide. To test this hypothesis, they crystallised a complex of SIRT5 with NAD^+ and a succinyl peptide and showed that, actually, the γ-carboxyl group of the succinyl moiety fits into the SIRT5 substrate pocket (Du et al. 2011).

SIRT5 is also an efficient desuccinylase of non-histone proteins (Sadhukhan et al. 2016), as well as a demalonylase (Du et al. 2011). When using N-terminal H3 peptides modified at the lysine 9 as substrates, the k_{cat}/K_m values for the demalonylation and desuccinylation reaction are, respectively, 6.1 and 4.3×10^3 M^{-1} s^{-1}, a 1000-fold higher than for deacetylation (Du et al. 2011). Consistent with these *in vitro* data is the finding that the level of malonylation of both mitochondrial and cytosolic proteins is much higher in SIRT5 knocked-out mice than in wild-type animals (Nishida et al. 2015).

The above results raise an interesting question. SIRT5 was classically considered as a mitochondrial protein. How is this localization reconciled with the fact that cytosolic proteins are demalonylated by the enzyme? Have the data obtained *in vitro* with histone peptides any functional significance? The answer to these questions is provided taking into account that two SIRT5 isoforms exist. Both of them possess a cleavable mitochondrial signal in their common N-terminus, but the isoform 1-specific C-terminus also contains a cytoplasmic topogenic sequence, which may allow it to be localized in both, mitochondria and cytosol after the N-terminus is cleaved (Matsushita et al. 2011) and the nuclear translocation may occur through the nuclear pores. Actually, the nuclear localization of SIRT5 has recently be demonstrated by western blot analysis of nuclear extracts of livers from wild type and SIRT5 knocked-out mice (Park et al. 2013).

The first report of a reader for propionyllysine was published in 2010, when Vollmuth et al. found that the two bromodomains (BD1 and BD2) of BRD4, a protein from the BET (bromodomain and extraterminal domain) family, were able to bind propionylated peptides, while butyryllysine-containing peptides were much weakly bound. BD2 recognises both acetyllysine ans propionyllysine-containing peptides with comparable affinity, but BD1 is two to threefold more specific for acetyllysine (Vollmuth and Geyer 2010). More recently, Flynn et al. used peptide arrays from the N-terminal region of histone H3 to check the binding of 49 bromodomains (Flynn et al. 2015). Thirty-five out of them were able to bind both, acetyllysine and propionyllysine peptides and those of a subset of bromodomain-containing proteins, namely CECR2, BRD9 and TAF1 not only bind the short propionyl group, but also the larger butyryl chain. As mentioned above, the second bromodomain of TAF1 also recognises crotonyllysine. The analysis of the crystal structure of BRD9 has revealed that the ligand pocket of the bromodomain is flexible enough to accommodate the large butyryl chain with an affinity comparable to that of acetyllysine (Flynn et al. 2015).

There are only a few clues as to the possible functions of the short-chain acylations of histones studied in this section. The propionylation of H3K23 in the leukemia U937 cells decreases during monocytic differentiation, but the acetylation level does not change. This finding led Liu et al. to propose that propionylation level of H3K23 is associated with U937 cell differentiation (Liu et al. 2009). These authors also remarked that, in spite of the similarity in histone acetylation levels among different cell lines, their propionylation levels are markedly different. Taking into account that the writers, erasers and readers of acetylation and propionylation are common (Table 1), these differences among the levels of both histone PTMs might point to a similar and yet distinct role.

The role of histone butyrylation has been recently studied in detail by Goudarzi et al. First, these authors found that the chromatin distribution and dynamic changes of H4K5ac and H4K8ac is clearly different from those of their butyrylated counterparts in mouse spermatogenesis. The use of this biological model allowed them to detect, through genome-wide approaches, that butyrylated H4 maps around TSSs as acetylated H4 does. Although

Table 1 Histone short-chain acylations other than acetylation

Modification	Writers	Erasers	Readers	Function
Crotonylation	p300	SIRT1-3	YEATS domains (Taf14, YEATS2, AF9)	Transcriptional activation
Propionylation	p300/ CBP	Class I and/or II HDACs	Many bromodomains	Differentiation
	MYST	SIRT1		
	PCAF?			
Butyrylation	p300/ CBP	Class I and/or II HDACs	Some bromodomains	Transcriptional activation
		SIRT5		
Malonylation	Unknown	SIRT5	Unknown	Unknown
Succinylation	Unknown	SIRT5	Unknown	Unknown

butyrylation of H4 is also associated with active transcription, it seems to play a role different from that of the acetylated histone, as butyrylation of H4K5, but not of H4K8, inhibits the binding of the bromodomain-containing protein Brdt to H4 acetylated peptides (Goudarzi et al. 2016).

4.3 Distinct Histone Acylation: A Sensor of the Metabolic State of the Cell?

The above results suggest that histone acetylation and other acylations may share similar functions, writers, erasers and readers, although some subtle and yet unresolved differences and competitiveness may be found among these PTMs. Obviously the histone code significance may be considerably enhanced in view of these novel modifications and a deep research will be needed to understand their meaning. Meanwhile, we wish to emphasize that the facts that all the histone PTMs mentioned in the present section use coenzyme A derivatives as acyl donors, that all of them are important metabolites, and that acyl-transfer enzymes may in many cases uses several of them, considerably expand our views on the relationships between metabolism and epigenetic modifications of histones. This issue has been the subject of several recent reviews (see, for instance, (Gut and Verdin 2013; Fan et al. 2015; Su et al. 2016b; Janke et al. 2015)).

As remarked by Lin et al. (2012), the differences in the ratio between histone acetylation and propionylation in several cell lines (Liu et al. 2009) may be simply due to the different concentrations of both acyl donors, acetyl-CoA and propionyl-CoA in the cells. Actually, *in vitro* experiments have shown that the ratio crotonyl-CoA/acetyl-CoA largely determines the level of crotonylation or acetylation of histones (Sabari et al. 2015). In our opinion, this is a crucial question. Of course, taking into account that many different histone acylations occur in nuclei it is obvious that the corresponding acyl-CoA substrates ought to be present in this cell compartment, but the diverse metabolic states of the cells may dramatically change the levels of the different nuclear acyl-CoA.

It is first pertinent to examine the metabolic origin of the different nuclear acyl-CoA molecules. First studies suggested that acetyl-CoA can diffuse across the nuclear pore in *S. cerevisiae* (Takahashi et al. 2006) and this idea has been peacefully extended to all eukaryotes, so it is frequent to speak about the "nucleocytosolic" compartment as opposed to the mitochondrial one when dealing with the distribution of acetyl-CoA. Some data seemed to sustain this assumption. For instance, the linking between the activity of ATP-citrate lyase and histone acetylation (Gut and Verdin 2013) was taken as a proof that the cytosol-generated acetyl-CoA was the substrate for histone acetylation. But, to the best of our belief, the free diffusion of CoA derivatives through the

nuclear pore has not yet been unequivocally proven. Moreover, as recently remarked by Boukouris et al. (2016), the energy of hydrolysis of the acetyl-CoA thioester bond is high enough to make the molecule so unstable that it requires being formed in the location in which it has to be used.

The almost simultaneous discovery that ATP-citrate lyase and acetyl-CoA synthetase (Wellen et al. 2009) as well as carnitine acetyltransferase (Madiraju et al. 2009) are also present in nuclei opened a novel perspective. The first two enzymes are typically cytoplasmatic; ATP-citrate lyase cleaves cytosolic citrate to yield acetyl-CoA and oxalacetate and acetyl-CoA synthetase is able to catalyse the formation of acetyl-CoA from acetate. The reaction of carnitine acetyltransferase, a classical mitochondrial enzyme, also yields acetyl-CoA from acetyl-carnitine. Not only these enzymes are also present in nuclei but a link between them and histone acetylation was found (Wellen et al. 2009; Madiraju et al. 2009). More recently, it has been found that the pyruvate dehydrogenase complex is present in nuclei and that it is functional in catalysing the formation of the acetyl-CoA required for histone modification (Sutendra et al. 2014).

These results provided an answer to the dilemma of the origin of nuclear acetyl-CoA, as aptly discussed in a recent review (Boukouris et al. 2016), because the substrates of the above mentioned enzymes can freely diffuse into nuclei. Nevertheless, they leave many things to solve, for instance, the mechanisms by which the mitochondrial pyruvate dehydrogenase complex is exported to nucleus once the mitochondrial topogenic signal has been removed (Sutendra et al. 2014).

Much less is known about the origin of other nuclear short-chain acyl-CoA derivatives required for the non-acetyl histone PTMs

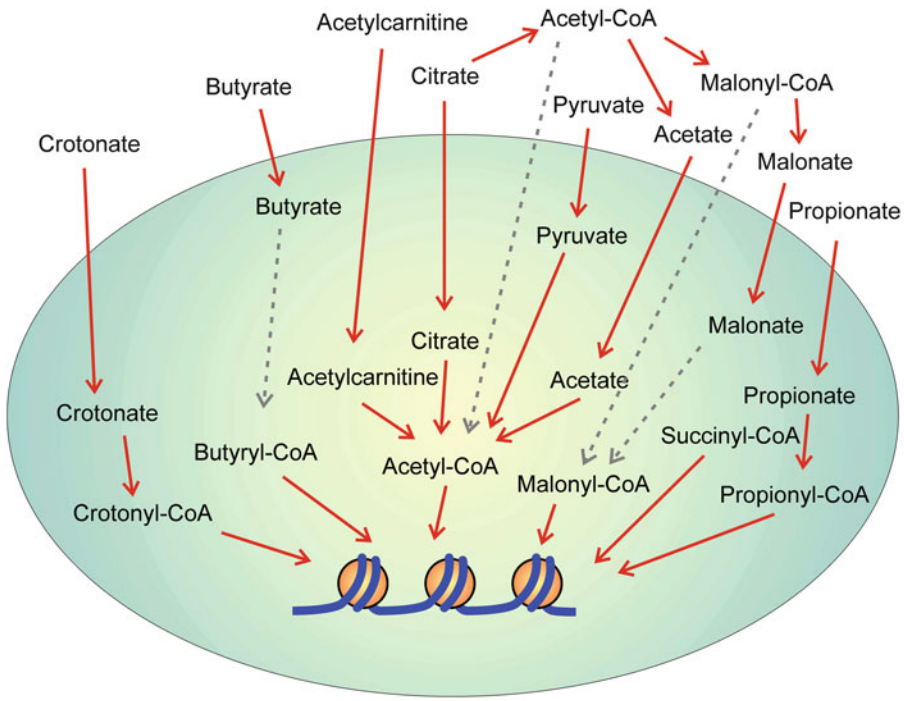

Fig. 1 Possible origin of the different nuclear short-chain acyl-CoA substrates used in histone acylation. The figure shows the relations between the nucleus (large oval) and the cytosol. The experimentally checked reactions are represented by *red arrows* (see the text for details on the corresponding enzymes). The putative reactions, including the translocation of coenzyme A derivatives, are denoted by *dashed*, *gray arrows*

mentioned above. It has been long recognized that acetyl-CoA synthetase accepts some other non-acetate molecules, propionate included, although butyrate is not a substrate for the enzyme (Patel and Walt 1987). It has been proposed, but not proven, that butyryl-CoA may be formed in nuclei at the expense of butyrate. Acyl-CoA synthetase 2, which is present in both, nuclei and cytosol of human HCT116 cells (Wellen et al. 2009) has been shown to catalyse the formation of crotonyl-CoA (Sabari et al. 2015).

The documented origin of nuclear acyl-CoA substrates is depicted in Fig. 1. It remains to be determined the origin of butyryl-, succinyl- and malonyl-CoA, including the possibility of their diffusion through the nuclear pores. At any rate, the metabolic origin of the different acyl-CoAs is different, so their relative concentrations may considerably change in response to the diverse metabolic states of the cells. We have already mentioned that in many instances a HAT enzyme may catalyse the transfer of several acyl groups to histone lysines and that the reaction rate may critically depend on the relative concentration of the donors, but no conclusive data on the possible functional role of the different acylations are available. In this regard, it should be mentioned that the level of both, histone acetylation and methylation depends on dietary factors (Gut and Verdin 2013) and that the epigenetic traits may be transgenerationally inherited (Vollmuth and Geyer 2010), although the mechanisms involved in this process are still controversial (Su et al. 2016b). The above considerations suggest that it would be worth studying in depth the dependence of the different histone acylations on the metabolic state of the cells.

5 From Local to Genome-Wide Approaches and Back Again

5.1 Early Local Studies

Initial studies on nucleosome remodelling and changes in histone PTMs were carried out at the level of selected loci. The indirect end-labelling technique, which was first described to map DNase I hypersensitive sites in *Drosophila* heat shock genes (Wu 1980), was soon adapted, in combination with micrococcal nuclease digestion, to map the accessible linker DNA, and so a picture of nucleosome positioning could be obtained. Although the resolution of the technique was low and it could only be applied to relatively small loci, its application allowed studying transcription-related changes in nucleosome positioning (see, for instance (Pérez-Ortín et al. 1987; Matallana et al. 1992)).

The locus-specific analysis of histone PTMs was possible once the chromatin immunoprecipitation (ChIP) technique started to be used (Crane-Robinson et al. 1997). Fragments of chromatin, obtained by micrococcal nuclease digestion or, more frequently, by sonication, were immunofractionated with antibodies raised against a given histone epigenetic mark. The recovery of immunoprecipitated DNA and its analysis allowed deciding which sequences are occupied by nucleosomes containing that epigenetic mark. In this way, the distribution of histone PTMs along a given gene or locus could be studied. Early methods, especially when chromatin fragments encompassing two or three nucleosomes were used, only gave medium resolution maps of the PTMs distribution, but the ChIP assays proved to be very useful to study transcription-associated changes in histone PTMs and to check the validity and limitations of the histone code hypothesis at the level of single genes or small loci. The ChIP assays may also be directed to locate a non-nucleosomal protein (a transcription factor, or a histone modifying enzyme, for instance) with the use of specific antibodies against that protein.

5.2 The Genomic Era

The advent of the omic approaches allowed analysing many aspects of chromatin structure over the entire genome. The analysis starts as in the single-gene approaches, but the identification of the DNA sequences is carried out by omic techniques, involving microarrays or high-

throughput sequencing and the corresponding bioinformatic treatment of data. The use of these approaches to study nucleosome occupancy, the distribution of histone variants and PTMs, as well as the dynamic changes in them was dealt with in the excellent review of Rando and Chang (2009).

By means of these genome-wide approaches highly valuable data have been obtained. Regarding nucleosome positioning (Zhang and Pugh 2011), it is a common feature in active genes that a nucleosome-free region (NFR) spans the TSS, with nucleosomes positioned both upstream and downstream. These nucleosomes are correlatively designated with minus and plus signs respectively. A recent study has revealed that in mouse embryo stem cells there exist two types of promoters enriched in the epigenetic mark H3K4me3, which differ in the wideness of the NFR. The wide NFRs contain transcription-associated histone variants and PTMs, but they have a non-canonical chromatin organisation, sensitive to nuclease digestion. The histones are present in heminucleosomes or nucleosomes lacking one or two H2A-H2B dimers, maintained by the action of remodellers (de Dieuleveult et al. 2016). In other cases, the presence of NFRs is due to DNA sequence determinants.

The distribution of histone PTMs was also studied along the human genome (see, for instance, (Wang et al. 2008)) and these studies provided information as to the co-occurrence of epigenetic marks along the genome, as well as to the frequency of the association of these marks with the different regions of the genes in their transcriptionally active or inactive states (Karmodiya et al. 2012).

In spite of the great value of the genome-wide approaches, they have an obvious limitation. In a certain sense, it can be said that the information provided by genome-wide approaches is similar to that given by statistical data. It is possible to know, for instance, that roughly 55% of patients suffering from colorectal cancer will survive at least 5 years after diagnosis. But these data do not give information as to the outcome of the illness of a particular patient, and yet the oncologist has to treat particular patients and not anonymous groups. The doctor needs to know the personal profile of every patient if a personalized medicine has to be applied. In an analogous manner, the knowledge of the common patterns of distribution of nucleosomes and of epigenetic marks at the level of the entire genome is not warrant for assuring that this pattern is displayed by a given gene.

It is obvious that details on chromatin structure and histone PTMs at selected loci can be obtained through genomic-wide approaches, but these methods are too expensive and time-consuming if only information on a few genes is required. Moreover, this information is often needed at different developmental stages, metabolic situations, etc., a need that would do the use of omic methods prohibitive. In other words, the above considerations suggest that the studies at single loci should be developed in parallel with the genome-wide approaches.

5.3 Experimental Determination of Nucleosome Occupancy at Selected Loci

To study in detail the chromatin organisation of a genetic locus it is first necessary to know the positions occupied by the nucleosomes. Micrococcal nuclease protection (MNP, Fig. 2) offer a convenient and affordable way to do so. Formaldehyde cross-linked chromatin is first digested with the nuclease to give fragments of mononucleosomal size. The DNA isolated from these fragments is then used as template for RT-qPCR. To do this, it is essential to design primers defining tiled amplicons of about 100 bp. Obviously, only the amplicons in which both of the primers lie within the template DNA, *i.e.*, those corresponding to micrococcal nuclease-protected regions, will be amplified, and the PCR signal will be proportional to the degree of protection, which, in turn, depends on the nucleosome occupancy. As the efficiency of the different sets of primers will ordinarily be different, a correction should be made by amplifying naked DNA of about 150–200 bp. This may be conveniently prepared by sonication

of naked genomic DNA. If the corrected signal is plotted against the position of each amplicon (usually measured at its centre) a graphic depicting the position of the nucleosomes may be obtained (Fig. 2). It has to be noted that nucleosome positioning, especially when results from DNA sequence motifs, is not absolutely strict. In other words, rotational determinants for nucleosome positioning usually define a series of positions differing by 10 bp, rather than a unique position. This is the reason by which more or less bell-shaped curves result in the plotting. Of course, the size of the amplicons influences the accuracy of the results and the maximum of the curve does not necessarily coincide with the position of the dyad axis of the nucleosomes.

We first used this method in 2011, also known as nucleosome-scanning (Infante et al. 2012), in combination with semi-quantitative PCR, to detect the position of nucleosomes in the promoter of murine *Gas1* gene (Sacilotto et al. 2011). An advantage of MNP is that it allows obtaining fine details in the transcription-related changes in nucleosome organisation. For instance, the murine *Egr1* gene has resulted to be a good example of the use of this method. This immediate-early gene is expressed to a very low

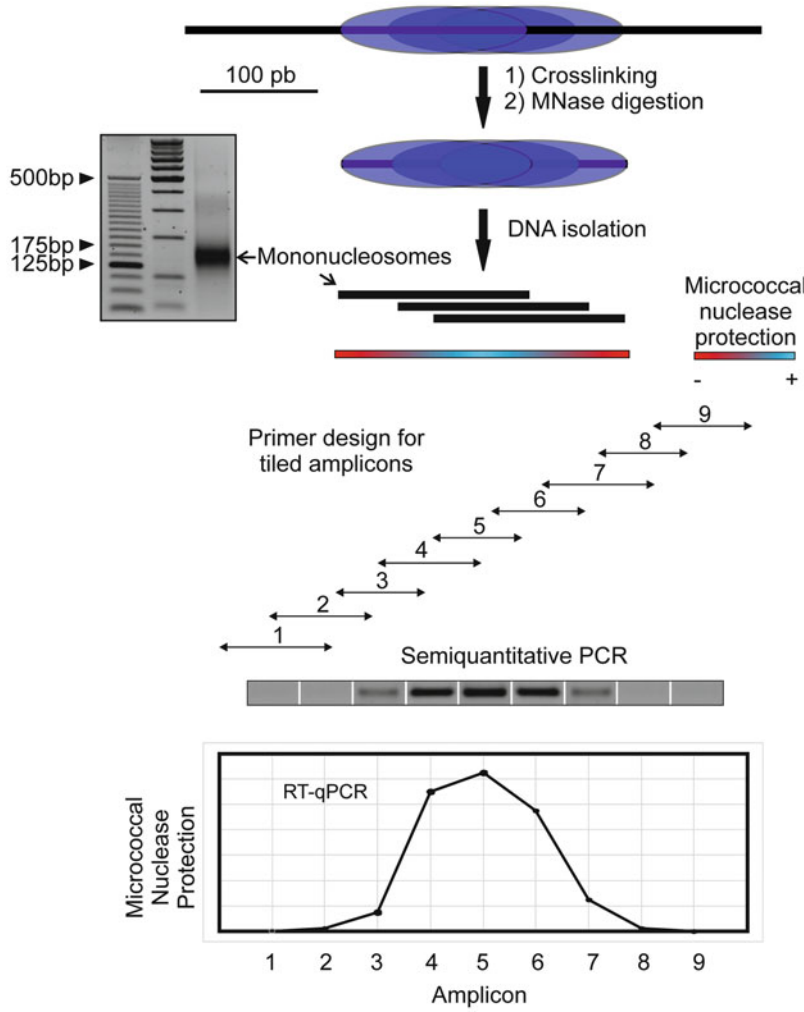

Fig. 2 The micrococcal nuclease protection (*MNP*) assay. Cross-linked chromatin is digested with micrococcal nuclease to give mononucleosomal fragments. The most common mechanism of sequence-directed nucleosome positioning involves rotational determinants and, as shown in the *top row*, each nucleosome actually is a family of 10 bp-spaced nucleosomes. Therefore, the protected DNA extends more than 147 bp, with the protection level diminishing at both sides. A PCR analysis with primers defining a series of tiled amplicons of about 100 bp will give the results depicted in the lower part of the figure. When RT-qPCR is used, and the DNA concentration is plotted against the position of the centre of each amplicons, the resulting graphic roughly depicts the position occupied by the nucleosome or family of nucleosomes

level in the non-stimulated mouse progenitor hepatocyte MLP29cell line, but it is rapidly induced after treating with 12-*O*-tetradecanoylphorbol-13-acetate (TPA). The *RNAPol-ChIP* technique, which measures real-time transcriptional rate (Sandoval and Rodríguez 2004), allows detecting a clear increase in transcription as soon as 5 min after adding TPA. Transcription reaches a maximum at 30 min and by 180 min it returns to the basal situation (Fig. 3), because the own product of the gene, once bound to a specific site in the promoter, recruits the NAB1/NAB2 repressors (Tur et al. 2010). By using a MNP assay, we found that the EGR1 site in the promoter of the gene is covered by nucleosome N − 2. Nevertheless, as shown in Fig. 4, soon after TPA induction a remodelling event results in the downstream sliding of N − 2, which allows the accessibility of the product of the gene to its target sequence, thus initiating the events that eventually led to the repression of the gene (Riffo-Campos et al. 2015). Nucleosome N − 1 is also remodelled upon transcription, and results partially evicted (Fig. 4), probably to facilitate the assembly of the mediator complex, that binds the *Egr1* promoter between the TSS and −400 (Wang et al. 2005).

5.4 The Identification of Histone PTMs and/or Chromatin-Interacting Factors at Single-Nucleosome Level

The location of epigenetic histone marks and/or protein factors at the level of a given, single nucleosome may be easily obtained through the *Nuc-ChIP* method (Sacilotto et al. 2011), which has been used by many authors. Essentially, *Nuc-ChIP* is a classical ChIP assay in which the immunoprecipitation step is carried out with mononucleosomes, isolated as described above for MNP assays (see Fig. 2). The DNA recovered from the immunoprecipitate is then amplified with the appropriate set of primers, corresponding to the amplicons covered by the nucleosomes of choice. In this way the presence of a given histone mark in a specific nucleosome can be detected.

This offers several interesting possibilities. First of all, the method detects a PTM only when it is present in a nucleosome-assembled histone, and not when a free, modified histone is bound to DNA, as it occurs in the above-mentioned wide NFRs (de Dieuleveult et al. 2016). A second example is given by the distribution of the double mark H3S10phK14ac. It has been known for some time that the promoter of immediate-early genes acquire this double mark as a prerequisite to their induction, as shown by

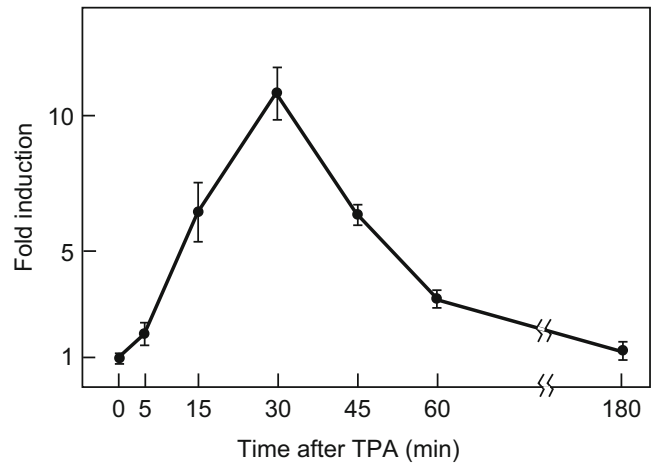

Fig. 3 Induction of mouse *Egr1* after TPA treatment of MLP29 cells. The actual expression level was determined by *RNApol-ChIP* (Sandoval and Rodríguez 2004) at several times after adding TPA. The figure has been constructed with the data reported by Tur et al. (2010)

classical ChIP analysis of sonicated chromatin in mouse *Fos* (Cheung et al. 2000; Thomson et al. 2001), *Jun* (Thomson et al. 2001) and *Egr1* (Tur et al. 2010), among other genes. A *Nuc-ChIP* assay allowed us to specify that H3 phosphoacetylation mainly affects nucleosome N + 1 in murine *Egr1* (Riffo-Campos et al. 2015). Working with the same biological model, it was found that the histone activating marks H3K9ac and H4K16ac are characteristic of nucleosome N − 1, while H3K4me3, another activating mark, is mainly found in N + 1 (Fig. 5). The latter finding of *Nuc-ChIP* agrees with the data obtained from genome-wide analyses, which

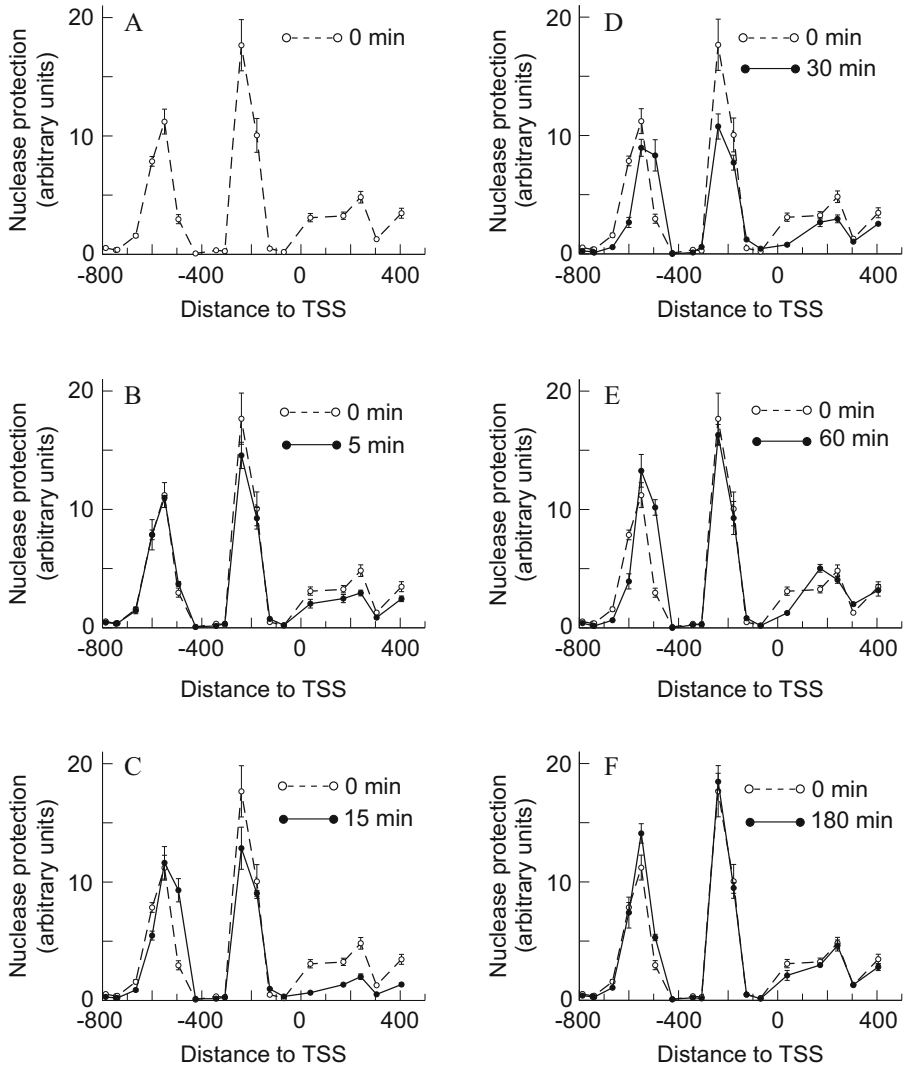

Fig. 4 Time-course of changes in nucleosome occupancy in the promoter and proximal coding region of the murine *Egr1* gene after TPA induction. The protection against nuclease digestion was determined and plotted against the distance to TSS. To facilitate comparisons, the nuclease protection at t = 0 min was shown in all the panels. The plotted experimental points correspond to the mean ± standard error of three determinations. This research was originally published in Riffo-Campos et al. (2015) © the American Society for Biochemistry and Molecular Biology

detected this histone PTM at the start of actively transcribed genes (Kimura 2013), but in other instances, the results obtained by *Nuc-ChIP* do not coincide with those of genomic approaches. For instance, *Nuc-ChIP* analysis showed that H3K9me3 is present in N + 1 of murine *Egr1* (Fig. 5D), while Wang et al. found that this mark is virtually absent from the environment of the TSS of 1000 active genes (Wang et al. 2008).

To further explore this apparent contradiction, we took advantage of another of the possibilities of *Nuc-ChIP*, namely, the analysis of non-histone proteins bound to a given nucleosome. Following this methodology, we explored the presence of the heterochromatin protein HP1-γ around the *Egr1* TSS, because HP1 proteins are known to recognise methylated lysine 9 of H3 through their chromodomain. HP1 proteins are characteristic of heterochromatin and they are typically involved in gene silencing. Recent genome-wide studies describe a mechanism for the silencing caused by HP1 proteins, which co-localize with H3K9me3 (Hiragami-Hamada et al. 2016). Curiously enough, HP1-γ is preferentially found in

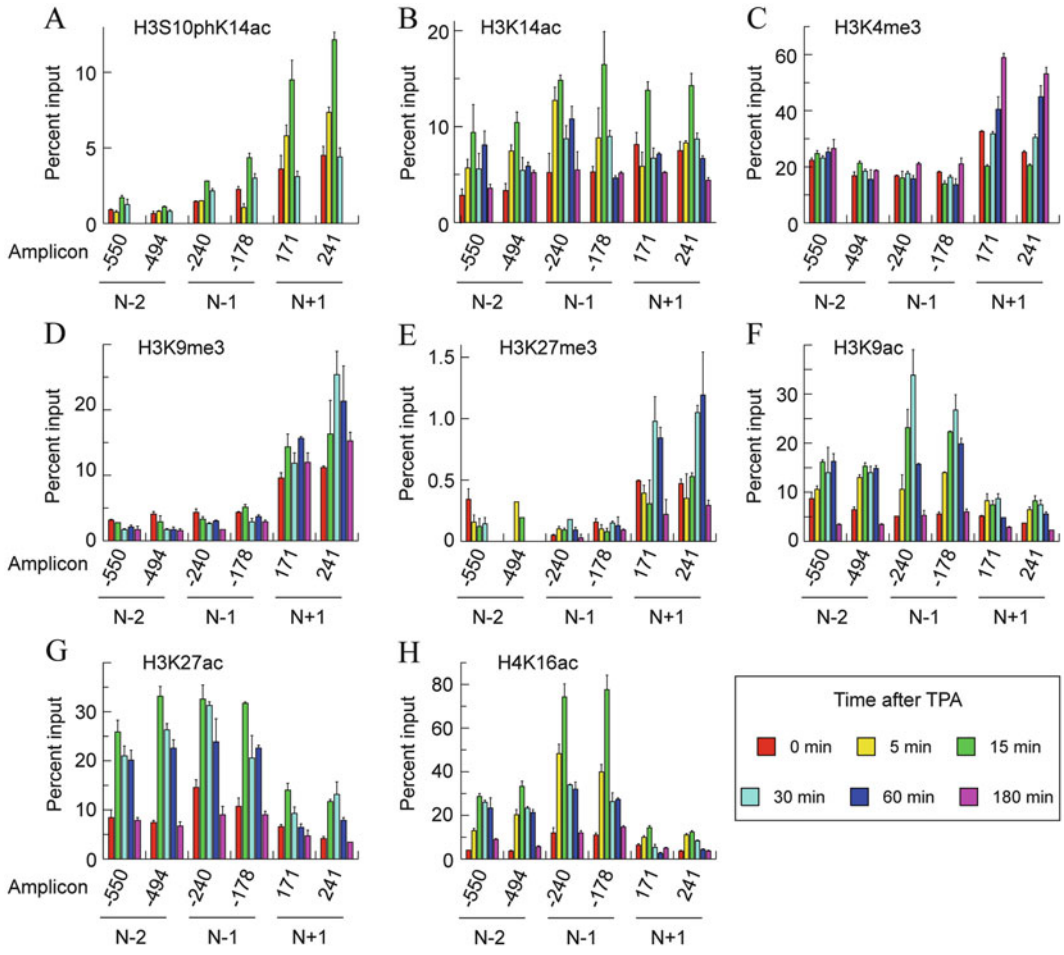

Fig. 5 Time-dependent changes in histone PTMs in nucleosomes −2, −1 and +1 of *Egr1* gene after adding TPA to MLP29 cells. Panels **a**–**h** show the levels of different modifications in a representative experiment, plotted as percent of input, for two amplicons in every nucleosome. *Error bars* represent the standard deviation of three determinations. The times after adding TPA are given in the inset at the *right* of the *lower row*. This research was originally published in Riffo-Campos et al. (2015) © the American Society for Biochemistry and Molecular Biology

Egr1 N + 1 (Fig. 6) and it co-maps with H3K9me3 (compare Figs. 5D and 6). Our results agree with those of Vakoc et al., also working with HP1-γ (Vakoc et al. 2005). Therefore, studies at single-nucleosome level, carried out by *Nuc-ChIP*, may aid to find exceptions to the general rules derived from genome-wide approaches. In the present instance, they suggest a distinct role for the different isoforms of HP1. This question deserves further study; it has been already mentioned that the interaction of HP1-α and HP1-β with H3K9me3 can be modulated by phosphorylation (Irving-Hooper and Binda 2015), and the possibility of a similar modulation in HP1-γ should be explored.

The *Nuc-ChIP* analysis can be carried out in a time-dependent manner after activation of a gene. In this way, the sequence of histone PTMs can be ascertained at single-nucleosome level. The order in which the different epigenetic events take place during gene activation or repression has represented a classical challenge in chromatin research (see (Mellor 2006) for a review), but early data were obtained by classical ChIP. Kim and Kim (Kim and Kim 2010), studying the β-globin gene and its locus control region, obtained valuable data with ChIP analysis of chromatin digested with micrococcal nuclease to a mononucleosomal level. Nevertheless, as the nucleosome positioning was not determined, the results cannot be explained at single-nucleosome resolution.

The TPA-induced transient induction of *Egr1* gene offers a convenient model to carry out these time-dependent, *Nuc-ChIP* studies (Fig. 5). A general observation is that, with the exception mentioned below, the modification state of the three nucleosomes studies returns to the basal level when the transient expression of the gene ceases. Apart from this general question, several conclusions can be drawn from these studies. First, H3 phosphoacetylation, which is an initial event in the induction of immediate-early genes (Crosio et al. 2003) is not required for sustained transcription, as it clearly diminishes prior to the peak of transcriptional rate of the gene (see Fig. 3). Second, H3K14ac and H4K16ac in the promoter precede other activating modifications, such as H3K9ac. Third, H3K4me3, which, as previously mentioned, fundamentally occurs in N + 1, does not return to the basal level at 180 min after stimulation. Probably, the permanence of this activating PTM, which co-occurs with the repressing mark H3K9me3 may assure an immediate activation of the gene in an eventual second round of transcription (see below for the meaning of the co-occurrence of bivalent marks).

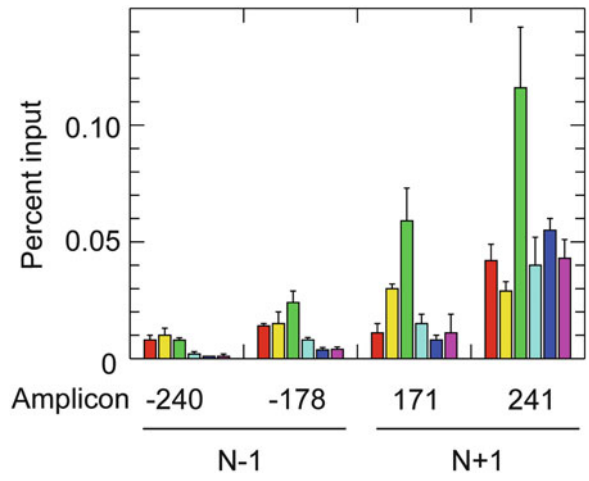

Fig. 6 Time-dependent binding of HP1-γ to nucleosomes −1 and +1 of *Egr1* gene after adding TPA to MLP29 cells. The experiment was carried out by *Nuc-ChIP* and the plot was done exactly as those in Fig. 5. The original experiment was carried out in our laboratory by A. L. Riffo-Campos, J. Castillo, G. López-Rodas and L. Franco (unpublished results)

6 The Presence of Multiple Histone PTMs

6.1 How Can Combinatorial Marks in a Single Nucleosome Be Detected?

It has been just shown how the nucleosomes of *Egr1* promoter are labelled by several different histone PTMs. Of course, this is not an isolated example and the number of similar cases reported in the literature is too huge to be listed here. Strahl and Davis, when proposing the histone code hypothesis (Strahl and Allis 2000), advanced that a combination of different histone PTMs may specify a given function, so the simultaneous presence of some epigenetic marks in nucleosomes may be functionally significant. It may also be possible that two or more histone distinct PTMs drive a given function when they are sequentially introduced in chromatin. Most of the published work on multiple histone PTMs deal with the combinatorial significance of several epigenetic marks. In the next sections, we will describe the methods used to detect the simultaneous presence of different PTMs, to analyse afterwards some functional properties of combinatorial marks.

Nuc-ChIP, just as classical ChIP, has a limitation. Let us suppose that a single nucleosome (N1 in Fig. 7A) contains two different epigenetic marks in its histones. If a *Nuc-ChIP* assay was carried out with the antibodies against these marks, and the recovered nucleosomal DNA is PCR-amplified with the primers defining the corresponding amplicons, the results will indicate that these two marks are present in N1. But this result does not necessarily imply a co-occurrence of the two marks in the same nucleosome. It might occur that one of the marks is present in N1 in a given cell while the other mark is present, also in N1 but in other cell of the sample used. The possibility also exists that being both PTMs present in the same cell, one of them occurs in one of the alleles and the second one in the other. In both instances, as shown in Fig. 7B, the results of the *Nuc-ChIP* analysis will be the same as in the case of co-occurrence of the PTMs (Sacilotto et al. 2011).

To decide between both possibilities, *reChIP* (Furlan-Magaril et al. 2009), which can be adapted to mononucleosomes and then known as *sequential Nuc-ChIP* (Sacilotto et al. 2011) may be carried out. The nucleosomes immunoprecipitated with a first antibody were recovered and subjected to a second *Nuc-ChIP* assay with an antibody against a different protein or epigenetic mark. The final immunoprecipitate was then PCR-analysed so that the amplified sequences correspond to nucleosomes carrying simultaneously both epitopes. Of course, the above method can be scaled up to obtain information at a genome-wide level and several methods have been recently described to improve these approaches (Sadeh et al. 2016; Shema et al. 2016).

6.2 Combinatorial Epigenetic Marks in Nucleosomes

In the last years, evidence in favour of the ubiquitous presence of combined marks is continuously increasing. Combination of PTMs may occur in a *trans*-histone or in a *cis*-histone mode (Rothbart and Strahl 2014; Su and Denu 2016). In the former case, two marks are present in different histone molecule (either in the same nucleosome or in neighbouring nucleosomes). In the latter, the marks belong to the same histone molecule. Some histone PTMs occur in a "paired" manner, *i. e.*, when one of the modifications is present in a nucleosome the second one is also frequently present. For instance, the pairs H3K27ac-H3K4me3 and H3K36me3-H3K27ac are characteristic, respectively, of active promoters and enhancers (Xiao et al. 2012) and the pair H3K9ac-H3K14ac is a hallmark of gene activation (Karmodiya et al. 2012).

The presence of a combination of epigenetic marks in a single nucleosome, either on the same histone molecule or in different histone copies within the octamer, requires an appropriate

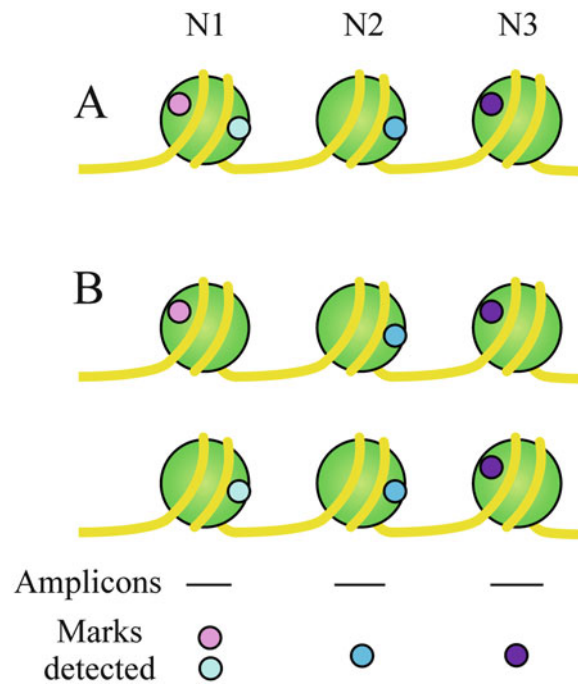

Fig. 7 A limitation of *Nuc-ChIP* exemplified by the case of co-occurrence of two different histone PTMs. They may actually co-occur in the same nucleosome N1, as in (**A**), but one of them may be present in N1 from a subset of cells of the analysed population and the second one in N1 from a different subset of cells (**B**). A similar situation would result if both marks are distributed between the two alleles in every cell. The finding of marks in N2 and N3, being present in every copy of the corresponding nucleosome, does not involve any ambiguity

combination of reader domains, which may reside either in the same or in different protein molecules.

There are proteins harbouring two different reader domains that may bind their specific marks. This is, for instance, the case of 14-3-3 proteins, which have been typically known as phospho-binding proteins. Both, mammalian 14-3-3 and their yeast homologues Bmh1 and Bmh2 are able to bind H3S10phK14ac, under stringent conditions (500 mM NaCl), but non-acetylated H3S10ph is bound with much less affinity, as revealed by isothermal titration calorimetry (Walter et al. 2008). Human BPTF (bromodomain PHD finger transcription factor) specifically recognises the pair H3K4me3-H4K16ac in a single nucleosome and the structural basis for this specificity has been established (Ruthenburg et al. 2011). The above examples illustrate the existence of readers for *cis*- and *trans*-histone combinations of marks.

Another recent example of a protein that recognises two marks is zinc finger MYND (Myeloid, Nervy and DEAF-1)-type containing 8 (ZMYND8), which specifically binds the combination of activating marks H3.1K36me2/H4K16ac. A structural basis for the simultaneous recognition of both marks has been postulated, and it is worth noting that ZMYND8 shows a strong preference for the canonical histone H3.1, when compared with the variant H3.3 (Adhikary et al. 2016). The interested reader may find more examples in the recent authoritative review of Su and Denu (Su and Denu 2016).

In other instances, recognition of combinatorial epigenetic marks is carried out by protein complexes in which there are at least two components, each of them harbouring a different reader domain. Many often, these complexes also contain components with catalytic domains that may either "*write*" or "*erase*" other histone PTMs in the same nucleosome or in a neighbour one. For instance, the HBO1 HAT complex possesses three PHD domains in two different subunits, namely ING4/5 and JADE1/2/3. The pull-down experiments of Saksouk et al. (2009)

confirmed that the PDH finger domains of ING4/5 specifically bind H3K4me3. The structural bases for this specificity were cleared up when the crystal structure of the $ING4_{PHD}$-H3K4me3 complex was solved (Hung et al. 2009). The PHD domains of JADE are essential for the association of HBO1 to chromatin (Saksouk et al. 2009). In this way, the HBO1 complex may be recruited to H3K4me3-containing nucleosomes and catalyse the acetylation of H3 (Hung et al. 2009).

The MOZ/MORF HAT complex provides another excellent example of multiple readers distributed among several subunits. The KAT6A/KAT6B subunit, which contains the catalytic HAT activity, also contains two PHD domains capable of recognising acetylated H3. A third PHD domain is present in the BRPF adaptor subunit, which also contains a bromodomain and an H3K36me3-interacting PWWP domain. Finally, an additional PHD domain, which binds H3K4me3, is present in the ING5 subunit (Klein et al. 2014). In this way, a complex network of epigenetic regulation is established, in which the combination of pre-existing histone PTMs determine the further activity of a "writer".

6.3 The Meaning of Bivalent Marks

Sequential Nuc-ChIP has been of invaluable aid to report the existence of bivalent epigenetic marks, *i. e.*, histone PTMs of opposing meaning (activating and repressing, for instance), that co-occur in the same nucleosome. The presence of these apparently contradictory epigenetic modifications was first reported in some stem cell genes. In an early review, this combination of activating and repressive marks was designed as "bivalent" and the authors reasoned that the coexistence of both marks may play the role of priming the genes both to expression or silencing as demanded by differentiation to specific cell lineages (Gan et al. 2007). Since then, the presence of bivalent marks and their association with differentiation and development have been widely documented (for a recent review, see (Harikumar and Meshorer 2015)). Recent examples include the *PLZF* gene, which encodes a transcription factor that drives T cell differentiation into natural killer T cell lineage. It contains nucleosomes in their promoter harbouring the bivalent marks H3K27me3 and H3K4me3, as determined by sequential ChIP (Dobenecker et al. 2015). More recently, by using an original sequential ChIP protocol at a genomic scale, have identified the widespread occurrence of the same bivalent marks in CD4+ memory T cells (Kinkley et al. 2016).

The co-occurrence of bivalent marks is not a property exclusive to stem cells or to cells involved in developmental commitment, and some examples have been recently found in tumour suppressor genes. By means of classical ChIP analysis, the presence of the activating marks H3K9ac, H3K14ac, H3K4me3 and the silencing mark H3K27me3 has been found in the promoter of the tumour suppressor *TXNIP* gene, although the results do not allow to know which of these marks occur at a single nucleosome level (Baldan et al. 2015). A genome-wide analysis, conducted in 8 glioma stem cell lines, allowed Lin et al. to conclude that H3K4me3 and H3K27me3 co-map in a set of genes. The suppressor gene *SLC17A7*, whose overexpression reduces the oncogenic phenotype of glioblastoma cells, is an interesting member of that set of genes (Lin et al. 2015). Sequential ChIP analyses, carried out in our laboratory, detected that the repressing mark H3K9me2 co-occurs in the N-1 nucleosome of the mouse suppressor gene *Gas1* with the activating mark H3K27ac and, to a lesser extent, with H3K4me3 and H4R3me2 (Sacilotto et al. 2011).

Although sequential ChIP has not been done to assess the co-occurrence of bivalent marks at single-nucleosome level, Fig. 5 shows that H3K4me3 and H3K27me3 are simultaneously present in the region of nucleosome +1 of murine *Egr1*. The functional meaning of these bivalent marks in suppressor genes and, perhaps, in immediate-early genes may be explained by the analogy proposed in Fig. 1 of the review by Harikumar and Meshorer (2015). A bivalent promoter is comparable to an anchored boat with the

sails up. Should the sails be lowered, the boat will remain still, but if the anchor is removed, she will immediately sail. In a bivalent gene, if the repressing mark is erased, transcription may immediately start, but if the activating mark is removed, the gene will be fixed in a repressed state.

It should be mentioned that the recently described method for the traceless synthesis of asymmetrically bivalent nucleosomes (Lechner et al. 2016) may allow obtaining valuable data on the mechanisms by which histone PTMs cross-talk.

7 Concluding Remarks

The field of histone PTMs is a rapidly changing area of research and every novel finding poses new questions to solve. Some of them have been put forward in the present review. The expanding views on "non-classical" histone PTMs require a deeper analysis of their enzymology as well as of the possible "readers" of these modifications.

The relationships between metabolism and epigenetics, which has attracted a deep attention in the last years, are far to be solved and many questions challenge the researchers in this field.

On the other hand, both the novel PTMs and some contradictory results on the distribution and meaning of the PTMs, which result from comparing genome-wide analyses with local studies, may imply a novel formulation of the histone code.

Acknowledgments This work was supported by grants from the Spanish Ministerio de Economía y Competitividad (FIS PI12/02110) and from Generalitat Valenciana (PROMETEO 2013–005). We are very indebted to Prof. Juan R. Viña for attracting our attention to the metabolic enzymes that "moonlight" in the nucleus.

Conflict of Interest The authors declare no conflict of interests.

Ethical Approval This article does not contain any studies with human participants or animals performed by any of the authors.

References

Adhikary S, Sanyal S, Basu M, Sengupta I, Sen S, Srivastava DK, Roy S, Das C (2016) Selective recognition of H3.1K36 dimethylation/H4K16 acetylation facilitates the regulation of all-trans-retinoic acid (ATRA)-responsive genes by putative chromatin reader ZMYND8. J Biol Chem 291:2664–2681

Allfrey VG, Faulkner R, Mirsky AE (1964) Acetylation and methylation of histones and their possible role in the regulation of RNA synthesis. Proc Natl Acad Sci U S A 315:786–794

Andrews FH, Shinsky SA, Shanle EK, Bridgers JB, Gest A, Tsun IK, Krajewski K, Shi X, Strahl BD, Kutateladze TG (2016) The Taf14 YEATS domain is a reader of histone crotonylation. Nat Chem Biol 12:396–398

Arents G, Moudrianakis EN (1993) Topography of the histone octamer surface: repeating structural motifs utilized in the docking of nucleosomal DNA. Proc Natl Acad Sci U S A 90:10489–10493

Arents G, Burlingame RW, Wang BC, Love WE, Moudrianakis EN (1991) The nucleosomal core histone octamer at 3.1 Å resolution: a tripartite protein assembly and a left-handed superhelix. Proc Natl Acad Sci U S A 88:10148–10152

Baldan F, Mio C, Lavarone E, Di Loreto C, Puglisi F, Damante G, Puppin C (2015) Epigenetic bivalent marking is permissive to the synergy of HDAC and PARP inhibitors on TXNIP expression in breast cancer cells. Oncol Rep 33:2199–2206

Ballestar E, Abad C, Franco L (1996) Core histones are glutaminyl substrates for tissue transglutaminase. J Biol Chem 271:18817–18824

Bao X, Wang Y, Li X, Li X, Liu Z, Yang T (2014) Identification of "erasers" for lysine crotonylated histone marks using a chemical proteomics approach. eLife 3:e02999

Basso M, Ratan RR (2013) Transglutaminase is a therapeutic target for oxidative stress, excitotoxicity and stroke: a new epigenetic kid on the CNS block. J Cereb Blood Flow Metab 33:809–818

Berger SL, Kouzarides T, Shiekhattar R, Shilatifard A (2009) An operational definition of epigenetics. Genes Dev 23:781–783

Berndsen CE, Albaugh BN, Tan S, Denu JM (2007) Catalytic mechanism of a MYST family histone acetyltransferase. Biochemistry 46:623–629

Boukouris AE, Zervopoulos SD, Michelakis ED (2016) Metabolic enzymes moonlighting in the nucleus: metabolic regulation of gene transcription. Trends Biochem Sci 41:712–730

Brownell JE, Zhou J, Ranalli T, Kobayashi R, Edmondson DG, Roth SY, Allis CD (1996) Tetrahymena histone acetyltransferase A: a homolog to yeast Gcn5p linking histone acetylation to gene activation. Cell 84:843–851

Chen Y, Sprung R, Tang Y, Ball H, Sangras B, Kim SC, Falck JR, Peng J, Gu W, Zhao Y (2007) Lysine propionylation and butyrylation are novel post-translational modifications in histones. Mol Cell Proteomics 6:812–819

Cheng Z, Tang Y, Chen Y, Kim S, Liu H, Li SSC, Gu W, Zhao Y (2009) Molecular characterization of propionyllysines in non-histone proteins. Mol Cell Proteomics 8:45–52

Cheung P, Tanner KG, Cheung WL, Sassone-Corsi P, Denu JM, Allis CD (2000) Synergistic coupling of histone H3 phosphorylation and acetylation in response to epidermal growth factor stimulation. Mol Cell 5:905–915

Crane-Robinson C, Hebbes TR, Clayton AL, Thorne AW (1997) Chromosomal mapping of core histone acetylation by immunoselection. Methods 12:48–56

Crosio C, Heitz E, Allis CD, Borrelli E, Sassone-Corsi P (2003) Chromatin remodeling and neuronal response: multiple signaling pathways induce specific histone H3 modifications and early gene expression in hippocampal neurons. J Cell Sci 116:4905–4914

Cutter AR, Hayes JJ (2015) A brief review of nucleosome structure. FEBS Lett 589:2914–2922

Daban J-R (2015) Stacked thin layers of metaphase chromatin explain the geometry of chromosome rearrangements and banding. Sci Rep 5:14891

de Dieuleveult M, Yen K, Hmitou I, Depaux A, Boussouar F, Dargham DB, Jounier S, Humbertclaude H, Ribierre F, Baulard C, Farrell NP, Park B, Keime C, Carrière L, Berlivet S, Gut M, Gut I, Werner M, Deleuze J-F, Olaso R, Aude J-C, Chantalat S, Pugh BF, Gérard M (2016) Genome-wide nucleosome specificity and function of chromatin remodellers in ES cells. Nature 530:113–116

Dobenecker M-W, Kim JK, Marcello J, Fang TC, Prinjha R, Bosselut R, Tarakhovsky A (2015) Coupling of T cell receptor specificity to natural killer T cell development by bivalent histone H3 methylation. J Exp Med 212:297–306

Dorigo B, Schalch T, Bystricky K, Richmond TJ (2003) Chromatin fiber folding: requirement for the histone H4 N-terminal tail. J Mol Biol 327:85–96

Du J, Zhou Y, Su X, Yu JJ, Khan S, Jiang H, Kim JH, Woo J, Kim JH, Choi BH, He B, Chen W, Zhang S, Cerione RA, Auwerx J, Hao Q, Lin H (2011) Sirt5 is a NAD-dependent protein lysine demalonylase and desuccinylase. Science 334:806–809

Eltsov M, Maclellan KM, Maeshima K, Frangakis AS, Dubochet J (2008) Analysis of cryo-electron microscopy images does not support the existence of 30-nm chromatin fibers in mitotic chromosomes in situ. Proc Natl Acad Sci U S A 105:19732–19737

Fan J, Krautkramer KA, Feldman JL, Denu JM (2015) Metabolic regulation of histone post-translational modifications. ACS Chem Biol 10:95–108

Finch JT, Klug A (1976) Solenoidal model for superstructure in chromatin. Proc Natl Acad Sci U S A 73:1897–1901

Flynn EM, Huang OW, Poy F, Oppikofer M, Bellon SF, Tang Y, Cochran AG (2015) A subset of human bromodomains recognizes butyryllysine and crotonyllysine histone peptide modifications. Structure 23:1801–1814

Furlan-Magaril M, Rincón-Arano H, Recillas-Targa F (2009) Sequential chromatin immunoprecipitation protocol: ChIP-reChIP. Methods Mol Biol 543:253–266

Gállego I, Castro-Hartmann P, Caravaca JM, Caño S, Daban JR (2009) Dense chromatin plates in metaphase chromosomes. Eur Biophys J 38:503–522

Gan Q, Yoshida T, McDonald OG, Owens GK (2007) Concise review: epigenetic mechanisms contribute to pluripotency and cell lineage determination of embryonic stem cells. Stem Cells 25:2–9

Garrity J, Gardner JG, Hawse W, Wolberger C, Escalante-Semerena JC (2007) N-lysine propionylation controls the activity of propionyl-CoA synthetase. J Biol Chem 282:30239–30245

Georgieva EI, López-Rodas G, Sendra R, Grobner P, Loidl P (1991) Histone acetylation in Zea mays. II biological significance of post- translational histone acetylation during embryo germination. J Biol Chem 266:18751–18760

Goudarzi A, Zhang D, Huang H, Barral S, Kwon OK, Qi S, Tang Z, Buchou T, Vitte AL, He T, Cheng Z, Montellier E, Gaucher J, Curtet S, Debernardi A, Charbonnier G, Puthier D, Petosa C, Panne D, Rousseaux S, Roeder RG, Zhao Y, Khochbin S (2016) Dynamic competing histone H4 K5K8 acetylation and butyrylation are hallmarks of highly active gene promoters. Mol Cell 62:169–180

Grigoryev SA, Woodcock CL (2012) Chromatin organization – the 30 nm fiber. Exp Cell Res 318:1448–1455

Gut P, Verdin E (2013) The nexus of chromatin regulation and intermediary metabolism. Nature 502:489–498

Haery L, Thompson RC, Gilmore TD (2015) Histone acetyltransferases and histone deacetylases in B- and T-cell development, physiology and malignancy. Genes Cancer 6:184–213

Harikumar A, Meshorer E (2015) Chromatin remodeling and bivalent histone modifications in embryonic stem cells. EMBO Rep 16:1609–1619

Hiragami-Hamada K, Soeroes S, Nikolov M, Wilkins B, Kreuz S, Chen C, De La Rosa-Velázquez IA, Zenn HM, Kost N, Pohl W, Chernev A, Schwarzer D, Jenuwein T, Lorincz M, Zimmermann B, Walla PJ, Neumann H, Baubec T, Urlaub H, Fischle W (2016) Dynamic and flexible H3K9me3 bridging via HP1β dimerization establishes a plastic state of condensed chromatin. Nat Commun 7:11310

Hung T, Binda O, Champagne KS, Kuo AJ, Johnson K, Chang HY, Simon MD, Kutateladze TG, Gozani O (2009) ING4 mediates crosstalk between histone H3

K4 trimethylation and H3 acetylation to attenuate cellular transformation. Mol Cell 33:248–256
Infante JJ, Law GL, Young ET (2012) Analysis of nucleosome positioning using a nucleosome-scanning assay. Methods Mol Biol 833:63–87
Irving-Hooper BK, Binda O (2015) A phosphotyrosine switch controls the association of histone mark readers with methylated proteins. Biochemistry 55:1631–1634
Iwahara T, Bonasio R, Narendra V, Reinberg D (2012) SIRT3 functions in the nucleus in the control of stress-related gene expression. Mol Cell Biol 32:5022–5034
Janke R, Dodson AE, Rine J (2015) Metabolism and epigenetics. Annu Rev Cell Dev Biol 31:473–496
Jiang T, Zhou X, Taghizadeh K, Dong M, Dedon PC (2007) N-formylation of lysine in histone proteins as a secondary modification arising from oxidative DNA damage. Proc Natl Acad Sci U S A 104:60–65
Karmodiya K, Krebs AR, Oulad-Abdelghani M, Kimura H, Tora L (2012) H3K9 and H3K14 acetylation co-occur at many gene regulatory elements, while H3K14ac marks a subset of inactive inducible promoters in mouse embryonic stem cells. BMC Genomics 13:424
Kim K, Kim A (2010) Sequential changes in chromatin structure during transcriptional activation in the β globin LCR and its target gene. Int J Biochem Cell Biol 42:1517–1524
Kimura H (2013) Histone modifications for human epigenome analysis. J Hum Genet 58:439–445
Kinkley S, Helmuth J, Polansky JK, Dunkel I, Gasparoni G, Fröhler S, Chen W, Walter J, Hamann A, Chung HR (2016) reChIP-seq reveals widespread bivalency of H3K4me3 and H3K27me3 in $CD4^+$ memory T cells. Nat Commun 7:12514
Klein BJ, Lalonde M-E, Côté J, Yang XJ, Kutateladze TG (2014) Crosstalk between epigenetic readers regulates the MOZ/MORF HAT complexes. Epigenetics 9:186–193
Kuo TF, Tatsukawa H, Kojima S (2011) New insights into the functions and localization of nuclear transglutaminase 2. FEBS J 278:4756–4767
Lai T-S, Lin C-J, Greenberg CS (2016) Role of tissue transglutaminase-2 (TG2)-mediated aminylation in biological processes. Amino Acids. doi:10.1007/s00726-016-2270-8
Längst G, Manelyte L (2015) Chromatin remodelers: from function to dysfunction. Genes (Basel) 6:299–324
Laurent BC, Treich I, Carlson M (1993) The yeast SNF2/SWI2 protein has DNA-stimulated ATPase activity required for transcriptional activation. Genes Dev 7:583–591
Lawrence M, Daujat S, Schneider R (2016) Lateral thinking: how histone modifications regulate gene expression. Trends Genet 32:42–56
Lechner CC, Agashe ND, Fierz B (2016) Traceless synthesis of asymmetrically modified bivalent nucleosomes. Angew Chem Int Ed 55:2903–2906
Leemhuis H, Packman LC, Nightingale KP, Hollfelder F (2008) The human histone acetyltransferase P/CAF is a promiscuous histone propionyltransferase. Chembiochem 9:499–503
Li G, Zhu P (2015) Structure and organization of chromatin fiber in the nucleus. FEBS Lett 589:2893–2904
Li Y, Sabari BR, Panchenko T, Wen H, Zhao D, Guan H, Wan L, Huang H, Tang Z, Zhao Y, Roeder RG, Shi X, Allis CD, Li H (2016) Molecular coupling of histone crotonylation and active transcription by AF9 YEATS domain. Mol Cell 62:181–193
Lin H, Su X, He B (2012) Protein lysine acylation and cysteine succination by intermediates of energy metabolism. ACS Chem Biol 7:947–960
Lin B, Lee H, Yoon J-G, Madan A, Wayner E, Tonning S, Hothi P, Schroeder B, Ulasov I, Foltz G, Hood L, Cobbs C (2015) Global analysis of H3K4me3 and H3K27me3 profiles in glioblastoma stem cells and identification of SLC17A7 as a bivalent tumor suppressor gene. Oncotarget 6:5369–5381
Liu B, Lin Y, Darwanto A, Song X, Xu G, Zhang K (2009) Identification and characterization of propionylation at histone H3 lysine 23 in mammalian cells. J Biol Chem 284:32288–32295
Loidl P (1988) Towards an understanding of the biological function of histone acetylation. FEBS Lett 227:91–95
López-Rodas G, Tordera V, Sánchez del Pino MM, Franco L (1989) Yeast contains multiple forms of histone acetyltransferase. J Biol Chem 264:19028–19033
López-Rodas G, Tordera V, Sánchez del Pino MM, Franco L (1991a) Subcellular localization and nucleosome specificity of yeast histone acetyltransferases. Biochemistry 30:3728–3732
López-Rodas G, Georgieva EI, Sendra R, Loidl P (1991b) Histone acetylation in Zea mays I: activities of histone acetyltransferases and histone deacetylases. J Biol Chem 266:18745–18750
Luger K, Mäder AW, Richmond RK, Sargent DF, Richmond TJ (1997) Crystal structure of the nucleosome core particle at 2.8 Å resolution. Nature 389:251–260
Madiraju P, Pande SV, Prentki M, Madiraju SRM (2009) Mitochondrial acetylcarnitine provides acetyl groups for nuclear histone acetylation. Epigenetics 4:399–403
Maeshima K, Imai R, Tamura S, Nozaki T (2014) Chromatin as dynamic 10-nm fibers. Chromosoma 123:225–237
Matallana E, Franco L, Pérez-Ortín JE (1992) Chromatin structure of the yeast *SUC2* promoter in regulatory mutants. Mol Gen Genet 231:395–400
Matsushita N, Yonashiro R, Ogata Y, Sugiura A, Nagashima S, Fukuda T, Inatome R, Yanagi S (2011) Distinct regulation of mitochondrial localization and stability of two human Sirt5 isoforms. Genes Cells 16:190–202

McConoughey SJ, Basso M, Niatsetskaya ZV, Sleiman SF, Smirnova NA, Langley BC, Mahishi L, Cooper AJL, Antonyak MA, Cerione RA, Li B, Starkov A, Chaturvedi RK, Bea MF, Coppola G, Geschwind DH, Ryu H, Xia L, Iismaa SE, Pallos J, Pasternack R, Hils M, Fan J, Raymond LA, Marsh JL, Thompson LM, Ratan RR (2010) Inhibition of transglutaminase 2 mitigates transcriptional dysregulation in models of Huntington's disease. EMBO Mol Med 2:349–370

Mellor J (2006) Dynamic nucleosomes and gene transcription. Trends Genet 22:320–329

Nishida Y, Rardin MJ, Carrico C, He W, Sahu AK, Gut P, Najjar R, Fitch M, Hellerstein M, Gibson BW, Verdin E (2015) SIRT5 regulates both cytosolic and mitochondrial protein malonylation with glycolysis as a major target. Mol Cell 59:321–332

Noh KM, Allis CD, Li H (2016) Reading between the lines: "ADD"-ing histone and DNA methylation marks toward a new epigenetic "Sum." ACS Chem Biol 11:554–563

Noma K, Allis CD, Grewal SIS (2001) Transitions in distinct histone H3 methylation patterns at the heterochromatin domain boundaries. Science 293:1150–1155

Nowak RP, Tumber A, Johansson C, Che KH, Brennan P, Owen D, Oppermann U (2016) Advances and challenges in understanding histone demethylase biology. Curr Opin Chem Biol 33:151–159

Park J, Chen Y, Tishkoff DX, Peng C, Tan M, Dai L, Xie Z, Zhang Y, Zwaans BMM, Skinner ME, Lombard DB, Zhao Y (2013) SIRT5-mediated lysine desuccinylation impacts diverse metabolic pathways. Mol Cell 50:919–930

Patel SS, Walt DR (1987) Substrate specificity of acetyl coenzyme A synthetase. J Biol Chem 262:7132–7134

Peng C, Lu Z, Xie Z, Cheng Z, Chen Y, Tan M, Luo H, Zhang Y, He W, Yang K, Zwaans BMM, Tishkoff D, Ho L, Lombard D, He T-C, Dai J, Verdin E, Ye Y, Zhao Y (2011) The first identification of lysine malonylation substrates and its regulatory enzyme. Mol Cell Proteomics 10:M111.012658

Pérez-Ortín JE, Estruch F, Matallana E, Franco L (1987) Fine analysis of the chromatin structure of the yeast *SUC2* gene and of its changes upon derepression. Comparison between the chromosomal and plasmid-inserted genes. Nucleic Acids Res 15:6937–6956

Rando OJ (2012) Combinatorial complexity in chromatin structure and function: revisiting the histone code. Curr Opin Genet Dev 22:148–155

Rando OJ, Chang HY (2009) Genome-wide views of chromatin structure. Annu Rev Biochem 78:245–271

Riffo-Campos ÁL, Castillo J, Tur G, González-Figueroa P, Georgieva EI, Rodríguez JL, López-Rodas G, Rodrigo MI, Franco L (2015) Nucleosome-specific, time-dependent changes in histone modifications during activation of the early growth response 1 (*Egr1*) gene. J Biol Chem 290:197–208

Rine J, Herskowitz I (1987) Four genes responsible for a position effect on expression from HML and HMR in *Saccharomyces cerevisiae*. Genetics 116:9–22

Rodríguez-Paredes M, Esteller M (2011) Cancer epigenetics reaches mainstream oncology. Nat Med 17:330–339

Rothbart SB, Strahl BD (2014) Interpreting the language of histone and DNA modifications. Biochim Biophys Acta 1839:627–643

Ruthenburg AJ, Li H, Milne TA, Dewell S, McGinty RK, Yuen M, Ueberheide B, Dou Y, Muir TW, Patel DJ, Allis CD (2011) Recognition of a mononucleosomal histone modification pattern by BPTF via multivalent interactions. Cell 145:692–706

Sabari BR, Tang Z, Huang H, Yong-Gonzalez V, Molina H, Kong HE, Dai L, Shimada M, Cross JR, Zhao Y, Roeder RG, Allis CD (2015) Intracellular crotonyl-CoA stimulates transcription through p300-catalyzed histone crotonylation. Mol Cell 58:203–215

Sacilotto N, Espert A, Castillo J, Franco L, López-Rodas G (2011) Epigenetic transcriptional regulation of the growth arrest-specific gene 1 (*Gas1*) in hepatic cell proliferation at mononucleosomal resolution. PLoS One 6:e23318

Sadeh R, Launer-Wachs R, Wandel H, Rahat A, Friedman N (2016) Elucidating combinatorial chromatin states at single-nucleosome resolution. Mol Cell 63:1–9

Sadhukhan S, Liu X, Ryu D, Nelson OD, Stupinski JA, Li Z, Chen W, Zhang S, Weiss RS, Locasale JW, Auwerx J, Lin H (2016) Metabolomics-assisted proteomics identifies succinylation and SIRT5 as important regulators of cardiac function. Proc Natl Acad Sci U S A 113:4320–4325

Sajan SA, Hawkins RD (2012) Methods for identifying higher-order chromatin structure. Annu Rev Genomics Hum Genet 13:59–82

Saksouk N, Avvakumov N, Champagne KS, Hung T, Doyon Y, Cayrou C, Paquet E, Ullah M, Landry AJ, Côté V, Yang XJ, Gozani O, Kutateladze TG, Côté J (2009) HBO1 HAT complexes target chromatin throughout gene coding regions via multiple PHD finger interactions with histone H3 tail. Mol Cell 33:257–265

Sandoval J, Rodríguez J (2004) RNAPol-ChIP: a novel application of chromatin immunoprecipitation to the analysis of real-time gene transcription. Nucleic Acids Res 32:e88

Schmitges FW, Prusty AB, Faty M, Stützer A, Lingaraju GM, Aiwazian J, Sack R, Hess D, Li L, Zhou S, Bunker RD, Wirth U, Bouwmeester T, Bauer A, Ly-Hartig N, Zhao K, Chan H, Gu J, Gut H, Fischle W, Müller J, Thomä NH (2011) Histone methylation by PRC2 is inhibited by active chromatin marks. Mol Cell 42:330–341

Sendra R, Rodrigo I, Salvador ML, Franco L (1988) Characterization of pea histone deacetylases. Plant Mol Biol 11:857–866

Sendra R, Salvador ML, Franco L (1991) A chromatin-associated histone deacetylase from pea (*Pisum sativum*). Plant Sci 78:43–51

Shema E, Jones D, Shoresh N, Donohue L, Ram O, Bernstein BE (2016) Single-molecule decoding of combinatorially modified nucleosomes. Science 352:717–721

Shi Y, Lan F, Matson C, Mulligan P, Whetstine JR, Cole PA, Casero RA, Shi Y (2004) Histone demethylation mediated by the nuclear amine oxidase homolog LSD1. Cell 119:941–953

Simpson RT (1978) Structure of the chromatosome, a chromatin particle containing 160 base pairs of DNA and all the histones. Biochemistry 17:5524–5531

Strahl BD, Allis CD (2000) The language of covalent histone modifications. Nature 403:41–45

Strahl BD, Ohba R, Cook RG, Allis CD (1999) Methylation of histone H3 at lysine 4 is highly conserved and correlates with transcriptionally active nuclei in *Tetrahymena*. Proc Natl Acad Sci U S A 96:14967–14972

Strahl BD, Briggs SD, Brame CJ, Caldwell JA, Koh SS, Ma H, Cook RG, Shabanowitz J, Hunt DF, Stallcup MR, Allis CD (2001) Methylation of histone H4 at arginine 3 occurs in vivo and is mediated by the nuclear receptor coactivator PRMT1. Curr Biol 11:996–1000

Su Z, Denu JM (2016) Reading the combinatorial histone language. ACS Chem Biol 11:564–574

Su J, Wang F, Cai Y, Jin J (2016a) The functional analysis of histone acetyltransferase MOF in tumorigenesis. Int J Mol Sci 17:99

Su X, Wellen KE, Rabinowitz JD (2016b) Metabolic control of methylation and acetylation. Curr Opin Chem Biol 30:52–60. doi:10.1016/j.cbpa.2015.10.030

Sutendra G, Kinnaird A, Dromparis P, Paulin R, Stenson TH, Haromy A, Hashimoto K, Zhang N, Flaim E, Michelakis ED (2014) A nuclear pyruvate dehydrogenase complex is important for the generation of Acetyl-CoA and histone acetylation. Cell 158:84–97

Takahashi H, McCaffery JM, Irizarry RA, Boeke JD (2006) Nucleocytosolic acetyl-coenzyme A synthetase is required for histone acetylation and global transcription. Mol Cell 23:207–217

Tan M, Luo H, Lee S, Jin F, Yang JS, Montellier E, Buchou T, Cheng Z, Rousseaux S, Rajagopal N, Lu Z, Ye Z, Zhu Q, Wysocka J, Ye Y, Khochbin S, Ren B, Zhao Y (2011) Identification of 67 histone marks and histone lysine crotonylation as a new type of histone modification. Cell 146:1016–1028

Taunton J, Hassig CA, Schreiber SL (1996) A mammalian histone deacetylase related to the yeast transcriptional regulator Rpd3p. Science 272:408–411

Thomson S, Clayton AL, Mahadevan LC (2001) Independent dynamic regulation of histone phosphorylation and acetylation during immediate-early gene induction. Mol Cell 8:1231–1241

Tur G, Georgieva E, Gagete A, López-Rodas G, Rodríguez J, Franco L (2010) Factor binding and chromatin modification in the promoter of murine *Egr1* gene upon induction. Cell Mol Life Sci:4065–4077

Vakoc CR, Mandat SA, Olenchock BA, Blobel GA (2005) Histone H3 lysine 9 methylation and HP1γ are associated with transcription elongation through mammalian chromatin. Mol Cell 19:381–391

van Holde KE (1989) Chromatin. Springer, New York

Vollmuth F, Geyer M (2010) Interaction of propionylated and butyrylated histone H3 lysine marks with Brd4 bromodomains. Angew Chem Int Ed Engl 49:6768–6772

Walter W, Clynes D, Tang Y, Marmorstein R, Mellor J, Berger SL (2008) 14-3-3 interaction with histone H3 involves a dual modification pattern of phosphoacetylation. Mol Cell Biol 28:2840–2849

Wang L, Dent SYR (2014) Functions of SAGA in development and disease. Epigenomics 6:329–339

Wang G, Balamotis MA, Stevens JL, Yamaguchi Y, Handa H, Berk AJ (2005) Mediator requirement for both recruitment and postrecruitment steps in transcription initiation. Mol Cell 17:683–694

Wang Z, Zang C, Rosenfeld JA, Schones DE, Barski A, Cuddapah S, Cui K, Roh T-Y, Peng W, Zhang MQ, Zhao K (2008) Combinatorial patterns of histone acetylations and methylations in the human genome. Nat Genet 40:897–903

Wapenaar H, Dekker FJ (2016) Histone acetyltransferases: challenges in targeting bi-substrate enzymes. Clin Epigenetics 8:59

Wellen KE, Hatzivassiliou G, Sachdeva UM, Bui TV, Cross JR, Thompson CB (2009) ATP-citrate lyase links cellular metabolism to histone acetylation. Science 324:1076–1080

Wu C (1980) The 5′ ends of *Drosophila* heat shock genes in chromatin are hypersensitive to DNase I. Nature 286:854–860

Xiao S, Xie D, Cao X, Yu P, Xing X, Chen C-C, Musselman M, Xie M, West FD, Lewin HA, Wang T, Zhong S (2012) Comparative epigenomic annotation of regulatory DNA. Cell 149:1381–1392

Xie Z, Dai J, Dai L, Tan M, Cheng Z, Wu Y, Boeke JD, Zhao Y (2012) Lysine succinylation and lysine malonylation in histones. Mol Cell Proteomics 11:100–107

Xu YM, Du JY, Lau ATY (2014a) Posttranslational modifications of human histone H3: an update. Proteomics 14:2047–2060

Xu G, Wang J, Wu Z, Qian L, Dai L, Wan X, Tan M, Zhao Y, Wu Y (2014b) SAHA regulates histone

acetylation, butyrylation, and protein expression in neuroblastoma. J Proteome Res 13:4211–4219

Yang XJ (2015) MOZ and MORF acetyltransferases: Molecular interaction, animal development and human disease. Biochim Biophys Acta 1853:1818–1826

Zhang Z, Pugh BF (2011) High-resolution genome-wide mapping of the primary structure of chromatin. Cell 144:175–186

Zhang K, Chen Y, Zhang Z, Zhao Y (2009) Identification and verification of lysine propionylation and butyrylation in yeast core histones using PTMap software. J Proteome Res 8:900–906

Zhao D, Guan H, Zhao Z, Mi W, Wen H, Li Y, Zhao Y, Allis CD, Shi X, Li H (2016) YEATS2 is a selective histone crotonylation reader. Cell Res 26:629–632

Adv Exp Med Biol - Protein Reviews (2017) 2:93–101
DOI 10.1007/5584_2017_60

Published online: 22 June 2017

Regulation of the Extracellular SERPINA5 (Protein C Inhibitor) Penetration Through Cellular Membranes

Felix C. Wahlmüller, Hanjiang Yang, Margareta Furtmüller, and Margarethe Geiger

Abstract

It is generally accepted that the phospholipid bilayer of the cell membrane is impermeable for proteins and peptides and that these molecules require special mechanisms for their transport from the extra- to the intracellular space. Recently there is increasing evidence that certain proteins/peptides can also directly cross the phospholipid membrane. SERPINA5 (protein C inhibitor) is a secreted protease inhibitor with broad protease reactivity and wide tissue distribution. It binds glycosaminoglycans and certain phospoholipids, which can modulate its inhibitory activity. SERPINA5 has been shown to be internalized by platelets, granulocytes, HL-60 promyelocytic leukemia cells, and by Jurkat lymphoma cells. Once inside the cell it can translocate to the nucleus. There are several indications that SERPINA5 can directly cross the phospholipid bilayer of the cell membrane. In this review we will describe what is known so far about the conditions, as well as the cellular and molecular requirements for SERPINA5 translocation through the cell membrane and for its penetration of pure phospholipid vesicles.

Keywords

Serpin • Protein C inhibitor • Translocation • Cell penetrating peptide • Phospholipid • Cell membrane

Abbreviations

LRP	LDL-receptor related protein, alpha-2-macroglobulin receptor
LUV	large unilamellar vesicle
PCI	protein C inhibitor
PE	phosphatidylethanolamine

F.C. Wahlmüller, H. Yang, M. Furtmüller, and M. Geiger (✉)
Department of Vascular Biology and Thrombosis Research, Center of Physiology and Pharmacology, Medical University Vienna, Schwarzspanierstrasse 17, 1090 Vienna, Austria
e-mail: margarethe.geiger@meduniwien.ac.at

1 Intra- and Extracellular Serpins

Serpins (*ser*ine *p*rotease *in*hibitors) are a superfamily of proteins that share a common core domain consisting of three β-sheets, 8–9 α-helices, and a solvent exposed reactive center loop (for review see (Huntington 2011)). Although most serpins are single-use suicide inhibitors of serine proteases, the family also contains non-inhibitory members and cross class inhibitors of other proteases (e.g. cysteine proteases) (Law et al. 2006; Pak et al. 2004). Serpins are involved in the regulation of blood coagulation, fibrinolysis, and many other important biological processes (Law et al. 2006). They also share the ability to bind non-protease ligands such as glycosaminoglycans (Geiger et al. 1991; Pratt et al. 1992; Tollefsen 1994; Quinsey et al. 2004), phospholipids (Wahlmuller et al. 2014; Malleier et al. 2007), DNA (Grigoryev et al. 1999; Abraham 1992), collagen (Koide et al. 1992), or hormones (Jerabek et al. 2001; Qi et al. 2011; Carrell et al. 2011; Zhou et al. 2008), which may modulate their protease inhibitory activity (Pratt et al. 1992; Wahlmuller et al. 2014; Malleier et al. 2007; Ecke et al. 1992), regulate hormone delivery (Carrell et al. 2011; Zhou et al. 2008), or contribute to other yet unknown biological effects.

It is generally accepted that some serpins are secreted, whereas others fulfill their functions inside the cell and, following cell fractionation, can be found in cytosolic and in nuclear fractions. Interestingly some serpins do not obey that rule, since they are found in- and outside the cell. Some intracellular serpins, which belong to serpin clade B, have also been found extracellularly (Izuhara et al. 2008). One example for a B-clade serpin with bi-topological distribution is plasminogen activator inhibitor 2 (PAI-2, SERPINB2) (Medcalf 2011; Stringer et al. 2012; Siefert et al. 2014). SERPINB2 was first discovered as an inhibitor of the plasminogen activator urokinase (Kawano et al. 1970). Only a small percentage of SERPINB2 is normally being glycosylated and secreted. The predominant part of SERPINB2 is not secreted and stays inside the cell as a non-glycosylated 45 kDa form (Genton et al. 1987). Further analysis revealed that SERPINB2 secretion is triggered by an inefficient secretion signal which consist of two rather hydrophobic domains close to the N-terminus (von Heijne et al. 1991). It is assumed that this might be a fine tuning system for secretion efficiency, as both domains are needed for SERPINB2 translocation. Yet the ability for facultative translocation is a very interesting feature of SERPINB2 and might be a regulatory factor for SERPINB2 availability (for review see (Medcalf and Stasinopoulos 2005)). On the other hand, some secreted serpins are also present inside the cell. These include alpha-1-antichymotrypsin (SERPINA3) (Santamaria et al. 2013), angiotensinogen (SERPINA8) (Garrido-Gil et al. 2013), pigment epithelium-derived factor (PEDF, SERPINF1) (Karakousis et al. 2001; Anguissola et al. 2011) and protein C inhibitor (PCI, SERPINA5) (Baumgartner et al. 2007; Yang et al. 2015). The variability of serpin localization might be a yet underestimated possibility for cells to adapt to different physiological situations or contribute to tissue specific functions. The localization duality of so called "secreted serpins" might be explained by optional intracellular localization due to variations in splicing, internalization of previously secreted protein, or other mechanisms.

There has long been general agreement that the cellular plasma membrane represents a barrier for proteins, and that these molecules can cross this barrier only via special mechanisms such as fluid-phase- or receptor-mediated endocytosis. Recently there is increasing evidence that proteins can also directly cross the cell membrane (Spatazza et al. 2013; Prochiantz 2013; Wu and Gehring 2014). Within these proteins domains rich in basic amino acids have been identified that were responsible for their ability to cross the plasma membrane. Peptides corresponding to these sequences as well as synthetic peptides with similar properties, so called cell-penetrating peptides, are now used for the intracellular delivery of diverse cargos (Said Hassane et al. 2010). However, the mechanism (s) of protein/peptide internalization is/are not

fully clear and may be different for different proteins/peptides. It has been proposed that positively charged protein domains interact with cell surface molecules such as negatively charged phospholipids and/or glycosaminoglycans. This leads to accumulation of the protein/peptide on the cell surface. In a second step the protein/peptide is internalized by the cell either by directly interacting with the phospholipid bilayer or by other mechanisms such as micropinocytosis (Wu and Gehring 2014; Alves et al. 2010). As far as serpins are concerned, several serpin-protease complexes bind to LDL-receptor related protein (LRP; alpha-2-macroglobulin receptor) and are cleared from the circulation by receptor mediated endocytosis via clathrin-coated pits (Strickland and Ranganathan 2003; Kasza et al. 1997; Zhou et al. 2015; Fazavana et al. 2016; Kounnas et al. 1996). So far no other way of serpin internalization by cells has been described. As outlined in detail below, we have indications that SERPINA5 can be internalized by cells in an unconventional manner, possibly directly through the phospholipid membrane.

2 Biochemistry and Biology of Protein C Inhibitor (PCI, SERPINA5)

Protein C inhibitor (PCI) is a protease inhibitor and a member of clade A of the serpin superfamily. The designation "protein C inhibitor (PCI)" was initially chosen, since it was discovered as an inhibitor of the anticoagulant protease activated protein C (Marlar and Griffin 1980; Suzuki et al. 1983). However, this name may be misleading, since PCI is a serpin with very broad protease reactivity, and for the interactions with several target proteases higher second order rate constants have been determined than for its interaction with activated protein C (for review see (Wahlmüller 2015)). In agreement with the accepted serpin nomenclature (Silverman et al. 2001) we will therefore use the terms SERPINA5/*SERPINA5* for the human protein/gene and serpinA5/*serpinA5* for the mouse protein/gene, respectively, rather than protein C inhibitor. SERPINA5 is a secreted protein. In man it is synthesized in many organs and tissues (Hayashi et al. 2004). So far it has been detected in almost every body fluid and secretion (Laurell et al. 1992). In mice, at least in adults, serpinA5 is almost exclusively expressed in the male and female reproductive tracts (Zechmeister-Machhart et al. 1996; Uhrin et al. 2000). Therefore it is not surprising that the only phenotype of serpinA5 knockout mice was infertility of homozygous males (Uhrin et al. 2000). The different tissue specific expression of SERPINA5 in man and mice makes it difficult to translate data from mouse studies to the human system. SERPINA5 binds heparin and other glycosaminoglycans (Geiger et al. 1991; Pratt and Church 1992; Li et al. 2007; Priglinger et al. 1994). Furthermore it binds a variety of phospholipids (Wahlmuller et al. 2014; Malleier et al. 2007). The majority of studies analyzing the interaction of SERPINA5 with glycosaminglycans and phospholipids has been performed *in vitro*. Only few data have been published showing the interaction of SERPINA5 with glycosaminoglycans and phospholipids in living cells or tissues (Malleier et al. 2007; Priglinger et al. 1994; Einfinger et al. 2015; Rieger et al. 2014).

3 Internalization of SERPINA5 by Cells

Prendes et al. have shown that human platelets contain SERPINA5, which can be derived from endogenous synthesis in megakaryocytes as well as from internalization (Prendes et al. 1999). In these studies it was also observed that in bone marrow sections SERPINA5 was present in the nucleus of megakaryocytes and granulocytes. Follow up *ex vivo* experiments revealed that SERPINA5 was internalized by cells and translocated to the nucleus (Baumgartner et al. 2007; Yang et al. 2015). Not all cells incorporated SERPINA5, but only ~10–15%. The molecular weight of SERPINA5 is

~57 kDa making it unlikely that it translocates to the nuclear compartment by simple diffusion. The observed nuclear localization of PCI therefore suggests the presence of a nuclear localization signal in the protein. The inspection of the SERPINA5 protein sequence revealed 2 putative classical NLS sequences, one localized in the A + -helix and the second in H-helix of SERPINA5. The functionality of both sequences was analyzed leading to the conclusion that the nuclear localization signal sequence in the H-helix was responsible for the observed translocation of SERPINA5 to nucleus (Sokolikova et al. unpublished data). In the following paragraphs we will characterize the cellular and molecular requirements for SERPINA5 internalization. We will also briefly describe the cells and methods used to allow the reader better interpretation of the data obtained.

3.1 Cells and Methods Used for Studying Internalization of SERPINA5

Internalization of SERPINA5 was studied *in vitro* with human peripheral blood granulocytes, with HL-60 cells (promyelocytic leukemia cells), and with Jurkat lymphoma cells. For visualization of SERPINA5 internalization cells were incubated with appropriately labeled SERPINA5 and analyzed by confocal laser scanning microscopy or transmission electron microscopy. For quantitation of SERPINA5 internalization cells were incubated with ^{125}I–labeled SERPINA5. In these experiments internalized radioactivity was quantified after proteolytic removal of cell surface associated radioactivity. For studying the molecular requirements for serpinA5 internalization, human cells (Jurkat) and recombinant intact or truncated mouse serpinA5 were used to be able to differentiate between internalized and endogenous protein by using antibodies specifically recognizing mouse serpinA5. Cells were incubated with intact or cleaved serpinA5, or with a truncated serpinA5 mutant lacking the first 18 amino acids. Thereafter subcellular fractions were prepared and analyzed SDS-PAGE and Western blotting. In addition to these *ex vivo* experiments *in vivo* experiments were performed, in which biotin-labeled SERPINA5 was injected into the tail vein of mice. After 30 min blood was drawn, and leukocytes were analyzed for the presence of incorporated SERPINA5 by confocal microscopy using Cy-2-labeled streptavidin for the detection of biotinylated SERPINA5. Experiments analyzing the cellular requirements and conditions for internalization were mainly done with granulocytes and with HL-60 cells (Baumgartner et al. 2007). Studies analyzing the protein requirements for cellular internalization were done with Jurkat lymphoma cells (Yang et al. 2015). For the characterization of the direct interaction of SERPINA5 with phospholipid membranes large unilamellar vesicles (LUVs) with different phospholipid compositions were used (Baumgartner et al. 2007).

3.2 Conditions and Cellular Requirements for the Internalization of SERPINA5

Internalization of SERPINA5 occurred at 37 °C as well as at 6 °C. It was very similar in the absence and presence of receptor-associated protein (RAP), which blocks the uptake of serpin/protease complexes via LRP (Fazavana et al. 2016; Croucher et al. 2006; Storm et al. 1997; Rodenburg et al. 1998; McKee et al. 2015; Jensen et al. 2009; Fayard et al. 2009). SERPINA5 internalization was also seen with cells with disrupted dynamin2 function. Taken together, these data suggest that internalization of SERPINA5 is endocytosis independent (Baumgartner et al. 2007).

Internalization of SERPINA5 by cells was decreased in the presence of heparin, suggesting that cell surface glycosaminoglycans play a role for SERPINA5 internalization or for its enrichment on the cell surface. Heparin also competes with binding of SERPINA5 to

phosphatidylserine and to oxidized phosphatidylethanolamine (PE), and binding of these phospholipids involves the heparin-binding site of SERPINA5, which is located in its H-helix (Malleier et al. 2007). Furthermore SERPINA5 can permeabilize bacterial membranes and thereby kill bacteria (Malmstrom et al. 2009). Also for this membrane permeabilizing effect the heparin binding site is necessary. Therefore, the fact that heparin interferes with the internalization of SERPINA5 does not necessarily mean that cellular glycosaminoglycans are involved. Heparin may compete with both, with binding of SERPINA5 to cell surface glycosaminoglycans/phopholipids as well as well as with the uptake mechanism itself. As indicated above, there are data in the literature that glycosaminoglycans are important for the accumulation of cell penetrating proteins on the cell surface, from where the proteins can use different routes through the cellular membrane. Priglinger et al. have shown that glycosaminoglycans present on the luminal surface of kidney cells (TCL-598) can bind SERPINA5 (Priglinger et al. 1994). *In vitro* glycosaminoglycans isolated from these cells stimulated the activity of SERPINA5 in a heparin-like manner (Geiger et al. 1991). At the time these studies were performed, a possible role of cellular glycosaminoglycans for the internalization of SERPINA5 has not been considered.

Duramycin, a cyclic peptide specifically interacting with the phospholipid PE, interfered in a dose dependent manner with the internalization of SERPINA5 by neutrophils suggesting the direct involvement of PE in the uptake (Baumgartner et al. 2007). The hypothesis that PE in the cell membrane is directly involved in the internalization is furthermore supported by the fact that PE-containing phospholipid vesicles interfere with the uptake of SERPINA5 by neutrophils. SERPINA5 can also get access to the intravesicular space of LUVs, suggesting that it can cross pure phospholipid membranes. This is only seen with PE-containing LUVs, but not with LUVs containing only phosphatidylcholine, again suggesting the involvement of PE. It seems that the conical shape of PE species with long chain fatty acids is more important for SERPINA5 membrane transduction than its ethanolamine head group, since diacylglycerol but not short chain PE, supported SERPINA5 internalization in a similar way (Baumgartner et al. 2007). As judged from experiments performed with PE containing LUVs, SERPINA5 did not cause pore formation in the phospholipid bilayer, but induced changes in its structure that are consistent with the formation of aqueous compartments within the membrane. The crystal structure of SERPINA5 was characterized in 2003 (Huntington et al. 2003). Phospholipid docking studies based on this structure were performed. These studies together with data obtained for the incorporation of site-specific SERPINA5 mutants into PE-containing phospholipid vesicles, are consistent with a model, in which PE is accommodated in a branched hydrophobic cavity between helix H and helix D of SERPINA5 (Baumgartner et al. 2007). This accommodation seems to be necessary for the phospholipid membrane insertion of SERPINA5. In the experiments with pure phospholipid vesicles - unlike in intact cells - SERPINA5 was not completely translocated to the core of the vesicles, suggesting that - in addition to the interaction of SERPINA5 with PE - additional transfer mechanisms are operative in cells.

3.3 Molecular Requirements for the Cellular Internalization of SERPINA5

Internalization was observed with both, SERPINA5 purified from human urine as well as with recombinant SERPINA5 expressed in E. coli. This suggests that glycosylation of the protein is not a requirement for its internalization. *In vitro* experiments analyzing the interaction of SERPINA5 with testisin (PRSS21), a GPI-anchored membrane serine protease, revealed that testisin cleaved SERPINA5 not only at its reactive site peptide bond, but additionally at a site close to its N-terminus. Upon this cleavage a peptide corresponding to helix A+ was released (Yang et al. 2015). This was seen

with human as well as with mouse serpinA5. N-terminally cleaved SERPINA5 forms lacking the first 11 amino acids (human SERPINA5) or the first 18 amino acids (mouse serpinA5), respectively, were not internalized by cells. Also a truncated serpinA5 mutant lacking the N-terminus was not internalized. Protease inhibitory activity and heparin binding were not affected by this N-terminal truncation. Proteolytic removal of the N-terminal helix A+ of SERPINA5 by local proteases may therefore restrict the entrance of SERPINA5 into cells and thereby regulate its possible intracellular functions. On the other hand, synthetic FITC-labeled peptides with amino acid sequences corresponding to the 11 N-terminal amino acids of human or the N-terminal 18 amino acids of mouse serpinA5, respectively, were internalized by Jurkat cells. The labeled SERPINA5 peptides were internalized to a much higher extent than FITC alone or FITC-labeled dextran, suggesting that the uptake of the peptides does not occur via simple fluid phase endocytosis. Staining of the incorporated FITC-labeled SERPINA5 peptides appeared homogenous. This was different from staining of internalized FITC-labeled TAT-peptide, which showed a punctate staining consistent with internalization via endocytosis. The TAT-peptide is a synthetic cell penetrating peptide with the sequence of the protein domain responsible for the cellular uptake of the HIV-1 trans-activator of transcription (TAT) protein. SERPINA5 peptides and the TAT-peptide therefore seem to use (a) different route(s) of internalization.

4 Conclusions and Perspectives

There are several indications suggesting that SERPINA5 is internalized by cells in a manner similar to that seen with cell penetrating peptides/proteins. However, so far there is no definitive proof for this assumption. The fact that internalization of a related heparin-binding serpin (SERPIND1, heparin cofactor II) was not observed under similar assay conditions does not justify the conclusion that the internalization is specific for SERPINA5. It can as well be a more general phenomenon seen with many proteins. Although several intracellular proteins interacting with SERPINA5 have been identified (Furtmüller et al. 2014) (Sokolikova et al., unpublished), it is not known if its internalization is biologically relevant. Further studies are needed to determine the intracellular functions of SERPINA5. So far all SERPINA5 internalization studies were done with cells growing in suspension (HL60 cell, Jurkat cells, and platelets). It is therefore also unclear if extracellular matrix components contribute to SERPINA5 internalization. In addition to exposed phospholipids and glycosaminoglycans on the cell surface, also substances in the vicinity of cells could influence SERPINA5 internalization either by causing local accumulation of the protein or by proteolytic removal of its N-terminal cell penetrating peptide. Further studies are needed to clearly define which features enable certain cells to internalize SERPINA5, while it is excluded from others. Such features could be the phospholipid composition of the cell membrane, the presence of surface exposed complex sugars, the transmembrane voltage potential, and/or cell-specific chaperone proteins or co-factors. The only *in vivo* data obtained so far are from experiments where labeled SERPINA5 was injected into the tail vein of mice. In these experiments Baumgärtner et al. have shown that injected SERPINA5 was detectable in the nucleus of peripheral blood granulocytes (Baumgartner et al. 2007). Therefore data obtained *ex vivo* with cells in suspension need to be confirmed with intact tissues and in the living organism. Thereby possible new ways of protein translocation could be identified which may be used not only by SERPINA5, but also by other proteins.

Acknowledgements This work was supported by grants P22792-B11 from the Austrian Science Fund (FWF) and 14064 from the "Medizinisch-wissenschaftlicher Fonds des Bürgermeisters der Bundeshauptstadt Wien" (both to MG).

Conflict of Interest The authors declare that they have no conflicts of interest.

Ethical Approval This article does not contain any studies with human participants or animals performed by any of the authors.

References

Abraham CR (1992) The role of the acute-phase protein alpha 1-antichymotrypsin in brain dysfunction and injury. Res Immunol 143(6):631–636

Alves ID, Jiao CY, Aubry S, Aussedat B, Burlina F, Chassaing G, Sagan S (2010) Cell biology meets biophysics to unveil the different mechanisms of penetratin internalization in cells. Biochim Biophys Acta 1798(12):2231–2239

Anguissola S, McCormack WJ, Morrin MA, Higgins WJ, Fox DM, Worrall DM (2011) Pigment epithelium-derived factor (PEDF) interacts with transportin sr2, and active nuclear import is facilitated by a novel nuclear localization motif. PLoS One 6(10):e26234

Baumgartner P, Geiger M, Zieseniss S, Malleier J, Huntington JA, Hochrainer K, Bielek E, Stoeckelhuber M, Lauber K, Scherfeld D, Schwille P, Waldele K, Beyer K, Engelmann B (2007) Phosphatidylethanolamine critically supports internalization of cell-penetrating protein c inhibitor. J Cell Biol 179(4):793–804

Carrell R, Qi X, Zhou A (2011) Serpins as hormone carriers: modulation of release. Methods Enzymol 501:89–103

Croucher D, Saunders DN, Ranson M (2006) The urokinase/PAI-2 complex: a new high affinity ligand for the endocytosis receptor low density lipoprotein receptor-related protein. J Biol Chem 281 (15):10206–10213

Ecke S, Geiger M, Binder BR (1992) Glycosaminoglycans regulate the enzyme specificity of protein-c inhibitor. Ann N Y Acad Sci 667:84–86

Einfinger K, Badrnya S, Furtmuller M, Handschuh D, Lindner H, Geiger M (2015) Phospholipid binding protein C inhibitor (PCI) is present on microparticles generated in vitro and in vivo. PLoS One 10(11): e0143137

Fayard B, Bianchi F, Dey J, Moreno E, Djaffer S, Hynes NE, Monard D (2009) The serine protease inhibitor protease nexin-1 controls mammary cancer metastasis through LRP-1-mediated MMP-9 expression. Cancer Res 69(14):5690–5698

Fazavana JG, Muczynski V, Proulle V, Wohner N, Christophe OD, Lenting PJ, Denis CV (2016) LRP1 contributes to the clearance of the factor VIIa/antithrombin complex. J Thromb Haemost. doi:10.1111/jth.13502

Furtmüller M, Yang H, Sarg B, Lindner H, Geiger M (2014) SerpinA5 is internalized by Jurkat lymphoma cells and regulates nuclear cathepsin L. Abstract Book, 7th International Symposium on Serpin Biology, Structure, and Function, Leogang, Austria, Abstract 67

Garrido-Gil P, Valenzuela R, Villar-Cheda B, Lanciego JL, Labandeira-Garcia JL (2013) Expression of angiotensinogen and receptors for angiotensin and prorenin in the monkey and human substantia nigra: an intracellular renin-angiotensin system in the nigra. Brain Struct Funct 218(2):373–388

Geiger M, Priglinger U, Griffin JH, Binder BR (1991) Urinary protein c inhibitor. Glycosaminoclycans synthesized by the epithelial kidney cell line tcl-598 enhance its interaction with urokinase. J Biol Chem 266(18):11851–11857

Genton C, Kruithof EK, Schleuning WD (1987) Phorbol ester induces the biosynthesis of glycosylated and nonglycosylated plasminogen activator inhibitor 2 in high excess over urokinase-type plasminogen activator in human u-937 lymphoma cells. J Cell Biol 104 (3):705–712

Grigoryev SA, Bednar J, Woodcock CL (1999) Ment, a heterochromatin protein that mediates higher order chromatin folding, is a new serpin family member 5. J Biol Chem 274(9):5626–5636

Hayashi T, Nishioka J, Kamada H, Asanuma K, Kondo H, Gabazza EC, Ido M, Suzuki K (2004) Characterization of a novel human protein C inhibitor (PCI) gene transgenic mouse useful for studying the role of PCI in physiological and pathological conditions. J Thromb Haemost 2(6):949–961

Huntington JA (2011) Serpin structure, function and dysfunction. J Thromb Haemost 9(Suppl 1):26–34

Huntington JA, Kjellberg M, Stenflo J (2003) Crystal structure of protein c inhibitor provides insights into hormone binding and heparin activation. Structure 11 (2):205–215

Izuhara K, Ohta S, Kanaji S, Shiraishi H, Arima K (2008) Recent progress in understanding the diversity of the human ov-serpin/clade b serpin family. Cell Mol Life Sci 65(16):2541–2553

Jensen JK, Dolmer K, Gettins PG (2009) Specificity of binding of the low density lipoprotein receptor-related protein to different conformational states of the clade e serpins plasminogen activator inhibitor-1 and proteinase nexin-1. J Biol Chem 284(27):17989–17997

Jerabek I, Zechmeister-Machhart M, Binder BR, Geiger M (2001) Binding of retinoic acid by the inhibitory serpin protein c inhibitor. Eur J Biochem 268 (22):5989–5996

Karakousis PC, John SK, Behling KC, Surace EM, Smith JE, Hendrickson A, Tang WX, Bennett J, Milam AH (2001) Localization of pigment epithelium derived factor (pedf) in developing and adult human ocular tissues. Mol Vis 7:154–163

Kasza A, Petersen HH, Heegaard CW, Oka K, Christensen A, Dubin A, Chan L, Andreasen PA (1997) Specificity of serine proteinase/serpin complex binding to very-low-density lipoprotein receptor and alpha2-macroglobulin receptor/low-density-lipoprotein-receptor-related protein. Eur J Biochem 248(2):270–281

Kawano T, Morimoto K, Uemura Y (1970) Partial purification and properties of urokinase inhibitor from human placenta. J Biochem 67(3):333–342

Koide T, Asada S, Nagata K (1992) Substrate recognition of collagen-specific molecular chaperone hsp47. Structural requirements and binding regulation. J Biol Chem 274(49):34523–34526

Kounnas MZ, Church FC, Argraves WS, Strickland DK (1996) Cellular internalization and degradation of antithrombin iii-thrombin, heparin cofactor ii-thrombin, and alpha 1-antitrypsin-trypsin complexes is mediated by the low density lipoprotein receptor-related protein. J Biol Chem 271(11):6523–6529

Laurell M, Christensson A, Abrahamsson PA, Stenflo J, Lilja H (1992) Protein C inhibitor in human body fluids. Seminal plasma is rich in inhibitor antigen deriving from cells throughout the male reproductive system. J Clin Invest 89(4):1094–1101

Law RH, Zhang Q, McGowan S, Buckle AM, Silverman GA, Wong W, Rosado CJ, Langendorf CG, Pike RN, Bird PI, Whisstock JC (2006) An overview of the serpin superfamily. Genome Biol 7(5):216

Li W, Adams TE, Kjellberg M, Stenflo J, Huntington JA (2007) Structure of native protein c inhibitor provides insight into its multiple functions. J Biol Chem 282 (18):13759–13768

Malleier JM, Oskolkova O, Bochkov V, Jerabek I, Sokolikova B, Perkmann T, Breuss J, Binder BR, Geiger M (2007) Regulation of protein C inhibitor (PCI) activity by specific oxidized and negatively charged phospholipids. Blood 109(11):4769–4776

Malmstrom E, Morgelin M, Malmsten M, Johansson L, Norrby-Teglund A, Shannon O, Schmidtchen A, Meijers JC, Herwald H (2009) Protein C inhibitor--a novel antimicrobial agent. PLoS Pathog 5(12): e1000698

Marlar RA, Griffin JH (1980) Deficiency of protein C inhibitor in combined factor v/viii deficiency disease. J Clin Invest 66(5):1186–1189

McKee CM, Ding Y, Zhou J, Li C, Huang L, Xin X, He J, Allen JE, El-Deiry WS, Cao Y, Muschel RJ, Xu D (2015) Protease nexin 1 induces apoptosis of prostate tumor cells through inhibition of x-chromosome-linked inhibitor of apoptosis protein. Oncotarget 6 (6):3784–3796

Medcalf RL (2011) Plasminogen activator inhibitor type 2: still an enigmatic serpin but a model for gene regulation. Methods Enzymol 499:105–134

Medcalf RL, Stasinopoulos SJ (2005) The undecided serpin. The ins and outs of plasminogen activator inhibitor type 2. FEBS J 272(19):4858–4867

Pak SC, Kumar V, Tsu C, Luke CJ, Askew YS, Askew DJ, Mills DR, Bromme D, Silverman GA (2004) Srp-2 is a cross-class inhibitor that participates in postembryonic development of the nematode caenorhabditis elegans: initial characterization of the clade l serpins. J Biol Chem 279(15):15448–15459

Pratt CW, Church FC (1992) Heparin binding to protein c inhibitor. J Biol Chem 267(13):8789–8794

Pratt CW, Whinna HC, Church FC (1992) A comparison of three heparin-binding serine proteinase inhibitors. J Biol Chem 267(13):8795–8801

Prendes MJ, Bielek E, Zechmeister-Machhart M, Vanyek-Zavadil E, Carroll VA, Breuss J, Binder BR, Geiger M (1999) Synthesis and ultrastructural localization of protein C inhibitor in human platelets and megakaryocytes. Blood 94(4):1300–1312

Priglinger U, Geiger M, Bielek E, Vanyek E, Binder BR (1994) Binding of urinary protein-c inhibitor to cultured human epithelial kidney tumor-cells (TCL-598) – the role of glycosaminoglycans present on the luminal cell-surface. J Biol Chem 269 (20):14705–14710

Prochiantz A (2013) Signaling with homeoprotein transcription factors in development and throughout adulthood. Curr Genomics 14(6):361–370

Qi X, Loiseau F, Chan WL, Yan Y, Wei Z, Milroy LG, Myers RM, Ley SV, Read RJ, Carrell RW, Zhou A (2011) Allosteric modulation of hormone release from thyroxine and corticosteroid-binding globulins. J Biol Chem 286(18):16163–16173

Quinsey NS, Greedy AL, Bottomley SP, Whisstock JC, Pike RN (2004) Antithrombin: in control of coagulation 1. Int J Biochem Cell Biol 36(3):386–389

Rieger D, Assinger A, Einfinger K, Sokolikova B, Geiger M (2014) Protein C inhibitor (PCI) binds to phosphatidylserine exposing cells with implications in the phagocytosis of apoptotic cells and activated platelets. PLoS One 9(7):e101794

Rodenburg KW, Kjoller L, Petersen HH, Andreasen PA (1998) Binding of urokinase-type plasminogen activator-plasminogen activator inhibitor-1 complex to the endocytosis receptors alpha2-macroglobulin receptor/low-density lipoprotein receptor-related protein and very-low-density lipoprotein receptor involves basic residues in the inhibitor. Biochem J 329(Pt 1):55–63

Said Hassane F, Saleh AF, Abes R, Gait MJ, Lebleu B (2010) Cell penetrating peptides: overview and applications to the delivery of oligonucleotides. Cell Mol Life Sci 67(5):715–726

Santamaria M, Pardo-Saganta A, Alvarez-Asiain L, Di Scala M, Qian C, Prieto J, Avila MA (2013) Nuclear alpha1-antichymotrypsin promotes chromatin condensation and inhibits proliferation of human hepatocellular carcinoma cells. Gastroenterology 144 (4):818–828. e814

Siefert SA, Chabasse C, Mukhopadhyay S, Hoofnagle MH, Strickland DK, Sarkar R, Antalis TM (2014) Enhanced venous thrombus resolution in plasminogen activator inhibitor type-2 deficient mice. J Thromb Haemost 12(10):1706–1716

Silverman GA, Bird PI, Carrell RW, Church FC, Coughlin PB, Gettins PG, Irving JA, Lomas DA, Luke CJ, Moyer RW, Pemberton PA, Remold-O'Donnell E, Salvesen GS, Travis J, Whisstock JC (2001) The serpins are an expanding superfamily of structurally similar but functionally diverse proteins.

Evolution, mechanism of inhibition, novel functions, and a revised nomenclature. J Biol Chem 276 (36):33293–33296

Spatazza J, Di LE, Joliot A, Dupont E, Moya KL, Prochiantz A (2013) Homeoprotein signaling in development, health, and disease: a shaking of dogmas offers challenges and promises from bench to bed. Pharmacol Rev 65(1):90–104

Storm D, Herz J, Trinder P, Loos M (1997) C1 inhibitor-C1s complexes are internalized and degraded by the low density lipoprotein receptor-related protein. J Biol Chem 272(49):31043–31050

Strickland DK, Ranganathan S (2003) Diverse role of ldl receptor-related protein in the clearance of proteases and in signaling. J Thromb Haemost 1(7):1663–1670

Stringer B, Udofa EA, Antalis TM (2012) Regulation of the human plasminogen activator inhibitor type 2 gene: cooperation of an upstream silencer and transactivator. J Biol Chem 287(13):10579–10589

Suzuki K, Nishioka J, Hashimoto S (1983) Protein C inhibitor. Purification from human plasma and characterization. J Biol Chem 258(1):163–168

Tollefsen DM (1994) The interaction of glycosaminoglycans with heparin cofactor II. Ann N Y Acad Sci 714:21–31

Uhrin P, Dewerchin M, Hilpert M, Chrenek P, Schofer C, Zechmeister-Machhart M, Kronke G, Vales A, Carmeliet P, Binder BR, Geiger M (2000) Disruption of the protein C inhibitor gene results in impaired spermatogenesis and male infertility. J Clin Invest 106(12):1531–1539

von Heijne G, Liljeström P, Mikus P, Andersson H, Ny T (1991) The efficiency of the uncleaved secretion signal in the plasminogen activator inhibitor type 2 protein can be enhanced by point mutations that increase its hydrophobicity. J Biol Chem 266 (23):15240–15243

Wahlmüller FC (2015) Protein C inhibitor. In: Geiger M, Wahlmüller FC, Furtmüller M (eds) The serpin family. Proteins with multiple functions in health and disease. Springer, Cham, pp 153–177

Wahlmuller FC, Sokolikova B, Rieger D, Geiger M (2014) New lipid interaction partners stimulate the inhibition of activated protein c by cell-penetrating protein C inhibitor. Thromb Haemost 111(1):41–52

Wu X, Gehring W (2014) Cellular uptake of the antennapedia homeodomain polypeptide by macropinocytosis. Biochem Biophys Res Commun 443(4):1136–1140

Yang H, Wahlmuller FC, Sarg B, Furtmuller M, Geiger M (2015) A+−helix of protein C inhibitor (PCI) is a cell-penetrating peptide that mediates cell membrane permeation of PCI. J Biol Chem 290(5):3081–3091

Zechmeister-Machhart M, Hufnagl P, Uhrin P, Xu J, Geiger M, Binder BR (1996) Molecular cloning and tissue distribution of mouse protein C inhibitor (PCI). Immunopharmacology 32(1–3):96–98

Zhou A, Wei Z, Stanley PL, Read RJ, Stein PE, Carrell RW (2008) The s-to-r transition of corticosteroid-binding globulin and the mechanism of hormone release. J Mol Biol 380(1):244–251

Zhou X, Liu Z, Shapiro L, Yang J, Burton GF (2015) Low-density lipoprotein receptor-related protein 1 mediates alpha1-antitrypsin internalization in cd4+ t lymphocytes. J Leukoc Biol 98(6):1027–1035

Adv Exp Med Biol - Protein Reviews (2017) 2:103–148
DOI 10.1007/5584_2017_93

Published online: 22 August 2017

Coding of Class I and II Aminoacyl-tRNA Synthetases

Charles W. Carter Jr

Abstract

The aminoacyl-tRNA synthetases and their cognate transfer RNAs translate the universal genetic code. The twenty canonical amino acids are sufficiently diverse to create a selective advantage for dividing amino acid activation between two distinct, apparently unrelated superfamilies of synthetases, Class I amino acids being generally larger and less polar, Class II amino acids smaller and more polar. Biochemical, bioinformatic, and protein engineering experiments support the hypothesis that the two Classes descended from opposite strands of the same ancestral gene. Parallel experimental deconstructions of Class I and II synthetases reveal parallel losses in catalytic proficiency at two novel modular levels—protozymes and Urzymes—associated with the evolution of catalytic activity. Bi-directional coding supports an important unification of the proteome; affords a genetic relatedness metric—middle base-pairing frequencies in sense/antisense alignments—that probes more deeply into the evolutionary history of translation than do single multiple sequence alignments; and has facilitated the analysis of hitherto unknown coding relationships in tRNA sequences. Reconstruction of native synthetases by modular thermodynamic cycles facilitated by domain engineering emphasizes the subtlety associated with achieving high specificity, shedding new light on allosteric relationships in contemporary synthetases. Synthetase Urzyme structural biology suggests that they are catalytically-active molten globules, broadening the potential manifold of polypeptide catalysts accessible to primitive genetic coding and motivating revisions of the origins of catalysis. Finally, bi-directional genetic coding of some of the oldest genes in the proteome places major limitations on the likelihood that any RNA World preceded the origins of coded proteins.

C.W. Carter Jr (✉)
Department of Biochemistry and Biophysics, University of North Carolina at Chapel Hill, Chapel Hill, NC 27599-7260, USA
e-mail: carter@med.unc.edu

Keywords
Bi-directional genetic coding • Modular deconstruction • Protozymes • Reflexivity • Synthetase class division • Urzymes

Abbreviations

aaRS	aminoacyl-tRNA synthetase(s)
TrpRS	tryptophanyl-tRNA synthetase
LeuRS	Leucyl-tRNA synthetase
HisRS	histidyl-tRNA synthetase
ATP	adenosine 5′ triphosphate
PPi	inorganic pyrophosphate
ASA	Solvent-accessible surface area
HSQC	Heteronuclear Single-Quantum Correlation
BEAST	Bayesian Evolutionary Analysis Sampling Trees

1 Introduction

> It is unlikely that the aminoacyl-tRNA synthetases played any specific role in the evolution of the genetic code; their evolutions did not shape the codon assignments. (Woese et al. 2000)

> A real understanding of the code origin and evolution is likely to be attainable only in conjunction with a credible scenario for the evolution of the coding principle itself and the translation system. (Koonin and Novozhilov 2009)

The first epigram begins the concluding section of an authoritative review of this field published in 2000. The review contains much information and detailed interpretations based on the best available data at that time. Much of the research and theory to emerge since that time, however, has pointed to the opposite conclusion, in keeping with the dialectic component always implicit in scientific research. Consistent with the spirit expressed in the second epigram, unprecedented experimental and bioinformatic studies of the earliest evolution of aminoacyl-tRNA synthetases (aaRS) now make a compelling case for their intimate and probably necessary participation, with tRNA, in the evolution of the universal genetic code and the shaping of codon assignments.

1.1 The RNA World Hypothesis

The results reviewed herein are especially relevant to the question of whether or not present day biology replaced a prior organization in which information storage and catalysis both were entirely the province of RNA (Gilbert 1986; Robertson and Joyce 2012), an idea with resilient support in the literature (Robertson and Joyce 2012; Bernhardt 2012; Breaker 2012; Yarus 2011a, b; Van Noorden 2009; Wolf and Koonin 2007). As argued elsewhere in detail (Carter and Wills 2017; Wills and Carter 2017), the actual evidence for such scenarios is remarkably thin. The catalytic repertoire of RNA is very limited, relative to that of proteins (Wills 2016) and appears to be incapable of the sophistication required to synchronize metabolism with genetics. Evidence from ever more impressive aptamer replicases (Horning and Joyce 2016; Sczepanski and Joyce 2014; Taylor et al. 2015; Attwater et al. 2013; Wochner et al. 2011) and the practical value of Selex experiments (Tuerck and Gold 1990), would support only a highly limited version of the RNA World hypothesis unless phylogenetic relationships connected them to biological ancestry. So far as we know, all nucleic acids in contemporary biology are synthesized by protein enzymes, much as, reciprocally, the synthesis of proteins from activated amino acids is catalyzed by an RNA template at the peptidyl transferase center of the ribosome (Noller 2004; Noller et al. 1992; Bowman et al. 2015; Petrov et al. 2014). Thus no phylogenetic basis exists for ancestral ribozymal polymerases.

Moreover, the proposal that aminoacyl-tRNA synthetase enzymes arose as a single pair of ancestors coded bi-directionally on opposite strands of the same RNA gene decisively undermines the heart of the RNA World scenario, by establishing that catalysis of aminoacylation by proteins emerged with scarcely non-random fidelity. Such lack of specificity would have been abolished by purifying selection, had there been any ribozymal system with higher fidelity.

Moreover, aminoacyl-tRNA synthetases, aaRS, represent a unique group of enzymes because, as the only genes in the proteome that, when translated by the rules of genetic coding, can then impose those rules, they compose a unique, reflexive interface between genes and gene products. This special relationship to the proteome lends considerable significance to the evolutionary phylogenetics of aaRS gene sequences (Chandrasekaran et al. 2013; Cammer and Carter 2010), i.e. to how the aaRS came to be encoded. I will argue that by studying the ancestral coding of contemporary aaRS, we are led directly to a deeper understanding of how the genetic code might have arisen far more rapidly as a collaboration between ancestral proteins and RNAs than would ever have been possible in a world based entirely on a single polymer type (Carter and Wills 2017; Wills and Carter 2017).

There is consensus on several important aspects of aaRS structural and sequence-derived phylogenetics. Notably, they form two utterly distinct superfamilies that, on several levels are as distinct as possible from each other. Class I aaRS active sites all assume a Rossmann dinucleotide binding fold first observed in lactate dehydrogenase and flavodoxin (Buehner et al. 1973) in which the active site forms at the interface between parallel β-strands and the amino termini of two helixes. In contrast, Class II aaRS active sites are formed from antiparallel β-strands.

These structural differences (Eriani et al. 1990a) motivated substantial effort to understand why and how nature would have divided the labor of tRNA aminoacylation in such a binary fashion (Delarue 2007; Delarue and Moras 1992; Ibba et al. 2005; Cusack 1995; Härtlein and Cusack 1995; Cusack 1993, 1994; Ribas de Pouplana and Schimmel 2001a, b, c; Schimmel and Ribas de Pouplana 2000; Schimmel 1991, 1996; Schimmel et al. 1993;). Answers to these questions have emerged from supplementing phylogenetic analysis (O'Donoghue and Luthey-Schulten 2003) with experimental deconstruction by protein engineering (Martinez et al. 2015; Carter 2014; Li et al. 2011, 2013; Pham et al. 2007, 2010) and recapitulation (Weinreb et al. 2014; Li and Carter 2013) complemented by novel phylogenetic metrics (Chandrasekaran et al. 2013; Cammer and Carter 2010).

Conclusions emanating from these studies change how we view the proteome and origin of genetic coding in important ways:

(i) Class I and II aaRS appear to have originated from complementary coding sequences on opposite strands of the same bi-directional ancestral gene (Martinez et al. 2015; Carter et al. 2014).
(ii) That gene complementarity has profound implications for the origin of genetic information, some of which had already been suggested by others (Rodin et al. 2009, 2011; Rodin and Rodin 2006a, b, Rodin and Rodin 2008;).
(iii) The inversion symmetry of complementary coding strands has recognizable consequences for protein secondary and tertiary structures, and the active site construction of the resulting Class I and II enzymes (Carter and Wills 2017; Carter et al. 2014), especially in light of the organization of the genetic code.
(iv) Complementary studies of the modular aaRS architectures of both synthetase classes (Schimmel et al. 1993; Carter 2014) led to the discovery of how the organization of tRNA coding elements record how amino acids behave in water and in protein folding (Carter and Wolfenden 2015, 2016).
(v) Whereas we can only begin to speculate on how such a gene emerged, it seems clear

that it arose from a peptide RNA partnership and not from an RNA World (Carter and Wills 2017; Carter 2015).

Thus, it now becomes possible to propose, in outline, a much more targeted program for studying how translation evolved.

1.2 The Hypothesis of Rodin and Ohno (1995)

Shortly after the aaRS Class division became apparent (Eriani et al. 1990a, b; Cusack 1993; Cusack et al. 1990, 1991) Rodin and Ohno published a remarkable hypothesis (Rodin and Ohno 1995). They used multi-family sequence alignments to establish consensus codons for the Class-defining motifs in the two superfamilies and found that codons for Class I PxxxxHIGH and KMSKS active-site catalytic motifs were almost exactly anticodons for Class II Motifs 2 and 1, respectively. That statistically significant, in-frame complementarity, illustrated in Fig. 1a, suggested that the contemporary aaRS superfamilies had at one time been coded by a single ancestral gene, one strand of which was transcribed and translated giving the ancestral Class I synthetase. Conversely, the opposite strand encoded the ancestral Class II synthetase.

The authors actually understated the statistical support for their case by not citing probabilities—10^{-8}–10^{-18}—of the observed alignments under the null hypothesis indicated by their jumble-testing z-scores. Perhaps for this reason, the hypothesis remained more or less dormant for almost a decade before it was revived by Carter and Duax (Duax et al. 2005; Carter and Duax 2002). Subsequent work has substantially strengthened the experimental and bioinformatic support for the hypothesis by articulating and testing predictions that it makes (Fig. 1b). Direct support for the hypothesis, discussed at length in this review, is made more relevant by related work on the origin of translation (Carter and Wills 2017; Wills 1993, 2004, 2016; Petrov and Williams 2015; Caetano-Anollés et al. 2013; Harish and Caetano-Anollés 2012) and the genetic code (Carter and Wolfenden 2015, 2016; Wolfenden et al. 2015).

1.3 The Origins of Symbolic Interpretation and Coding

Biological nucleic acid sequences represent an exquisite repository of information relevant to managing stimuli from the world at large. For our purposes, it is useful to distinguish between two types of information stored in nucleic acids. Information about the chemical environment of biology defines how amino acids behave in water; gene sequences exploit that information by configuring amino acid sequences capable of folding into functional proteins.

The information in genes furnishes the blueprints for assembling proteins via the ribosomal read-write apparatus. Genes constitute a set of programs, written in the language of the genetic code, and expressed as a sequence of codons, or symbols consisting of three consecutive nucleotide bases, each with a specific meaning—start, a particular amino acid belongs here, stop. Equally important is the translation table embedded in transfer RNA. This second type of information specifies the conversion of the symbolic information in codons into specific amino acids. It has recently become apparent that this conversion corresponds closely to the phase transfer equilibria that enable translated gene sequences to fold and function. It represents the programming language in which genes are written and self-organization has embedded it efficiently and robustly into tRNA base sequences, primarily in the acceptor stem and anticodon.

The aaRS connect codons, hence messages in mRNA to amino acids via the translation table in the genetic code, each synthetase performing specific tRNA aminoacylation to enforce the rule specifying that a particular codon means that a particular amino acid is to be inserted whenever the anticodon of its cognate tRNA matches a codon in the message. As the synthetases are themselves made according to

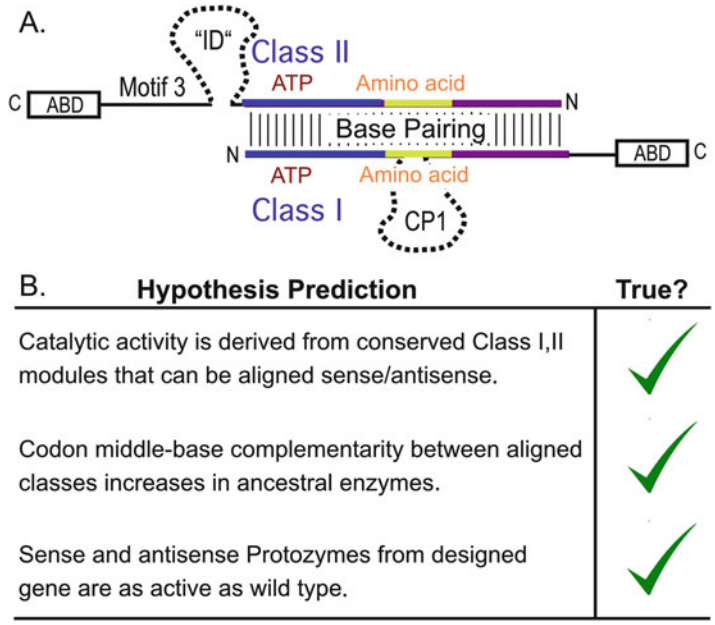

Fig. 1 The hypothesis of Rodin and Ohno (1995). (**a**) Schematic of the hypothesis. Genes for Class I and Class II aaRS are aligned in opposite directions as they would be oriented in an ancestral gene bearing the coding sequences on opposite strands. *Vertical lines* denote the extent of ancestral bi-directional coding, indicated by base-pairing of the coding sequences identified first in the Class-defining motifs in each superfamily. Large domains—the two anticodon-binding domains at the C-terminus of each Class and an insertion domain, ID in Class II, CP1 in Class I—are indicated by *boxes* and *dashed lines*, respectively. Substrate binding sites for the amino acid activation reaction, ATP and amino acid, are indicated. (**b**) Summary of published evidence supporting the hypothesis, to be discussed in detail in this review

specific mRNA sequences, their connection to the genetic code is deeply reflexive or self-referential: once translated, they themselves become sensitive to the impact that water has on their constituent amino acids and fold into active conformations. Those folded conformations subsequently execute the symbolic rules in the genetic coding table to make themselves and all other proteins (Fig. 2; (Carter and Wolfenden 2016)).

At the nucleic acid level, the molecular nature of this information, and how it is preserved from one generation to the next, are well understood in terms of base-pairing, as are the general structural mechanisms by which this base sequence information is read out by transcription, and converted first to protein sequences by the ribosome during translation and then to folded, active enzymes. Principles of protein folding are also beginning to be understood, at least in outline (Fersht 2000; Dill and MacCallum 2012; Baker 2000). Key to understanding the origin and evolution of each of these mechanisms is the element of "interpretation"—rephrasing the encoded information into a more flexible form capable of a greatly extended range of functionalities.

How the genetic code became embedded in tRNA sequences and how mRNA sequences originated, however, have been essentially blank pages. High probability synthetase•tRNA complexes were essential to launching translation. The probability of implementing molecular recognition and interpretation via self-organization (Wills 1993; Johnson and Lam 2010; Füchslin and McCaskill 2001; Küippers 1979; Eigen and Schuster 1977) and natural selection (Dennett 1995) decrease sharply the more sophisticated the system. Thus, it seems

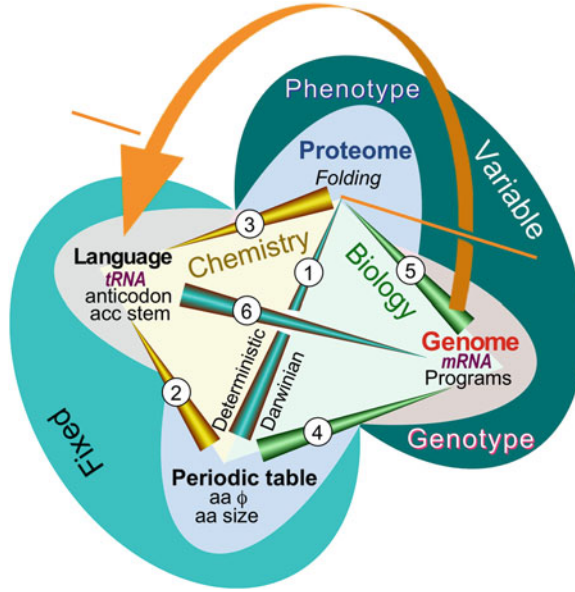

Fig. 2 Aminoacyl-tRNA synthetases and their cognate tRNAs furnish the reflexive elements necessary to translate the genetic code (*orange arrow*). The code connects their gene sequences, via their folded structures, to the enzymes that can enforce the coding rules in the codon table. Network analysis of the Central Dogma of Molecular Biology accommodates new evidence relating both tRNA identity elements and protein folding directly to the free energies of phase transfer equilibria of amino acid side chains (Carter and Wolfenden 2015, 2016; Wolfenden et al. 2015). Two of the nodes of a tetrahedron—physical properties of amino acids and the codon assignment table—reside in the realm of chemistry. They are "fixed" because they obey chemical equilibria. The other two nodes—gene sequences and protein folding—are dynamic processes that transcend chemistry because they are variable and form the basis for the evolution of diversity through self-organization and natural selection. The network connects RNA and Protein worlds via six edges: *1*. Protein folding depends on both amino acid polarity and size (Wolfenden et al. 2015), properties that play a role analogous to those of elements in chemistry, in that the amino acids form a kind of "periodic table" on which the folding of proteins is based. *2*. tRNA bases encode amino acid size and polarity separately (Carter and Wolfenden 2015). The acceptor stem codes for amino acid sizes; the bases of the anticodon code for amino acid polarities. Amino acid properties therefore dictate how tRNA bases are recognized by aminoacyl-tRNA synthetases. *3*. tRNA codes are related to protein folding. Together, statements (*1*) and (*2*) imply that for the aminoacyl-tRNA synthetases, the code (and mRNA sequences) must define folded structures that bind specifically to particular tRNAs in order to read the language of genetics. *4*. Gene sequences (mRNA) are analogous to computer programs. Genetic instructions assemble amino acids according to their physical properties in ways that, when translated according to the programming language in tRNA (in *5*), yield functional proteins (enzymes, motors, switches, regulators). *5*. mRNA sequences (i.e., the genotype) determine amino acid sequences in proteins, and hence how amino acid sizes and polarities are exploited to produce different folded proteins. The spontaneous folding of amino acid sequences gives rise to functions (i.e., the phenotype) that ultimately determine whether or not a particular sequence survives natural selection. Changes accumulated in gene sequences result from selection acting on the phenotype. (*4*) and (*5*) localize how selection incorporates information about amino acid behavior into gene sequences, hence depict the evolutionary dimension in biology. *6*. The evolution of mRNA sequences only makes sense in the context of the translation table (or programming language) established by the genetic code. The circularity of arrows (5), (3), and (6) illustrates a somewhat deeper self-referential element than those identified in molecular biology by Hofstadter as generators of complexity according to Gödel's incompleteness theorem (Hofstadter 1979) (Adapted, with permission, from Carter and Wolfenden (2016))

likely that translation began with smaller, less specific complexes, hence a simpler, less precise, and probably redundant alphabet. The recent experimental work reviewed here points clearly to molecular models with just those properties. These and other arguments (Carter and Wills

2017; Wills and Carter 2017). imply that genetic coding arose in a flexible, rudimentary implementation that later underwent successive refinements that completed the code (Carter and Wills 2017).

Given that the aaRS are probably the first and only gene products (ie., of the second type of information) with the ability to interpret the first type of information (ie., the genetic code translation table), it should come as no surprise that their molecular phylogenies contain potentially useful information concerning how they arose and began translating genetic messages. Retracing evolution is a unique subset of reconstructing the past, i.e. of history. It can be argued that the effort is fruitless as one cannot run the tape in reverse, that important and relevant witnesses are all extinct, and in particular that there is no way to test hypotheses. Our work (Chandrasekaran et al. 2013; Cammer and Carter 2010; Martinez et al. 2015; Carter 2014, 2015; Li et al. 2011, 2013; Pham et al. 2007, 2010; Weinreb et al. 2014; Li and Carter 2013; Carter et al. 2014, 2016; Rodin et al. 2009; Carter and Wolfenden 2015, 2016; Carter and Duax 2002; Wolfenden et al. 2015; Sapienza et al. 2016), and that of others (O'Donoghue and Luthey-Schulten 2003; Petrov and Williams 2015; Caetano-Anollés et al. 2013; Harish and Caetano-Anollés 2012; Caetano-Anollés 2015; Sun and Caetano-Anollés 2008), tends to rebut this objection. In reality, molecular phylogenies of the Class I and II aaRS have proven to be a rich source of unexpected insights into how translation became possible and robust tools now enable us to investigate, and even recapitulate key events from the past history of life.

2 Evidence for Bi-directional Coding Ancestry: Molecular Phylogenies, Urzymes, and Protozymes

The broader evidence now supporting the hypothesis of Rodin and Ohno (1995) began with analysis of superpositions of the three-dimensional structures of Class I and II aaRS, as illustrated in Fig. 1 and described in Sect. 2.1. Section 2.2 reviews the experimental characterization of the parallel catalytic activities and amino acid specificities of the deconstructed hierarchies from both classes. Problems raised by experimental recapitulation of putative evolutionary events connecting the ancestral forms to the contemporary enzymes are discussed in Sect. 2.3. A new distance metric for phylogenetic analysis of protein superfamilies related by bi-directional coding ancestry is reviewed in Sect. 2.4, together with its possible use in identifying how synthetases for the 20 canonical amino acids may have diversified from a single ancestral gene.

2.1 Protein Engineering and Experimental Deconstruction

The overall strategy of these studies has been to deconstruct Class I and II aaRS into genes for their component modules, use enzyme kinetics to characterize their catalytic activities and specificities, and validate their authenticity. Recapitulation of putative evolutionary intermediates by partial reconstruction also has been carried out, although to a lesser extent, as described in Sect. 2.3.

Deconstruction Genes coding for intermediate modules were made using molecular biological techniques. For Class II aaRS in which the active site is formed by a continuous, uninterrupted coding sequence, deconstruction can be accomplished using PCR amplification of the desired region (Li et al. 2011). For Class I aaRS, however, the active site—and Urzyme—are discontinuous, requiring more aggressive protein engineering (Pham et al. 2007, 2010). Two aspects of the fusion and solubilization of the Class I Urzymes required amino acid sequence modification: (i) the intervening insertion element had to be removed and the two ends fused together, and (ii) an extensive surface area of

nonpolar side chains, exposed by the removal of entire domains, needed to be modified to enhance solubility. In constructing Urzymes for TrpRS and LeuRS, both operations were accomplished using the Design module in the Rosetta program (Dantas et al. 2003).

Urzymes Multiple sequence and especially multiple structure alignments furnish the basic tools for constructing molecular phylogenies (O'Donoghue and Luthey-Schulten 2003) (Fig. 3). Superimposing three-dimensional structures of proteins within the same superfamily reveals that certain modules are shared by all family members, whereas others differ distinctly from member to member. The most conserved modules generally contain the active sites, and for that reason alone are likely candidates for evolutionary intermediates. For both aaRS classes, modules shared by all ten superfamily members contain essentially their intact active sites built from ~130 residues (Pham et al. 2007; Carter and Duax 2002). These modules have been expressed independently of the rest of the contemporary gene from two Class I and one Class II aaRS and shown to exhibit ~60% of the transition state stabilization of the full-length enzymes (Li et al. 2011; Pham et al. 2007, 2010). Their extensive conservation and enzymatic activities earned them the descriptor "Urzyme" from the German prefix Ur = primitive, authentic, original plus enzyme.

Protozymes Mildvan published a series of studies in which he excerpted the ATP binding sites of three different P-loop ATPases—F1 ATPase (Chuang et al. 1992a, b), DNA polymerase (Mullen et al. 1993), and adenylate kinase (Fry et al. 1985, 1988)—and demonstrated that they retained ligand-dependent structures similar to that observed in the full-length proteins. All three ATP binding sites consist of ~50 residue β-α-β secondary structures with a glycine-rich loop between the first strand and helix, and appear homologous in these respects to the Class I aaRS ATP binding sites. That precedent motivated further deconstruction of the Class I and II Synthetase Uryzmes, both of which contain ATP binding sites of approximately the length—46 residues—studied by Mildvan. Expression and fluorescence titration of ATP by these 46-mers established that they, too, bind ATP tightly, motivating investigation of their possible catalytic properties. ATP binding sites from both Class I and II aaRS accelerated amino acid activation by 10^6-fold (Martinez et al. 2015), and led to their designation as "protozymes" from "proto" = first.

The hierarchy—monomer > catalytic domain > Urzyme > protozyme (Fig. 4)—illustrates the parallel evolution of both Class I and Class II aaRS providing details abstracted in Fig. 3. Of particular interest are the following:

(i) Red and blue modules are interrupted by an insertion (connecting peptide 1 CP1 (Burbaum and Schimmel 1991)) in the Class I Uryzme but continuous in the Class II Urzyme.
(ii) The protozyme module (blue) occurs at the amino terminus of the Class I and at the carboxy terminus of Class II aaRS Urzymes.
(iii) Transition-state stabilization free energies for amino acid activation assayed by PPi exchange for each catalyst, $\Delta G k_{cat}/K_M/k_{non} = -RT\ln(k_{cat}/K_M/k_{non})$, are approximately linearly related to its mass (Martinez et al. 2015). Note that transition-state stabilization free energies are logarithmically related to the rate enhancements.

Catalytic activities of Class I (Pham et al. 2007, 2010)and II (Li et al. 2011, 2013) Urzymes were the first observations to substantively validate predictions implied by Rodin and Ohno for the bi-directional genetic coding of Class I and II aaRS. The third observation establishes a crucial pre-requisite for the evolution of catalytic activity in general: insofar as catalysis is required to synchronize the rates of chemical reactions in the cell, it is essential that different enzyme families across the proteome evolve so as to preserve parallel increases in rate enhancement.

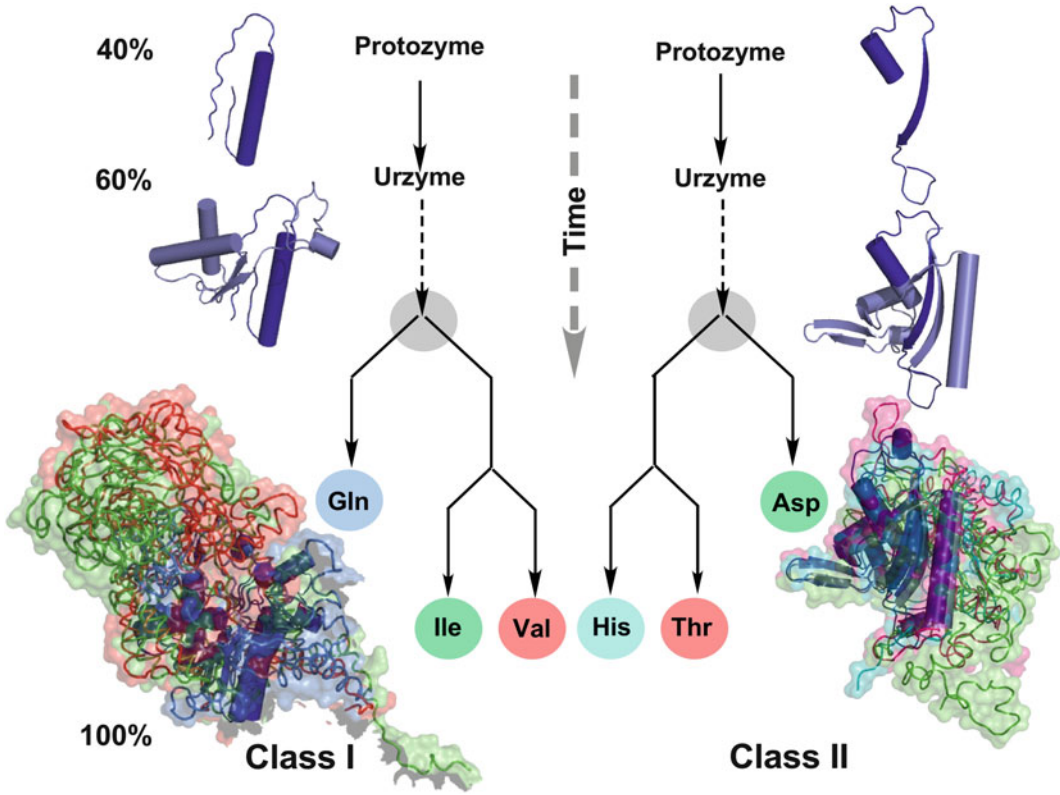

Fig. 3 Inferring protein family trees from molecular anatomies. Structures of three class I and class II aaRS have been rotated into a common orientation using their atomic coordinates and colored differently. α-Helical secondary structures are drawn as cylinders; extended β-structures as ribbons with *arrows* indicating their direction. Larger, more differentiated structures are drawn as *noodles*, surrounded by their surfaces. Differences in the recent structures at the *bottom* are highlighted by modules of one color that are absent in other structures. Such differences can be quantified and used to construct the genealogies in the center. Modules that are most similar in all three are colored *dark blue* and are inferred to be present in the common ancestor. Circles represent essentially modern aaRS. The three structures in each aaRS class are labeled with their three-letter abbreviations. There is consensus that they were present together with twelve other aaRS in the last universal common ancestor (LUCA) of all living organisms (Fournier and Alm 2015; Fournier et al. 2011). Novel results described here are the construction, expression, and experimental testing of ancestral forms called urzymes and protozymes, which are found, essentially without variation in all contemporary species and which retain substantial fractions—60% and 40% respectively—of the catalytic activity of the contemporary enzymes. The similarity between the class I and II genealogies is evidence that the two families evolved coordinately (Courtesy of *Natural History*, Carter, CW Jr. (2016) *Natural History*: 125:28–33)

Characterization Overexpressing Urzymes from both Classes leads to their accumulation in inclusion bodies. Washed inclusion bodies contain >50% Urzyme in such cases, and therefore represent a significant purification. Inclusion bodies solubilized in 6 M guanidinium hydrochloride can be renatured by size exclusion chromatography on superdex 75, which also yields essentially pure Urzyme. Active-site titration (Fersht et al. 1975; Francklyn et al. 2008) shows that between 35–70% of the molecules in various preparations contribute to the observed activity seen in pyrophosphate exchange assays (Francklyn et al. 2008). TrpRS and HisRS Urzymes accelerate the rates of amino acid activation (assayed by pyrophosphate exchange) and tRNA aminoacylation by 10^9-fold and 10^6-fold, respectively (Li et al. 2013). These values are consistent with measurements of the uncatalyzed rates for the two reactions, as spontaneous amino

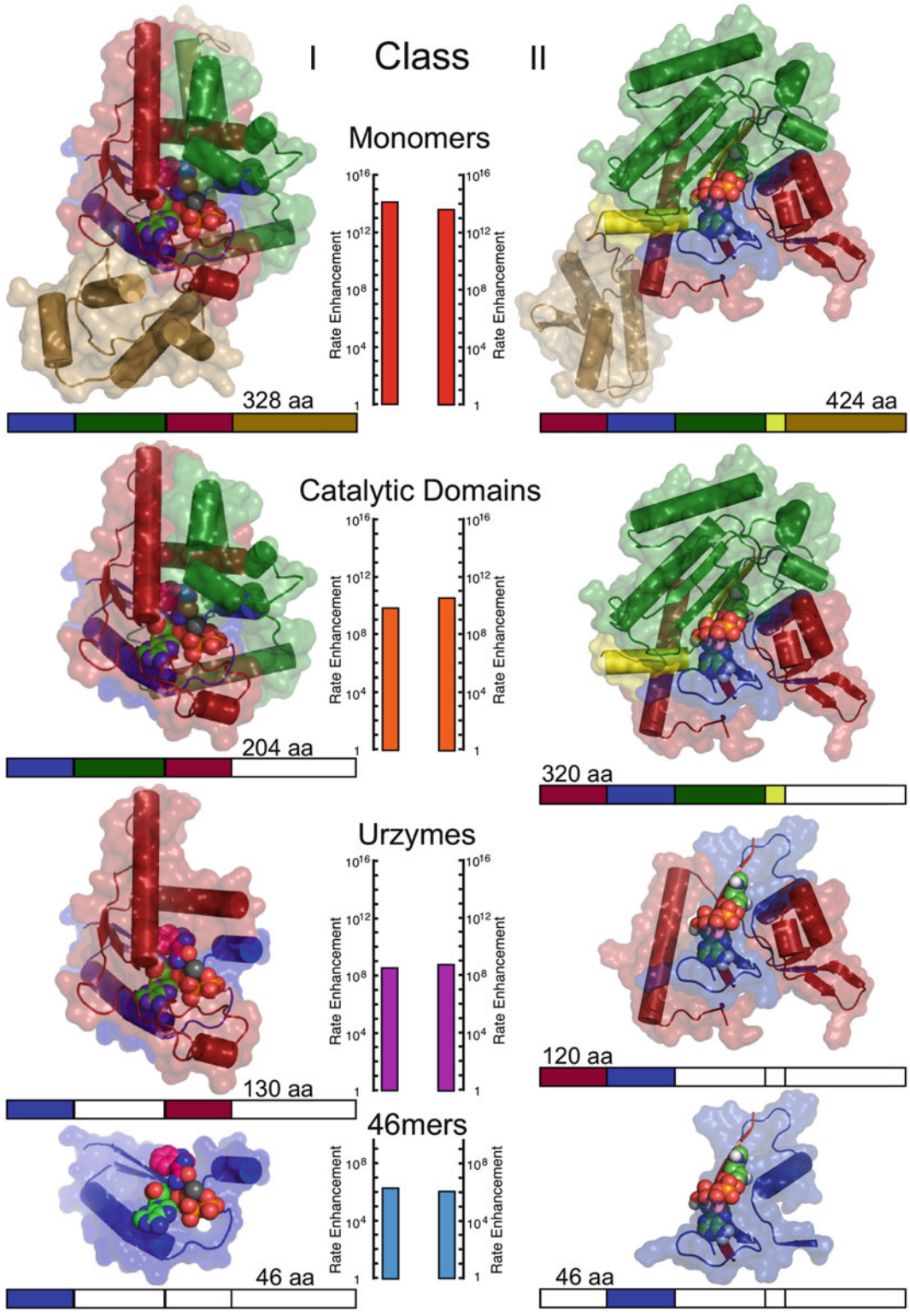

Fig. 4 Deconstruction of Class I tryptophanyl (PDB code 1MAU)- and Class II histidyl (PDB code 2EL9)-tRNA synthetases into successively smaller fragments that retain catalytic activity (Woese et al. 2000; Yarus 2011a, b; Van Noorden 2009; Wolf and Koonin 2007; Martinez et al. 2015). Graphics for smaller constructs are

acid activation (Kirby and Younas 1970) is ~1000-fold slower than are either spontaneous acylation (Wolfenden and Liang 1989) or peptide bond formation from activated amino acids (Schroeder and Wolfenden 2007; Sievers et al. 2004).

As protozymes isolated from the two aaRS Classes have only ~40% of the mass of Urzymes, they are substantially weaker catalysts, activating cognate amino acids 10^6 times faster than the uncatalyzed rate. PPi exchange assays were incubated for 14 days and assayed at intervals of several days (Martinez et al. 2015). The specificities of amino acid activation by wild-type and bi-directionally coded protozymes, and their possible acylation activities have yet to be determined.

Validation Establishing the authenticity of the catalytic activities observed for the aaRS Urzymes and protozymes is obviously of great importance, and is a matter to which considerable attention has been paid (Carter 2014; Li et al. 2011, 2013; Pham et al. 2007, 2010; Carter et al. 2014). They are much weaker catalysts than full length enzymes, and consequently, their activities can much more readily be attributed to very small amounts of various kinds of contaminating enzymes, including, of course, the full-length native homologs present in all cell extracts. In addition to the absence of activity in conventional controls carried out using extracts prepared from cells containing empty cloning vectors, authenticity was established by four controls:

(i) Steady-state kinetic experiments show that Urzyme and protozyme activities saturate at amino acid concentrations several orders of magnitude higher than is required to saturate the full-length enzymes. This argument is strengthened by the specificity spectra determined for the Class I LeuRS and Class II HisRS Urzymes (Fig. 5; (Carter et al. 2014; Carter 2015)).
(ii) Cryptic catalytic activity is released when Urzymes expressed as fusion proteins with maltose-binding protein are treated with TEV protease.
(iii) Active-site mutations and modular variants containing minor additional mass at the N- and C-termini alter the measured activity.
(iv) Active-site titration confirms that a major fraction of molecules contribute to the observed activity (aaRS Urzymes only; it is unclear that the protozymes would exhibit a pre-steady state burst, which is a requisite for active-site titration).

All these results implicate the actual genetic construct in the observed activity, and contaminating activities cannot account for either (ii), (iii), or (iv).

2.2 Class I and II aaRS Deconstructions Exhibit Parallel Catalytic Hierarchies

Catalytic Rate Enhancements Correlate with Catalyst Mass Deconstructions (Fig. 4) reveal surprisingly consistent increases in transition-state stabilization with additional masses in the ascending hierarchies (Carter et al. 2014; Carter 2015). Catalyst masses range

Fig. 4 (continued) derived from coordinates of the full-length enzymes. *Colored bars* below each structure denote the modules contained within each structure; white segments are deleted. The number of amino acids (aa) in each construct is noted. Measured catalytic rate enhancements for ^{32}PPi exchange, relative to the uncatalyzed second-order rate (kcat/Km)/knon are plotted on vertical scales aligned in the center of the figure and are colored from *blue* (slower) to *red* (faster) (This research was originally published in the *Journal of Biological Chemistry* Martinez et al. (2015) ©American Society of Biochemistry and Molecular Biology)

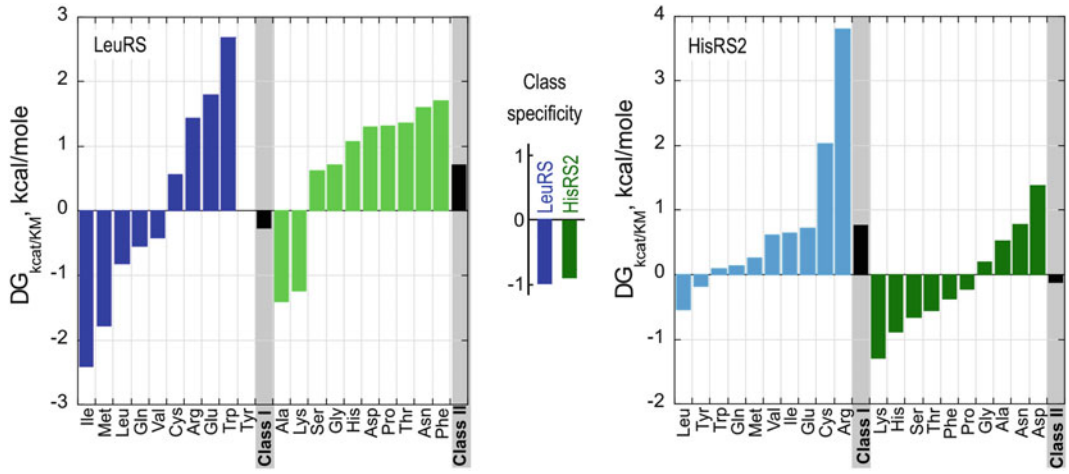

Fig. 5 Amino acid specificity spectra of Class I LeuRS and Class II HisRS2 Urzymes. The mean net free energy for specificity of Class I and II Urzymes for homologous vs. heterologous substrates, i.e., ΔG(kcat/KM)ref – ΔG (kcat/KM)amino acid (i), where ref is the cognate amino acid, is approximately 1 kcal/mole for both Class I and II Urzymes (*center*). Class I amino acids are colored *blue*; Class II amino acids are colored *green*. *Bold colors* denote substrates from the homologous Class; *pastel colors* denote heterologous substrates (From Carter (2015))

by 70-fold from ~6.5 KD to 450 KD, and the constructs derived from each Class are distributed differently with respect to size. Class I deconstructions are a "low resolution" map because they include two modular hybrids—catalytic domain and Urzyme plus anticodon-binding domain—between the Urzyme and the full length monomers. The Class II constructs, on the other hands, include high resolution divisions—increments of 6, 20, and 26 residues—at approximately the 126-residue size of the Urzyme. Across this entire range of deconstructions, transition-state stabilization energies increase linearly with the number of residues (Martinez et al. 2015). Moreover, the slopes for each Class are the same within 5%.

Class I, II Constructs at Each Stage Have the Same Catalytic Proficiencies A second remarkable result of the aaRS deconstruction is that the linear relationships between transition-state stabilization free energy and the number of residues also have the same *intercepts*. This implies strongly that throughout the evolutionary history of the two synthetase Classes, they retained comparable catalytic proficiencies (Martinez et al. 2015). The importance of this observation is that the synthetase superfamilies form a tightly interdependent autocatalytic set coupled by the fact that each is required to operate with approximately the same throughput of aminoacylated tRNAs for translation of all amino acids within the current genetic alphabet (Carter and Wills 2017). Their enzymatic activities must, therefore, have remained quite comparable for all relevant amino acids over the duration of the synthetase superfamily growth from short peptides to long polypeptides. It was not obvious, however, that experiments would confirm that expectation. Nevertheless, aaRSs from both Classes appear to have been capable of parallel increases in both size and catalytic proficiency, consistent with continuously providing comparable quantities of aminoacyl-tRNAs for all amino acids throughout the evolutionary tuning of the genetic code.

Class I and II Urzymes Are Promiscuous Catalysts That Nonetheless Have Comparable Amino Acid Specificity Essentially complete amino acid specificity spectra have been determined for amino acid activation by the Class I

LeuRS and Class II HisRS Urzymes (Fig. 5) (Carter et al. 2014; Carter 2015). Remarkably, the two catalysts retain a significant preference for the class of amino acid substrates for which their parent enzymes were specific. The LeuRS Urzyme prefers not to activate Class II amino acids; the HisRS2 Urzyme prefers not to activate Class I amino acids. The degree of specificity, evaluated as the free energy of the specificity ratio, $\Delta Gk_{cat}/K_M(I/II)$ and $\Delta Gk_{cat}/K_M(II/I)$, are ~ -1 kcal/mole for both Urzymes. This value is roughly 20% of that for the full-length enzymes. It means that given equimolar concentrations of all 20 amino acids, the Class I Urzyme will activate an amino acid from the wrong class roughly one time in 5, whereas a native aaRS will typically active an incorrect amino acid roughly one time in 5000. Thus, aaRS Urzymes are promiscuous with respect to amino acid recognition, but retain the Class preferences of the full-length enzymes from which they were derived for amino acids within their own class.

As noted below, the problem of evolving high amino acid specificity is more subtle than might appear from the initial studies in Fig. 5. An important possibility is that specificities were enhanced in the presence of cognate tRNAs, as is true for several contemporary aaRS (Farrow et al. 1999; Ibba and Soll 2004; Uter et al. 2005; Sherlin and Perona 2003). Work is in progress to characterize tRNA specificity in a similar fashion, and to determine whether or not the amino acid specificity spectra (Fig. 5) improve in the presence of cognate tRNAs.

Wild-Type and Bi-directional Protozyme Gene Products from Both Classes Have the Same Catalytic Proficiencies Section 2.4 discusses in greater detail the extent to which experimental and bioinformatics results have confirmed the hypothesis of Rodin and Ohno that the original ancestral genes for Class I and II aaRS were fully complementary. It is worthwhile noting here that wild type Class I and II protozymes were excerpted directly from full-length TrpRS and HisRS genes. Although those coding sequences retain a strong trace of their bi-directional coding ancestry, they are distinctly not complementary. To test the prediction that a fully complementary protozyme gene could be achieved, the computer design program, Rosetta, already used extensively in the re-design of Class I Urzymes, was adapted to impose coding complementarity on the two protozyme genes, resulting in a single gene with two different functional translation products, one from each strand (Martinez et al. 2015).

Analysis of the peptides coded by the resulting bi-directional gene showed that the four gene products—Class I and II; designed and wild type—have nearly the same catalytic proficiency, $\Delta Gk_{cat}/K_M = +3.5 \pm 0.8$ kcal/mole. The amino acid sequences of the designed protozymes are quite different from the WT sequences. This agreement therefore suggests that the catalytic activities of the Class I and II protozymes may be consistent with a very large number of different sequences that share only simple patterns based on a reduced alphabet of fewer amino acids, consistent with their possible emergence at a time when the amino acid alphabet was both smaller and less faithfully implemented.

Designed Protozymes Have High Turnover, Low Specificity The steady-state kinetic parameters for WT and designed protozymes revealed yet another remarkable comparison. Although the overall second-order rate constants, $\Delta Gk_{cat}/K_M$, are very nearly the same, their similar values arise from quite different values for the turnover number and amino acid substrate affinity. The WT protozymes, perhaps because they were excerpted from the full length proteins, retain higher ground-state substrate affinities but have lower turnover numbers, whereas the designed Protozymes have higher turnover numbers and weaker ground-state affinities (Martinez et al. 2015). The differences in both parameters are about 100-fold, leaving their k_{cat}/K_M ratios unchanged.

Without intending to do so, by enforcing genetic complementarity the design process also enhanced the turnover number while weakening amino acid affinity (Fig. 6). Specific binding of

cognate, versus non-cognate amino acids cannot be improved without increasing the binding affinity of the cognate complex, so increased ground state amino acid affinities are a prerequisite for enhanced discrimination between competing substrates. Thus, deconstructions of both aaRS Classes exhibit parallel enhancements that improved fitness by increasing both catalysis and specificity. Notably, the higher turnover number and lower amino acid affinity of the designed, bi-directionally coded protozymes match properties expected for a emerging rudimentary coding apparatus.

2.3 Recapitulation

Modular Engineering of TrpRS One of the best ways to validate and utilize knowledge gained from the reconstruction of ancestral forms is to recapitulate putative evolutionary steps by reconstructing and testing intermediates (Bridgham et al. 2009; Dean and Thornton 2007; Thornton 2004). The deconstruction of the Class I and II aaRS has afforded such opportunities (Li et al. 2011; Li and Carter 2013). Those investigations cast new light on synthetase function and evolution.

Two putative TrpRS constructs intermediate between the Urzyme and full-length enzyme

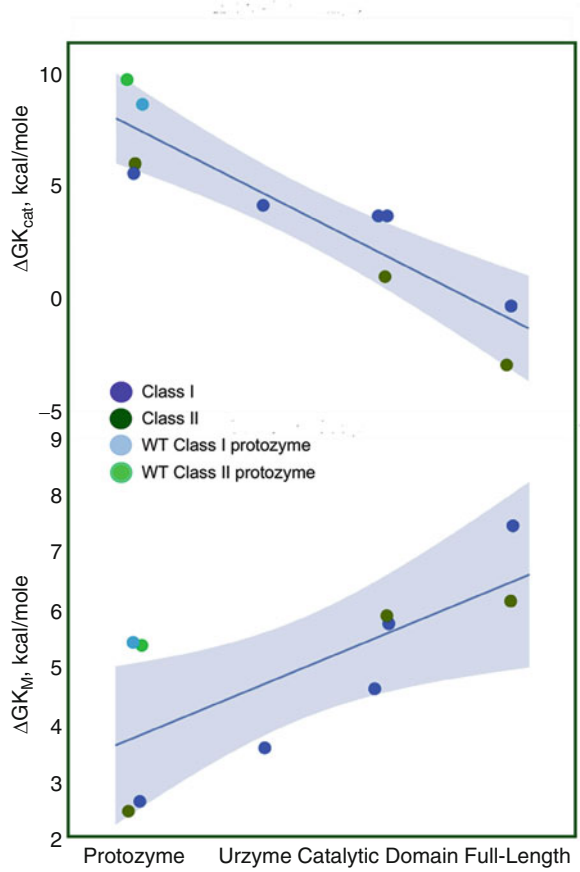

Fig. 6 Parallel sequential improvements in catalytic rate enhancement (*top*) and ground-state amino acid affinity (*bottom*) associated with modular enhancements of Class I (*blue*) and Class II (*green*) aminoacyl-tRNA synthetase evolution. Increased amino acid specificity requires higher affinity binding of cognate amino acids, to differentially release non-cognate complexes. Thus, the behavior of the ground-state amino acid affinity is a surrogate for specificity. Both catalytic proficiency and specific recognition of cognate amino acids therefore improve with more sophisticated modularity. *Pastel colors* show that imposing bi-directional coding on the protozymes increases both k_{cat} and K_M proportionately

involved the re-insertion of the CP1 fragment to restore the catalytic domain and the covalent joining of the anticodon-binding domain to the Urzyme (Li and Carter 2013). Comparison of these modular variants showed that, although both intermediate species exhibited modest increases in catalytic proficiency, neither was any better than the Urzyme, either in aminoacylation or in discriminating between cognate tryptophan and non-cognate tyrosine (Li and Carter 2013). There are two notable interpretations of this surprising result. First, as neither intermediate construct would have sufficiently increased fitness to be selected, it suggests that the apparently separate evolutionary enhancements must have occurred coordinately, either because one of the two had already begun to function *in trans*, or because one or the other, or both modules could "grow" by smaller modular additions that did endow enhanced fitness (Li and Carter 2013). Second, the modular thermodynamic cycle involving full-length TrpRS, the two distinct intermediates (Li and Carter 2013), and the Urzyme allowed measurement of a $\Delta\Delta G^{\ddagger} \sim -5$ kcal/mole coupling energy between the CP1 and anticodon-binding domains in the transition state of the amino acid activation reaction by full-length TrpRS (Li and Carter 2013), shedding new light on the general problem of intramolecular signaling or allostery (Carter et al. 2017; Chandrasekaran and Carter 2017; Chandrasekaran et al. 2016).

Mechanistic studies on intact TrpRS had previously identified a profound intramolecular coupling, $\Delta\Delta G^{\ddagger} \sim -5$ kcal/mole necessary for catalytic assist by the active-site Mg^{2+} ion (Weinreb and Carter 2008) and achieving full catalytic proficiency by the full-length enzyme (Weinreb et al. 2012, 2014; Carter et al. 2017; Weinreb and Carter 2008). A five-way coupling interaction, $\Delta\Delta G^{\ddagger} \sim -5$ kcal/mole, was also measured between four residues in an allosteric switching region 20 Å from the active-site metal that mediates the shear involved in domain movement during catalysis (Kapustina et al. 2007). A related study (Weinreb et al. 2014) confirmed that the same coupling energy was used in the transition state to enforce the specific selection of cognate tryptophan vs non-cognate tyrosine. Thus, the modular thermodynamic cycle provided a key link connecting the long-range coupling observed previously directly to the domain movement: the four switching side chains (I4, F26, Y33, and F37), the Mg^{2+} ion, and both domains all move coordinately in the transition state (Carter et al. 2017; Carter 2017).

Modular Engineering of HisRS Three conserved motifs are recognized in Class II aaRS: Motif 1 and Motif 2 compose the HisRS Urzyme. The third, Motif 3, however, lies well outside the Urzyme. It is separated by a long and variable insertion domain, C-terminal to the Urzyme, much as the long and variable CP1 insertion interrupts the Class I Urzyme. Exploratory modular engineering of interactions in the Class II HisRS yielded several intriguing observations (Li et al. 2011). (i) Motif 3 could be fused together with the HisRS Urzyme to produce a module whose catalytic activity is intermediate between that of the Urzyme and that of Ncat, the HisRS catalytic domain containing both Motif 3 and the insertion domain (Augustine and Francklyn 1997). (ii) Catalytic proficiency of the Motif 3-supplemented HisRS Urzyme is further enhanced by adding six additional residues N-terminal to the Urzyme (Li et al. 2011). (iii) The six-residue N-terminal fragment functions synergistically with Motif 3. Effects of the five modules estimated by regression methods from all of the measurements (Fig. 7) distinctly resemble those evaluated on the basis of more thorough investigations of Class I constructs.

2.4 Middle Codon-Base Pairing: A New Phylogenetic Distance Metric

Bi-directional Genetic Coding Left a Detectable Trace in Contemporary Sequences Sense/antisense alignment of coding sequences from different protein families introduced a new, phylogenetic distance metric—the percentage of middle codon bases that are complementary in

all-by-all in-frame bi-directional alignments of multiple sequence alignments from the two families. As an example, aligning the TrpRS Class I Uryzme against the HisRS Motif 2 (Pham et al. 2007) revealed that the region of quite extensive codon-anticodon complementarity identified by Rodin and Ohno could be extended to include ~75% of both Urzyme sequences, provided that the first and third codon bases were excluded. Outside regions of very high conservation as found in the Class-defining signatures of the aaRS, a transient ancestral use of dual strand coding, followed by an extended period of adaptive radiation would rapidly degrade the complementarity of the two strands. The highly conservative nature of the genetic code, together with wobble property of the third codon base (Crick 1966) mean that loss

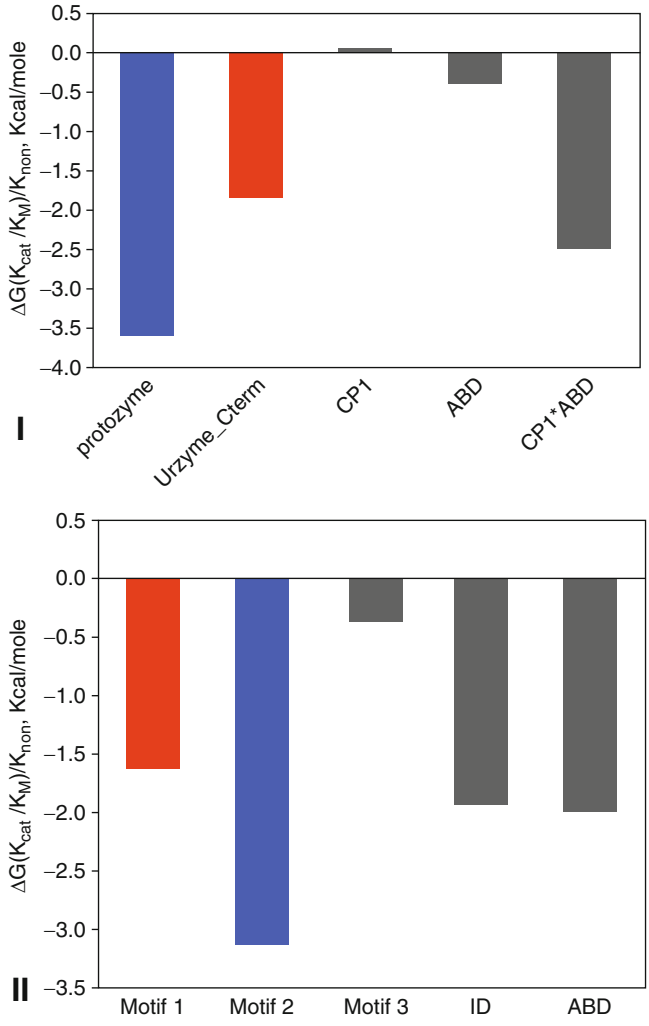

Fig. 7 Corresponding modules make similar relative contributions to catalysis by Class I and II aaRS. The Protozymes are colored *blue*; the remainder of the Urzymes *red*; and additional modules, including the insertion domains and anticodon-binding domains *grey*. Differences between the two Classes include the fact that Class II Motif 3 has no corresponding module in Class I aaRS, and the insertion and anticodon-binding domains have not been examined separately in Class II, so their synergistic interaction, which is quite large in Class I aaRS, cannot be estimated

in the middle-base pairing occurs much more slowly as sequences diverge than that in the first codon bases on each strand, each of which is opposite a wobble base on the opposite strand (Fig. 8a). The trace of bi-directional coding ancestry can thus be recovered by structurally-informed middle codon-base alignments of sufficient numbers of contemporary sequences (Fig. 8b) (Chandrasekaran et al. 2013). To wit, if the number of sequences aligned is sufficiently high (~10^4 comparisons in (Chandrasekaran et al. 2013), the standard error of the mean is reduced to a tiny fraction of the differences between the pairing frequencies of Class I vs Class II alignments and those (0.25) expected under the null hypothesis that one base in four would be complementary.

Elevated Codon Middle-Base Pairing in Multiple Antiparallel Alignments Between Different Class I and II aaRS Coding Sequences Occurs Generally Throughout all aaRS Superfamilies The significance of the published study of middle codon-base pairing (Chandrasekaran et al. 2013) raises a potential question because the statistics were accumulated for alignments of a Class IC (TrpRS) with a Class IIA (HisRS) synthetase. Neither of these synthetases was likely to have been among the earliest to appear. To establish the significance of the middle codon-base pairing distance metric, we therefore extended this analysis to include eleven aaRS, balancing the three subclasses by including six from Class I (TrpRS, TyrRS, LeuRS, IleRS, GluRS, GlnRS) and five from Class II (HisRS, ProRS, AspRS, AsnRS, PheRS; N. Chandrasekaran, personal communication). The alignments included 64 amino acids surrounding the PxxxxHIGH and KMSKS sequences in Class I aaRS and the Motif 1 and 2 sequences in Class II aaRS in (Chandrasekaran et al. 2013) to enhance confidence. The trace of ancestral bi-directional coding remains significant.

This extended database samples multiple comparisons between all subclasses within each Class, and hence include pairs of aaRS that presumeably appeared at different times along the evolution of the code. The statistical structure of this new database is shown in Fig. 9. The bi-directional alignments add an average of ~0.07 ± 0.007 to the fraction of codon middle-base pairing over those within the same aaRS Class. The difference between within- and between-classes accounts for ~60% of the variance in observed pairing ($R^2 = 0.60$), and the Student t-test probability for a ratio of the slope to its standard error as large as 10 is ~10^{-14}.

Ancestral Sequence Reconstruction Extends the Phylogenetic Evidence for Bi-directional Coding Significantly Backward in Time Ancestral gene reconstruction (Benner et al. 2007; Stackhouse et al. 1990) has become broadly used to resurrect ancestral enzymes (Gaucher et al. 2008) and signaling proteins (Dean and Thornton 2007; Thornton 2004; Hanson-Smith et al. 2010; Andreini et al. 2008; Ortlund et al. 2007; Bridgham et al. 2006; Thornton et al. 2003). Given the evidence for significant residual codon middle-base pairing in contemporary Class I and Class II sense/antisense alignments (Fig. 8b), it was of interest to extend the technique to the quantitative comparison of distinct gene families whose evolutionary descent might have been tightly coupled by bi-directional genetic coding at the origins of translation. That prediction led to the expectation that reconstructed node sequences of both superfamilies might exhibit increased codon middle-base pairing as reconstructed nodes from each family are aligned in opposite directions. This test is distinct from the construction of phylogenetic trees from multiple sequence alignments of related proteins, because it compares separate reconstructions of distinct families carried out independently and aligned only after the nodes have been reconstructed. The resulting appearance of increased codon middle-base pairing (Fig. 8c) is therefore a significant, orthogonal verification of the Rodin-Ohno hypothesis (Chandrasekaran et al. 2013).

Codon Middle-Base Pairing May Contain Evidence for Very Early Stages of Genetic

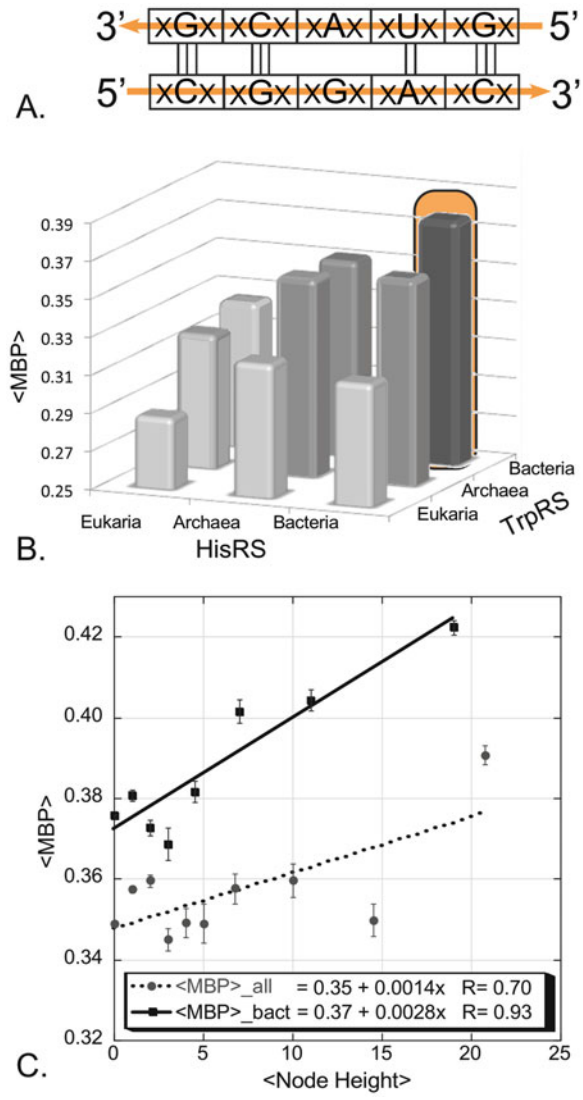

Fig. 8 Codon middle-base pairing (<MBP>) furnishes a new phylogenetic distance metric. (**a**) Transient bi-directional coding is rapidly lost after the constraint is released. First and third bases lose complementarity much faster than the middle bases, which retain residual base-pairing into contemporary sequences. (**b**) Comparison of middle codon-base pairing in all-by-all alignments of "Urgene" sequences excerpted from ~200 contemporary HisRS and TrpRS sequences (Chandrasekaran et al. 2013). (**c**) Node-dependence of middle codon-base pairing in antiparallel alignments of middle bases from ancestral sequences reconstructed independently for the TrpRS and HisRS Urzyme multiple sequence alignments. *Solid line* is for bacterial sequences, *dashed line* is for all bacterial, archaeal, and eukaryotic sequences (**b** and **c** adapted with permission from the Society for Molecular Biology and Evolution. Chandrasekaran et al (2013)

Coding The breadth of the histograms in Fig. 9 and consensus subdivisions of the two aaRS Classes into parallel subclasses, one large and two small, suggest that further examination of the middle-base pairing metric may eventually provide clues about the order in which pairs of aaRS speciated, and hence the order in which amino acids appeared in coding relationships. We constructed putative phylogenetic trees from the aligned amino acid sequences of eleven aaRS

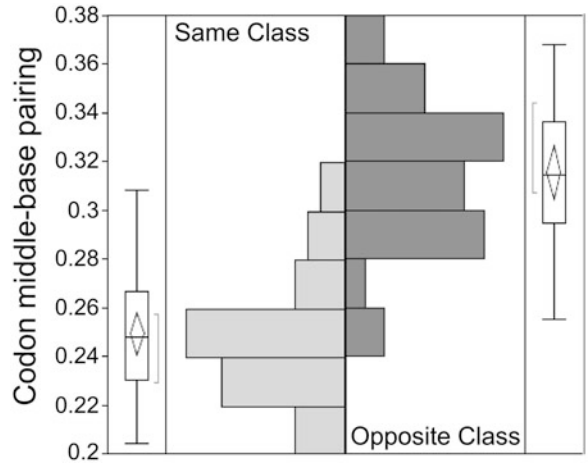

Fig. 9 Extended analysis of mean codon middle-base pairing. Results from (Chandrasekaran et al. 2013) have been updated to include alignments of ~200 sequences from each of eleven contemporary synthetases (Asp, Asn, Glu, Gln, His, Ile, Leu, Pro, Phe, Trp, Tyr). Histograms are shown for the fraction of base pairing between middle codon bases for antisense alignments from the same and opposite aaRS Classes, as indicated. The difference between the two mean values indicated by *horizontal lines* in the logos outside the histograms is 0.067, which is ~14 times the standard error. Further statistics of the comparison are discussed in the text and shown in Fig. 10

(six Class I and five Class II; Fig. 10a) and from the middle base-pairing distance metric (Fig. 10b) to illustrate this possibility. Significantly, there is only one significantly lower middle codon-base pairing metric among the all-by-all comparison of the subclasses—subclasses Ib and IIc appear to be more distantly related than all of the other subclasses. Thus, the distance metric implies comparable distances between all aaRS subclasses of each class to those of the other. Although based on partial data, this analysis is nevertheless interesting because it suggests ancestral genes in which the two principal subclasses are swapped (Fig. 10b): strands of the presumptive ancestral gene encoded ancestral Class Ia Ile-like and Class IIb Asp-like protozymes. Similarly, the next most prominent middle-base pairing metric relates sequences of Class IIa ProRS those of Class Ib GlnRS. Further work in this direction is in progress, and will require developing improved analytical tools for using the new distance metric, along with ways to deal with the ancestral sequence reconstructions built from amino acid alphabets of decreasing size (Wills 2016; Markowitz et al. 2006; Wills et al. 2015).

These data suggest that we now potentially have the tools to address directly the question of which stepwise bifurcations were actually involved, and in which order, leading to the universal genetic code. That code is one of a tiny number of near optimal codes that have the dual properties of high redundancy and resistance to mutation (Freeland and Hurst 1998). It therefore must have been discovered by a process of feedback-constrained symmetry-breaking phase transitions, or "boot-strapping". The underlying necessity for these transitions is discussed in detail elsewhere (Carter and Wills 2017; Wills and Carter 2017). Among the first of these symmetry-breaking transitions relevant to the genetic code was the aaRS class division that divided the amino acids into two distinct classes, as discussed in Sect. 4.

3 Structural Biology of Ancestral Synthetases

Most of what we know about the structures of Urzyme and Protozyme models for ancestral

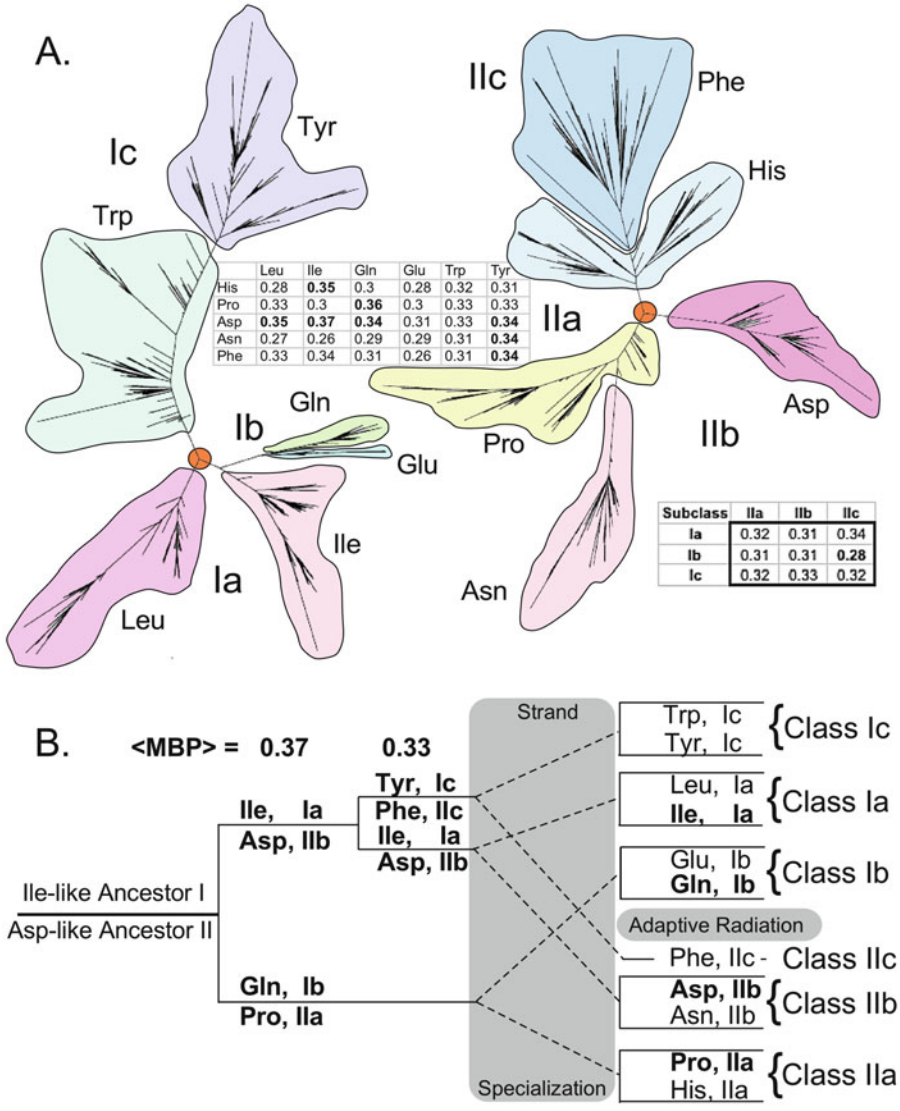

	Leu	Ile	Gln	Glu	Trp	Tyr
His	0.28	**0.35**	0.3	0.28	0.32	0.31
Pro	0.33	0.3	**0.36**	0.3	0.33	0.33
Asp	**0.35**	**0.37**	**0.34**	0.31	0.33	**0.34**
Asn	0.27	0.26	0.29	0.29	0.31	**0.34**
Phe	0.33	0.34	0.31	0.26	0.31	**0.34**

Subclass	IIa	IIb	IIc
Ia	0.32	0.31	0.34
Ib	0.31	0.31	**0.28**
Ic	0.32	0.33	0.32

Fig. 10 Extended analysis of the middle codon-base pairing metric confirms previous statistical evidence for ancestral bi-directional coding. Approximately 200 sequences, broadly distributed among the three canonical domains of life were assembled for 64 amino acid residues from 11 of the 20 canonical aminoacyl-tRNA synthetases (Unpublished data of S. N. Chandrasekaran). The 64 residues included the 46 residues of the protozymes together with 18 residues of the KMSKS and Motif I loops from the respective aaRS classes. Tables embedded in the figure show the mean middle codon-base pairing metrics for the all-by-all comparison of the 11 aaRS, and the corresponding average values for the canonical subclasses. (**a**) Independent phylogenetic trees drawn from the complete 192-base sequences of each class. (**b**) A putative tree drawn according to distances from the middle codon-base pairing metric for a 64-base subset of the sequences in **a**

aaRS has been inferred from crystal structures of full-length enzymes. Thus, for example, all structures depicted in figures herein were prepared by excerpting relevant coordinates from the corresponding pdb files. However, work has begun on the challenging task of providing more reliable and detailed structural data.

TrpRS Urzyme Is a Catalytically Active Molten Globule Attempts to crystallize Urzymes, either alone or as maltose-binding-protein fusions, has not yet been successful. It has, however, been possible to prepare isotopically labeled samples of active TrpRS Urzyme. Preliminary ^{15}N-^{1}H HSQC spectra from those samples supported an unexpected, but not unprecedented conclusion—the TrpRS Urzyme is not a folded protein, but has many of the properties expected from a catalytically active molten globule (Sapienza et al. 2016). The HSQC spectrum has a reasonable dispersion of values in the ^{15}N dimension, but, even in the presence of ATP and a non-reactive tryptophan analog all ~80 peaks are contained between 8–8.5 ppm in the ^{1}H dimension, which is characteristic of proteins that are not fully folded. The conclusion that it is probably a molten globule is reinforced by the fact that the temperature dependence of CD spectrum exhibits cold denaturation, and that Thermaflour measurements of thermal melting in the presence of Sypro Orange dye exhibit high fluorescence at all temperatures below ~45 °C, above which fluorescence decreases non-cooperatively over a range of ~30 °C. Both cold denaturation and high fluorescence over broad temperature ranges in the presence of Sypro Orange are characteristic of limited tertiary structure as in molten globules (Sapienza et al. 2016).

The likely possibility that the TrpRS Uryzme is a catalytically active molten globule has considerable significance in light of the work of Hilvert (Pervushin et al. 2007) and (Hu 2014), showing that the native chorismate mutase dimer and an engineered monomeric form that is a molten globule exhibit comparable rate accelerations—and hence transition state stabilization—by distinctly different strategies. The high, positive $T\Delta S^{\ddagger}$ implies even greater enthalpic contribution to transition state stabilization. Thus, thee molten globular catalyst achieves a substantially higher $-\Delta H^{\ddagger}$ to overcome the entropic cost of restricting the molten conformation of the catalyst when it binds to the transition state. The additional flexibility of the molten globular ensemble appears enable it to wrap more tightly around the transition state configuration of the substrate than can the properly folded native form of the enzyme.

The Potential Manifold for Catalytic Activity by Poorly Structured Polypeptides May Thus Be Much Larger Than Was Thought Possible Two molten globular polypeptides therefore exhibit high rate accelerations. At least one of these does so by forming substantially tighter bonds in the transition state than are possible with the native enzyme. This plasticity opens the possibility that many similar structural ensembles might act catalytically, and hence that a wider range of polypeptides might exhibit catalytic activity.

Peptide Catalysts Are Far Superior to Ribozymes The superiority of peptide catalysts is widely recognized. However, because it is so much easier to generate and select catalytic aptamers from RNA than it is from protein combinatorial libraries, it is unclear that this wide recognition comes with an appreciation of just how superior polypeptide catalysts are, in principle. Wills (2016) has compared the combinatorial possibilities for making an active site with proteins to those available for ribozymes. The combinatorial advantage of protein active sites arises because amino acids are only half the volume of nucleotide bases, meaning that contact to a transition state can arise from a greater number of amino acids. This advantage is compounded by the fact that there are five times as many choices of amino acids. As a result, proteins have an advantage somewhere between a million- and a billion-fold over RNA, which is what is observed experimentally (Carter and Wills 2017).

Hecht's work (Patel et al. 2009; Moffet et al. 2003; Kamtekar et al. 1993) has demonstrated that a large proportion of molecules within patterned combinatorial libraries actually do form molten globules. The relatively low free energy barriers associated with assuming catalytically competent conformations, together with the vastly enhanced abilities of amino acid side chains to engineer nanoscale chemistry argue

that catalytic activity is likely to arise and evolve much more rapidly from populations of peptides than from libraries of RNA. Thus, demonstrating that catalytic proficiency does not require the evolution of properly folded proteins represents a considerable expansion in their potential catalytic repertoire.

4 The Basis for the AARS Class Division

Because they activate amino acids by catalyzing adenylation by ATP, the aminoacyl-tRNA synthetases are arguably among the earliest enzymes to emerge during the origin of life. Absent catalysts, amino acid activation is both the slowest kinetically and most irreversible thermodynamically of the chemical reactions necessary for protein synthesis (Carter et al. 2014). The former distinction means that activation is ~1000 times slower than acyl transfer to tRNA or peptide bond formation from activated intermediates and represents the principal kinetic barrier to making peptides in a pre-biotic context. The latter means that amino acid activation is one of the hardest reactions in biology to drive to completion. It is probably not accidental that it became driven by ATP hydrolysis, which can deliver an additional free energy pulse once the pyrophosphate liberated by amino acid activation is subsequently hydrolyzed, assuring that activation goes to completion.

That two distinct protein superfamilies emerged to couple amino acid activation to ATP hydrolysis represented a conundrum that remained unanswered until a quite recent investigation connecting coding properties of tRNA bases with the physical chemistry of amino acid side-chain phase transfer and protein folding equilibria (Carter and Wolfenden 2015, 2016; Wolfenden et al. 2015) provided the first clues to a possible answer (see Fig. 2). One puzzling aspect of dividing the 20 canonical amino acids into two distinct groups is that the resulting classes appear to have quite similar diversity in their representation of the various physical chemical properties. Subclass B activates Glu, Gln, and Lys in Class I and Asp, Asn, and Lys in Class II. Subclass C activates Trp and Tyr in Class I and Phe in Class II. The similar diversity within each class leaves open the possibility that the two synthetase Classes appeared sequentially and not simultaneously. Although most authors have been reluctant to comment on their order of appearance (Woese et al. 2000), several have argued for a sequential appearance (Safro and Klipcan 2013; Klipcan and Safro 2004; Smith and Hartman 2015).

4.1 Class I, II aaRS Have Highly Interdependent Active-Site Constructions

Sequence conservation within the synthetase active sites furnishes the strongest evidence that the two Classes appeared simultaneously and not sequentially (Carter et al. 2014; Carter 2015). Functional residues in each site—those whose functional groups directly influence the chemistry of the two substrates, as opposed to side chains within the conserved signatures that interact with the rest of the protein—are drawn entirely from the set of amino acids activated by the opposite aaRS Class (Fig. 11). This phenomenon is especially conspicuous for the Class-defining signature residues. For example, seven residues from the HIGH and KMSKS motives of Class I active sites interact with the ATP substrate; whereas the two remaining hydrophobic, Class I, I and M residues, respectively, coordinate movement of the two signatures because they are embedded in a hydrophobic core of the anticodon-binding domain.

Although further work on this question is certainly worthwhile, there appear to be functional reasons why active-site residues are deployed quite differently in each Class. Although these differences have not been delineated systematically, they appear to produce dissimilar transition-state stabilization mechanisms (Perona and Gruic-Sovulj 2013; Zhang et al. 2006). With some exceptions—TrpRS residue D132 is a Class II amino acid conserved in the amino acid substrate binding sites of several Class I aaRS—the residues that obey this particular asymmetry

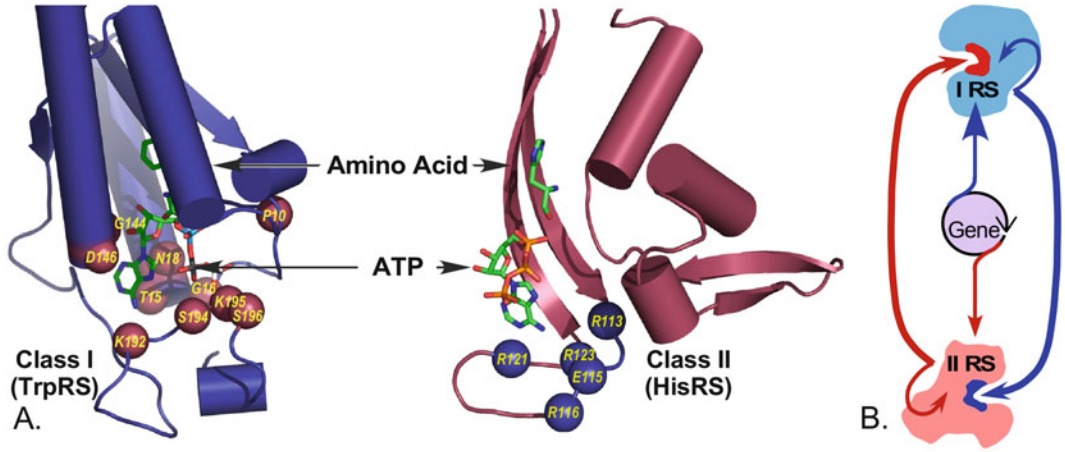

Fig. 11 Functional active-site residues in all members of Class I are drawn exclusively from the set of amino acids activated by Class II aaRS, and vice versa. (**a**) The two sets of Class-defining residues have quite distinct functional groups; Class I active-site residues consist of histidine, glycine, proline, asparagine, threonine, lysine, and aspartic acid; Class II active-site residues consist of arginine and glutamic acid. It is highly inconceivable that this differentiation is accidental. (**b**) The differentiation of active-site catalytic residues effectively creates a hypercycle-like interdependence of Class I and II ancestral forms (Eigen and Schuster 1977)

are located in the respective ATP binding sites, and their functional differentiation is likely to be related to functional differentiation in the mechanism for ATP activation. Class I aaRS appear to use a dynamic Mg^{2+} ion that moves with the PPi leaving group bound by the KMSKS loop during the transition state (Carter et al. 2017) and appear to stabilize additional negative charge in a dissociative transition state involving an α-metaphosphate (Carter et al. 2017). Class II aaRS appear to stabilize a pentavalent α-phosphoryl group transition state with multiple Mg^{2+} ions that are bound directly by protein residues in a manner reminiscent of the two-metal transition state stabilization of polymerases (Steitz and Steitz 1993).

Some variation in these patterns occurs in eukaryotic synthetases, which are much more highly differentiated than bacterial aaRS and have adapted their catalytic mechanisms to accommodate and perhaps to sustain the accumulation of modules, called *physiocrines* (Guo and Schimmel 2013; Guo et al. 2010), with additional functions, whose selective advantages have been proposed to require modifying the active-site configurations (Yang et al. 2004, 2007).

These putative mechanistic differences are consistent with the differential use of Class II histidine, asparagine, lysine and serine to stabilization of a (PO_3^-) metaphosphate transition state by Class I aaRS, and of Class I arginine—stabilization with Mg^{2+} of pentavalent phosphoryl transition state assisted by glutamic acid coordination of Mg^{2+} by Class II aaRS. As the active sites are almost certainly the oldest parts of an enzyme, it seems highly unlikely that either aaRS Class could ever have managed without the other because of the necessity to provide activated amino acids from the opposite set for their own translation.

Mechanistic differentiation as outlined here may have deeper evolutionary significance in light of a series of asymmetries at primary, secondary, and tertiary structural levels. These are described in Sects. 4.2, 4.3 and 4.4.

4.2 Amino Acid Side Chain Volume May Underlie the Class Distinction

It seems reasonable to seek a basis for the striking division between the two amino acid

classes from among the various physical descriptors that differentiate amino acid chemical behaviors. The obvious diversity within each class complicates the question. Given a matrix with one amino acid per row and columns giving its class and candidate descriptors, one can compare the various linear models relating properties to amino acid Class. Most proposed predictors are corrupted by attempts to impose correlations with the buried (or exposed) surface areas in proteins. Three predictors stand apart from this difficulty: the "polar requirement" (Woese et al. 1966), and the phase transfer free energies for water-to-cyclohexane (Wolfenden 2007; Gibbs et al. 1991; Wolfenden et al. 1979a; Wolfenden et al. 1979b) and vapor-to-cyclohexane (Radzicka and Wolfenden 1988). The former resulted from an ingenious attempt to test the hypothetical correlation between an amino acid property and the codon table. The resulting scale was derived from paper chromatography of the amino acids in solutions of varying content of dimethylpyridine, to alter the mobility in accordance with the phase transfer behavior. However, that scale is highly idiosyncratic and cannot be recapitulated without an extensive investigation into the properties of paper chromatography, which is rarely if ever used today. In contrast, both the latter measures represent pure physico-chemical equilibria unrelated to possible interactions either with carbohydrates in the paper support or with nucleic acids (Fig. 12).

The three different properties are not linearly independent. The polar requirement is uncorrelated with the vapor-to-cyclohexane equilibria ($R^2 = 0.06$; $P = 0.26$) but well-correlated with the water-to-cyclohexane equilibria ($R^2 = 0.62$; $P < 0.0001$). However, the two phase transfer equilibria themselves are uncorrelated ($R^2 = 0.01$; $P = 0.69$). Thus, they are distinctly different metrics, whereas the polar requirement resembles the hydrophobicity measured by the water-to-cyclohexane transfer equilibrium.

The second relevant point is how the three values correlate with the degree of side chain exposure in folded proteins measured by the solvent accessible surface area, ASA. That metric is, itself, subject to uncertainty as discussed elsewhere (Carter and Wolfenden 2015; Wolfenden et al. 2015), where it is argued that the values published by Moelbert (Moelbert et al. 2004) represent the least ambiguous values. Moreover, amino acids cysteine and proline violate all characterizations of this sort, owing to alternative influences—exposure in turn segments, coordination of metals and disulfide linkages—that lead to highly variant distributions between surface and core. Given those assumptions, and by a substantial margin, the best model for the ASA values is achieved by a linear combination of water-to-cyclohexane and vapor-to-cyclohexane free energies ($R^2 = 0.94$; all $P < 0.001$). The polar requirement performs less well in combinations (Fig. 13), indicating that the information in the polar requirement is redundant with that in the transfer free energy from water to cyclohexane. Thus, the vapor-to-cyclohexane transfer free energy provides new, complementary information, allowing a nearly complete prediction of ASA.

The original purpose in developing the polar requirement was to account for regularities in the genetic code. It appears, however, that tRNA identity elements are more reliably related in detail to the phase transfer free energies (Carter and Wolfenden 2015, 2016) than to the polar requirement value.

4.3 tRNA Acceptor Stem and Anticodon Have Independent Coding Properties

In a paper that now appears increasingly prescient, Schimmel et al. (1993) argued that the dual domain structures of aaRS and tRNAs and experimental demonstrations that many aaRS could specifically aminoacylate tRNA acceptor stems in the absence of the anticodon stem loops implied an earlier phase of genetic coding. They proposed that aaRS catalytic domains and tRNA acceptor stems may have implemented an "operational RNA code" that enabled them to begin to align aminoacyl-acceptor stems according to an

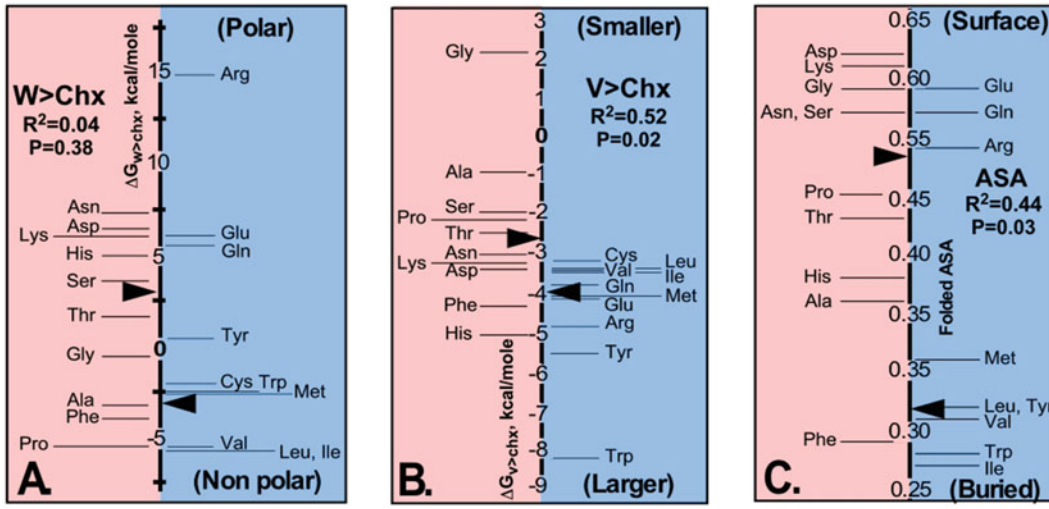

Fig. 12 Comparisons of the phase transfer free energies of the Class I (*blue*) and II (*red*) amino acids. (**a**) Water to cyclohexane transfer free energies, or hydrophobicity. (**b**) Vapor to cyclohexane transfer free energies, which are closely related to side chain volume ($R^2 = 0.88$). (**c**) Exposed surface areas of amino acid side chains in folded proteins, estimated by (Moelbert et al. 2004). Median values are indicated by *black arrow* points. Statistics for regression models expressing each property as a function of amino acid Class are given below the titles. Extremes for each property are indicated at the *top* and *bottom* of the Class I half of each *panel* (Adapted from Carter and Wolfenden (Carter and Wolfenden 2015))

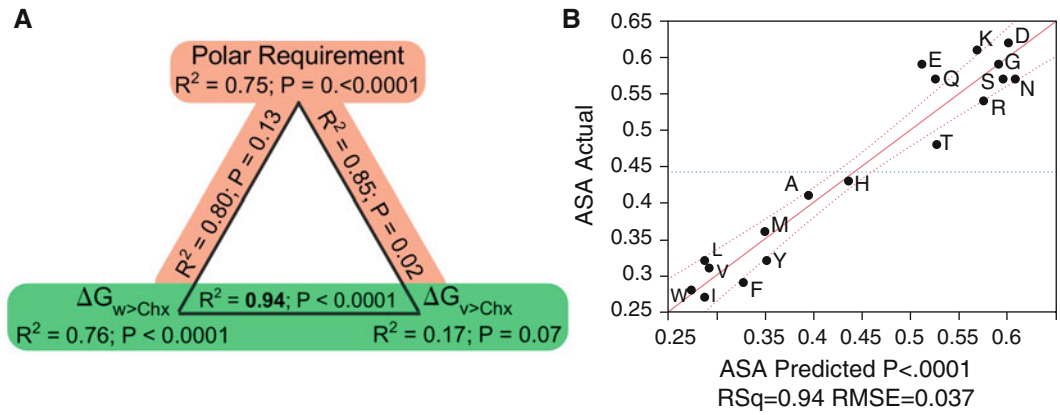

Fig. 13 Basis sets for protein folding. The polar requirement (Woese et al. 1966) was the earliest effort to find such a basis set. Performance of the polar requirement is compared here with two other, more fundamentally derived amino acid properties. (**a**) Summary of regression models for the residual accessible surface area in folded proteins, ASA, (Moelbert et al. 2004) using amino acid properties as predictors. All three metrics are related to the ASA. Polar requirement alone is correlated with ASA nearly as well as is the water to cyclohexane transfer free energy, to which it is highly correlated. Edges of the triangle give statistics for bi-variate models involving two of the three predictors. *Green* background indicates satisfactory models; *red* background indicates models that have inferior statistics, either because they do not explain the variation in ASA, or because the polar requirement contribution is insignificant, or both. (**b**) The optimal model given across the *bottom* edge of **a** leads to quite satisfactory prediction of the ASA for all canonical amino acids excepting proline and cysteine, for which there are consensus factors leading to their being outliers

ancestral messenger RNA (Henderson and Schimmel 1997). The anticodon stem-loop and corresponding binding domains in the synthetases were assimilated later.

The more recent demonstration that aaRS Urzymes could acylate tRNA complemented the experimental acylation of acceptor stems (Francklyn et al. 1992; Francklyn and Schimmel 1989, 1990), reinforcing the suggestion of Schimmel, et al., and highlighting the question of what, specifically, might that operational code have consisted? To answer this question, various potential properties of the 20 canonical amino acids were assembled into a table with one line per amino acid. Each property was listed in a separate column. Separate tables included additional columns representing acceptor stem and anticodon bases forming identity elements (compiled by Giegé (Giegé et al. 1998)) according to a binary code using one bit for whether a base is a purine (−1) or a pyrimidine (1) and another bit for whether its Watson-Crick base pairing formed three (1) or two (−1) hydrogen bonds. Regression models were then constructed for each property as a dependent variable using the coding element columns as independent variables (Carter and Wolfenden 2015).

Not surprisingly, all such models provided excellent correlations with each physical property if sufficiently many coefficients were used. To differentiate "predictive" models from models using sufficiently many coefficients that they overfitted the noise, two non-canonical amino acids, selenocysteine (Sec) and pyrrolysine (Pyl), outside the training set were used for cross-validation. There was a clear distinction between models capable of predicting the properties of the two amino acids in the test set, and those that did so poorly. "Predictive" models had a small variance in predicting the test set (Sec, Pyl). They differed distinctly, depending on whether the identity elements used as independent variables came from the acceptor stem or from the anticodon (Fig. 14). Bases in the acceptor stem provide uniquely predictive codes for the side-chain size, whether or not it is branched at the β-carbon, and whether or not the side chain has a carboxyl group. Most other side-chain properties, notably including the hydrophobicity, are specified by the anticodon (Carter and Wolfenden 2015).

The unique and restricted coding properties of the acceptor stem provide substantive support for the proposal that an "operational RNA code" preceded the universal genetic code carried by the anticodon bases. Details of the acceptor stem code suggest in addition that the properties most important for that code were size, β-branching, and carboxylate side chains. In turn, those properties argue that genetic coding began before it became useful to encode side chains necessary to form hydrophobic cores, and hence before coding specified folded tertiary structures (Carter and Wolfenden 2015). In fact, the central features of the acceptor stem code specify requirements for forming extended chain β-structures, like those identified by modeling interactions between peptide β-structures and RNA (Carter 1975; Carter and Kraut 1974). These requirements suggest a selective advantage that could have favored the emergence of such an operational code from a pre-existing population of oligopeptides and oligonucleotides that interacted according to a direct, stereochemical code based upon mutual structural complementarity. Moreover, it is consistent with the notion, elaborated in Sects. 2.4 and 5.B, that ancestral synthetases, and especially protozymes were coded using a reduced alphabet, leading to "statistical proteins" (Wills 2016; Vestigian et al. 2006; Woese 1967, 1969).

4.4 Bi-directional Coding Implies Two Interpretations of the Same Genetic Information

To test the Rodin-Ohno hypothesis directly, we adapted the Rosetta multistate design algorithm (Leaver-Fay et al. 2011) to craft polypeptide sequences to stabilize two alternative backbone configurations—Class I and Class II protozymes— simultaneously and subject to the constraint that amino acids selected to stabilize

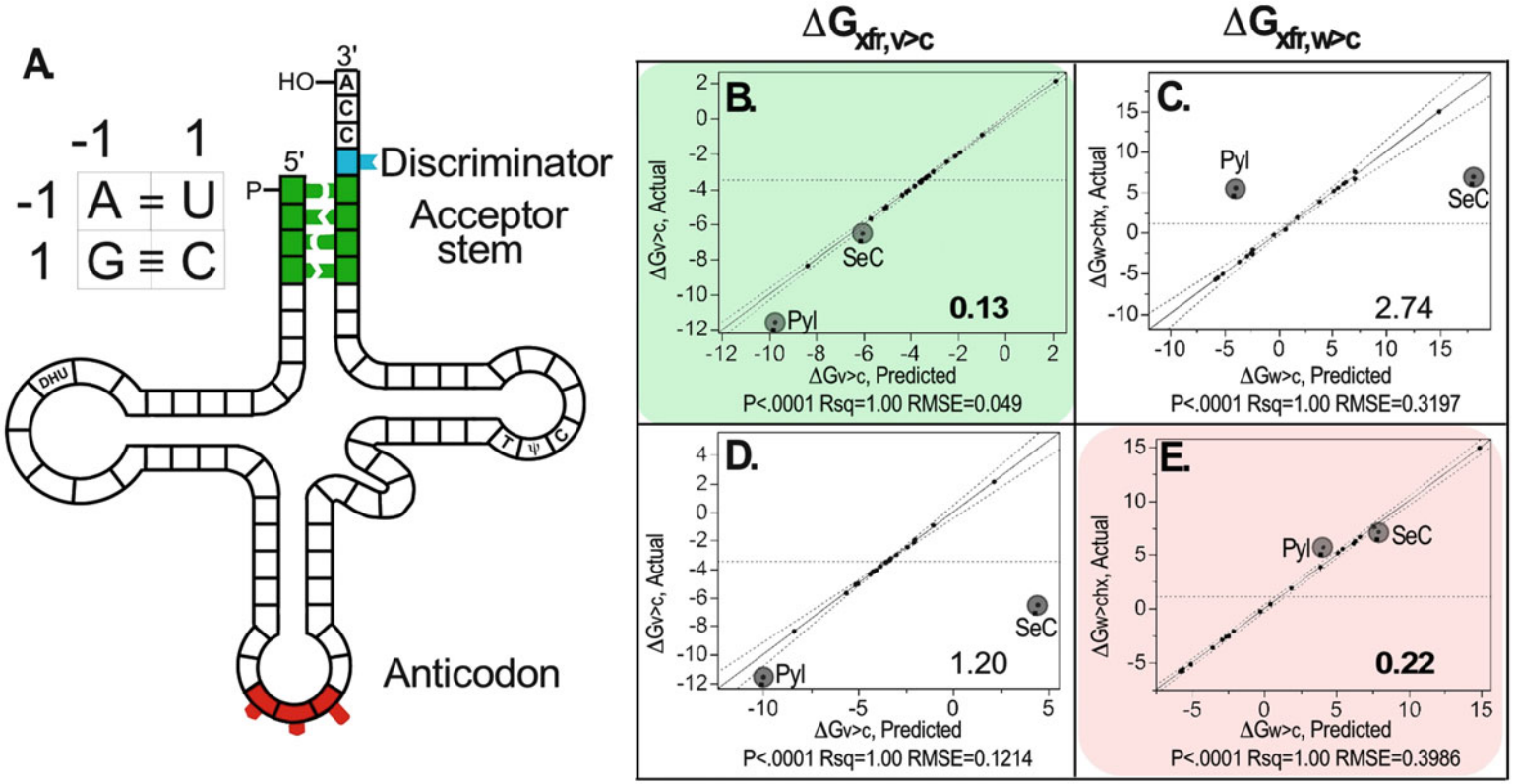

Fig. 14 Coding assignments in the tRNA acceptor stem and anticodon bases (Carter and Wolfenden 2015, 2016). tRNA coding of amino acid properties. (**a**) Binary representation of tRNA coding showing the acceptor stem (*green*) and anticodon (*red*). (**b**–**e**) Correlations between experimental values for ΔGw > c (**c** and **e**) and ΔGv > c (**b** and **d**) and those calculated from the best regression models. (**b** and **c**) show models for the acceptor stem bases; **d** and **e** show models for the anticodon bases. (**b**–**e**) are arranged as a 2^2 factorial design for the two tRNA coding regions (down the vertical) and the two physicochemical properties (across the horizontal). Coefficients trained on the 20 canonical amino acids ((Carter and Wolfenden 2015); see SI Appendix, Tables S2 and S4) were used to predict values for Sec and Pyl for cross-validation. *Lower right-hand corners* of **b**–**e** show RMS relative errors for cross-validation. Colored backgrounds show which of the four models make low variance predictions for the test-set of selenocysteine and pyrrolysine, which were not included in the training set. Plots prepared using JMP (SAS 2015) (From Carter and Wolfenden (2015))

one backbone have codons complementary to those of amino acids at the corresponding position on the other strand. Those constraints enforced bi-directional coding and produced one gene from which we could express a Class I Protozyme in one orientation and a Class II Protozyme in the other orientation Fig. 15 (Martinez et al. 2015).

Contemporary aaRS genes are obviously coded uni-directionally (there is, however, evidence that bi-directional coding might have survived to contemporary organisms in isolated cases (Carter and Duax 2002; LéJohn et al. 1994a, b; Yang and LéJohn 1994). The degree of middle codon-base pairing in sufficiently detailed, all-by-all comparisons may therefore allow two different mechanisms to be distinguished: (i) strand specialization, in which the two strands of daughter genes developed mutations that eliminated bi-directional coding in order to achieve sufficiently improved fitness (Fig. 16a), and (ii) adaptive radiation of bi-directional genes that would have preserved high middle codon-base pairing until more recent times (Fig. 16b). At what point the strand specialization actually occurred along the sequence of bifurcations during code expansion should have left distinguishable signatures in patterns of the middle codon-base pairing distance metric.

Bi-directional coding means that the two aaRS Classes are derived from alternative interpretations of the same ancestral genetic information, much as in visual puzzles with complementary interpretations of figure and ground (Fig. 17). The Watson-Crick base-pairing rules and the repeating twofold symmetry relating backbones of opposite nucleic acid strands means that the two strands of the designed Protozyme gene contain only one set of unique information, represented in complementary

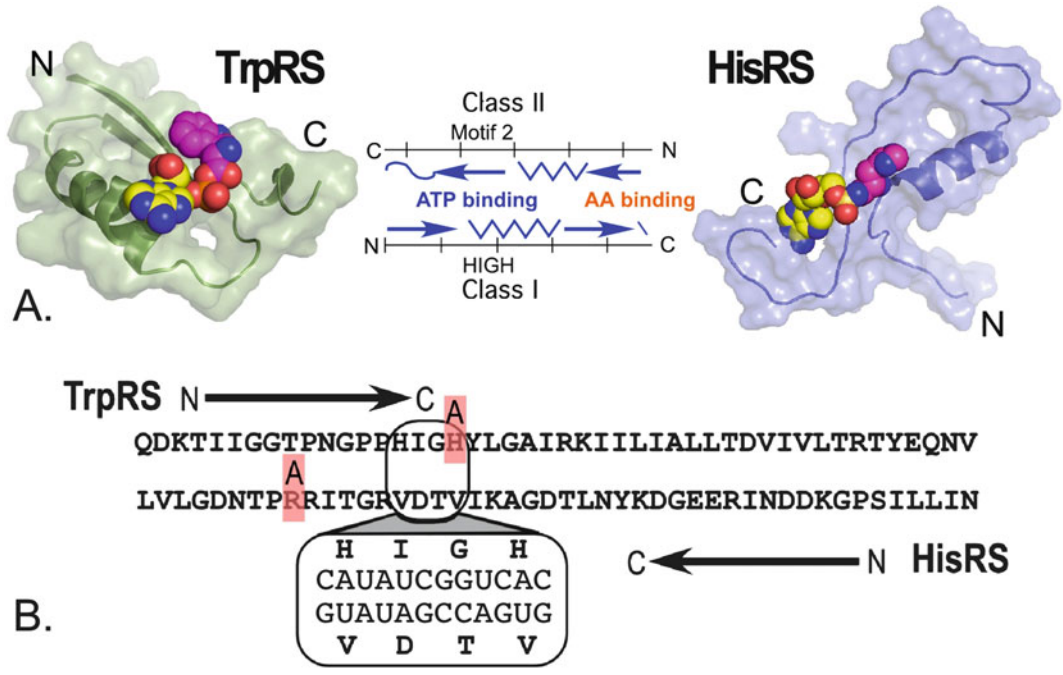

Fig. 15 A designed bi-directional gene encoding a Class I Protozyme on one strand and a Class II Protozyme on the opposite strand (Martinez et al. 2015). (**a**) Structural scaffolds that constrained Rosetta amino acid selections while enforcing complementary codons on opposite strands. *Scheme* in the *center* indicates locations of substrate binding sites. (**b**) Translated sequences from the designed gene. Alanine mutations used to validate authenticity of activity are highlighted in *red* above the corresponding active-site residues. Zoomed region illustrates complementary coding sequences (This research was originally published in the *Journal of Biological Chemistry* Martinez et al. (2015) ©American Society of Biochemistry and Molecular Biology)

forms by either strand. The opposite strand has no additional information! Yet that information can support two entirely different interpretations with similar functions, depending on how it is read. This unexpected duality unifies the two aaRS superfamilies. Unification is commonly sought by physicists, but is very unusual in structural biology.

5 Inversion Symmetries in Structure and Function Maximally Differentiate the Two aaRS Classes

Anomalies described in Sect. 4 appeared at first to be unrelated curiosities. In fact, however, they all assume coherent interpretations as inversion symmetries in the structural and functional implications of bi-directional coding for the organizational levels —primary, secondary, tertiary— of the familiar Linderstrøm-Lang (Linderstrøm-Lang 1952) hierarchy. Moreover, these inversion symmetries may have significantly impacted the emergence of genetic coding (Carter and Wills 2017). This section incorporates these relationships into a unified framework: multi-level molecular disambiguation.

The Genes of Bi-directionally Coded Ancestral Class I and Class II aaRS Were as Different as Possible from Each Other Although the sugar-phosphate backbones of two complementary strands of a nucleic acid can be interconverted by twofold symmetry operations, their sequences can be interconverted only via the complementarity operation of base-pairing. This means that the mutational path from one strand to its complement is as long as possible: bi-directionally coded genes are maximally differentiated with respect to mutation, and it is essentially inconceivable that random mutational events could achieve that interconversion.

Primary Amino Acid Sequences of Ancestral Class I and Class II aaRS Were as Different as Possible from Each Other Primary structures of proteins are intimately related via the genetic code to their nucleic acid (RNA or DNA) coding sequences. For this reason, ancestral, bi-directionally coded aaRS ancestors are maximally differentiated from one another.

Secondary Structures of Class I and II aaRS Were Similar to Each Other Unlike primary and tertiary structures, the ancestral Class I and II aaRS secondary structures were very likely similar, with crucial differences outlined in the next paragraph. Secondary structural similarity arises from the fact that formation of α-helical and extended β-structures is driven largely by periodic patterns of similar side chain properties—heptapeptide repeats of non-polar side chains forming α-helices and alternating dipeptide patterns forming extended β-structure. Such periodicities reflect across from one coding strand to the other [See Fig. 6b of Ref. (Chandrasekaran et al. 2013)].

Tertiary Structures of Proteins Coded by Bi-directional Genes Have the Interesting Property of Being in a Real Sense Inside Out, One to the Other A curious feature in the organization of the genetic code (Zull and Smith 1990) means that amino acids that are confined to cores of folded proteins have codons whose anticodons encode residues invariably found on the surface [See Fig. 6a of Ref. (Chandrasekaran et al. 2013)]. Thus, whereas secondary structures in bi-directionally coded pairs of proteins are largely reflected across the two coding strands, solvation patterns of their respective side chains are inverted. Surfaces of helices and strands that are exposed in folded structures of one Class are buried in those of the other.

Use of Side Chains from Opposite Classes Maximizes Differentation of Catalytic Mechanisms The active site differentiation (Fig. 11) results in significant mechanistic disambiguation of the active-site chemistries of Class I and II aaRS. Mutations that might lead to interconversion from one mechanism to the other would therefore be most likely to be lethal,

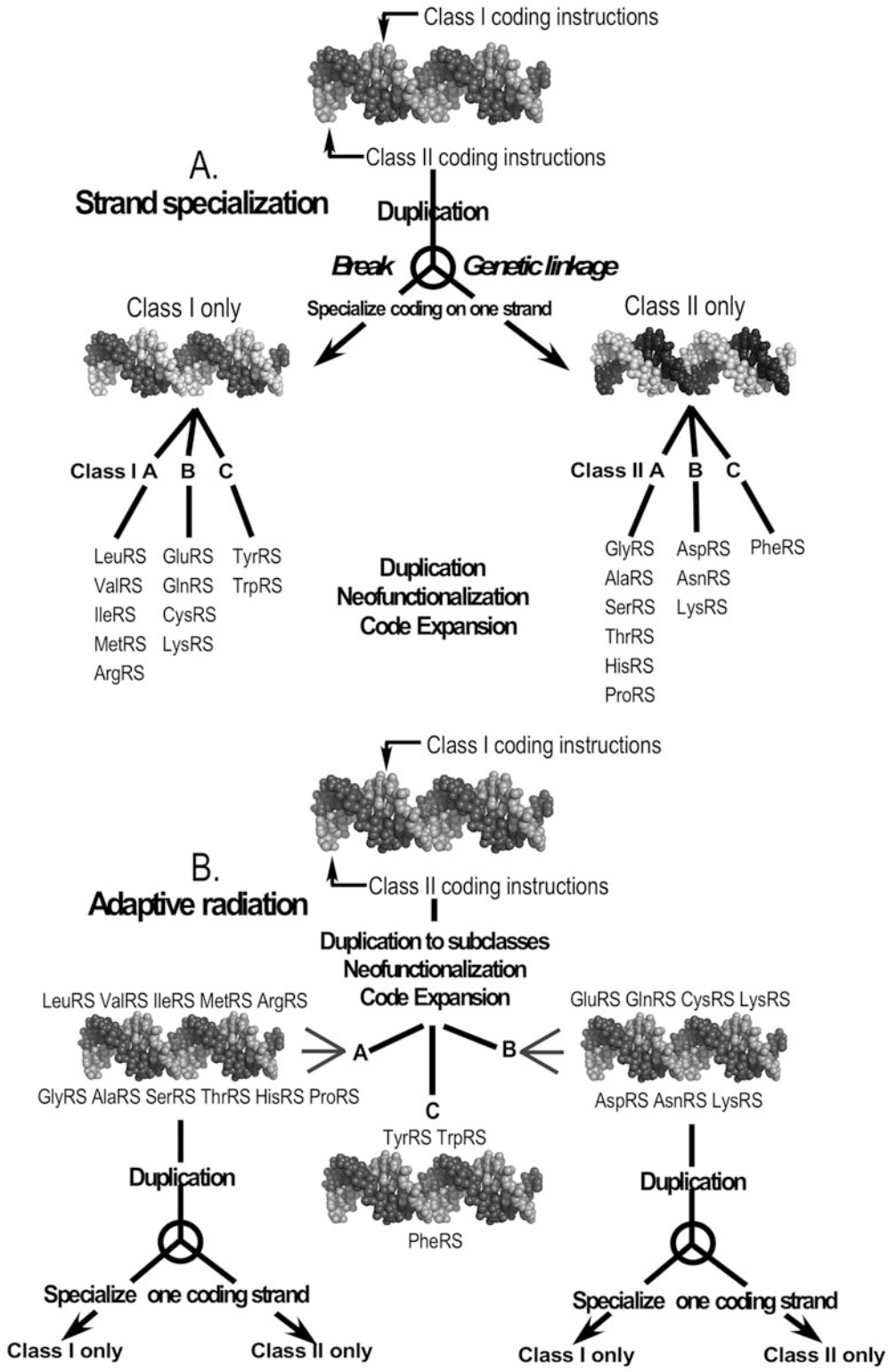

Fig. 16 Alternative mechanisms for genetic code expansion. (**a**) Strand specialization. Daughters produced by gene duplication evolve first by breaking the genetic linkage between bi-directional coding sequences, producing specialized genes that express from only one of the two strands. (**b**) Adaptive radiation. The code is

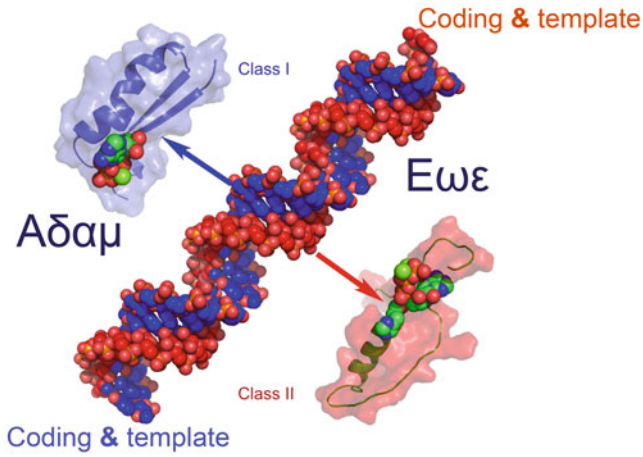

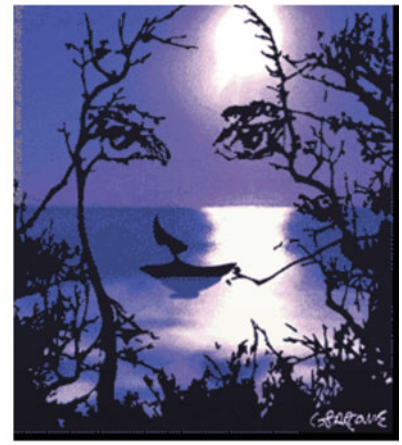

"Twilight Face", © Gianni A. Sarcone, giannisarcone.com. All rights reserved.

Fig. 17 Two different interpretations of the same unique information. (**a**) The bi-directional Protozyme gene in Fig. 14 has two possible translation products, one from each strand. One double-stranded gene constructed by the computer program "Rosetta" produces two different, equally functional protozymes from instructions on opposite strands. Each strand thus serves as a gene, coding for a peptide, as well as a template for duplication. We have chosen to call the two strands Αδαμ and Εωε, using Greek names to distinguish these molecular ancestors from our mythical human ancestors. Although there is only a single unique set of instructions, that information has two distinct and functional interpretations, depending on which strand is read (Courtesy of Carter *Natural History* CW, Jr. (2016) *Natural History* 125:28–33.) (**b**) This duality is a biological implementation of the familiar visual puzzle, which also has two distinct and equally valid interpretations (Gianni Sarcone, with permission)

adding a measure of secuity to the mechanistic integrity of the Class.

Substrate Recognition Differentiates Large from Small Amino Acid Side Chains The only significant aspect of the canonical 20 amino acids for which there is a statistically significant difference between the two classes is the size of the side chain (Carter and Wolfenden 2015; Wolfenden et al. 2015). It would seem more than coincidental that amino acid size is also the primary source of differentiation in the tRNA acceptor stem operational code (Carter and Wolfenden 2015, 2016). Side chain volume thus appears to underlie the initial differentiation between aaRS substrates that eventually enabled the development of the current genetic code.

6 Evolutionary Implications

The genetic code represents one of the deepest unsolved puzzles associated with the origin of life. An important possible reason why it has remained such an outstanding problem is that much of the interdisciplinary community concerned with the origin of life has been preoccupied by the RNA World hypothesis, under which the code remains an even more challenging enigma than it needs to be. Under that

Fig. 16 (continued) expanded by producing pairs of bi-directional genes, both strands of which have specialized functions. (**a**) and (**b**) should lead to different patterns in the degree of middle codon-base pairing (Adapted with permission from the Society for Molecular Biology and Evolution. Chandrasekaran et al. (2013))

hypothesis, the code was "discovered" by ribozymes seeking to improve their severely limited catalytic potential and was perhaps assisted by stereochemical complementarity of nucleotide triplets whose structures were complementary to those of amino acids, for which they eventually became (either) codons or anticodons (Yarus 2011a; Yarus et al. 2009). The typical argument (Koonin 2011) is that amino acids were first recruited by ribozymes as "co-factors" that enhanced the diversity and proficiency of ribozymes. As their superior catalytic functions became manifest, increasingly polymerized forms of amino acids arose through some form of selection, leading to the translation system now used throughout biology. One of many substantial problems with this narrative is that there really is no rational mechanism for bootstrapping the code into existence in an RNA world (Carter and Wills 2017).

This review promised a dialectical survey of ways in which recent advances in understanding the evolution of the aminoacyl-tRNA synthetases have tended to refute the contention that these enzymes "…did not shape the codon assignments". A substantial number of unexpected results have been put in evidence since that judgment was formulated. Do those observations contribute to "a credible scenario for the evolution of the coding principle itself and the translation system"? Remarkably, the answer appears to be substantively affirmative as outlined in greater detail elsewhere (Carter and Wills 2017; Wills and Carter 2017). In brief, each of the unexpected oddities arising from recent aaRS research now can be seen as necessary and sufficient vestiges of a bootstrapping process that began deep in a very primitive RNA/peptide world that prefigured relationships in Fig. 2 at an elemental level. Its built-in and robust reflexivity enabled a massive acceleration of the search for a near optimal genetic code. Further, these results were accomplished using a variety of effective new tools and ways of thinking, with which to explore the many interstices remaining to be explored.

Assembling the pieces reviewed here into a coherent refutation of the RNA World narrative begins with the conclusion that contemporary protein structures represent an archive of their origins and evolutionary expansion.

6.1 Protein Structures Were Probably Not Completely Overwritten But Left an Interpretable Archive of Their Evolutionary Origin in Bi-directional Genetic Coding

Successive experimental deconstruction of both Class I and Class II aaRS reveals parallel structural and catalytic hierarchies. Catalytic domains, Urzymes, and Protozymes represent increasingly deeply, broadly conserved motifs. The relative ease in identifying them and the robustness of their experimental characterization compose a substantial string of evidence that the hierarchies apparent in Figs. 3 and 4 represent not a palimpsest of an RNA World (Benner et al. 1989), but a legitimate archive (Danchin 2007)—evident in the contemporary structures—from which we have been able to read out, and reconstruct reasonable models for successive stages in their evolution.

Evolutionary reconstruction is kin to similar scientific problems, such as chemical and enzyme kinetic mechanisms, that present formidable barriers having to do with limitations placed by time. Kinetic mechanisms imply limiting structures, transition states, which by virtue of their extremely short lifetimes, cannot normally be directly detected. The inability to re-play the tape of evolution, on the other hand, creates analogous problems. In both cases, direct study of the objects of greatest interest is either difficult or impossible. These time-related barriers, in turn, dictate the logical framework necessary to progress. Koch's postulates concerning infectious disease were an early expression of this framework, and these were re-formulated by Fersht (1999) to shape the evidence for a particular intermediate in a reaction path. This logical process entails three elements: characterization of the putative intermediate, demonstration that it can be formed from

preceding structures fast enough to lie on the path, and demonstration that it can react fast enough to lie on the path. By analogy, a legitimate evolutionary intermediate must be identified, and prepared. Then, plausible evolutionary changes must be outlined—and if possible tested—to account for its initial appearance and its subsequent conversion to the next intermediate in a reasonable timeframe.

The aaRS superfamilies behave consistently with this logical framework. Like Matryoshka dolls, elemental Class I and II active sites both lie within their protozymes, which form the ATP binding sites. Protozymes themselves compose a bit less than half the Urzymes, which contain the nuts and bolts of the catalytic domain. The function of the TrpRS Urzyme within the full-length enzyme is, however, entangled with coordinated motions of the CP1 and ABD domains (Kapustina et al. 2006, 2007; Li et al. 2015; Budiman et al. 2007; Kapustina and Carter 2006). Recent combinatorial perturbation studies have implicated these motions in long-range allosteric effects crucial to both catalysis (Weinreb et al. 2009, 2012) and specificity (Weinreb et al. 2014; Li and Carter 2013; Carter et al. 2017) in TrpRS. The synthetase phylogenies therefore represent rich and, as yet only minimally tapped, resources of information about the evolutionary development of catalysis, specificity, and allostery.

Beginning with the audacious proposal of Rodin and Ohno (1995) and culminating with the experimental demonstration of a bi-directional gene for the Class I and II Protozymes (Martinez et al. 2015), the trajectory of aaRS research has produced diverse experimental and bioinformatic confirmations of the predictions of bi-directional coding (Fig. 1). Substantive validation of the unification of the two synthetase Classes implies a need to re-annotate proteomic databases. In particular, if, as appears to be the case, a bi-directional synthetase protozyme gene preceded most of the proteome, then phylogenies (Wolf and Koonin 2007; ; Aravind et al. 1998, 2002; Leipe et al. 2002; Wolf et al. 1999) that imply that the Class I synthetase superfamily branched off a different root quite late in the emergence of the proteome cannot also be correct unless modified in important ways to reflect the substantially finer modularity of proteins in general and the staged appearance of different modules.

For the moment, suffice it to say that the direct evidence for the bi-directional coding hypothesis appears exceptionally strong both for Protozymes (Martinez et al. 2015) and for Urzymes (Li et al. 2013). Section 3 developed the implications of bi-directional coding for the differentiation of the genes themselves and their implications for primary, secondary, and tertiary structures of the corresponding synthetases, and thence for their catalytic and coding functions. In the following section, we see how these aspects of synthetase phylogeny and structural biology, viewed coherently as outlined in Sect. 5, also in fact fulfill important requirements for bootstrapping complexity from simplicity.

6.2 Bi-directional Coding Was Probably Essential to Stabilize the Emergence of Translation

From the standpoint of information processing, genetic coding differs fundamentally from replication. It is, arguably, one of the most significant and puzzling among the transformations that produced biology from chemistry. It is perhaps the key event that enabled the creation of a multiplicity of sufficiently tunable catalytic activities to synchronize the rates necessary for cellular metabolism, Sect. 2.1. It seems surprising that (Woese et al. 2000) would have summarily dismissed the possibility that the evolution of the aminoacyl-tRNA synthetases—the executors of the genetic code—had much to do with the development of the code itself.

The alternative argument, that synthetase evolution actually was the *sine qua non* of what generated the code, has been articulated in considerable detail elsewhere [(Carter and Wills 2017; Wills and Carter 2017) and refs cited

therein]. Key aspects of that argument are as follows:

(i) Primary structures generated by bi-directional coding are maximally different from one another, hence cannot be "fused" via functional mutants.
(ii) Coding relationships in tRNA acceptor stems and anticodons are consistent with at least two distinct stages during which synthetase-tRNA recognition participated in indirect (i.e., "genetic") coding (Carter and Wolfenden 2015, 2016). The earlier stage is eminently consistent with a very small amino acid alphabet consisting of one or at most two bits. Moreover, this result implies the tetrahedral network (Fig. 2) connecting four nodes, two in the nucleic acid world—tRNA (the programming language) and mRNA (the programs) to two nodes in the protein world—amino acid physical chemistry and protein folding (Carter and Wolfenden 2015, 2016; Wolfenden et al. 2015).
(iii) A two-bit alphabet competing with anything pre-existing in any RNA coding world having higher sophistication would have been rapidly eliminated by purifying selection because it would degrade more sophisticated messages.
(iv) (a–c) imply that genetic coding must have been built from scratch in an implementation executed by protein aaRSs.
(v) Bi-directionally coded aaRS Protozymes and Urzymes represent a credible origin of the reflexivity necessary for efficiently bootstrapping the full genetic code into existence.

This bulleted list correlates with the elements of inversion symmetry relating the two aaRS Classes suggesting that the fundamentals of aaRS evolution (Sect. 3) closely match requirements for the emergence of genetic coding (Sect. 5.B(a)–(e)).

Bi-directional Coding Is Unexpected Because It Limits Genetic Diversity An indeterminate, but presumably significant fraction of all possible mutations that might enhance the fitness of both products from a bi-directional gene are forbidden by the complementarity constraint. It also appears likely that many such mutations would also decrease the fitness of the translated product from the opposite strand. Recent unpublished computational analysis (Silvert and Simonson 2016) suggests that the cost of bi-directional coding may be smaller than previously thought. Computational construction of bi-directional genes for all pairwise combinations of 500 pfam domains revealed that the number of pairs whose bi-directional genes in all 6 relative reading frames were homologous to consensus sequences from contemporary sequence alignments was unexpectedly high. Thus, the inversion symmetry of the universal genetic code observed by Zull and Smith (Zull and Smith 1990) may actually have played a key role in the eventual selection of the universal genetic code by optimizing the number of potentially functional bi-directional genes.

In any case, co-linear bi-directional coding does exact a price. The quest for diversity is severely limited by constraining both strands of a gene to have functional interpretations. That price must have been paid for by strong contemporary selective advantages. Two definitive properties—gene linkage (Pham et al. 2007) and gene differentiation (Carter and Wills 2017; Wills and Carter 2017)—together with the interdependence of all aaRS genes, may have compensated for this limitation while error rates were very high, and consequently made bi-directional coding an inevitable requirement for the emergence of coded protein synthesis.

Bi-directional Ensures Coexpression of Expressed Genes It seems reasonable that the two classes of amino acid substrates differed sufficiently that coded protein synthesis could not have been launched without (at least) two specialized kinds of aaRS. The distinction between amino acid substrates of Class I and II aaRS is closely related to the roles those amino acids play in protein folding and the apparently earlier

distinctions based on size, β-branching, and carboxylate side chains (Carter and Wolfenden 2015, 2016) are conspicuously appropriate for defining secondary structures in coded peptides. Bi-directional coding of amino acid activating enzymes with two specificities would have created a durable and ready-made basis for beginning to define coded peptides with rudimentary functional distinctions. If so, then before amino acid activation and acylation reactions became compartmentalized, bi-directional coding would have linked the two gene products, ensuring that both kinds of aaRS were produced in the same places and at the same times.

Bi-directional Coding Assures the Stability Necessary to Initiate and Sustain Genetic Diversity More generally, the inversion symmetry of bi-directional aaRS gene coding fulfills a number of criteria necessary for the stability and survival of emerging quasispecies in the face of what have come to be called "error catastrophes" (Eigen and Schuster 1977; Koonin 2011; Orgel 1963; Eigen 1971). The relatively low fidelity of the Urzymes characterized thus far and the evidence that they themselves are highly evolved means that their origins lie in populations of molecules, called "quasispecies" that achieve similar functions, but have multiple sequences (Eigen et al. 1988). The centroids of quasispecies are powerful "attractors" because they are sufficiently isolated in sequence space that variants with lower function will eventually be eliminated unless they "revert" toward the centroid. It is difficult therefore for a quasispecies to "bifurcate" , because clusters of functional sequences are separated by large regions of inactive species. The most important barrier to generating multiple aaRS was therefore to establish two species with similar catalytic function that were sufficiently differentiated that they could form stable, independent quasispecies [See Fig. 2 of (Carter and Wills 2017). Figure 18 summarizes how bi-directioinal coding provides the requisite differentiation to establish a "boot block" for the self-organization of genetic coding (Carter and Wills 2017; Wills and Carter 2017) in a peptide RNA collaboration.

The Genetic Code Is Much too Unusual to Have Been Discovered by Chance Among the challenges associated with genetic coding is to understand how so much amino acid physical chemistry became embedded into both tRNA and mRNA sequences. The combinatorics of genetic coding have been analyzed multiple ways by multiple investigators. The conclusion of these studies has been that for every code with the properties of the universal genetic code, there are perhaps a million other potential codes that

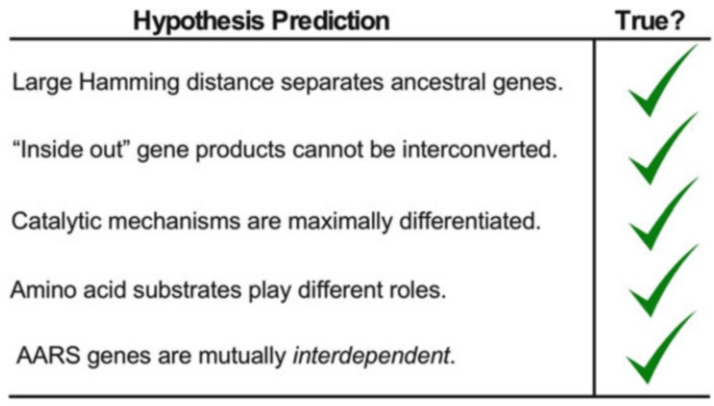

Fig. 18 Summary of how the surprising aspects of aaRS evolutionary history actually helped to facilitate the stabilization of quasi-species bifurcations associated with the earliest genetic coding. At each level of the Linderstrøm-Lang hierarchy (Linderstrøm-Lang 1952), from coding strands to secondary, to tertiary structure and mechanism, bi-directional coding decisively differentiates between the two aaRS Classes

are less optimal (Freeland and Hurst 1998). That estimate should probably be revised as both the apparent temporal appearance of encoded amino acid physical chemistry and bi-directional coding impose even more stringent requirements, making the universal code even more special than Freeland &Hurst appreciated.

In any RNA world, selecting amino acid sequences that fold into functional proteins depends entirely on natural selection. This implies an essentially trial-and-error search. As Koonin has pointedly noted by invoking multiple universes, such a specialized code is inaccessible by random processes in our universe (Koonin 2011). The alternative, which thus appears mandatory, is to provide a bootstrapping algorithm, by which a simple process can be endowed with the necessary characteristics to build complexity using its own resources.

The bootstrapping metaphor is quite intimately embedded into the framework of genetic coding. As noted (Carter and Wolfenden 2015, 2016), the code comprises a programming language and an associated set of programs written using that language. In this sense, it closely resembles a computer operating system, as Williams has noted elsewhere (Bowman et al. 2015; Petrov and Williams 2015; Anton et al. 2015). The key here is that computer operating systems are built around a simple set of instructions sufficient to enable the hardware, by executing those instructions, to build successively more sophisticated levels of functionality using a very limited set of alternatives. We believe that genetic coding must have arisen from an analogous "boot block" (Carter and Wills 2017), some of whose key relationships are illustrated in Fig. 19.

As shown in Fig. 19, bi-directionally coded protein aaRS are uniquely equipped to implement the crucial feedback loop necessary to bootstrap genetic coding, namely sensing the impacts of the local nano-environment on component amino acids that lead to protein folding rules. This feedback loop assures that amino acid sequences incapable of folding or whose functions are inferior are rapidly eliminated because the "rule executors" are themselves governed by the same phase transfer equilibria as all proteins. It cannot operate in any system using ribozymal aaRS. Bi-directional synthetase genes and the coding rules (Fig. 19) therefore together compose an existence proof that genetic coding could have evolved from humble origins by discovering both foldable sequences and optimal coding relationships much more rapidly than would have been possible in a pre-existing RNA world.

Interdependence Helped Assure Survival of Both Synthetase Classes The bullet list at the beginning of this section differentiates the products of a bi-directional gene at all levels. This multilevel differentiation sustains their underlying functional separation. The probability that mutations could eventually fuse their functions is minimized by the decisive mechanistic disambiguation [see Fig. 2 of Ref. (Carter and Wills 2017)]. Further, dependence of the functions coded by each strand on the gene products of both strands defines a hypercycle-like coupling (Eigen and Schuster 1977) to ensure that the two gene products have enhanced ability to survive high error rates, as in Figs. 17 and 18. In this sense, the liability we see today in bi-directional coding—tight genetic linkage—was probably a significant strength before chemistry became localized in cells.

6.3 Catalysis Arose from Simple, Promiscuous Molten Globules

The progression of transition-state stabilization free energies illustrated in Fig. 4 already suggests that catalytic proficiency developed progressively during the evolutionary maturation of the aaRS. Protozymes with ~50 amino acid residues produce >40% and Urzymes with ~130 amino acid residues produce ~60% of the transition state stabilization of modern enzymes. The specificity spectra in Fig. 5 suggest that aaRS Urzymes had achieved only 20% of their contemporary specificity. That distinction between catalysis and specificity sharply delineates discrete events in their evolutionary history (Fig. 6). Thus, most of the specificity appears to have

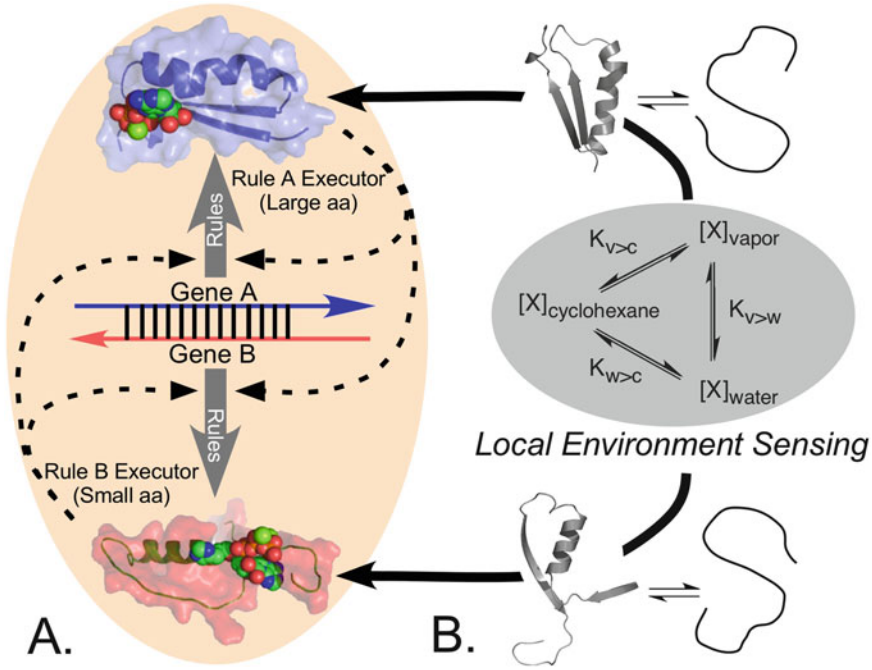

Fig. 19 Reflexivity in the emergence of the genetic code. Bi-directional Protozyme and putative Urzyme genes compose an existence proof for an intrinsic coding feedback loop that cannot exist in an RNA world. These genes are potentially translated (*thick grey arrows*; rules) by themselves (rule executors; *thin dashed arrows*). Both genes, in turn, must fold according to the behavior of amino acid phase transfer equilibria (local environment sensing) in order to execute the coding rules (*thick black arrows*). This feedback loop greatly enhances the ability of such genes to serve as "boot block" in bootstrapping development of more sophisticated genetic coding

evolved after the synthetases had developed most of their catalytic proficiency. Preliminary published experiments suggest that amino acid specificity can be achieved only by invoking allosteric interactions between domains in the contemporary enzymes (Weinreb et al. 2014; Li and Carter 2013; Carter et al. 2017) (vide infra; Sect. 2.3).

The surprising catalytic proficiency of the aaRS protozymes suggests that the earliest transition-state stabilization mechanisms arose by positioning backbone binding determinants and only later made use of active-site side chains. A pertinent example is the N-terminal array of four unsatisfied hydrogen bond donors in alpha helices, which became a foundation for stabilizing phosphate—and pyrophosphate—binding (Hol et al. 1978) and which is an important part of the Class I protozyme. It is not as yet known whether or not specific active-site side chains in the protozymes function in the same manner as they appear to do in the Urzymes and full-length enzymes. The loss of activity in the active-site mutant protozymes suggests that these side chains do contribute to transition-state stabilization, but more detailed functional studies will be necessary to delineate precisely their functional role.

Similarly, it appears likely that the Urzyme level of evolutionary development may utilize tight transition-state binding associated with a large unfavorable negative entropy change as suggested for the TrpRS Urzyme (Sapienza et al. 2016) and a chorismate mutase molten globular variant (Hu 2014). This possibility, combined with the discussion in Sect. 3 of the superiority of peptide catalysts suggests strongly that the emergence and selection of catalytic activity itself was vastly more efficient and hence more rapid for peptide, than for ribozymal catalysts. Moreover, if tight transition-state binding is common among molten peptide molten

globules, selection would recruit catalysts from a much larger manifold of sequences. The large negative TΔS term may ultimately limit the potential transition-state stabilization free energy of molten globules, and hence create in addition a selective advantage for evolving sequences that stabilize folded structures with more rigid transition-state complementarity (Amyes and Richard 2013). Finally, as noted above, enhancing substrate specificity likely required the emergence of allosteric effects that cannot develop within the Urzyme framework alone.

7 Outstanding Questions

Finally, it remains to outline areas that remain unresolved, where future experimental efforts can be most productive. We pose some of these questions in this section.

Do the Coding Relationships Identified in tRNA Acceptor Stems and Anticodons Preclude Evolutionary Inclusion of any Non-canonical Amino Acids into the Genetic Code? This insightful question, posed by a reviewer, opens up the possibility that the selection of the canonical 20 amino acids might also have a physical basis if, for example, norleucine was excluded because it had an inappropriate combination of size and polarity. None of the possible tests of this idea appears to be feasible without comparable experimental measurements of the phase transfer free energies of the non-canonical amino acids. A vexing related question is how the distinction first emerged between tRNA acceptor stems recognized by ancestral Class I and II aaRS. Unpublished efforts to answer this question have not yet been fruitful.

What Was the Scale of Modularity in the Earliest Evolution of Proteins? The most serious challenge to the various scenarios described in this review is the significant evidence from Koonin's group (Koonin and Novozhilov 2009; Koonin 2011; Aravind et al. 2002; Leipe et al. 2002; Wolf et al. 1999) and others (Caetano-Anolles et al. 2007, 2013) that speciation of the Class I aaRS did not occur until relatively late in the generation of the proteome. Those studies are based on the most current thinking on phylogenetic reconstruction, yet they appear to be inconsistent with a fundamental role for objects like the bi-directional Protozyme gene products near the root of the proteome. Our view is that this conundrum arises from failure to appropriately recognize fine-scale modularity in constructing trees for domains. Thus, we believe that the putative bi-directional Protozyme gene was ancestral not only to the aaRSs but to many other families of related function, and that horizontal modular transfers may have been important before molecular biology created cellular species (Wolf et al. 1999; Soucy et al. 2015). Under this alternative hypothesis, the late branching of Class I aaRS represents a subsequent process associated with refinement of the aaRS specificities, once the proteome as a whole had emerged from a simpler alphabet.

Although the evidence implies that we can infer the modular outlines of evolutionary succession from the structural hierarchies, the assembly of contemporary enzymes from these reconstructed ancestral modules necessarily involved overwriting some details that therefore remain speculative. Our view is that the clearest guides to the actual ancestry remains experimental characterization of the functionality of modules clearly related by phylogenetic methods to contemporary proteins, and that the ability now to investigate the experimental recapitulation of intermodular interactions, both *in cis* and *in trans*, along lines developed with the TrpRS (Li and Carter 2013) and HisRS (Li et al. 2011) Urzymes remains a key direction for further research, including both the assembly of Urzymes from protozymes and the other modules present in the Urzymes (Pham et al. 2007) and the assembly of modern aaRS from Urzymes in the presence of homologs of CP1, the Class II insertion domains, and the anticodon-binding domains of both classes.

Recent work appears to be moving toward a consensus consistent with our view. In particular, Caetano-Anolles (Caetano-Anollés and Caetano-Anollés 2016) now recognizes that the P-loop hydrolase domain genes are among the more ancient genes, without acknowledging that the Class I protozyme appears to be a reasonable ancestral form, not only of the Class I synthetases, but also of the P-loop hydrolases themselves.

Was Specific Aminoacylation of tRNA Originally Catalyzed by Ribozymes? The aaRS protozymes appear to be efficient catalysts of amino acid activation. It remains, among other things to be tested, to characterize their amino acid preferences. More important, however, is to determine whether or not they can also accelerate the transfer of activated amino acids to tRNA. The Class I protozyme lacks even the rudiments of a surface with which to bind the tRNA acceptor stem, whereas the Class II protozyme does retain such rudiments. Thus, it is possible that the ancestral protozymes were not entirely symmetrical in their catalytic repertoire, and that the Class II protozyme may have been uniquely able to acylate the tRNA acceptor stem. In any case, it appears that it is much more straightforward to use Selex procedures to isolate RNA aptamers that use activated amino acids to acylate tRNA than it is to find comparable aptamers capable of activating amino acids by reaction with ATP (Niwa et al. 2009; Suga et al. 1998). Thus, it is both conceivable and worth testing whether or not if accompanied by protozymes, such aptamers might have accelerated tRNA acylation from amino acids and ATP.

How Simple an Amino Acid Alphabet Can Still Support an Active Bi-directional Protozyme Gene? Answers to this question appear to be fundamental to understanding the origins of genetic coding. Fortunately, the wherewithal to answer it appears to be in place. The middle codon-base pairing metric of bi-directional coding appears to show sufficient variation between pairs of Class I and II aaRS Ur-genes (Figs. 9 and 10) to support a semi-quantitative map of bifurcations that best account for the order in which the amino acids were assimilated into the growing genetic code (Chandrasekaran et al. 2013), (Chandrasekaran, personal communication). The BEAST computer program has been adapted to utilize transition probability matrices of decreasing order, consistent with identifying nodes in the elaboration of the code (Markowitz et al. 2006), (Wills, personal communication). The multistate algorithm by which Rosetta imposes gene complementarity can be modified for testing models of code development by generating bi-directional protozyme genes whose catalytic activities can then be compared. These tools will become even more useful if and when it becomes possible to design a *bona fide* Ur-gene having all three of the modules identified originally by Pham et al. (2007).

How Did Cognate tRNAs Evolve to Distinguish Between the Two aaRS Classes? This question appears to pose a much more difficult problem. The aaRS class distinction was straightforward to identify from the initial observation of a group of aaRSs that lacked the HIGH and KMSKS catalytic signatures characteristic of all aaRS sequences available at that time (Eriani et al. 1990a, b). Notwithstanding the evidence accumulated to date from a much larger tRNA research community, it is not yet possible to identify sequence signatures—outside the identity elements that define the amino acid specificities of the synthetases—that differentiate the recognition by one or the other synthetase Class. Thus, whereas it is possible in principle, even in the face of horizontal gene transfer (Ardell and Andersson 2006), to attempt to establish a tree along which the aaRS genes radiated to enlarge the amino acid alphabet, no such exercise appears possible yet for their cognate tRNAs. It is possible that the approaches used by Caetano-Anollès (Caetano-Anollés and Caetano-Anollés 2016) are capable of identifying appropriate patterns in the tRNA multiple sequence

alignments, but thus far, that does not appear to have been a goal. Thus, a full understanding of the "tree" of amino acid acylation to tRNA in the emergence of translation, even in principle, appears still to lie ahead.

Acknowledgments Research from the Carter laboratory was supported by the National Institutes of General Medical Sciences, GM 78228 and GM40906. I am grateful for the comments of an anonymous referee, and for similar input from E. First.

Conflict of Interest The author is unaware of any conflicts of interest.

References

Amyes TL, Richard JP (2013) Specificity in transition state binding: the Pauling model revisited. Biochemistry 52:2021–2035. doi:10.1021/bi301491r

Andreini C, Bertini I, Cavallaro G, Holliday GL, Thornton JM (2008) Metal ions in biological catalysis: from enzyme databases to general principles. J Biol Inorg Chem 13:1205–1218. doi:10.1007/s00775-008-0404-5

Anton SP, Gulen B, Norris AM, Kovacs NA, Bernier CR, Lanier KA, Fox GE, Harvey SC, Wartell RM, Hud NV, Williams LD (2015) History of the ribosome and the origin of translation. PNAS 112(50):15396–15401

Aravind L, Leipe DD, Koonin EV (1998) Toprim—a conserved catalytic domain in type IA and II topoisomerases, DnaG-type primases, OLD family nucleases and RecR proteins. Nucleic Acids Res 26 (18):4205–4213

Aravind L, Anantharaman V, Koonin EV (2002) Monophyly of class I aminoacyl tRNA synthetase, USPA, ETFP, photolyase, and PP-ATPase nucleotide-binding domains: implication for protein evolution in the RNA world. Proteins Struct Funct Genet 48:1–14

Ardell DH, Andersson SGE (2006) TFAM detects co-evolution of tRNA identity rules with lateral transfer of histidyl-tRNA synthetase. Nucleic Acids Res 34 (3):893–904. doi:10.1093/nar/gkj449

Attwater J, Wochner A, Holliger P (2013, December) In-ice evolution of RNA polymerase ribozyme activity. Nat Chem 5:1101–1018. doi:10.1038/NCHEM.1781

Augustine J, Francklyn C (1997) Design of an active fragment of a class II aminoacyl-tRNA synthetase and its significance for synthetase evolution. Biochemistry 36:3473–3482

Baker D (2000, May 4) A surprising simplicity to protein folding. Nature 405:39–42

Benner SA, Ellington AD, Tauer A (1989, September) Modern metabolism as a palimpsest of the RNA world. Proc Nati Acad Sci USA 86:7054–7058

Benner SA, Sassi SO, Gaucher EA (2007) Molecular paleoscience: systems biology from the past. Adv Enzymol Relat Areas Mol Biol 75:9–140

Bernhardt HS (2012) The RNA world hypothesis: the worst theory of the early evolution of life (except for all the others). Biol Direct 7:23

Bowman JC, Hud NV, Williams LD (2015) The ribosome challenge to the RNA world. J Mol Evol 80:143–161. doi:10.1007/s00239-015-9669-9

Breaker RR (2012) Riboswitches and the RNA world. Cold Spring Harb Perspect Biol 4:a003566. doi:10.1101/cshperspect.a003566

Bridgham JT, Carroll SM, Thornton JW (2006) Evolution of hormone-receptor complexity by molecular exploitation. Science 312(7):97–101

Bridgham JT, Ortlund EA, Thornton JW (2009) An epistatic ratchet constrains the direction of glucocorticoid receptor evolution. Nature 461:515–519

Budiman M, Knaggs MH, Fetrow JS, Alexander RW (2007) Using molecular dynamics to map interaction networks in an aminoacyl-tRNA synthetase. Prot Struct Funct Bioinf 68:670–689

Buehner M, Ford GC, Moras D, Olsen KW, Rossmann MG (1973) D-Glyceraldehyde 3-phosphate Dehydrogenase: three dimensional structure and evolutionary significance. Proc Nat Acad Sci USA 70:3052–3054

Burbaum J, Schimmel P (1991) Structural relationships and the classification of aminoacyl-tRNA synthetases. J Biol Chem 266(26):16965–16968

Caetano-Anollés G (2015) Ancestral insertions and expansions of rRNA do not support an origin of the ribosome in its peptidyl transferase center. J Mol Evol 80:162–165. doi:10.1007/s00239-015-9677-9

Caetano-Anollés D, Caetano-Anollés G (2016) Piecemeal buildup of the genetic code, ribosomes, and genomes from primordial tRNA building blocks. Lifestyles 6:43. doi:10.3390/life6040043

Caetano-Anolles G, Kim HS, Mittenthal JE (2007) The origin of modern metabolic networks inferred from phylogenomic analysis of protein architecture. Proc Nat Acad Sci USA 104(22):9358–9363. doi:10.1073 pnas.0701214104

Caetano-Anollés G, Wang M, Caetano-Anollés D (2013) Structural phylogenomics retrodicts the origin of the genetic code and uncovers the evolutionary impact of protein flexibility. PLoS One 8(8):e72225. doi:10.1371/journal.pone.0072225

Cammer S, Carter CW Jr (2010) Six rossmannoid folds, including the class I aminoacyl-tRNA synthetases, share a partial core with the anticodon-binding domain of a class II aminoacyl-tRNA synthetase. Bioinformatics 26(6):709–714. doi:10.1093/bioinformatics/btq039

Carter CW Jr (1975, March) Cradles for molecular evolution. New Sci 27:784–787

Carter CW Jr (2014) Urzymology: experimental access to a key transition in the appearance of enzymes. J Biol Chem 289(44):30213–30220. doi:10.1047/jbcR114.576495

Carter CW Jr (2015) What RNA world? Why a peptide/RNA partnership merits renewed experimental attention. Lifestyles 5:294–320. doi:10.3390/life5010294

Carter CW Jr (2017) High-dimensional mutant and modular thermodynamic cycles, molecular switching, and free energy transduction. Annu Rev Biophys 46:433–453. doi:10.1146/annurev-biophys-070816-033811

Carter CW Jr, Duax WL (2002) Did tRNA synthetase classes arise on opposite strands of the same gene? Mol Cell 10:705–708

Carter CW Jr, Kraut J (1974) A proposed model for interaction of polypeptides with RNA. Proc Nat Acad Sci USA 71(2):283–287

Carter CW Jr, Wills PR (2017) Interdependence, reflexivity, fidelity, and impedance matching: the need for an alternative to the RNA world. BioRxiv. doi:10.1101/139139

Carter CW, Jr., Wolfenden R (2015) tRNA acceptor-stem and anticodon bases form independent codes related to protein folding. Proc Nat Acad Sci USA 112 (24):7489–7494. doi:http://www.pnas.org/cgi/doi/10.1073/pnas.1507569112

Carter CW Jr, Wolfenden R (2016) Acceptor-stem and anticodon bases embed amino acid chemistry into tRNA. RNA Biol 13(2):145–151. doi:10.1080/15476286.2015.1112488

Carter CW Jr, Li L, Weinreb V, Collier M, Gonzales-Rivera K, Jimenez-Rodriguez M, Erdogan O, Chandrasekharan SN (2014) The Rodin-Ohno hypothesis that two enzyme superfamilies descended from one ancestral gene: an unlikely scenario for the origins of translation that will not be dismissed. Biol Direct 9:11

Carter J, Charles W., Chandrasekaran SN, Weinreb V, Li L, Williams T 2016 Combining multi-mutant and modular thermodynamic cycles to measure energetic coupling networks in enzyme catalysis. In: Pearson A, Benedict J (eds) Structural dynamics, American Crystallographic Association annual meeting, 2016. American Crystallographic Association

Carter CW Jr, Chandrasekaran SN, Weinreb V, Li L, Williams T (2017) Combining multi-mutant and modular thermodynamic cycles to measure energetic coupling networks in enzyme catalysis. Struct Dyn 4:032101

Chandrasekaran SN, Carter CWJ (2017) Adding torsional interaction terms to the anisotropic network model improves the PATH performance, enabling detailed comparison with experimental rate data. Struct Dyn 4:032103

Chandrasekaran SN, Yardimci G, Erdogan O, Roach JM, Carter CW, Jr (2013) Statistical evaluation of the Rodin-Ohno hypothesis: sense/antisense coding of ancestral class I and II aminoacyl-tRNA synthetases. Mol Biol Evol 30(7):1588–1604. doi:10.1093/molbev/mst070

Chandrasekaran SN, Das J, Dokholyan NV, Carter CW Jr (2016) A modified PATH algorithm rapidly generates transition states comparable to those found by other well established algorithms. Struct Dyn 3:012101. doi:10.1063/1.4941599

Chuang W-J, Abeygunawardana C, Pedersen PL, Mildvan AS (1992a) Two-dimensional NMR, circular dichroism, and fluorescence studies of PP-50, a synthetic ATP-binding peptide from the b-subunit of mitochondrial ATP synthase. Biochemist 31:7915–7921

Chuang W-J, Abeygunawardana C, Gittis AG, Pedersen PL, Mildvan AS (1992b) Solution structure and function in trifluoroethanol of PP-50, an ATP-binding peptide from F_1ATPase. Arch Biochem Biophys 319 (1 May 10):110–122

Crick FHC (1966) Codon-anticodon pairing: the wobble hypothesis. J Mol Biol 19:548–555

Cusack S (1993) Sequence, structure and evolutionary relationships between class 2 aminoacyl-tRNA synthetases: an update. Biochimie 75:1077–1081

Cusack S (1994) Evolutionary implications. Nat Struct Mol Biol 1:760

Cusack S (1995) Eleven down and nine to go. Nat Struct Biol 2:824–831

Cusack S, Berthet-Colominas C, Härtlein M, Nassar N, Leberman R (1990) A second class of synthetase structure revealed by X-ray analysis of *Escherichia coli* seryl-tRNA synthetase at 2.5 Å. Nature 347 (6290):249–255

Cusack S, Härtlein M, Leberman R (1991) Sequence, structural and evolutionary relationships between class 2 aminoacyl-tRNA synthetases. Nucl Acid Res 109(13):3489–3498

Danchin A (2007) Archives or palimpsests? Bacterial genomes unveil a scenario for the origin of life. Biol Theor 2(1):1–10

Dantas G, Kuhlman B, Callender D, Wong M, Baker D (2003) A large scale test of computational protein design: folding and stability of nine completely redesigned globular proteins. J Mol Biol 332 (2):449–460

Dean AM, Thornton JW (2007) Mechanistic approaches to the study of evolution: the functional synthesis. Nat Rev Genet 8(September):675

Delarue M (2007) An asymmetric underlying rule in the assignment of codons: possible clue to a quick early evolution of the genetic code via successive binary choices. RNA 13:1–9

Delarue M, Moras D (1992) Aminoacyl-tRNA synthetases: partition into two classes. In: Eckstein F, Lilley DMJ (eds) Nucleic acids and molecular biology, vol 6. Springer, Berlin/Heidelberg, pp 203–224

Dennett DC (1995) Darwin's dangerous idea: evolution and the meanings of life. Simon and Schuster, New York

Dill KA, MacCallum JL (2012) The protein-folding problem, 50 years on. Science 338:1042–1046

Duax WL, Huether R, Pletnev V, Langs D, Addlagatta A, Connare S, Habegger L, Gill J (2005) Rational genomes: antisense open reading frames and codon bias in short chain oxido reductase enzymes and the evolution of the genetic code. Prot Struct Funct Bioinf 61:900–906

Eigen M (1971) Selforganization of matter and the evolution of biological macromolecules. Naturwissenschaften 58:465–523

Eigen M, Schuster P (1977) The hypercyde: a principle of natural self-organization part a: emergence of the hypercycle. Naturwissenschaften 64:541–565

Eigen M, McCaskill JS, Schuster P (1988) Molecular quasi-species. J Phys Chem 92:6881–6891

Eriani G, Delarue M, Poch O, Gangloff J, Moras D (1990a) Partition of tRNA synthetases into two classed based on mutually exclusive sets of sequence motifs. Nature 347(9):203–206

Eriani G, Dirheimer G, Gangloff J (1990b) Aspartyl-tRNA synthetase from *Escherichia coli*: cloning and characterisation of the gene, homologies of its translated amino acid sequence with asparaginyl- and lysyl-tRNA synthetases. Nucleic Acids Res 18:7109–7117

Farrow MA, Nordin BE, Schimmel P (1999) Nucleotide determinants for tRNA-dependent amino acid discrimination by a Class I tRNA synthetase. Biochemistry 38:16898–16903

Fersht AR (1999) Structure and mechanism in protein science. W. H. Freeman and Company, New York

Fersht AR (2000) Transition-state structure as a unifying basis in protein-folding mechanisms: contact order, chain topology, stability, and the extended nucleus mechanism. Proc Nat Acad Sci USA 97(4):1525–1529

Fersht AR, Ashford JS, Bruton CJ, Jakes R, Koch GLE, Hartley BS (1975) Active site titration and aminoacyl adenylate binding stoichiometry of amionacyl-tRNA synthetases. Biochemist 14(1):1–4

Fournier GP, Alm EJ (2015) Ancestral reconstruction of a pre-LUCA aminoacyl-tRNA synthetase ancestor supports the late addition of Trp to the genetic code. J Mol Evol 80:171–185. doi:10.1007/s00239-015-9672-1

Fournier GP, Andam CP, Alm EJ, Gogarten JP (2011) Molecular evolution of aminoacyl tRNA synthetase proteins in the early history of life. Orig Life Evol Biosph 41:621–632

Francklyn C, Schimmel P (1989, February 2) Aminoacylation of RNA Minihelices with Alanine. Nature 337:478–481

Francklyn C, Schimmel P (1990, November) Enzymatic aminoacylation of an eight-base-pair microhelix with histidine. Proc Nati Acad Sci USA 87:8655–8659

Francklyn C, Musier-Forsyth K, Schimmel P (1992) Small RNA helices as substrates for aminoacylation and their relationship to charging of transfer RNAs. Eur J Biochem 206:315–321

Francklyn CS, First EA, Perona JJ, Hou Y-M (2008) Methods for kinetic and thermodynamic analysis of aminoacyl-tRNA synthetases. Methods 44:100–118

Freeland SJ, Hurst LD (1998) The genetic code is one in a million. J Mol Evol 47:238–248

Fry DC, Kuby SA, Mildvan AS (1985) NMR studies of the MgATP binding site of adenylate kinase and of a 45-residue peptide fragment of the enzyme. Biochemistry 24:4680–4694

Fry DC, Byler DM, Sisu H, Brown EM, Kuby SA, Mildvan AS (1988) Solution structure of the 45-residue MgATP-binding peptide of adenylate kinase as examined by 2-D NMR, FTIR, and CD spectroscopy. Biochemistry 27:3588–3598

Füchslin RM, McCaskill JS (2001) Evolutionary self-organization of cell-free genetic coding. Proc Natl Acad Sci USA 98:9185–9190

Gaucher EA, Govindarajan S, Ganesh OK (2008) Palaeotemperature trend for precambrian life inferred from resurrected proteins. Nature 451 (Feb 7):704–707

Gibbs PR, Radzicka A, Wolfenden R (1991) The anomalous hydrophilic character of proline. J Am Chem Soc 113:4714–4715

Giegé R, Sissler M, Florentz C (1998) Universal rules and idiosyncratic features in tRNA identity. Nucleic Acids Res 26(22):5017–5035

Gilbert W (1986) The RNA world. Nature 319:618

Guo M, Schimmel P (2013, March) Essential nontranslational functions of tRNA synthetases. Nat Chem Biol 9:145–153

Guo M, Yang X-L, Schimmel P (2010, September) New functions of aminoacyl-tRNA synthetases beyond translation. Nat Rev Mol Cell Biol 11:668–674

Hanson-Smith V, Kolaczkowski B, Thornton JW (2010) Robustness of ancestral sequence reconstruction to phylogenetic uncertainty. Mol Biol Evol 27 (9):1988–1999

Harish A, Caetano-Anollés G (2012) Ribosomal history reveals origins of modern protein synthesis. PLoS One 7(3):e32776. doi:10.1371/journal.pone.0032776

Härtlein M, Cusack S (1995) Structure, function and evolution of Seryl-tRNA synthetases: implications for the evolution of aminoacyl-tRNA synthetases and the genetic code. J Mol Evol 40:519–530

Henderson BS, Schimmel P (1997) RNA-RNA interactions between oligonucleotide substrates for aminoacylation. Bioorg Med Chem 5(6):1071–1079

Hofstadter DR (1979) Gödel, Escher, Bach: an eternal golden braid. Basic Books, Inc, New York

Hol WJG, van Duijnen PT, Berensen HJC (1978) The α-helix dipole and the properties of proteins. Nature 273:443–446

Horning DP, Joyce GF (2016) Amplification of RNA by an RNA polymerase ribozyme. Proc Nat Acad Sci USA 113(35):9786–9791

Hu H (2014) Wild-type and molten globular chorismate mutase achieve comparable catalytic rates using very different enthalpy/entropy compensations. Sci China 57(1):156–164. doi:10.1007/s11426-013-5021-7

Ibba M, Soll D (2004) Aminoacyl-tRNAs: setting the limits of the genetic code. Genes Dev 18:731–738

Ibba M, Francklyn C, Cusack S (2005) Aminoacyl-tRNA synthetases. MBIU, Landesbioscience, Georgetown

Johnson BR, Lam SK (2010) Self-organization, natural selection, and evolution: cellular hardwareand genetic software. Bioscience 60:879–885. doi:10.1525/bio.2010.60.11.4

Kamtekar S, Schiffer JM, Xiong H, Babik JM, Hecht MH (1993) Protein design by binary patterning of polar and non-polar amino acids. Science 262:1680–1685

Kapustina M, Carter CW Jr (2006) Computational studies of tryptophanyl-tRNA synthetase ligand binding and conformational stability. J Mol Biol 362:1159–1180

Kapustina M, Hermans J, Carter CW Jr (2006) Potential of mean force estimation of the relative magnitude of the effect of errors in molecular mechanics approximations. J Mol Biol 362:1177–1180

Kapustina M, Weinreb V, Li L, Kuhlman B, Carter CW Jr (2007) A conformational transition state accompanies tryptophan activation by *B. stearothermphilus* tryptophanyl-tRNA synthetase. Structure 15:1272–1284

Kirby AJ, Younas M (1970) The reactivity of phosphate esters. Reactions of diesters with nucleophiles. J Chem Soc B 418:1165–1172

Klipcan L, Safro M (2004) Amino acid biogenesis, evolution of the genetic code and aminoacyl-tRNA synthetases. J Theor Biol 228:389–396

Koonin EV (2011) The logic of chance: the nature and origin of biological evolution. Pearson Education/FT Press Science, Upper Saddle River

Koonin EV, Novozhilov AS (2009) Origin and evolution of the genetic code: the Universal Enigma. IUBMB Life 61(2):99–111. doi:10.1002/iub.146

Küippers B (1979) Towards an experimental analysis of molecular self-organization and precellular Darwinian evolution. Naturwissenschaften 66:228–243

Leaver-Fay A, Jacak R, Stranges PB, Kuhlman B (2011) A generic program for multistate protein design. PLoS One 6(7):e20937

Leipe DD, Wolf YI, Koonin EV, Aravind L (2002) Classification and evolution of P-loop GTPases and related ATPases. J Mol Biol 317:41–72

LéJohn HB, Cameron LE, Yang B, MacBeath G, Barker DS, Willams SA (1994a, February 11) Cloning and analysis of a constitutive heat shock (cognate) protein 70 gene inducible by L-glutamine. J Biol Chem 269:4513–4522

LéJohn HB, Cameron LE, Yang B, Rennie SL (1994b, February 11) Molecular characterization of an NAD-specific glutamate dehydrogenase gene inducible by L-glutamine: antisense gene pair arrangement with L-glutamine-inducible heat shock 70-like protein gene. J Biol Chem 269:4523–4531

Li L, Carter CW, Jr (2013) Full implementation of the genetic code by tryptophanyl-tRNA synthetase requires intermodular coupling. J biol Chem 288:34736–34745. doi:10.1074/jbc.M113.510958

Li L, Weinreb V, Francklyn C, Carter CW Jr (2011) Histidyl-tRNA synthetase urzymes: class I and II aminoacyl-tRNA synthetase urzymes have comparable catalytic activities for cognate amino acid activation. J Biol Chem 286:10387–10395. doi:10.1074/jbc.M110.198929

Li L, Francklyn C, Carter CW Jr (2013) Aminoacylating urzymes challenge the RNA world hypothesis. J Biol Chem 288:26856–26863. doi:10.1074/jbc.M113.496125

Li R, Macnamara LM, Leuchter JD, Alexander RW, Cho SS (2015) MD simulations of tRNA and aminoacyl-tRNA synthetases: dynamics, folding, binding, and allostery. Int J Mol Sci 16:15872–15902. doi:10.3390/ijms160715872

Linderstrøm-Lang KU (1952) The lane medical lectures. Stanford University Press, Stanford

Markowitz S, Drummond A, Nieselt K, Wills PR (2006) Simulation model of prebiotic evolution of genetic coding. In: Rocha LM, Yaeger LS, Bedau MA, Floreano D, Goldstone RL, Vespignani A (eds) Artificial Life, vol 10. MIT Press, Cambridge, MA, pp 152–157

Martinez L, Jimenez-Rodriguez M, Gonzalez-Rivera K, Williams T, Li L, Weinreb V, Niranj Chandrasekaran S, Collier M, Ambroggio X, Kuhlman B, Erdogan O, Carter CWJ (2015) Functional class I and II amino acid activating enzymes can be coded by opposite strands of the same gene. J Biol Chem 290(32):19710–19725. doi:10.1074/jbc.M115.642876

Moelbert S, Emberly E, Tang C (2004) Correlation between sequence hydrophobicity and surface-exposure pattern of database proteins. Protein Sci 13:752–762

Moffet DA, Foley J, Hecht MH (2003) Midpoint reduction potentials and heme binding stoichiometries of de novo proteins from designed combinatorial libraries. Biophys Chem 105:231–239

Mullen GP, Vaughn JB, Jr., Mildvan AS (1993) Sequential proton NMR resonance assignments, circular dichroism, and structural properties of a 50-residue substrate-binding peptide from DNA polymerase I. Arch Biochem Biophys 301(1 February 15):174–183

Niwa N, Yamagishi Y, Murakami H, Suga H (2009) A flexizyme that selectively charges amino acids activated by a water-friendly leaving group. Bioorg Med Chem Lett 19:3892–3894

Noller H (2004) The driving force for molecular evolution of translation. RNA 10:1833–1837

Noller HF, Hoffarth V, Zimniak L (1992, June 5) Unusual resistance of peptidyl transferase to protein extraction procedures. Science 256:1416–1419

O'Donoghue P, Luthey-Schulten Z (2003) On the evolution of structure in aminoacyl-tRNA synthetases. Microbiol Mol Biol Rev 67(4):550–573

Orgel LE (1963) The maintenance of the accuracy of protein synthesis and its relevance to ageing. Proc Nat Acad Sci USA 49:517–521

Ortlund EA, Bridgham JT, Redinbo MR, Thornton JW (2007) Crystal structure of an ancient protein:

evolution by conformational epistasis. Science 317:1544–1548
Patel SC, Bradley LH, Jinadasa SP, Hecht MH (2009) Cofactor binding and enzymatic activity in an unevolved superfamily of de novo designed 4-helix bundle proteins. Protein Sci 18:1388–1400
Perona JJ, Gruic-Sovulj I (2013) Synthetic and editing mechanisms of aminoacyl-tRNA synthetases. Top Curr Chem. doi:10.1007/128_2013_456
Pervushin K, Vamvaca K, Vogeli B, Hilvert D (2007) Structure and dynamics of a molten globular enzyme. Nat Struct Mol Biol 14(December):1202–1206
Petrov AS, Williams LD (2015) The ancient heart of the ribosomal large subunit: a response to Caetano-Anolles. J Mol Evol 80:166–170. doi:10.1007/s00239-015-9678-8
Petrov AS, Bernier CR, Hsiao C, Norris AM, Kovacs NA, Waterbury CC, Stepanov VG, Harvey SC, Fox GE, Wartell RM, Hud NV, Williams LD (2014) Evolution of the ribosome at atomic resolution. Proc Nat Acad Sci USA 111(28):10251–10256
Pham Y, Li L, Kim A, Erdogan O, Weinreb V, Butterfoss G, Kuhlman B, Carter CW Jr (2007) A minimal TrpRS catalytic domain supports sense/antisense ancestry of class I and II aminoacyl-tRNA synthetases. Mol Cell 25:851–862
Pham Y, Kuhlman B, Butterfoss GL, Hu H, Weinreb V, Carter CW Jr (2010) Tryptophanyl-tRNA synthetase urzyme: a model to recapitulate molecular evolution and investigate intramolecular complementation. J Biol Chem 285:38590–38601. doi:10.1074/jbc.M110.136911
Radzicka A, Wolfenden R (1988) Comparing the polarities of the amino acids: side-chain distribution coefficients between the vapor phase, cyclohexane, 1-0ctanol, and neutral aqueous solution. Biochemistry 27(5):1664–1670
Ribas de Pouplana L, Schimmel P (2001a) Two classes of tRNA synthetases suggested by sterically compatible dockings on tRNA acceptor stem. Cell 104:191–193
Ribas de Pouplana L, Schimmel P (2001b) Operational RNA code for amino acids in relation to genetic code in evolution. J Biol Chem 276:6881–6884
Ribas de Pouplana L, Schimmel P (2001c) Aminoacyl-tRNA synthetases: potential markers of genetic code development. TIBS 26(10):591–596
Robertson MP, Joyce GF (2012) The origins of the RNA world. Cold Spring Harb Perspect Biol 4:a003608. doi:10.1101/cshperspect.a003608
Rodin SN, Ohno S (1995) Two types of aminoacyl-tRNA synthetases could be originally encoded by complementary strands of the same nucleic acid. Orig Life Evol Biosph 25:565–589
Rodin SN, Rodin A (2006a) Partitioning of aminoacyl-tRNA synthetases in two classes could have been encoded in a strand-symmetric RNA world. DNA Cell Biol 25:617–626
Rodin SN, Rodin A (2006b) Origin of the genetic code: first aminoacyl-tRNA synthetases could replace isofunctional ribozymes when only the second base of codons was established. DNA Cell Biol 25:365–375
Rodin SN, Rodin AS (2008) On the origin of the genetic code: signatures of its primordial complementarity in tRNAs and aminoacyl-tRNA synthetases. Heredity 100:341–355
Rodin A, Rodin SN, Carter CW Jr (2009) On primordial sense-antisense coding. J Mol Evol 69:555–567
Rodin AS, Szathmáry E, Rodin SN (2011) On origin of genetic code and tRNA before translation. Biol Direct 6:14
Safro M, Klipcan L (2013) The mechanistic and evolutionary aspects of the 2′- and 3′-OH paradigm in biosynthetic machinery. Biol Direct 8:17
Sapienza PJ, Li L, Williams T, Lee AL, Carter CW Jr (2016) An ancestral tryptophanyl-tRNA synthetase precursor achieves high catalytic rate enhancement without ordered ground-state tertiary structures. ACS Chem Biol 11:1661–1668. doi:10.1021/acschembio.5b01011
SAS (2015) JMP: the statistical discovery software, 10 edn. SAS Institute, Cary
Schimmel P (1991) Classes of aminoacyl-tRNA synthetases and the establishment of the genetic code. Trend Biol Sci 16(1):1–3
Schimmel P (1996) Origin of genetic code: a needle in the haystack of tRNA sequences. Proc Nat Acad Sci USA 93:4521–4522
Schimmel P, Ribas de Pouplana L (2000) Footprints of aminoacyl-tRNA synthetases are everywhere. TIBS 25(5):207–209
Schimmel P, Giegé R, Moras D, Yokoyama S (1993) An operational RNA code for amino acids and possible relationship to genetic code. Proc Nat Acad Sci USA 90:8763–8768
Schroeder GK, Wolfenden R (2007) The rate enhancement produced by the ribosome: an improved model. Biochemist 46:4037–4044
Sczepanski JT, Joyce GF (2014) A cross-chiral RNA polymerase ribozyme. Nature 515:440–442. doi:10.1038/nature13900
Shepherd J, Ibba M (2014) Relaxed substrate specificity leads to extensive tRNA mischarging by streptococcus pneumoniae class I and class II aminoacyl-tRNA synthetases. mBio 5 (5):e01656–e01614. doi:10.1128/mBio.01656-14
Sherlin LD, Perona JJ (2003, May) tRNA-dependent active site assembly in a class I aminoacyl-tRNA synthetase. Structure 11:591–603. doi:10.1016/S0969-2126(03)00074-1
Sievers A, Beringer M, Rodnina MV, Wolfenden R (2004) The ribosome as an entropy trap. Proc Nat Acad Sci USA 101:7897–7901
Silvert M, Simonson T (2016) Creation and analysis of an algorithm creating overlapping genes. Laboratoire de Biochimie – École Polytechnique, Palaiseau
Smith TF, Hartman H (2015) The evolution of class II aminoacyl-tRNA synthetases and the first code. FEBS Lett 589(23):3499–3507

Soucy SM, Huang J, Gogarten JP (2015, August) Horizontal gene transfer: building the web of life. Nat Rev Gen 16:472

Stackhouse J, Presnell SR, McGeehan GM, Nambiar KP, Benner SA (1990) The ribonuclease from an extinct bovid ruminant. FEBS Lett 262(1):104–106

Steitz TA, Steitz JA (1993) A general two-metal-ion mechanism for catalytic RNA. Proc Natl Acad Sci U S A 90(July):6498–6502

Suga H, Lohse PA, Szostak JW (1998) Structural and kinetic characterization of an acyl transferase ribozyme. J Am Chem Soc 120:1151–1156

Sun F-J, Caetano-Anollés G (2008) Evolutionary patterns in the sequence and structure of transfer RNA: a window into early translation and the genetic code. Plos One 3 (7):e2799

Taylor AI, Pinheiro VB, Smola MJ, Morgunov AS, Peak-Chew S, Cozens C, Weeks KM, Herdewijn P, Holliger P (2015) Catalysts from synthetic genetic polymers. Nature 518:427–430

Thornton JW (2004, May) Resurrecting ancient genes: experimental analysis of extinct molecules. Nat Rev Genet 5:366–375

Thornton JW, Need E, Crews D (2003) Resurrecting the ancestral steroid receptor: ancient origin of estrogen signaling. Science 301:714–1717

Tuerck C, Gold L (1990) Systematic evolution of ligands by exponential enrichment: RNA ligands to bacteriophage T7 DNA polymerase. Science 249:505–510

Uter NT, Gruic-Sovulj I, Perona JJ (2005) Amino acid-dependent transfer RNA affinity in a class I aminoacyl-tRNA synthetase. J Biol Chem 280 (25):23966–23977. doi:10.1074/jbc.M414259200

Van Noorden R (2009, May 13) RNA world easier to make. Nature published online. doi:10.1038/news.2009.471

Vestigian K, Woese CR, Goldenfeld N (2006) Collective evolution and the genetic code. Proc Nat Acad Sci USA 103:10696–10701

Weinreb V, Carter CW Jr (2008) Mg^{2+}-free *B. stearothermophilus* tryptophanyl-tRNA synthetase activates tryptophan with a major fraction of the overall rate enhancement. J Am Chem Soc 130:1488–1494

Weinreb V, Li L, Kaguni LS, Campbell CL, Carter CW Jr (2009, July 15) Mg2+−assisted catalysis by B. stearothermophilus TrpRS is promoted by allosteric effects. Structure 17:1–13

Weinreb V, Li L, Carter CW, Jr. (2012) A master switch couples Mg^{2+}-assisted catalysis to domain motion in B. stearothermophilus tryptophanyl-tRNA synthetase. Structure 20

Weinreb V, Li L, Chandrasekaran SN, Koehl P, Delarue M, Carter CW Jr (2014) Enhanced amino acid selection in fully-evolved tryptophanyl-tRNA synthetase, relative to its urzyme, requires domain movement sensed by the D1 switch, a remote. Dynamic Packing Motif J Biol Chem 289:4367–4376. doi:10.1074/jbc.M113.538660

Wills PR (1993) Self-organization of genetic coding. J Theor Biol 162:267–287

Wills PR (2004) Stepwise evolution of molecular biological coding. In: Pollack J, Bedau M, Husbands P, Ikegami T, Watson RA (eds) Artificial life IX. MIT Press, Cambridge, pp 51–56

Wills PR (2016) The generation of meaningful information in molecular systems. Phil Trans R Soc A A374:20150016. doi:10.1098/rsta.20150066

Wills PR, Carter CW Jr (2017) Insuperable problems of an initial genetic code emerging from an RNA world. BioRxiv. doi:10.1101/140657

Wills PR, Nieselt K, McCaskill JS (2015) Emergence of coding and its specificity as a physico-informatic problem. Orig Life Evol Biosph published online; pagination not yet available. doi:10.1007/s11084-015-9434-5

Wochner A, Attwater J, Coulson A, Holliger P (2011, April 8) Ribozyme-catalyzed transcription of an active ribozyme. Science 332:209–212

Woese C (1967) The genetic code. Harper & Row, New York

Woese C (1969) Models for the evolution of codon assignments. J Mol Biol 43:235–240

Woese CR, Dugre DH, Saxinger WC, Dugre SA (1966) The molecular basis for the genetic code. Proc Natl Acad Sci U S A 55:966–974

Woese CR, Olsen GJ, Ibba M, Soll D (2000) Aminoacyl-tRNA synthetases, the genetic code, and the evolutionary process. Microbiol Mol Biol Rev 64 (1):202–236

Wolf YI, Koonin EV (2007) On the origin of the translation system and the genetic code in the RNA world by means of natural selection, exaptation, and subfunctionalization. Biol Direct 2:14

Wolf YI, Aravind L, Grishin NV, Koonin EV (1999) Evolution of aminoacyl-tRNA synthetases—analysis of unique domain architectures and phylogenetic trees reveals a complex history of horizontal gene transfer events. Genome Res 9:689–710

Wolfenden R (2007, May 5) Experimental measures of amino acid Hydrophobicity and the topology of Transmembrane and globular proteins. J Gen Physiol 129:357–362. doi:10.1085/jgp.200709743

Wolfenden R, Liang Y-L (1989) Contributions of solvent water to biological group-transfer potentials: mixed anyhydrides of phosphoric and carboxylic acids. Bioorg Chem 17:486–489

Wolfenden R, Cullis PM, Southgate CCF (1979a) Water, protein folding, and the genetic code. Science 206:575–577

Wolfenden R, Andersson L, Cullis PM, Southgate CCF (1979b) Affinities of amino acid side chains for solvent water. Biochemistry 20:849–855

Wolfenden R, Lewis CA, Yuan Y, Carter CW Jr (2015) Temperature dependence of amino acid hydrophobicities. Proc Nat Acad Sci USA 112 (24):7484–7488. doi:10.1073/pnas.1507565112

Yang B, LéJohn HB (1994, February 11) NADP +−activable, NAD+ −specific glutamate dehydrogenase purification and immunological analysis. J Biol Chem 269:4506–4512

Yang XL, Schimmel P, Ewalt KL (2004) Relationship of two human tRNA synthetases used in cell signaling. Trends Biochem Sci 29(5):250–256

Yang X-L, Guo M, Kapoor M, Ewalt KL, Otero FJ, Skene RJ, McRee DE, Schimmel P (2007) Functional and crystal structure analysis of active site adaptations of a potent anti-angiogenic human tRNA synthetase. Structure 15:793–805

Yarus M (2011a) Life from an RNA world: the ancestor within. Harvard University Press, Cambridge, MA

Yarus M (2011b) Getting past the RNA world: the initial Darwinian ancestor. Cold Spring Harb Perspect Biol 3:a003590. doi:10.1101/cshperspect.a003590

Yarus M, Widmann J, Knight R (2009) RNA-amino acid binding: a stereochemical era for the genetic code. J Mol Evol 69:406–429

Zhang C-M, Perona JJ, Ryu K, Francklyn C, Hou Y-M (2006) Distinct kinetic mechanisms of the two classes of aminoacyl-tRNA synthetases. J Mol Biol 361:300–311. doi:10.1016/j.jmb.2006.06.015

Zull JE, Smith SK (1990) Is genetic code redundancy related to retention of structural information in both DNA strands? TIBS 15:257–261

Adv Exp Med Biol - Protein Reviews (2017) 2:149–161
DOI 10.1007/5584_2017_62

Published online: 22 June 2017

Regulation of Nephrin Phosphorylation in Diabetes and Chronic Kidney Injury

Benoit Denhez and Pedro Geraldes

Abstract

Diabetes is the leading cause of microalbuminuria and end-stage renal failure in industrial countries. Disruption of the filtration barrier, seen in almost all nephrotic diseases and diabetes, is the result of the loss or effacement of the podocyte foot process, notably damage of proteins within the slit diaphragm such as nephrin. For many years, nephrin has been viewed as a structural component of the slit diaphragm. It is now well recognized that nephrin contains several tyrosine residues in its cytoplasmic domain, which influences the development of glomerular injury. In this review, we propose an overview of nephrin signaling pathways in kidney injury.

Keywords

Nephrin • Nephropathy phosphatases • Podocyte • SHP-1

Abbreviations

DN	diabetic nephropathy
FP	foot process
NF-B	nuclear factor-kappa B
LPS	lipopolysaccharides
PAN	puromycin aminonucleoside
PI3K	phosphatidylinositol 3-kinase
PS	protamin sulfate
SD	slit diaphragm
SHP-1	Src homology 2 domain phosphatase 1

B. Denhez and P. Geraldes (✉)
Research Center of the Centre Hospitalier Universitaire de Sherbrooke and Departments of Medicine, Division of Endocrinology, Université de Sherbrooke, 3001 12e Ave Nord, Sherbrooke, Québec J1H 5N4, Canada
e-mail: Pedro.Geraldes@USherbrooke.ca

People living with diabetes are at high risk of developing complications affecting both the macrovascular and microvascular systems. Complications of the large vessels include coronary artery diseases, atherosclerosis and peripheral arterial disease, while complications disturbing small vessels include neuropathy, retinopathy and nephropathy, the latter being the focus of this review. Diabetic nephropathy is the leading cause of end-stage renal disease in the world and is linked with both high economic cost and morbidity (Collins et al. 2007). Unfortunately, there are limited ways to prevent the progression of the disease, which can ultimately result in kidney failure. The two main contributors to the disease are chronic hyperglycemia and hypertension (The Writing Team for the Diabetes Control and Complications Trial/

Epidemiology of Diabetes Interventions and Complications Research Group 2002; Epstein and Sowers 1992).

1 Diabetic Nephropathy

The first clinical manifestation of diabetic nephropathy (DN) is albuminuria, which is defined by abnormal high levels of the protein albumin in the urine. At the early stage, patients with DN will exhibit elevated glomerular filtration rate. As the disease progress, albuminuria will rise and the glomerular filtration rate will decline. Eventually, DN will evolve to end-stage renal disease, with very low glomerular filtration rate levels (<15 mL/min/1.73m^2) in which dialysis or kidney transplant will be required to prevent death (Dronavalli et al. 2008). Histopathological studies from the kidney cortex revealed that one of the first structures affected by DN is the glomerulus. The glomerulus is composed of three main cell types (mesangial cells, endothelial cells and podocytes). Diabetes-induced glomerulus dysfunction is characterized by the expansion of the mesangium, extracellular matrix deposition, thickening of the basal membrane, and dedifferentiation and cell death of the podocytes. Loss of the podocytes is believed to be one of the strongest predictors of DN progression (Meyer et al. 1999). The importance of podocytes in preserving renal functions in DN was highlighted by morphometric observations from kidney biopsies of diabetic patients which showed a significant reduction in numbers of podocytes in patients with short duration of diabetes before the apparition of microalbuminuria or other markers of the disease (Meyer et al. 1999; Pagtalunan et al. 1997; White et al. 2002). It is clear now that the mechanisms of diabetes-induced complications of the glomerular dysfunction are very complex and involve crosstalk between the mesangial cells, the endothelial cells and the podocytes (Kriz et al. 1998; Siddiqi and Advani 2013; Schlondorff and Banas 2009). In this review, the focus will be on the podocytes.

2 The Podocytes

Podocytes are highly specialized epithelial cells found in the kidney glomerulus that participate in blood filtration by creating a physical barrier around the blood capillaries. They are composed of three distinct morphological structures: the cellular body, the main process and the foot process (FP). Main processes of the podocytes are cytoplasmic projections that emerge from their cellular body. They further divide into smaller projections called FP that create a zipper-like structure with another FP of the neighboring podocytes. This highly organized zipper-like structure is responsible for filtering molecules and proteins found in the blood by their molecular sizes (Pavenstädt et al. 2003; Karnovsky and Ryan 1975). The FP expresses various integrins, notably the α3β1 integrin, that anchors the podocyte to the glomerular basement membrane (Sachs and Sonnenberg 2013). The integrity of the podocyte FP is very dependent on a structure found between adjacent FP called the slit diaphragm (SD). The SD can be best described as a multiprotein complex that regulates podocyte homeostasis and function (Reiser et al. 2000a; Verma et al. 2016). The essential role of the SD on podocyte ability to filtrate the blood was highlighted in various kidney diseases. The most striking example is the mutation of the protein nephrin which causes the earliest and most severe nephrotic syndrome (Greka and Mundel 2012).

3 Nephrin

The discovery of nephrin in 1998 was made by identifying the genetic mutation responsible for the congenital nephrotic syndrome of the Finnish type (NPHS1), which is one of the most severe forms of nephrotic syndrome (Kestilä et al.

1998). This finding underlined the critical role of nephrin in the maturation and function of the glomerulus, and marked a new era in glomerular disease research. Nephrin is a transmembrane protein of the *immunoglobulin-like* family. Its extracellular domain is composed of 8 *igG-like* domains and a single *fibronectin type 3* domain. It was first believed that nephrin was only expressed in the kidney, but recent studies confirmed its expression in the pancreatic β-cells playing a role in glucose-stimulated insulin release and cell survival signaling (Fornoni et al. 2010; Kapodistria et al. 2015; Jeon et al. 2012). Nephrin expression in the kidney is specific to the podocytes and is located in the SD (Fig. 1). Moreover, nephrin can be found in a detergent resistant cellular membrane compartment called lipid raft. Knockout mouse studies showed that the extracellular domain of nephrin interacts with nephrin and NEPH1 of the adjacent podocytes to link neighboring foot process together in a highly organized manner (Wartiovaara et al. 2004; Khoshnoodi et al. 2003).

3.1 Nephrin Phosphorylation

Sequencing of the intracellular domain of nephrin across various species revealed multiple tyrosine residues, which are evolutionally conserved suggesting that this portion of nephrin may have functional importance. Of them, many tyrosine residues are recognized by proteins that have SH2 domains. Previous data have demonstrated that the SRC-family kinase FYN had the highest affinity for nephrin and was the most potent at increasing nephrin tyrosine phosphorylation (Li et al. 2004; Verma et al. 2003). Since then, multiple studies discovered that phosphorylation of these tyrosine residues is critical to the regulation of various intracellular pathways in the podocytes. Those pathways include remodeling of the actin cytoskeleton, activation of the PI3 kinase/Akt pathway, calcium signaling and endocytosis of nephrin (Patrakka and Tryggvason 2007; Jones et al. 2009; Li et al. 2015; Quack et al. 2011) (Fig. 2).

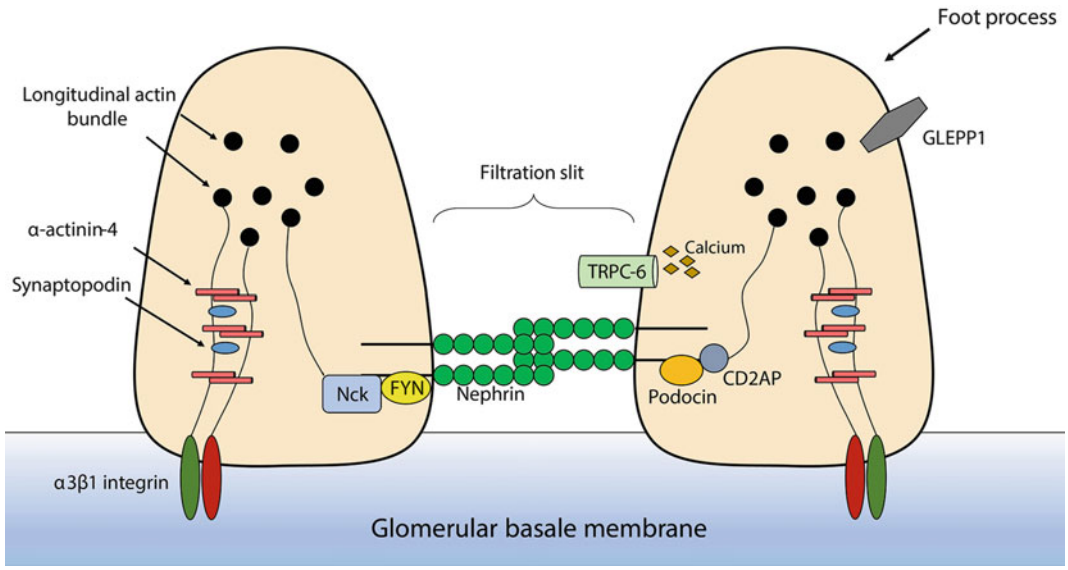

Fig. 1 Representative image of the foot process of the podocytes

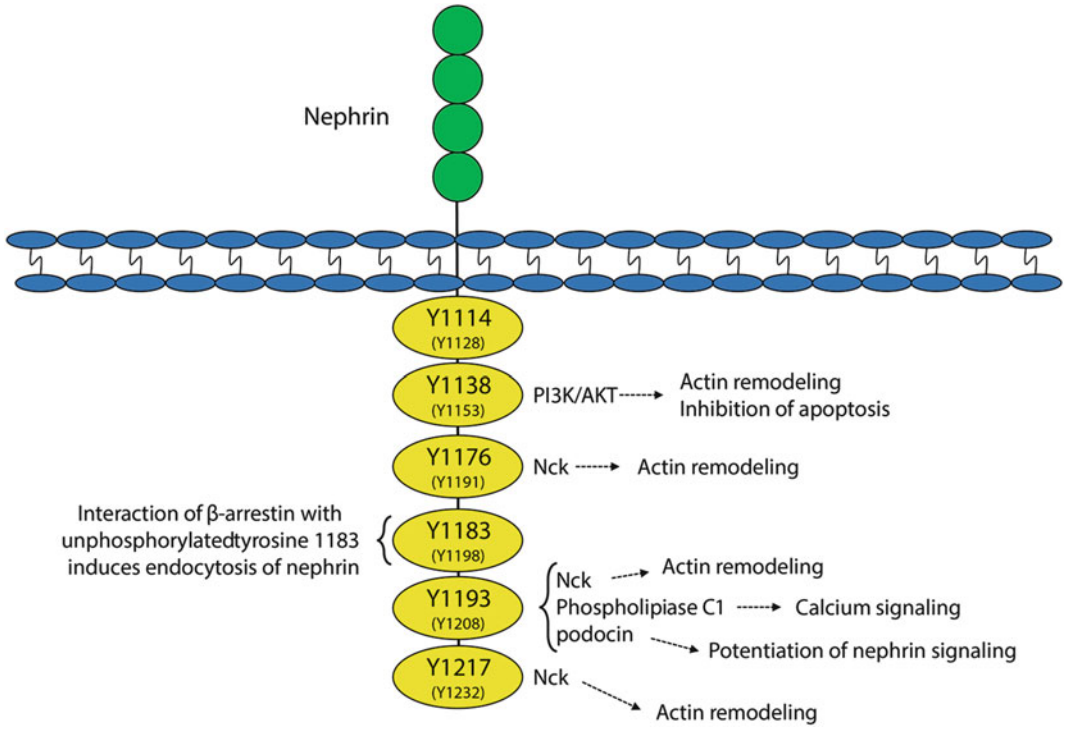

Fig. 2 Tyrosine residues in the cytoplasmic compartment of nephrin

3.2 Actin Remodeling

In 2006, two important studies by Pawson and Holzmann showed the crucial role of nephrin tyrosine phosphorylation in the regulation of actin remodeling in the podocytes. This remodeling required interaction of nephrin with both NCK1 and NCK2, two adaptor proteins containing three SH3 domains and a single SH2 domain. Both studies reported that triggering phosphorylation of tyrosine residues (Y1176, Y1193 and Y1208) of nephrin enhanced its interaction with NCK1 and NCK2, resulting in the formation of actin tails (Jones et al. 2006; Verma et al. 2006a). The role of the interaction of nephrin with NCK in maintaining kidney function was first highlighted using the NCK1 deficient mice and the podocyte specific NCK2 knockout mice, which developed glomerulosclerosis and podocyte FP fusion (Jones et al. 2009). These observations were further confirmed in a study by Dr. Jones' laboratory, who has generated mice with mutations in the tyrosine residues responsible of nephrin interaction with NCK. Mice expressing nephrin mutated at tyrosine 1176, 1193 and 1217 showed progressive proteinuria with aging, which was accompanied with podocyte foot process effacement, dilated capillary loops and thickening of the basal membrane. Moreover, these mice were more susceptible to heparin and lipopolysaccharides (LPS) induced kidney injury (New et al. 2016). This study clearly demonstrated that nephrin-mediated regulation of the actin cytoskeleton is required in both keeping a healthy glomerulus and during the recovery process after kidney injury.

3.3 Regulation of Calcium

The importance of calcium regulation in the podocytes was emphasized when gain-of-function mutation of the transient receptor potential cation channel 6, or TRPC6, was linked to focal segmental glomerulosclerosis, a glomerular

disease which ultimately leads to end-stage renal disease (Reiser et al. 2005; Winn et al. 2005). Calcium signaling in the podocytes is linked to the remodeling of the actin cytoskeleton, which is essential in maintaining a healthy filtration barrier (Greka and Mundel 2011). A previous study showed that phosphorylation of the tyrosine 1193 of nephrin promoted its interaction with phospholipase C-γ1 and triggered calcium mobilization (Harita et al. 2009). It was found that nephrin is implicated in the inhibition of the activity of TRPC6, but in a non-tyrosine-dependent mechanism (Kanda et al. 2011).

3.4 PI3K/Akt Pathway

The AKT family of proteins (Akt1, Akt2 and Akt3) are serine/threonine kinases that are involved in multiple cellular pathways including cell survival, proliferation, migration and actin remodeling. The phosphoinositide 3-kinase (PI3K) is composed of a catalytic subunit called p110 and a regulatory subunit called p85. Activation of Akt is made by a complex signaling cascade which starts with activated receptor tyrosine kinases, such as the platelet-derived growth factor receptor (PDGF) and the insulin receptor (IR). Upon activation, receptor tyrosine kinase activates PI3K through direct interaction or with a scaffolding protein such as the insulin receptor subtrat-1 (IRS-1). Activated PI3K phosphorylates phosphatidylinositol-4,5-bisphosphate (PIP2) to form phosphatidylinositol-3,4,5-triphosphate (PIP3). Then, Akt translocates to the membrane to be stimulated by both PIP3 and PDK1 (Manning and Cantley 2007). In podocytes, Akt2, and not Akt1, is critical for podocyte survival and function in various kidney diseases (Canaud et al. 2013). Interestingly, Akt2 is the major isoform activated upon insulin stimulation (Kim et al. 2000; Cho 2001; Garofalo et al. 2003).

The regulation and activation of the PI3K/Akt pathways by nephrin was initially associated with nephrin interaction with CD2AP and podocin, which are two proteins implicated in podocyte function found in the SD (Huber et al. 2003). Overexpression of nephrin in podocytes increased basal Akt phosphorylation, which is associated with an increased interaction of p85 subunit with nephrin on phosphorylated tyrosine residue 1138. The increased interaction between both proteins resulted in the reduction of actin stress fiber formation in cultured podocytes (Zhu et al. 2008).

4 Nephrin Phosphorylation in the Development of Mature Glomerulus

The first evidence that nephrin phosphorylation could be involved in the maturation of the glomerulus came from immunofluorescence experiments indicating that nephrin phosphorylation was greatly induced in the development of the glomerulus in mice (Verma et al. 2006b). Interestingly, the same group could not detect nephrin phosphorylation in the mature glomerulus, which contradicts results from other studies (Jones et al. 2009; Denhez et al. 2015; Verma et al. 2015). One possible explanation is the sensitivity of the antibodies used in these studies. Furthermore, mice expressing the triple mutant of nephrin did not exhibit abnormal filtration barrier and maturation of the glomerulus, which strongly suggests that nephrin-mediated actin regulation is not required for the maturation of the glomerulus, or that other pathways can compensate for the loss of nephrin mediated actin remodeling. Nonetheless, these results do not rule out that other nephrin tyrosine residues could be essential for the development of the glomerulus (New et al. 2016). As described above, the fundamental role of nephrin phosphorylation in the mature glomerulus was underlined by the presence of proteinuria and glomerular abnormalities in mice lacking of nephrin tyrosine residues related to actin regulation. Unfortunately, there is no indication that nephrin tyrosine residues involved in other cellular pathways such as calcium signaling or PI3K activation could play a role in maintaining kidney function in the mature glomerulus.

5 Nephrin Expression in Various Models of Glomerular Injury

The notion that the disruption of nephrin expression could lead to glomerular damage came from the observation that patients with congenital nephrotic syndrome of the Finnish type possessed mutations on the gene coding for nephrin (Hulkko et al. 2014). Subsequent studies revealed that the vast majority of these mutations contributed to impaired trafficking of nephrin to the cellular membrane. Downregulation of nephrin expression was observed in a number of glomerular disease, including lupus nephritis and DN (Doublier et al. 2003; Perysinaki et al. 2011), whereas some studies reported that expression of nephrin was not affected in proteinuric kidney disease. Patrakka and collaborators observed that the mRNA and protein expression of nephrin, using immunohistochemistry and in situ hybridization, was similar between pediatric minimal change nephrosis patients and controls (Patrakka et al. 2001). Quack and collaborator showed that high glucose level exposure in cultured podocytes activated PKC-α activity causing the phosphorylation on nephrin threonine residues 1120 and 1125 (Quack et al. 2011). These phosphorylation sites subsequently increased nephrin interaction with β-arrestin2 promoting nephrin endocytosis. The authors reported that the interaction of PKC-α with nephrin was dependant of the adaptor protein PICK1. Moreover, deletion of PKC-α in diabetic mice prevented the loss of nephrin expression and development of DN (Menne et al. 2006). Other than weakening of the structural integrity of the SD, loss of nephrin expression has been shown to promote cellular pathways contributing to glomerular injury. Hussain and collaborators demonstrated that nephrin deficiency activated the nuclear factor-kappa B (NF-κB), a transcription factor known to be upregulated in various glomerular diseases (Hussain et al. 2009; Zheng et al. 2006; Fujihara et al. 2007; Takano et al. 2001). The authors reported that cultured podocytes expressing a truncated mutant of nephrin exhibited elevated levels of NF-κB transcriptional activity and a shift of aPKC-ζ expression from the nucleus to the cytoplasm, which induced the phosphorylation of the cytoplasmic IκB causing its dissociation with NF-κB and subsequently its translocation to the nucleus (Hussain et al. 2009). More importantly, the rescue of nephrin expression prevented the increased NF-κB activation, suggesting that loss of nephrin expression could be a driving factor in NF-κB dependant glomerular diseases.

6 Nephrin Phosphorylation in Various Models of Acute Kidney Injury

Multiple studies sought to find if nephrin tyrosine phosphorylation was affected in various types of kidney injury. Typical mouse models of acute kidney injury include the puromycin aminonucleoside (PAN) nephropathy, the protamine sulfate (PS), and the LPS treatment. In these models, both PAN nephropathy and LPS treatment reduced nephrin tyrosine 1176/1193 phosphorylation levels (Jones et al. 2009; Zhu et al. 2008). It is believed that PAN nephropathy mimics minimal-change nephropathy in humans. Both diseases are characterized by almost no visible glomerular change on light microscopy but the major changes occurred in the structural integrity of the podocyte FP (Ryan and Karnovsky 1975; Löwenborg et al. 2000). Multiple studies that evaluated nephrin tyrosine phosphorylation in PAN models reported a stark decrease in its phosphorylation levels, in which the lowest expression of nephrin phosphorylation was observed when proteinuria reached its highest level (Jones et al. 2009; Zhu et al. 2008; Li et al. 2006). Moreover, human glomerulonephritis treatment with glucocorticoids exerted its actions by increasing the phosphorylation of nephrin (Ohashi et al. 2011). In contrast, the rat Heymann nephritis and PS-induced damage to the kidney significantly increased nephrin phosphorylation at tyrosine 1176/1193, while reperfusion of the kidney with heparin sulfate, which reversed podocyte FP spreading by PS, restored

nephrin phosphorylation to baseline levels. (Li et al. 2004; Verma et al. 2006a; New et al. 2016). In addition, another study found that preventing the increased phosphorylation levels of nephrin following PS treatment abrogated the podocyte FP effacement (Verma et al. 2015). On the other hand, mice expressing nephrin mutated at tyrosine 1176, 1193 and 1217 did not exhibit reduction in FP effacement in reperfused kidney with heparin sulfate suggesting that nephrin mediated remodeling of the actin cytoskeleton is required to restore the integrity of the FP in this model (New et al. 2016). Taken together, these data suggest that the homeostasis of the podocyte structure and its FP integrity by nephrin is a fine balance that can be disrupted by tipping it toward both sides.

7 Regulation of Tyrosine Phosphorylation of Nephrin

Ample evidence from *in vitro* studies showed that FYN and SRC kinases have the highest affinity for nephrin and are the most potent at increasing nephrin phosphorylation (Li et al. 2004; Verma et al. 2003; Jones et al. 2006). FYN was found to mostly phosphorylate nephrin tyrosine 1176, 1993 and 1217, which as we discussed above are required for nephrin interaction with NCK adaptor proteins. It is now widely accepted that regulation of cellular signaling mediated by phosphorylation is a fine balance between the activity of kinases and phosphatases. A change in either part of this balance can lead to various consequences, including diseases like cancer, diabetes and rheumatoid arthritis (Hendriks et al. 2013; Echwald et al. 2002; Hinks et al. 2006). Since nephrin phosphorylation is required for a healthy glomerulus, a better understanding of cellular mechanisms that contribute to the inhibition of nephrin-mediated intracellular pathways could be of therapeutic interest. One of the potential mechanisms is the increase interactions of nephrin with tyrosine phosphatases, which can dephosphorylate tyrosine residues of nephrin, leading to the inhibition of its cellular signaling pathways. Glomerular epithelial protein 1 (GLEPP1) is the most well-characterized tyrosine phosphatase in podocytes and is highly expressed on the apical membrane of the cells (Thomas et al. 1994; Wang et al. 2000). GLEPP1 deficient mice showed abnormal podocyte morphology and elevated blood pressure after uninephrectomy (Wharram et al. 2000). In cultured mouse podocytes, expression profile of selected phosphatases was detected by quantitative PCR and demonstrated that PTP1B, Src homology-2 domain phosphatase-2 (SHP-2), PTP-proline, glutamate, serine and threonine sequences (PTP-PEST), and PTPD2 were expressed in podocytes (Reiser et al. 2000b).

7.1 PTP1B

The first evidence that phosphatases could regulate nephrin phosphorylation was shown in a study from Dr. Takano's group. They found that PTP1B could bind to nephrin and dephosphorylate tyrosine 1193 and 1217 (Fig. 3). Moreover, inhibition or overexpression of PTP1B in podocytes drastically altered their actin cytoskeleton and remodeling, further reinforcing the idea that phosphatases can regulate nephrin-mediated cellular signaling actions (Aoudjit et al. 2011). In addition, the same group reported that inhibition of PTP1B significantly improved albuminuria and proteinuria following kidney injury in mice treated with PAN or adryamicin treatment (Kumagai et al. 2014).

7.2 SHP-1

Recently, our laboratory reported that Src homology 2 domain phosphatase 1 (SHP-1) can bind nephrin and reduce its tyrosine phosphorylation levels (Denhez et al. 2015). SHP-1 is part of the *non-receptor-like* family of tyrosine phosphatases. SHP-1 contains two SH2 domains (N-SH2 and C-SH2) which control both its activation and interaction with its targets. In its non-active state, the N-terminal SH2 domain

binds to the phosphatase catalytic domain of SHP-1 (Fig. 3). Binding of the C-terminal SH2 domain with the phosphorylated tyrosine of a targeted substrate disrupts the interaction of the N-SH2 domain with the phosphatase domain liberating the catalytic phosphatase domain to induce dephosphorylation of the tyrosine residues of its substrate. Activation of SHP-1 can also be enhanced by the phosphorylation of its tyrosine 536 and 546 residues (Wang et al. 2011; Uchida et al. 1994; Yoshida et al. 1999; Neel et al. 2003). SHP-1 is a negative modulator of multiple signaling pathways linked to growth factors, which includes platelet-derived growth factor, vascular endothelial growth factor and insulin signaling (Neel et al. 2003; Wu et al. 2003). Results from both our group and other laboratories found that hyperglycemia and diabetes increased the expression of SHP-1 in various cell types causing cellular growth factor inhibition (Geraldes et al. 2009; Mima et al. 2012; Drapeau et al. 2013; Lizotte et al. 2016). In podocytes, hyperglycemia induced a persistent increase of SHP-1 expression, due to epigenetic modification in the SHP-1 promoter (Lizotte et al. 2016) leading to insulin signaling resistance, podocyte dysfunction and cell death, and DN. This resulted in blunted Akt and ERK activation upon insulin stimulation in podocytes, both of which are associated with pro survival functions of insulin (Drapeau et al. 2013; Lizotte et al. 2016).

7.3 SHP-1 and Nephrin Tyrosine Phosphorylation

Results from our laboratory demonstrated that overexpression of SHP-1 significantly reduced phosphorylation of tyrosine 1176, 1993 and 1217 residues of nephrin suggesting that SHP-1 could be a negative modulator of nephrin-mediated actin remodeling. Moreover, using cultured human podocytes, our group showed that cells exposed to high levels of glucose significantly exhibited elevated SHP-1 expression, which was associated with reduced nephrin tyrosine phosphorylation. In addition, overexpression of the dominant negative form of SHP-1 prevented high glucose levels-induced inhibition of nephrin phosphorylation in DN (Denhez et al. 2015).

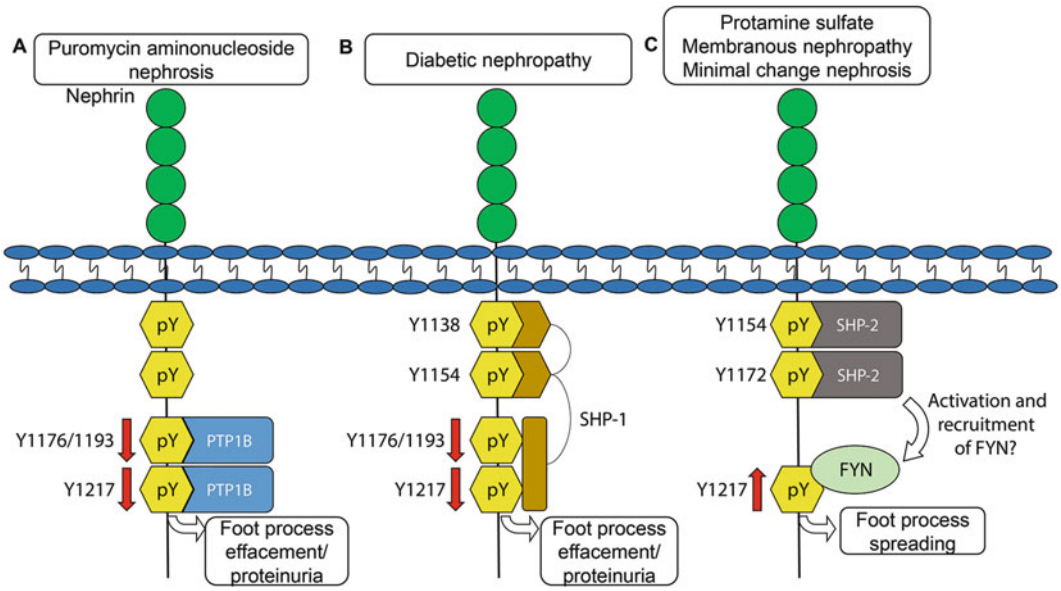

Fig. 3 Protein tyrosine phosphatase interaction and mechanism of action with nephrin tyrosine phosphorylation

7.4 SHP-2

Whereas SHP-1 is considered as a negative regulator of cell proliferation and dephosphorylated receptors of growth factors, SHP-2, on the other hand, is generally viewed as a positive signal transducer. Functional deletion of the *Shp-2* gene in mice induced death of the embryos at mid-gestation (Saxton et al. 1997). Both cells isolated from the SHP-2 null mice and expressing the catalytically inactive cysteine-to-serine mutant of SHP-2 exhibited decreased signal transduction activation upon growth factors and cytokine stimulation (Feng 1999; Neel et al. 2003). A recent study observed an enhanced nephrin phosphorylation activation on tyrosine 1191 and 1208 residues in cells that expressed both the CD16-nephrin chimera and SHP-2 (Verma et al. 2015). The same group also reported that the phosphorylation of tyrosine 542 of SHP-2 is increased in both minimal-change nephrosis and membranous nephropathy.

8 The Podocyte and Nephrin Phosphorylation in DN

Multiple studies showed that podocytes are the first cell affected by diabetes and disruption of the structural integrity of the SD could be a potential site that hyperglycemia causes podocyte injury (Ellis et al. 1987; Torbjörnsdotter et al. 2005; Steffes et al. 2001). There are multiple hypotheses to explain the dysfunction of podocytes in DN that contributes to reduced podocyte density in the glomerulus. Interestingly, in both rodent models and human kidney samples, it has been found that nephrin expression is significantly reduced by diabetes (Doublier et al. 2003; Aaltonen et al. 2001). The dysfunction of the podocyte SD in DN raises the question of whether nephrin tyrosine phosphorylation could be modulated. Few studies in the literature evaluated the phosphorylation levels of nephrin in rodent models of diabetes. Of those, opposite results have been reported. One study has observed an increase in tyrosine phosphorylation of nephrin in early DN (Dessapt-Baradez et al. 2014) whereas we and others have demonstrated a decrease in tyrosine phosphorylation levels (Denhez et al. 2015; Batchu et al. 2016; Mima et al. 2012). One possible explanation for these differences could be the model used to study kidney complications in a context of diabetes. The study that observed an increase in nephrin phosphorylation used the streptozotocin-induced diabetic mouse model, which can produce renal morphology variability in response to hyperglycemia (Gurley et al. 2006). Moreover, no difference in the podocyte FP width was shown in streptozotocin mice compared to non-diabetic mice. In contrast, we and other groups found that podocyte cell death and FP effacement occurred in Akita mice (Drapeau et al. 2013; Susztak et al. 2006). Duration of diabetes could be another explanation for these discrepancies. Increase nephrin tyrosine phosphorylation was observed at 13 weeks of diabetes, while our group reported that nephrin tyrosine phosphorylation was decreased after 20 weeks of diabetes. This raises the possibility that the mechanism leading to decreased nephrin tyrosine phosphorylation only occurs after prolonged chronic hyperglycemia.

9 Conclusion

The discovery of nephrin greatly improved our understanding of the podocyte function and revealed the central role of this protein in maintaining the structure of the podocyte slit diaphragm. Further studies showed that its intracellular domain is involved in the regulation of multiple signaling pathways that are required to preserve the foot process architecture in mature glomerulus. These findings raised the possibility that the disruption of the homeostasis of nephrin phosphorylation may participate in the pathogenesis and the progression of various kidney diseases. Particularly in DN, podocyte dysfunction could be a critical factor in disease progression. We and others reported that tyrosine phosphorylation of nephrin is reduced by hyperglycemia and diabetes, which may contribute to

DN development and progression. A better understanding of the mechanisms leading to the reduction of nephrin phosphorylation and its consequences in DN may provide new therapeutic strategies to prevent the progression of chronic kidney disease.

Compliance with Ethical Standards We do not have any conflicts of interest. Also, there is no animal or human participants in the study.

Conflicts of Interest The authors declare that they have no conflicts of interest.

Ethical Approval This article does not contain any studies with human participants or animals performed by any of the authors.

References

Aaltonen P, Luimula P, Aström E, Palmen T, Grönholm T, Palojoki E, Jaakkola I, Ahola H, Tikkanen I, Holthöfer H (2001) Changes in the expression of nephrin gene and protein in experimental diabetic nephropathy. Lab Invest 81(9):1185–1190

Aoudjit L, Jiang R, Lee TH, New LA, Jones N, Takano T (2011) Podocyte protein, Nephrin, is a substrate of protein tyrosine phosphatase 1B. J Signal Transduct 2011:376543

Batchu SN, Majumder S, Bowskill BB, White KE, Advani SL, Brijmohan AS, Liu Y, Thai K, Azizi PM, Lee WL, Advani A (2016) Prostaglandin I2 receptor Agonism preserves β-cell function and attenuates albuminuria through nephrin-dependent mechanisms. Diabetes 65(5):1398–1409

Canaud G, Bienaimé F, Viau A, Treins C, Baron W, Nguyen C, Burtin M, Berissi S, Giannakakis K, Muda AO, Zschiedrich S, Huber TB, Friedlander G, Legendre C, Pontoglio M, Pende M, Terzi F (2013) AKT2 is essential to maintain podocyte viability and function during chronic kidney disease. Nat Med 19 (10):1288–1296

Cho H (2001) Insulin resistance and a diabetes mellitus-like syndrome in mice lacking the protein kinase Akt2 (PKBbeta). Science 292(5522):1728–1731

Collins AJ, Kasiske B, Herzog C, Chavers B, Foley R, Gilbertson D, Grimm R, Liu J, Louis T, Manning W, McBean M, Murray A, St Peter W, Xue J, Fan Q, Guo H, Li Q, Li S, Qiu Y, Li S, Roberts T, Skeans M, Snyder J, Solid C, Wang C, Weinhandl E, Zhang R, Arko C, Chen S-CC, Dalleska F, Daniels F, Dunning S, Ebben J, Frazier E, Hanzlik C, Johnson R, Sheets D, Wang X, Forrest B, Berrini D, Constantini E, Everson S, Eggers P, Agodoa L (2007) Excerpts from the United States renal data system 2006 annual data report. Am J Kidney Dis 49 (1 Suppl 1):A7

Denhez B, Lizotte F, Guimond M-OO, Jones N, Takano T, Geraldes P (2015) Increased SHP-1 protein expression by high glucose levels reduces nephrin phosphorylation in podocytes. J Biol Chem 290 (1):350–358

Dessapt-Baradez C, Woolf AS, White KE, Pan J, Huang JL, Hayward AA, Price KL, Kolatsi-Joannou M, Locatelli M, Diennet M, Webster Z, Smillie SJ, Nair V, Kretzler M, Cohen CD, Long DA, Gnudi L (2014) Targeted glomerular angiopoietin-1 therapy for early diabetic kidney disease. J Am Soc Nephrol 25 (1):33–42

Doublier S, Salvidio G, Lupia E, Ruotsalainen V, Verzola D, Deferrari G, Camussi G (2003) Nephrin expression is reduced in human diabetic nephropathy evidence for a distinct role for glycated albumin and angiotensin II. Diabetes 52(4):1023–1030

Drapeau N, Lizotte F, Denhez B, Guay A, Kennedy CR, Geraldes P (2013) Expression of SHP-1 induced by hyperglycemia prevents insulin actions in podocytes. Am J Phys Endocrinol Metab 304(11):98

Dronavalli S, Duka I, Bakris GL (2008) The pathogenesis of diabetic nephropathy. Nat Clin Pract Endocrinol Metab 4(8):444–452

Echwald SM, Bach H, Vestergaard H, Richelsen B, Kristensen K, Drivsholm T, Borch-Johnsen K, Hansen T, Pedersen O (2002) A P387L variant in protein tyrosine phosphatase-1B (PTP-1B) is associated with type 2 diabetes and impaired serine phosphorylation of PTP-1B in vitro. Diabetes 51 (1):1–6

Ellis EN, Steffes MW, Chavers B, Mauer SM (1987) Observations of glomerular epithelial cell structure in patients with type I diabetes mellitus. Kidney Int 32(5):736–741

Epstein M, Sowers JR (1992) Diabetes mellitus and hypertension. Hypertension 19(5):403–418

Feng GS (1999) Shp-2 tyrosine phosphatase: signaling one cell or many. Exp Cell Res 253(1):47–54

Fornoni A, Jeon J, Santos JV, Cobianchi L (2010) Nephrin is expressed on the surface of insulin vesicles and facilitates glucose-stimulated insulin release. Diabetes 42:190

Fujihara CK, Antunes GR, Mattar AL, Malheiros DM, Vieira JM Jr, Zatz R (2007) Chronic inhibition of nuclear factor-kappaB attenuates renal injury in the 5/6 renal ablation model. Am J Physiol 292(1):F92–F99

Garofalo RS, Orena SJ, Rafidi K, Torchia AJ, Stock JL, Hildebrandt AL, Coskran T, Black SC, Brees DJ, Wicks JR, McNeish JD, Coleman KG (2003) Severe diabetes, age-dependent loss of adipose tissue, and mild growth deficiency in mice lacking Akt2/PKB beta. J Clin Invest 112(2):197–208

Geraldes P, Hiraoka-Yamamoto J, Matsumoto M, Clermont A, Leitges M, Marette A, Aiello LP, Kern TS, King GL (2009) Activation of PKC-delta and

SHP-1 by hyperglycemia causes vascular cell apoptosis and diabetic retinopathy. Nat Med 15 (11):1298–1306

Greka A, Mundel P (2011) Balancing calcium signals through TRPC5 and TRPC6 in podocytes. J Am Soc Nephrol 22(11):1969–1980

Greka A, Mundel P (2012) Cell biology and pathology of podocytes. Annu Rev Physiol 74:299–323

Gurley SB, Clare SE, Snow KP, Hu A, Meyer TW, Coffman TM (2006) Impact of genetic background on nephropathy in diabetic mice. Am J Physiol Renal Physiol 290(1):22

Harita Y, Kurihara H, Kosako H, Tezuka T, Sekine T, Igarashi T, Ohsawa I, Ohta S, Hattori S (2009) Phosphorylation of nephrin triggers Ca2+ signaling by recruitment and activation of phospholipase C-γ1. J Biol Chem 284(13):8951–8962

Hendriks WJAJ, Elson A, Harroch S, Pulido R, Stoker A, den Hertog J (2013) Protein tyrosine phosphatases in health and disease. FEBS J 280(2):708–730

Hinks A, Worthington J, Thomson W (2006) The association of PTPN22 with rheumatoid arthritis and juvenile idiopathic arthritis. Rheumatology 45(4):365–368

Huber TB, Hartleben B, Kim J, Schmidts M, Schermer B, Keil A, Egger L, Lecha RL, Borner C, Pavenstädt H, Shaw AS, Walz G, Benzing T (2003) Nephrin and CD2AP associate with phosphoinositide 3-OH kinase and stimulate AKT-dependent signaling. Mol Cell Biol 23(14):4917–4928

Hulkko J, Patrakka J, Lal M, Tryggvason K, Hultenby K, Wernerson A (2014) Neph1 is reduced in primary focal segmental glomerulosclerosis, minimal change nephrotic syndrome, and corresponding experimental animal models of adriamycin-induced nephropathy and puromycin aminonucleoside nephrosis. Nephron Extra 4(3):146–154

Hussain S, Romio L, Saleem M, Mathieson P, Serrano M, Moscat J, Diaz-Meco M, Scambler P, Koziell A (2009) Nephrin deficiency activates NF-kappaB and promotes glomerular injury. J Am Soc Nephrol 20 (8):1733–1743

Jeon J, Leibiger I, Moede T, Walter B, Faul C, Maiguel D, Villarreal R, Guzman J, Berggren P-OO, Mundel P, Ricordi C, Merscher-Gomez S, Fornoni A (2012) Dynamin-mediated Nephrin phosphorylation regulates glucose-stimulated insulin release in pancreatic beta cells. J Biol Chem 287(34):28932–28942

Jones N, Blasutig IM, Eremina V, Ruston JM, Bladt F, Li H, Huang H, Larose L, Li S, Takano T, Quaggin SE, Pawson T (2006) Nck adaptor proteins link nephrin to the actin cytoskeleton of kidney podocytes. Nature 440(7085):818–823

Jones N, New LA, Fortino MA, Eremina V, Ruston J, Blasutig IM, Aoudjit L, Zou Y, Liu X, Yu G-LL, Takano T, Quaggin SE, Pawson T (2009) Nck proteins maintain the adult glomerular filtration barrier. J Am Soc Nephrol 20(7):1533–1543

Kanda S, Harita Y, Shibagaki Y, Sekine T, Igarashi T, Inoue T, Hattori S (2011) Tyrosine phosphorylation–dependent activation of TRPC6 regulated by PLC-γ1 and nephrin: effect of mutations associated with focal segmental glomerulosclerosis. Mol Biol Cell 22 (11):1824–1835

Kapodistria K, Tsilibary E-PP, Politis P, Moustardas P, Charonis A, Kitsiou P (2015) Nephrin, a transmembrane protein, is involved in pancreatic beta-cell survival signaling. Mol Cell Endocrinol 400:112–128

Karnovsky MJ, Ryan GB (1975) Substructure of the glomerular slit diaphragm in freeze-fractured normal rat kidney. J Cell Biol 65(1):233–236

Kestilä M, Lenkkeri U, Männikkö M, Lamerdin J, McCready P, Putaala H, Ruotsalainen V, Morita T, Nissinen M, Herva R, Kashtan CE, Peltonen L, Holmberg C, Olsen A, Tryggvason K (1998) Positionally cloned Gene for a novel glomerular protein—nephrin—is mutated in congenital Nephrotic syndrome. Mol Cell 1(4):575

Khoshnoodi J, Sigmundsson K, Ofverstedt L-GG, Skoglund U, Obrink B, Wartiovaara J, Tryggvason K (2003) Nephrin promotes cell-cell adhesion through homophilic interactions. Am J Pathol 163 (6):2337–2346

Kim YB, Peroni OD, Franke TF, Kahn BB (2000) Divergent regulation of Akt1 and Akt2 isoforms in insulin target tissues of obese Zucker rats. Diabetes 49 (5):847–856

Kriz W, Gretz N, Lemley KV (1998) Progression of glomerular diseases: is the podocyte the culprit? Kidney Int 54(3):687–697

Kumagai T, Baldwin C, Aoudjit L, Nezvitsky L, Robins R, Jiang R, Takano T (2014) Protein tyrosine phosphatase 1B inhibition protects against podocyte injury and proteinuria. Am J Pathol 184(8):2211–2224

Li H, Lemay S, Aoudjit L, Kawachi H, Takano T (2004) Src-family kinase Fyn phosphorylates the cytoplasmic domain of nephrin and modulates its interaction with podocin. J Am Soc Nephrol 15(12):3006–3015

Li H, Zhu J, Aoudjit L, Latreille M, Kawachi H, Larose L, Takano T (2006) Rat nephrin modulates cell morphology via the adaptor protein Nck. Biochem Biophys Res Commun 349(1):310–316

Li X, Chuang PY, D'Agati VD, Dai Y, Yacoub R, Fu J, Xu J, Taku O, Premsrirut PK, Holzman LB, He JC (2015) Nephrin preserves podocyte viability and glomerular structure and function in adult kidneys. J Am Soc Nephrol 26(10):2361–2377

Lizotte F, Denhez B, Guay A, Gévry N, Côté AM, Geraldes P (2016) Persistent insulin resistance in Podocytes caused by epigenetic changes of SHP-1 in diabetes. Diabetes 65:3705

Löwenborg EKM, Jaremko G, Berg UB (2000) Glomerular function and morphology in puromycin aminonucleoside nephropathy in rats. Nephrol Dial Transplant 15(10):1547–1555

Manning BD, Cantley LC (2007) AKT/PKB signaling: navigating downstream. Cell 129(7):1261–1274

Menne J, Meier M, Park JK, Boehne M, Kirsch T, Lindschau C, Ociepka R, Leitges M, Rinta-Valkama J,

Holthofer H, Haller H (2006) Nephrin loss in experimental diabetic nephropathy is prevented by deletion of protein kinase C alpha signaling in-vivo. Kidney Int 70(8):1456–1462

Meyer TW, Bennett PH, Nelson RG (1999) Podocyte number predicts long-term urinary albumin excretion in Pima Indians with Type II diabetes and microalbuminuria. Diabetologia 42(11):1341–1344

Mima A, Kitada M, Geraldes P, Li Q, Matsumoto M, Mizutani K, Qi W, Li C, Leitges M, Rask-Madsen C, King GL (2012) Glomerular VEGF resistance induced by PKCδ/SHP-1 activation and contribution to diabetic nephropathy. FASEB 26(7):2963–2974

Neel BG, Gu H, Pao L (2003) The 'Shp'ing news: SH2 domain-containing tyrosine phosphatases in cell signaling. Trends Biochem Sci 28(6):284–293

New LA, Martin CE, Scott RP, Platt MJ, Chahi KA, Stringer CD, Lu P, Samborska B, Eremina V, Takano T, Simpson JA, Quaggin SE, Jones N (2016) Nephrin tyrosine phosphorylation is required to stabilize and restore podocyte foot process architecture. J Am Soc Nephrol 27:2422

Ohashi T, Uchida K, Uchida S, Sasaki S, Nitta K (2011) Dexamethasone increases the phosphorylation of nephrin in cultured podocytes. Clin Exp Nephrol 15 (5):688–693

Pagtalunan ME, Miller PL, Jumping-Eagle S, Nelson RG, Myers BD, Rennke HG, Coplon NS, Sun L, Meyer TW (1997) Podocyte loss and progressive glomerular injury in type II diabetes. J Clin Investig 99(2):342348

Patrakka J, Tryggvason K (2007) Nephrin--a unique structural and signaling protein of the kidney filter. Trends Mol Med 13(9):396–403

Patrakka J, Ruotsalainen V, Ketola I, Holmberg C, Heikinheimo M, Tryggvason K, Jalanko H (2001) Expression of nephrin in pediatric kidney diseases. J Am Soc Nephrol 12(2):289–296

Pavenstädt H, Kriz W, Kretzler M (2003) Cell biology of the glomerular podocyte. Physiol Rev 83(1):253–307

Perysinaki GS, Moysiadis DK, Bertsias G, Giannopoulou I, Kyriacou K, Nakopoulou L, Boumpas DT, Daphnis E (2011) Podocyte main slit diaphragm proteins, nephrin and podocin, are affected at early stages of lupus nephritis and correlate with disease histology. Lupus 20(8):781–791

Quack I, Woznowski M, Potthoff SA, Palmer R, Konigshausen E, Sivritas S, Schiffer M, Stegbauer J, Vonend O, Rump LC, Sellin L (2011) PKC alpha mediates beta-arrestin2-dependent nephrin endocytosis in hyperglycemia. J Biol Chem 286 (15):12959–12970

Reiser J, Kriz W, Kretzler M, Mundel P (2000a) The glomerular slit diaphragm is a modified adherens junction. JASN 11(1):1–8

Reiser J, Pixley FJ, Hug A, Kriz W, Smoyer WE, Stanley ER, Mundel P (2000b) Regulation of mouse podocyte process dynamics by protein tyrosine phosphatases rapid communication. Kidney Int 57(5):2035–2042

Reiser J, Polu KR, Möller CC, Kenlan P, Altintas MM, Wei C, Faul C, Herbert S, Villegas I, Avila-Casado C, McGee M, Sugimoto H, Brown D, Kalluri R, Mundel P, Smith PL, Clapham DE, Pollak MR (2005) TRPC6 is a glomerular slit diaphragm-associated channel required for normal renal function. Nat Genet 37(7):739–744

Ryan GB, Karnovsky MJ (1975) An ultrastructural study of the mechanisms of proteinuria in aminonucleoside nephrosis. Kidney Int 8(4):219–232

Sachs N, Sonnenberg A (2013) Cell-matrix adhesion of podocytes in physiology and disease. Nat Rev Nephrol 9(4):200–210

Saxton TM, Henkemeyer M, Gasca S, Shen R, Rossi DJ, Shalaby F, Feng GS, Pawson T (1997) Abnormal mesoderm patterning in mouse embryos mutant for the SH2 tyrosine phosphatase Shp-2. EMBO J 16 (9):2352–2364

Schlondorff D, Banas B (2009) The Mesangial cell revisited: no cell is an Island. J Am Soc Nephrol 20 (6):1179–1187

Siddiqi FS, Advani A (2013) Endothelial-podocyte crosstalk: the missing link between endothelial dysfunction and albuminuria in diabetes. Diabetes 62 (11):3647–3655

Steffes MW, Schmidt D, McCrery R, Basgen JM (2001) Glomerular cell number in normal subjects and in type 1 diabetic patients. Kidney Int 59:2104

Susztak K, Raff AC, Schiffer M, Böttinger EP (2006) Glucose-induced reactive oxygen species cause apoptosis of podocytes and podocyte depletion at the onset of diabetic nephropathy. Diabetes 55 (1):225–233

Takano T, Cybulsky AV, Yang X, Aoudjit L (2001) Complement C5b-9 induces cyclooxygenase-2 gene transcription in glomerular epithelial cells. Am J Physiol 281(5):F841–F850

The Writing Team for the Diabetes Control and Complications Trial/Epidemiology of Diabetes Interventions and Complications Research Group (2002) Effect of intensive therapy on the microvascular complications of type 1 diabetes mellitus. JAMA 287(19):2563–2569

Thomas PE, Wharram BL, Goyal M, Wiggins JE, Holzman LB, Wiggins RC (1994) GLEPP1, a renal glomerular epithelial cell (podocyte) membrane protein-tyrosine phosphatase. Identification, molecular cloning, and characterization in rabbit. J Biol Chem 269(31):19953–19962

Torbjörnsdotter TB, Perrin N, Jaremko GA (2005) Widening of foot processes in normoalbuminuric adolescents with type 1 diabetes. Pediatr Nephrol 20:750

Uchida T, Matozaki T, Noguchi T, Yamao T, Horita K, Suzuki T, Fujioka Y, Sakamoto C, Kasuga M (1994) Insulin stimulates the phosphorylation of Tyr538 and the catalytic activity of PTP1C, a protein tyrosine phosphatase with Src homology-2 domains. J Biol Chem 269(16):12220–12228

Verma R, Wharram B, Kovari I, Kunkel R, Nihalani D, Wary KK, Wiggins RC, Killen P, Holzman LB (2003) Fyn binds to and phosphorylates the kidney slit diaphragm component nephrin. J Biol Chem 278 (23):20716–20723

Verma R, Kovari I, Soofi A, Nihalani D, Patrie K, Holzman LB (2006a) Nephrin ectodomain engagement results in Src kinase activation, nephrin phosphorylation, Nck recruitment, and actin polymerization. J Clin Investig 116(5):1346–1359

Verma R, Kovari I, Soofi A, Nihalani D, Patrie K, Holzman LB (2006b) Nephrin ectodomain engagement results in Src kinase activation, nephrin phosphorylation, Nck recruitment, and actin polymerization. J Clin Invest 116(5):1346–1359

Verma R, Venkatareddy M, Kalinowski A, Patel SR, Salant DJ, Garg P (2015) Shp2 associates with and enhances nephrin tyrosine phosphorylation and is necessary for foot process spreading in mouse models of podocyte injury. Mol Cell Biol 36(4):596–614

Verma R, Venkatareddy M, Kalinowski A, Patel SR, Garg P (2016) Integrin ligation results in nephrin tyrosine phosphorylation in vitro. PLoS One 11(2):e0148906

Wang R, St John PL, Kretzler M, Wiggins RC, Abrahamson DR (2000) Molecular cloning, expression, and distribution of glomerular epithelial protein 1 in developing mouse kidney. Kidney Int 57 (5):1847–1859

Wang W, Liu L, Song X, Mo Y, Komma C, Bellamy HD, Zhao ZJ, Zhou GW (2011) Crystal structure of human protein tyrosine phosphatase SHP-1 in the open conformation. J Cell Biochem 112(8):2062–2071

Wartiovaara J, Ofverstedt L-GG, Khoshnoodi J, Zhang J, Mäkelä E, Sandin S, Ruotsalainen V, Cheng RH, Jalanko H, Skoglund U, Tryggvason K (2004) Nephrin strands contribute to a porous slit diaphragm scaffold as revealed by electron tomography. J Clin Invest 114(10):1475–1483

Wharram BL, Goyal M, Gillespie PJ, Wiggins JE, Kershaw DB, Holzman LB, Dysko RC, Saunders TL, Samuelson LC, Wiggins RC (2000) Altered podocyte structure in GLEPP1 (Ptpro)-deficient mice associated with hypertension and low glomerular filtration rate. J Clin Invest 106(10):1281–1290

White KE, Bilous RW, Marshall SM, Nahas M, Remuzzi G, Piras G, Cosmo S, Viberti G (2002) Podocyte number in normotensive type 1 diabetic patients with albuminuria. Diabetes 51 (10):3083–3089

Winn MP, Conlon PJ, Lynn KL, Farrington MK (2005) A mutation in the TRPC6 cation channel causes familial focal segmental glomerulosclerosis. Science 308:1801

Wu C, Sun M, Liu L, Zhou GW (2003) The function of the protein tyrosine phosphatase SHP-1 in cancer. Gene 306:1–12

Yoshida K, Kharbanda S, Kufe D (1999) Functional interaction between SHPTP1 and the Lyn tyrosine kinase in the apoptotic response to DNA damage. J Biol Chem 274(49):34663–34668

Zheng L, Sinniah R, Hsu SI (2006) In situ glomerular expression of activated NF-kappaB in human lupus nephritis and other non-proliferative proteinuric glomerulopathy. Virchows Arch 448(2):172–183

Zhu J, Sun N, Aoudjit L, Li H, Kawachi H, Lemay S, Takano T (2008) Nephrin mediates actin reorganization via phosphoinositide 3-kinase in podocytes. Kidney Int 73(5):556–566

Adv Exp Med Biol - Protein Reviews (2017) 2:163–179
DOI 10.1007/5584_2017_88

Published online: 17 August 2017

The Structure-Forming Juncture in Oxidative Protein Folding: What Happens in the ER?

Mahesh Narayan

Abstract

The folding of disulfide bond containing proteins proceeds in a biphasic manner. Initially, cysteines are oxidized to form disulfide bonds. Structure is largely absent during this phase. Next, when a minimally correct number of native linkages of disulfide bonds have been acquired, the biopolymer conformationally folds into the native, or a native-like, state. Thus, at the end of this "oxidative folding" process, a stable and biologically active protein is formed. This review focuses on dissecting the "structure-forming step" in oxidative protein folding. The ability to follow this pivotal step in protein maturation in somewhat detail is uniquely facilitated in "oxidative" folding scenarios. We review this step using bovine pancreatic Ribonuclease A as a model while recognizing the impact that this step has in subcellular trafficking and protein aggregation.

Keywords

Cis-trans proline isomerization • Endoplasmic reticulum • Oxidative folding • Protein trafficking • Rate-determining step • Structure-forming step • Thiol-disulfide exchange

Abbreviations

$3S_{NNU}$	Unstructured three-disulfide-bond-containing intermediate with one or more non-native disulfide linkages
$3S_{NU}$	Unstructured three-disulfide-bond-containing intermediate with native disulfide linkages

M. Narayan (✉)
Department of Chemistry, The University of Texas at El Paso, 500 W. University Ave, El Paso, TX, USA79968,
e-mail: mnarayan@utep.edu

$3S_{NUx,y,z}$	Unstructured three-disulfide-bond-containing intermediate with native disulfide linkages where x, y and z, refer to the cis- or trans- orientations of the X-Pro peptide bonds around prolines 93, 114 and 117, respectively
$U_{x,y,z}$	Unstructured disulfide-intact intermediate where x,y, and z refer to the cis- or trans- orientations of the X-Pro peptide bonds around prolines 93, 114 and 117, respectively
Des species	a folding intermediate lacking one disulfide bond
DTT^{ox}	Oxididized dithiothreitol
DTT^{red}	Reduced Dithiothreitol
ER	Endoplamic Reticulum
GSH	Reduced glutathione
GSSG	Oxidized glutathione
RNase A	bovine pancreatic ribonuclease A

1 Introduction

Disulfide bonds are the predominant covalent links that stabilize proteins over the usual non-covalent forces such as ionic interactions, Van der Waal's forces, hydrogen bonding and hydrophobic associations (Poland and Scheraga 1965; Pace et al. 1988). Disulfide bonds are found to exist in proteins that are secreted outside cells or stride the membranes of cells wherein a particularly harsh environment necessitates the existence of covalent bonds to support the tertiary structure.

Oxidative protein folding describes the procedure by which disulfide-bond-containing proteins mature to their biologically active form (Arolas et al. 2006; Thornton 1981; Narayan et al. 2000; Wedemeyer et al. 2000; Welker et al. 2001a, b). Oxidative protein folding involves the formation of disulfide bonds via oxidation of cysteine residues in the fully-reduced protein, followed by the conformational folding of the biopolymer to acquire the native state. It is a multi-step process involving chemical reactions such as oxidation, reduction, and thiol-disulfide exchange, and physical, non-covalent interactions as previously mentioned. It takes place within the oxidizing environment of the endoplasmic reticulum (ER).

The study of oxidative protein folding via "classical" folders such as the four-disulfide bovine pancreatic Ribonuclease A (RNase A), leech carboxypeptidase inhibitor, hen egg white Lysozyme, the three-disulfide-containing Bovine Pancreatic Trypsin Inhibitor, the two-disulfide RNase T1 among others have provided a wealth of information about the mechanism by which the protein gradually acquires its tertiary structure (Pace et al. 1988; Narayan et al. 2000; Arolas et al. 2004; Ewbank and Creighton 1993a, b; Oas and Kim 1988; Pace and Creighton 1986; Radford et al. 1992; Roux et al. 1999; van den Berg et al. 1999; Weissman and Kim 1995; Yu et al. 1995). The ability to better control elements of protein folding by studying oxidative protein folding pathways as opposed to studies focusing on conformational folding trajectories has been instrumental in revealing facets of protein folding that would otherwise elude inquiry (Narayan et al. 2000; Wedemeyer et al. 2000; Welker et al. 2001a, b). These include understanding the origin of kinetic traps, rate-determining steps in protein folding, heterogeneity ion folding pathways, dead-end species, among others (Narayan et al. 2000; Wedemeyer et al. 2000; Welker et al. 2001a, b; Weissman and Kim 1995).

The use of a "reductionist" physical chemistry approach to dissect the mechanism by which proteins fold within the ER has been key to unravelling the proceedings within this intracellular "black-box". The application of experimental protocols and biophysical tools to understand oxidative protein folding has been thoroughly reviewed in a previous edition of this series and elsewhere (Narayan 2011; Hidaka and Shimamoto 2013). We initiate this review by recapitulating our current understanding of the "structure-forming step" which has been made possible through a series of disulfide-intact folding studies and some oxidative folding scenarios. Using the structure-forming step in RNase A as a

template, we merge the interplay between a purely physical conformational process, viz. proline isomerization, with a chemical event, viz., thiol-disulfide exchange to examine the "chances" of successful acquisition of a native (biologically active) structure. The objective is to underscore the oxidative folding process which often involves a competition between chemical reactions and physical structure-forming reactions. The ability of one to dominate in rate over the other often dictates the outcome. The "state" that the intermediate that is poised to fold, resides in, often simply per chance, attenuates its "fate"; i.e. whether it folds fruitfully, or recycles back to the unfolded ensemble.

2 Oxidative Folding of RNase A

In the following sections we will revisit the oxidative folding of RNase A to recapitulate features characteristic of oxidative protein folding. Particular emphasis will be paid to the structure-forming step in oxidative protein folding using that of RNase A as an example. The folding of ribonuclease has served as a paradigm for understanding the physicochemical processes governing the regeneration of disulfide-bond-containing proteins and the folding of those proteins that lack the covalent linkage (cytosolic proteins). There are several reasons for this: It possesses a sufficient number of disulfide bonds to introduce a degree of complexity in the folding trajectory while still remaining analytically tractable for biophysical studies. By contrast, proteins with three or fewer disulfide bonds may not adequately represent the complexity of proteins that are processed through the ER (and those with greater than four disulfide bonds make separation of folding intermediates extremely difficult). The oxidative folding trajectory of RNase A encompasses factors and features including kinetic traps, local unfolding processes, temperature-dependent variations, and on-pathway intermediates that serve as a "one-pot prototype" for researchers studying oxidative protein folding (Narayan et al. 2000; Wedemeyer et al. 2000; Welker et al. 2001a, b). The details of the formation of disulfide bonds as the protein gets sequentially oxidized has been exceptionally well-characterized in that we have details of both entropic and enthalpic tendencies that impact the formation of cysteines. The disulfide-intact folding of RNase A has also been studied in-depth; with these studies serving as an analog for studying conformational folding. Within this ambit, the conformational folding of this protein has been found to proline-isomerization dependent and limited. Together, the exhaustive characterization of RNase A folding (disulfide-coupled and conformational) and the variety of pathways it adopts to acquire the native state make RNase A folding pathways exemplar for researchers and students of protein folding.

RNase A is a four-disulfide-bond containing protein that has been used as a model to understand the mechanism by which proteins fold. The native disulfide bonds in this protein are located as follows: [65–72], [40–95], [26–84], and [58–110]. The process of oxidative folding is initiated by introducing the fully-reduced protein into an "oxidative" environment involving a suitable buffer and an appropriate redox couple such as GSSG/GSH or DTT^{ox}/DTT^{red} (Rothwarf and Scheraga 1993a, b, c, d). The concentrations of the elements within the couple are chosen such as to obtain a "net" oxidizing potential.

Oxidative folding of RNase A begins with the initial oxidation of fully-reduced RNase A (R) to form an ensemble of one-disulfide-bond-containing (1S) intermediates. The preparation of R and analysis of the oxidative folding intermediates and their kinetics of formation has been previously described (Narayan 2011; Rothwarf and Scheraga 1993a, b, c, d) and will be summarized in brief here:

Native RNase A, usually sourced commercially, is denatured and reduced by introduction into a buffer containing a denaturing agent and a strong reducing agent for a period of 1 h (pH 8, 100 mM TriHCl, 6 M Gdn, 100 mM DTT^{red}). R is then desalted and introduced into a folding buffer (pH 8, 100 mM Tris-HCl, 100 mM DTT^{ox}). Note that small quantities of DTT^{red} are automatically generated from the reduction of DTT^{ox} by cysteines in reduced RNase A as a

byproduct of the oxidative folding process. Samples from the regeneration mixture are periodically withdrawn and blocked with a suitable thiol-blocking agent such as Aminomethylethanethiosulfonate (AEMTS) (Rothwarf and Scheraga 1993a, b, c, d). Blocking with this cationic reagent facilitates fractionation of the regeneration ensemble by their disulfide content and its subsequent kinetics analysis (Rothwarf and Scheraga 1993a, b, c, d). Periodically, the presence of structured intermediates that may populate the regeneration pathway can be identified by the application of a brief reduction pulse [1 mM DTT^{red}, pH 8, 2 min, no AEMTS]. The pulse serves to reduce all unstructured species back to R. By contrast, any structured intermediates and N possess buried disulfides that are not impacted by the pulse. This serves to facilitate the separation and collection of these intermediates (and N). The intermediates can be easily characterized for enzymatic activity, disulfide mapping, thermal stability and structure by first blocking their cysteines with AEMTS to prevent reshuffling. Once the disulfide-bond-connectivity has been established, the remaining cysteines can be mutated (for eg, to Alanine) to facilitate further characterization of the intermediates (Xu and Scheraga 1998; Iwaoka et al. 1998).

In RNase A, eight cysteines can form 28 distinct 1S isomers. The frequency by which individual isomers populate the 1S landscape depends upon both entropic and enthalpic contributions (Poland and Scheraga 1965; Kauzmann 1959; Xu et al. 1996; Volles et al. 1999). For example, the probability of forming a disulfide bond between cysteines 26 and 110 of RNase A is entropically highly disfavored (Xu et al. 1996). This is because these cysteines are the farthest away from each other in the chain and the resulting loop generated upon forming the [26–110] disulfide bond results in the largest loss of entropy to the peptide chain. In contrast, by purely entropic considerations, both [65–72] and [58–65] have the highest and equal probabilities of formation. Enthalpic interactions on the other hand can also influence the distribution of disulfide connectivities (Xu et al. 1996; Volles et al. 1999). Favorable enthalpic interactions bring the chain together and reduce the entropic penalty that would normally result upon disulfide-bond-induced loop closure. By contrast, unfavorable side-chain derived enthalpic interactions around the neighborhood of cysteines poised to form a disulfide bond would reduce the propensity to form that particular disulfide bond (Xu et al. 1996; Volles et al. 1999).

A second feature of the 1S ensemble is the unstructured nature of the populace. Though the protein is no longer as “free” as R, there is no evidence of structure within this ensemble. Nevertheless, attempts to characterize this ensemble by intramolecular distance measurements using FRET revealed constraints within the chain (Navon et al. 2001). The 1S ensemble, devoid of essential structure, is readily reduced back to R because it is unable to protect its disulfide bonds from the reducing agent (Narayan et al. 2000). Note that the reducing agent is present as part of the redox couple or is generated after the first cycle of disulfide bond formation in any protein). The 1S isomers are also able to freely isomerize intramolecularly with the equilibrium distribution of the 1S ensemble dictated by the entropic and enthalpic influences described above (Narayan et al. 2000; Wedemeyer et al. 2000; Welker et al. 2001a, b).

The oxidation of cysteines to disulfides continues with resulting 2S, 3S and 4S ensembles populating the folding landscape (Rothwarf and Scheraga 1993a, b, c, d); Fig. 1]. The 2S, 3S and 4S in RNase A are still unstructured and as a result their disulfides can be reduced easily or isomerize (with the exception of the 4S ensemble wherein intramolecular isomerization is not possible). Independent of the strength of the redox couple and folding conditions, a distribution of R-4S species emerges such that the species are in equilibrium with each other. The number of isomers within each ensemble in this equilibrium is governed by the number of cysteine residues in the protein. In RNase A, there are predicted to be 28 1S isomers, 210 2S isomers, 320 3S isomers and 104 4S isomers. Detailed experimental investigation of the 1S ensemble has confirmed

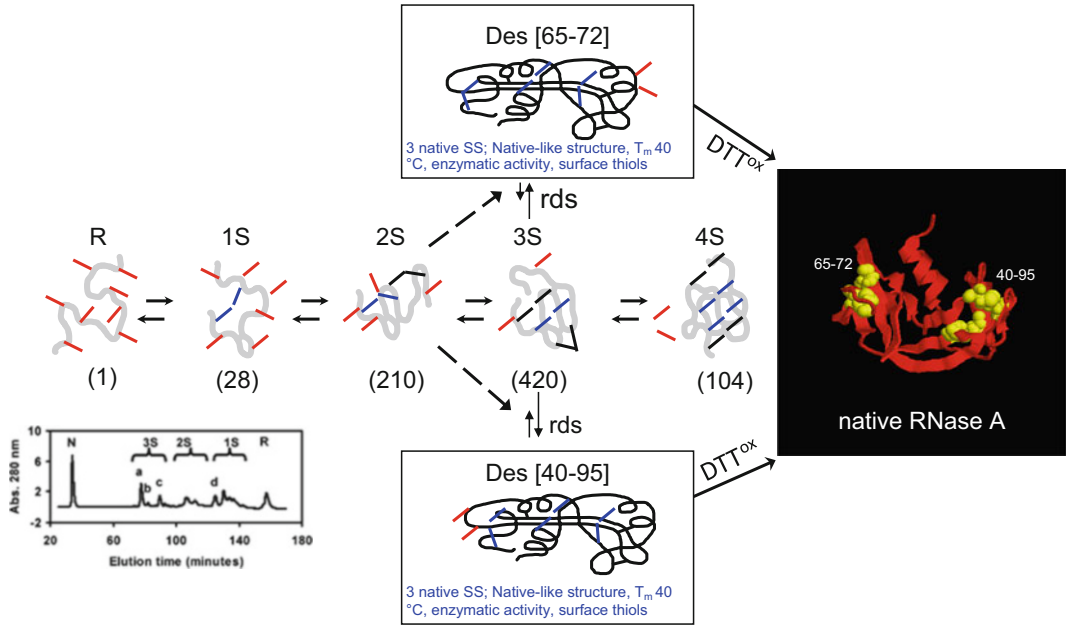

Fig. 1 Regeneration pathway of Ribonuclease A (pH 8, 25 °C; $DTT^{ox/red}$) depicting key features of the oxidative folding trajectory (Narayan et al. 2000). The fully-reduced protein R becomes increasingly oxidized to form ensembles of 1S, 2S, 3S, and 4S species wherein the numerals refer to the numbers of disulfide bonds in a species belonging to an ensemble. The possible number of isomers in each ensemble is also listed below each *n*S species. R-4S are unstructured and prone to thiol-disulfide exchange reactions (oxidation, reduction, reshuffling). Therefore, they are shown in equilibrium with one another. Select 3S molecules with native disulfide bonds can fold to form des [65–72] and des [40–95] (or 3S* species) in which native disulfide bonds are protected from thiol-disulfide-exchange reactions. The native protein (N) emerges from the 3S* species via oxidation of the remaining cysteines. The inset is a typical HPLC chromatogram in which the folding mixture is successfully fractionated using a thiol-blocking agent

the presence of all 28 1S isomers in the oxidative folding trajectory of RNase A in both the 1S ensemble and the 2S ensemble (Xu et al. 1996; Volles et al. 1999).

2.1 The Structure-Forming Step in the Oxidative Folding of RNase A

Two intermediates having three disulfide bonds each, viz. des [65–72] and des [40–95] (also called 3S* species, with the asterisk denoting structure), have been identified in the 3S ensemble to possess native-like structure (Rothwarf et al. 1998a, b); Fig. 2]. The terminology, des [x–y] reflects the missing disulfide bond in each species. Des [65–72] and des [40–95] possess melting point temperatures of 38 °C each and enzymatic activities of 95% and 5%, respectively, relative to native RNase A. These values perhaps reflect the "contribution" of the missing disulfide to the correct and stable orientation of the catalytic domain.

The native protein, N, is formed from these des species through the oxidation of their remaining cysteines (Fig. 2). The native protein is stable (T = 65 °C) and possesses 100% biological activity.

There are features pertaining to the formation of the 3S* species from the 3S ensemble that are particularly relevant to the folding landscape. As long as the folding conditions are below the melting point of the 3S* species, their formation from 3S is irreversible. This permits the 3S* species to be removed from the equilibrium distribution of 3S species (and from the R-4S pool). It facilitates the rapid formation of N, given that

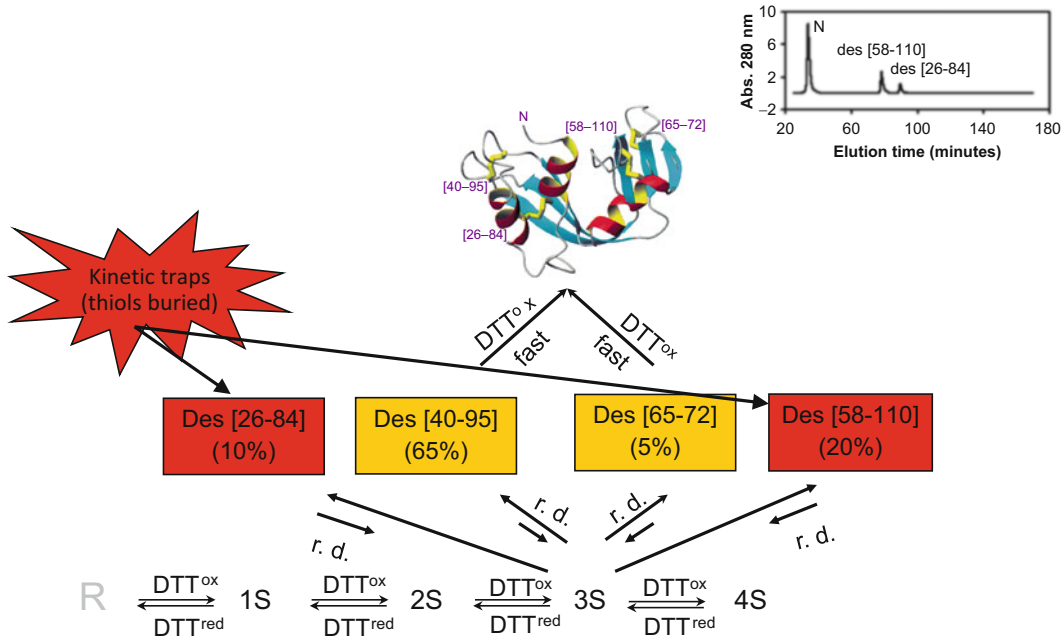

Fig. 2 Regeneration pathways of RNase A at 15 °C * (Welker et al. 1999). In addition to the characteristic features observed in Fig. 1, two kinetically trapped appear in the low-temperature regeneration pathway, These species, viz. des [26–84] and des [58–110] persist for over 4 days after initiating regeneration. They contain native, disulfide bonds, native-like structure but buried cysteines (which prevents their oxidation to N; making them kinetically trapped). With thermal transitions around 20 °C, they simply return to the pool of unstructured 3S isomers if regeneration is carried out at 25 °C. The inset is a typical HPLC chromatogram showing the products of the low-temperature refolding process when most of the unstructured intermediates had converted to N, leaving behind the two kinetically trapped species

there is no more intramolecular reshuffling and the remaining two cysteines are suitably spatially "positioned" to form a disulfide bond. It is notable that the formation of N from 3S* is also irreversible under normal folding conditions for the aforementioned reasons. Thus the acquisition of structure (specifically via the 3S* species, in RNase A) transitions the folding intermediates from an otherwise endless cycle of oxidation, reduction and reshuffling reactions to an intermediate that can acquire the final folded topology (N) at a much faster rate.

In RNase A, the formation of the 3S* species from the 3S ensembles constitutes the rate-determining step in the process R→N (Rothwarf et al. 1998a, b). It is a composite step involving thiol-disulfide exchange reactions (reshuffling or isomerization reactions) between isomers within the 3S ensemble and, a conformational folding step resulting in native-like structure. The conformational folding step results in the burial of the existing disulfide bonds and insulates them for further reshuffling (back to the 3S ensemble of isomers).

Of interest is the fact that two other 3S* species are also populated at lower temperatures. Des [58–110] and des [26–84] emerge onto the folding landscape when oxidative regeneration (refolding) is carried out at 15 °C; but not at room temperature (Welker et al. 1999); Fig. 2. These observations suggest that their thermal transitions reside between 15 and 25 °C. Furthermore, both des [58–110] and des [26–84] persist in the oxidative folding landscape even after all other intermediates have been consumed to form N, suggesting that they are kinetically trapped species (Welker et al. 2001a, b). Analysis of the tertiary structure of RNase A reveals that disulfides [58–110] and [26–84] are buried in the native structure. Therefore, there is a steric

barrier to the oxidation of cysteines 26 and 84 and cysteines 58 and 110, making des [26–84] and des [58–110] kinetically trapped. Energetically, a local unfolding event is required to expose either pair of cysteines for oxidation to the respective disulfide (Welker et al. 2001a, b). The free energy of the local unfolding process however is commensurate with the free energy of global unfolding. As a result both species are vulnerable to back-reshuffling to the 3S ensemble rather than oxidation to N.

3 Deconvoluting the Formation of 3S* from 3S

There are a total of 420 3S isomeric species that, in principle, can populate the 3S ensemble. Of these, 416 species contain one or more non-native disulfide bonds and are termed $3S_{NNU}$ (to denote the presence of non-native disulfide bonds and that the species lack structure). Any 3S species that contains one or more non-native disulfide bonds prevents it from conformational folding (Narayan et al. 2000; Wedemeyer et al. 2000; Welker et al. 2001a, b). Thus, there exists, a pool of potentially 416 species that are in equilibrium with each other through thiol-disulfide exchange (isomerization) reactions (Narayan et al. 2000). These 416 species are also in equilibrium with the rest of the unstructured species that populate the RNase A folding landscape. As discussed earlier, this equilibrium is established through oxidation and reduction reactions. Four of the 3S isomers (among the 420 species) contain only native disulfide bonds. These species are unstructured and termed $3S_{NU}$ to distinguish them from other, non-native disulfide-bond-containing, unstructured 3S species. The formation of $3S_{NU}$ takes place from $3S_{NNU}$ via isomerization of the sole non-native disulfide bond in the $3S_{NNU}$ species (Fig. 3). Thus, only those $3S_{NNU}$ species that possess two native bonds and one non-native bond can directly isomerize to $3S_{NU}$.

All four possible $3S_{NU}$ have two possible "fates" (Fig. 3). (1) The $3S_{NU}$ species can isomerize back (back-reshuffle) to a $3S_{NNU}$ species and eventually to any of the 3S isomers. This process happens by thiol-disulfide exchange reactions that are "chemical" in nature. (2) $3S_{NU}$ can conformationally fold to form a 3S* species. The 3S* species, as previously discussed, possess native-like structure (below their melting temperatures). As a result, they protect their native disulfide bonds from further intramolecular thiol-disulfide exchange (isomerization) reactions. The conformational folding process is physical in nature and involves the formation of (via secondary and tertiary interactions) near-native-like structure in RNase A. The native-like 3S* species do not backreshuffle to $3S_{NU}$ and therefore, $3S_{NU} \rightarrow 3S^*$ is unidirectional.

The formation of N from 3S* is also unidirectional via the oxidation of the remaining two cysteines in 3S*.

4 The Rate-Determining Step in RNase A Oxidative Folding

There are unimolecular and biomolecular steps in RNase A oxidative folding. The unimolecular processes are the intramolecular isomerization reactions within the 1S, 2S and 3S ensembles (R and 4 S cannot chemically isomerize). The unimolecular processes are pH dependent since they involve thiol-disulfide exchange reactions. The isomerization may also be biomolecular if it involves an external thiol-disulfide isomerase (such as Protein Disulfide Isomerase (PDI) (Gilbert 1990)) which can facilitate reshuffling. In fact, at an intracellular pH of ~6.7, "intramolecular" thiol-disulfide exchange reactions are likely to be intermolecular, because of PDI involvement, and therefore biomolecular. This is because the thiols of PDI are highly acidic with a pKa of 5.7. They would then be deprotonated at pH 6.7 and can engage/facilitate disulfide exchange in the substrate.

Bimolecular processes include, in addition to the above, oxidation and reduction reactions that help transition R towards N (via 1S, 2S, etc). These reactions are bimolecular because they either involve a small-molecule-based external redox couples, viz. GSSG/GSH, or PDI which

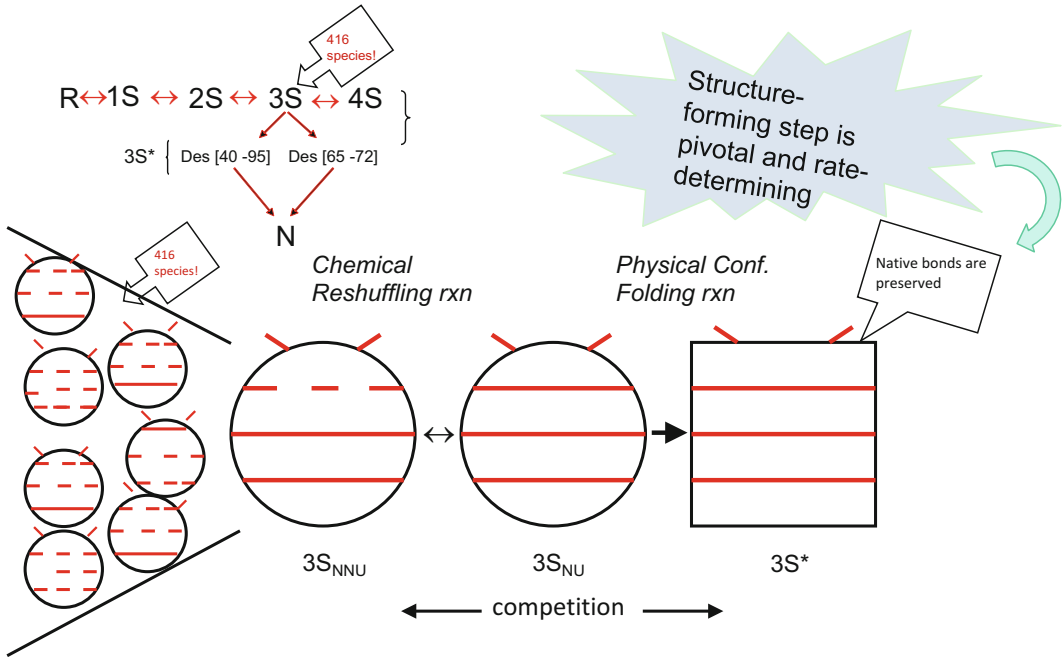

Fig. 3 Structure-coupled oxidative folding steps involves competition between chemical thiol-disulfide exchange rxns and a physical conf. folding rxn. The $3S_{NU}$ species can either conformationally fold to 3S* and structurally protect its disulfide bonds from further reshuffling or, it can reshuffle back to the 3S ensemble via $3S_{NNU}$

can also act as a reducing/oxidizing agent. Under laboratory settings, the choice and concentration of the small-molecule couple can be selected to attenuate the rate of the bimolecular steps and potentiate the regeneration landscape. For example, the use of $DTT^{ox}/^{red}$ facilitates the study of oxidative folding in the laboratory by virtue of DTT^{ox} being a relatively weak oxidizing agent (compared to GSSG) (Rothwarf and Scheraga 1993a, b, c, d). Furthermore, since DTT^{ox} does not form mixed disulfides with the protein thiols, it simplifies the folding landscape and facilitates the identification of intermediates that populate the folding trajectory (Xu et al. 1996; Volles et al. 1999).

It is quite obvious that the rate-determining step in the oxidative folding of RNase A is dependent on the nature of the redox reagent, presence of oxidoreductase chaperones such as PDI, temperature, etc. For example, in the absence of any redox couple and under unaerobic conditions, the rate-determining step in RNase A oxidative folding would be the formation of 1S from R. However, under "standard" folding conditions, the rate-determining step involves the formation of two 3S* species, viz. des [65–92] and des [40–95], from the 3S ensemble.

The rate limiting-step in RNase folding is the 3S to 3S* step (Fig. 3). It is the structure-forming juncture in the oxidative folding of RNase A. It is also, very often, the rate-determining step in oxidative folding of other proteins.

Using RNase A folding as a model, we will discuss why this is so in the following section. Understanding this step provides a window into protein folding and as a result, subcellular trafficking, in the endoplasmic reticulum. Towards this, we will examine the formation of 3S* from 3S using the formation of N from disulfide-intact denatured protein (U), as an analog. We will also review data that have been gathered on the formation of 3S* from 3S as a function of pH.

It is to be noted that the statistical rate of regeneration of RNase A is likely to be commensurate with its disulfide complexity. I.e., a four-disulfide-bond-containing protein is likely to

regenerate much more slowly that say, a one disulfide-bond-containing protein. This is because it is likely to populate an exponentially greater number of non-native disulfide-bond-containing intermediates. Conversely, the statistical regeneration rate of a one-disulfide-bond-containing protein with only two cysteines in the sequence is like to be higher than a corresponding one-disulfide-bond-containing protein with three cysteines in the sequence. The actual regeneration rate is compounded by a variety of folding factors that may impact disulfide-bond-acquisition and conformational folding of each protein. The thermodynamic stabilities of intermediates and the presence of kinetic traps also influence folding rates. For example, in RNase A both des [26–84] and des [58–110], the two kinetically trapped species, persist in the regeneration mixture for a period of days; similar to the trap found in BPTI. The thermodynamic stabilities of des [65–72] and des [40–95] are likely similar to those of other intermediates because they are found on the regeneration pathways at room temperature. In vivo, the thermodynamic stability may be somewhat compromised as the ambient temperature is 37 °C and likely closer to the melting points of some intermediates in proteins.

5 The Folding of Disulfide-Intact RNase A: Role of Proline Isomerization

RNase A has 4 Prolines at positions 42, 93, 114 and 117. In native RNase A (N), two of these prolines possess cis X − Pro peptide bonds (Tyr 92 − Pro 93 and Asn 113 − Pro 114), while the other two are trans X − Pro peptide bonds (Lys 41 − Pro 42 and Val 116 − Pro 117) (Wlodawer et al. 1988). When disulfide-intact bovine pancreatic ribonuclease A (RNase A) is unfolded (U), the X − Pro peptide bonds undergo cis − trans isomerization and eventually equilibrate to form a distribution of cis and trans conformers around their respective X-Pro peptide bonds. Under unfolded conditions, the equilibrium distribution is skewed to favor the trans conformation (70:30). Even though almost iso-energetic, the kinetic barrier between the conformers is large due to the presence of the double bond. The barrier height significantly restricts the cis isomerization rate and necessitates the presence of a catalyst (such as peptidyl prolyl isomerase (PPI)). In the presence of tertiary structure, the isomerization is expected to be even slower or non-existent. Therefore, in the native (or native-like) state, the prolines are said to be either "cis" or "trans" locked. Under such conditions, it is likely that "local" fluctuations are necessary to permit isomerization (or access to PPI).

In sum and substance, multiple species having different conformations about these X − Pro peptide bonds are present in the unfolded state of the protein. For example, the statistical fraction of the unfolded biopolymer which contains "all-cis" X-Pro peptide bonds would equal 0.3X0.3X0.3X0.3 = 0.0081 0r 0.81% of the unfolded molecules. By contrast, the fraction of unfolded molecules possessing all-trans linkages would equal (0.7)^4 = 24%; and so on.

When fully-denatured, disulfide-intact, RNase A (U), is allowed to refold in a folding buffer, there are multiple phases associated with the refolding process (Houry et al. 1994, 1995; Houry and Scheraga 1996). These phases, termed U_{vf}, U_f, U_s^{II}, and U_s^{I} associate with refolding time constants on the millisecond, millisecond to second, second to tens of seconds, and hundreds of seconds time scales, respectively (Houry et al. 1994, 1995; Houry and Scheraga 1996). These phases have been attributed to proline isomerization that is a part of the trajectory to the native structure; and precede the formation of native structure. The differences in conformations at the X − Pro peptide bonds result in different refolding rates for these unfolded species. For example, those unfolded disulfide-intact RNase A molecules that per chance possess the X-Pro conformations that coincide with the native (locked) X-Pro conformations would be "primed" to fold to N. Therefore, their refolding time constants would be the shortest. By contrast, those unfolded RNase A molecules with their X-pro bonds exactly out of phase w.r.t. their

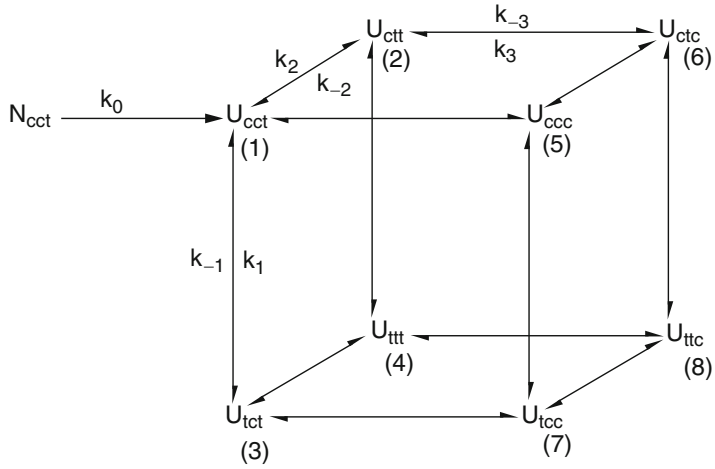

Fig. 4 Box model. The Proline isomerization depending (un)folding of disulfide-intact isomerase is illustrated by a "box" model. The time taken to fold (U → N) is dependent upon the disposition of X-Pro peptide bonds around the three essential prolines of RNase A. In the native state, the X-Pro peptide bonds around prolines 93, 114, 117 are locked in the cis, cis, and trans state. However, in the unfolded state, there are eight possible combinations the three X-Pro peptide bonds could adopt. Thus, the refolding time is fastest for U_{cct}; an unfolded intermediate whose X-Pro peptide bonds, per chance, is in the same conformation as that in N

dispositions in N would be the slowest to refold. The former scenario has been validated using a "double-jump" experiment in which native RNase A was introduced into unfolding conditions before being rapidly reintroduced into a refolding buffer (via dilution). The dwell-time of 1s in the "unfolding condition", prior to the second "jump" into refolding conditions, is sufficient to result in the complete loss of tertiary structure. However, the time spent in the unfolded state (1s) is not sufficient for the prolines to isomerize to their equilibrium unfolded state. Thus, reintroduction into "folding conditions" immediately after the 1s "unfolding condition dwell-time" resulted in a rapid (milli-second time constant) and monophasic folding of RNase A to N. By varying the "dwell-time" in the unfolded state, other phases were populated as a function of increasing time "spent" in the unfolded state.

These data, along with other data involving sequential mutations of the prolines alanine (which favors a trans-locked state) indicate that three of the four prolines, viz. 93, 114, 117 are "essential" to RNase A disulfide-intact folding. I. e., they impact the rate of conformational folding of RNase A (the U → N process). No effect on the refolding kinetics of the protein is observed from the isomerization of the X − Pro 42 peptide bond.

Based on the individual contributions of the three essential prolines to the refolding kinetics of RNase A, a box model for the conformational folding of RNase A has been proposed (Fig. 4). Given the reversible nature of the N to U transitions, for simplicity we will examine disulfide-intact conformational unfolding of RNase A using the box model.

Each vertex of the box represents one of the eight possible isomeric states that the three prolines could exist in. For example, U_{cct} indicates an unfolded state with proline 93, 114 and 117 in their native conformations [the subscripts refer to the cis or trans states and the order in which they appear relate to 93, 114 and 117, respectively]. In other words, it is the product formed from N (N_{cct}) when the native protein introduced into unfolding conditions with an "unfolded state dwell-time" of 1s. Thus U_{cct} lies closest to N since its prolines are already "aligned" with the native state conformation. Consequentially, it possesses the fastest refolding time (millisecond time constant) as proline isomerization is not involved when going from U_{cct} to N_{cct}. As the prolines start

isomerizing (by permitting U_{cct} to remain in an unfolding mileu for longer time frames), the time to refold back to N increases and the disulfide-intact unfolded intermediates occupy vertices farther away from the U_{cct} vertex. It is to be noted that the box model considers "one isomerization" at a time even though the isomerization reactions are likely independent of one another. The intermediate U_{ctt} is two steps away from folding to N_{cct} because Pro 114 is in the trans state in U_{ctt} and needs to isomerize to cis (U_{cct}) before becoming locked in the native state (N_{cct}). U_{ctt} must proceed via U_{cct} before it can become N_{cct}. The disulfide-intact intermediate Utcc is the farthest from U_{cct} (and from N_{cct}) since its prolines are in exactly the opposite conformation as the native state. It must proceed via three steps (intermediates) before it can fold to N (N_{cct}).

Using disulfide-intact RNase A as an example, the box model elegantly illustrates rate-determining features that may be encountered steps in the conformational folding of a protein. In RNase A, conformational folding is particularly complicated by the need for three (of four) prolines to isomerize to their native dispositions prior to conformational folding (and "locking-in" of those prolines via tertiary interactions).

6 The Structure-Forming Step in Oxidative Protein Folding

We now integrate our understanding of the 3S to 3S* transition in the oxidative folding of RNase A along with our knowledge of disulfide-intact RNase A conformational folding to delineate the structure-forming juncture in oxidative protein folding.

The four possible $3S_{NU}$ species are expected to be conformationally nearly identical to U. The only difference is the lack of a fourth native disulfide bond in $3S_{NU}$ relative to U. Therefore, each of the four $3S_{NU}$ species can exist in potentially eight "locally" heterogenous conformations via variations in the dispositions of the three essential prolines. For example, $3S_{NU}$ species lacking the [40–95] disulfide bond could exist as an ensemble of the following unfolded state intermediates: $3S_{NU\ cct}$; $3S_{NU\ ctt}$; $3S_{NU\ ctc}$; $3S_{NU\ ccc}$; $3S_{NU\ tct}$; $3S_{NU\ tcc}$; $3S_{NU\ ttc}$; $3S_{NU\ ttt}$.

From the discussion involving the time constants for the proline-isomerization-dependent/limited U → N processes, we can infer that similar time-constants and folding constraints characterize the $3S_{NU}$ to 3S* conformational transition. Therefore, we can reconsider the box model within the context of oxidative folding pathway (Fig. 5a). This is possible by incorporating both, chemical oxidative folding elements and physical (in this case proline isomerization and conformational folding) feature, in the box model. This is achieved by placing (each of the four) three-disulfide-containing $3S_{NU}$ species at the corresponding proline-conformation dependent vertex. An example involving a $3S_{NU}$ species lacking the [40–95] disulfide bond is shown within the context of the box model (Fig. 5a).

From prior reading, it is evident that a $3S_{NU}$ species that has its prolines in the native conformation ($3S_{NU\ cct}$) is poised to fold on a millisecond time-scale to 3S* (or $3S^*_{cct}$) (Fig. 5b). Thus, such a species ($3S_{NU\ cct}$) can "outcompete" the competing chemical thiol-disulfide exchange reaction that would otherwise result in $3S_{NU}$ becoming reshuffled to $3S_{NNU}$ (Fig. 5b). Three other species ($3S_{NUctt}$; $3S_{NUccc}$; $3S_{NU\ tct}$) are also likely to outcompete and therefore, evade, the reshuffling "threat" (Fig. 5b). While each of these species is one step away from $3S_{NUcct}$ and likely to possess millisecond to second folding time-constants, they remain at a greater "risk" of becoming reshuffled to $3S_{NNU}$ than is $3S_{NU\ cct}$. The remainder of the [40–95] $3S_{NU}$ isomers are likely to become back-reshuffled to $3S_{NNU}$ considering their prolonged refolding times.

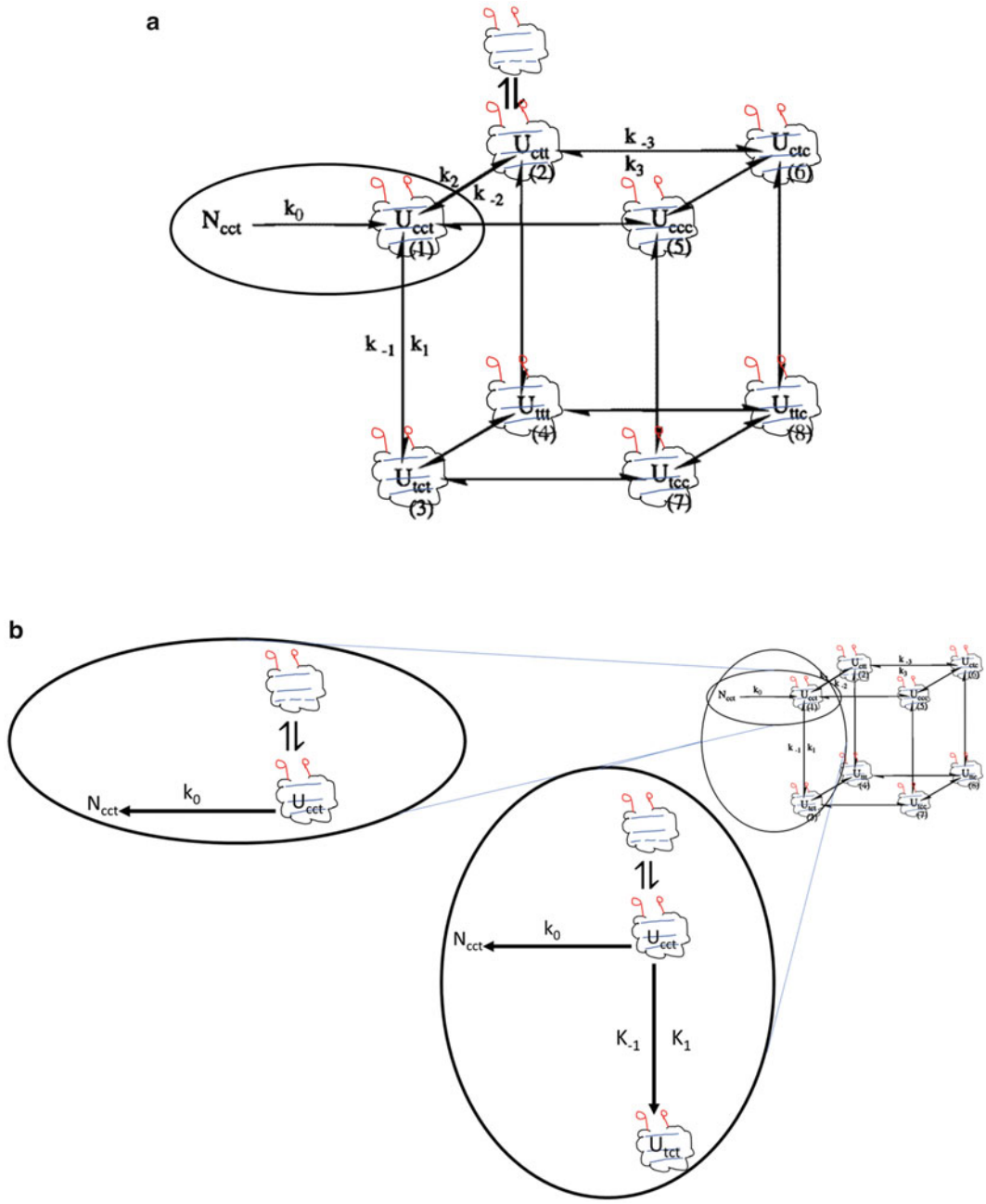

Fig. 5 (**a**) Proline-isomerization and the 3S → 3S* transition. Superimposition of a typical $3S_{NU}$ species over the box model. For example, a 3_{NU} species lacking the [40–95] disulfide bond can have eight different conformations of the X-Pro peptide bond around the three essential prolines. There are three other 3_{NU} species, all of which are poised to fold; but are proline-isomerization limited. (**b**) Two 3_{NU} species with different conformations around their X-Pro peptide bonds. $3_{NU\ cct}$ possesses the native conformation of X-pro peptide bonds and can rapidly (millisecond time-scale) fold to form $3S^*_{cct}$ while evading reshuffling to $3S_{NNU}$. By contrast $3S_{NU\ tct}$ is two steps away from being able to form $3S^*_{cct}$. Its time to refold to $3S^*_{cct}$ is therefore longer and while likely to fold to 3S*, it "risks" being reshuffled to $3S_{NNU}$

6.1 Factors Impacting the Competition Between Conformational Folding and Chemical Reshuffling ($3S_{NNU} \leftrightharpoons 3S_{NU} \rightarrow 3S^*$)

It is to be noted that the chemical disulfide-reshuffling reaction is highly pH dependent and therefore slight changes in the pH within the ER can amplify (or diminish) reshuffling rates. An increase in pH will favor reshuffling rates and may tilt the competition towards chemical reshuffling and formation of $3S_{NNU}$ since moderate changes in pH do not impact proline isomerization rates. However, unlike pH changes (fluctuation in these are not very plausible), the presence of an oxidoreductase can more practically impact chemical reshuffling. Furthermore, the presence of PDI is also likely to tilt the outcome of the $3S_{NNU} \leftrightharpoons 3S_{NU} \rightarrow 3S^*$ process towards $3S_{NNU}$ formation. This is because though PDI has no outcome on proline isomerization, it is likely to enhance the reshuffling process; making it competitive even at pH 7.4 with the conformational folding of fast folders. The presence of subcellular peptidyl prolyl isomerase can accelerate the isomerization of X-Pro peptide bonds and facilitate slower folding isomers to fold faster. Other factors that can increase thiol-disulfide exchange could include high density of substrates within the ER, thereby permitting intermolecular thiol-disulfide exchange. Overall, the scenarios is likely to be complicated by a variety of "folding" considerations.

7 Conclusion

The ability of a disulfide-bond containing protein to rapidly bury its disulfide bonds within native structure is key towards maturation. Thus conformational folding to a native or native-like state is critical. Any compromise in this process will result in "back-reshuffling" to the equilibrium pool of unstructured intermediates. The same principle holds true for purely conformational folders (cytosolic proteins). Conformational folding to form the native structure in such proteins exists in competition with water, salts, other amino acids and other proteins. Delays in folding increase the chances of terminal misfolding and degradation.

Cargo trafficking through the ER has an uphill journey before it can get successfully secreted. We anticipate that the first principles of protein folding, gleaned from test-tube studies, are applicable to the more complex confines of the ER. This is because "ex-vitro" experiments have relied on conditions that somewhat mimic those found in the confines of cellular compartments. The choice of pH, redox couples, inclusion of relevant chaperones in folding studies of RNase A and other disulfide-bond-containing proteins have been designed bearing in mind the intracellular milieu found within the ER. Furthermore, across slight variations in folding conditions, many proteins only demonstrate changes in the "rates of regeneration". Others adopt alternative pathways with the regenerative flux redistributed between the original and new-found pathways.

Yet some other variations in conditions can be expected that may impact regeneration rate but are unlike to impact the folding trajectory. For example, a primary difference between test-tube experiments and folding within the ER is the presence of high protein concentrations in the latter space. This could increase the tendency of the biopolymers to aggregate before they can fold; thereby reducing their "yield" and/or regeneration rate. Furthermore, the complexity of the ER is such that multiple chaperones and folding factors are likely to act in concert on the disulfide-bond-containing substrate trafficking through. Nevertheless, even under such conditions, the fundamental principles governing protein folding in the ER and in the cytoplasm still remain the same as has been derived from a robust choice of physico-chemical conditions applied by a many number of researchers in this field.

In the ER, the "commitment" to secretion is in competition with statistically higher tendencies

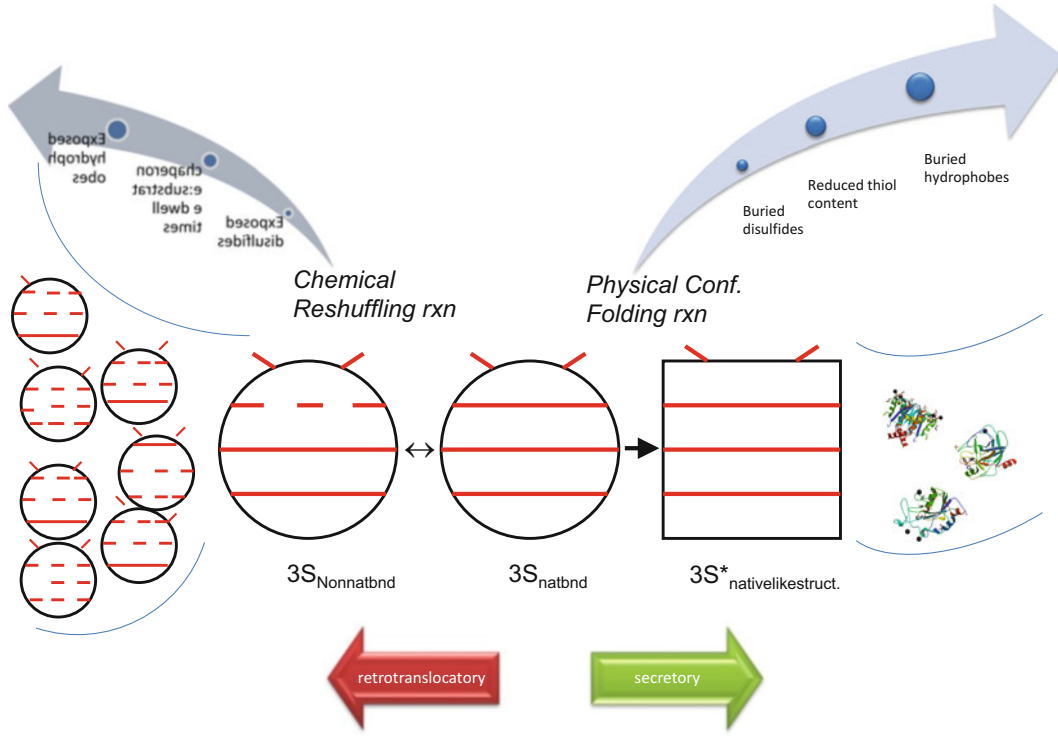

Fig. 6 Within the ER, a disulfide-bond-containing protein has two fates. It can either fold oxidatively fold successfully and get secreted outside the ER. Or, it can misfold. Terminal or successive misfolding would trigger retrotranslocatory apparatus and result in degradation. *In vivo*, there are several factors affecting the "fate" of a disulfide-bond-containing protein and traffic within the ER

or factors that bias the cargo towards retrotranslocation (Fig. 6). For example, the myriad number of non-native chemical and physical isomers increase the proteins' "dwell-time" in the unfolded state. This leads to a risk of misfolding, aggregation and retrotranslocation. To personify, it is clearly in the best "interests" of the protein to fold- a discussion for a later review. The ability to fold however, is predicated upon the "per chance" occurrence of the correct pre-folding conditions. I.e., by the chance occurrence of a sufficient number of native disulfide bonds that can trigger conformational folding; by the chance occurrence of the "native" complement of X-Pro peptide bonds. Extraneous factors such as biological catalysts that increase the frequency with which the per chance occurrence of intrinsic native factors are sampled simply provide yet another opportunity for the protein to fold and protect its key features (disulfide bonds, prolines, salt-bridges, van der Waal's forces) from dismantling. They do not influence the functional structure of the protein which is simply encoded in its sequence.

A thorough understanding of protein folding pathways is essential for facilitating the expression and folding of proteins not only for basic research but also for commercial applications as well. These include peptides like insulin and immunotoxins such as conotoxin (Kubo et al. 1996; Hober et al. 1997; Milner et al. 1999; Yang et al. 1999; Bulaj et al. 2003; Bulaj and Olivera 2008). Such an understanding is also critical for the introduction of non-native motifs within proteins including catalytic cysteines. A number of papers have also reviewed the techniques used to increase the rate of folding and the yield of the biologically active folded form in the aforementioned scenarios (de Marco 2009; Berkmen 2012; Ke and Berkmen 2014;

Stewart-Jones et al. 2015). Some of the strategies include co-expression of chaperones or the addition of small molecule folding adjuvants, tagging constructs of either leader sequences that export disulfide bond containing proteins to the appropriate folding loci in the cell or include helper proteins that can assist in folding, high-throughput selection of suitable clones that eliminate redundant disulfide bonds, and tuning of redox conditions. The overarching objective in all these cases is to sway the competition between folding and aggregation to favor rapid folding and burial of hydrophobic residues. Inroads have also been made to introduce disulfide bonds and also replace cysteines with Selenocysteine as potential mechanisms to intramolecularly catalyze disulfide bond formation (Arai et al. 2017). Other techniques have explored and exploited pro-domains in catalyzing disulfide-associated folding (Hidaka et al. 2000). Whereas the results have met with success, here too, the principles gathered from experimentally determine protein folding trajectories apply. Cysteines that are buried have the potential to result in the formation of kinetically-trapped intermediates and reduce folding yields/slow down regeneration rates (Narayan et al. 2001). Thus, incorrectly introduced cysteines can be detrimental. Furthermore, the introduction of every additional cysteine in a protein adds to the total number of intermediates in the folding ensemble. Particularly, it specifically populates the non-native ensemble and would therefore likely delay oxidative folding when considered from a statistical view-point.

In sum and substance, an intimate knowledge of oxidative folding mechanisms drives an understanding of subcellular trafficking, events that can promote misfolding and the emergence of diseases associated with improper folding such as Parkinson's, Alzheimer's, Huntington and mad-cow among others. Such a knowledge can also guide the efficient regeneration of proteins that have found biomedical and industrial use.

Acknowledgement MN acknowledges NIH 1SC3 GM111200 01A1. The author wishes to thank Ms. Brenda Rubi Torres for creating some of the artwork in this chapter and Mr. Gyan M. Narayan for help with the manuscript. This work, is in part, an outcome of pedagogical techniques used by the author for a Biophysical Chemistry class taught by him in Spring 2016 (CHEM 4335). MN would like to acknowledge Jose A. Barragan, Homero R. Garcia, Natalia Luna, Vanessa I. Navarro, Stefani Perez Torres, and Alejandro Rodriguez for engaging in scintillating discussions on the subject of "The Structure-Forming Juncture in Oxidative Protein Folding: What happens in the ER?"

This work is in Compliance with Ethical Standards.

Conflicts of Interest The author declares no conflicts of interest.

Ethical Approval This article does not contain any studies with human participants or animals performed by any of the authors.

References

Arai K, Takei T, Okumura M, Watanabe S, Amagai Y, Asahina Y, Moroder L, Hojo H, Inaba K, Iwaoka M (2017) Preparation of Selenoinsulin as a long-lasting insulin analogue. Angew Chem Int Ed Engl 56:5522–5526

Arolas JL, Bronsoms S, Lorenzo J, Aviles FX, Chang JY, Ventura S (2004) Role of kinetic intermediates in the folding of leech carboxypeptidase inhibitor. J Biol Chem 279:37261–37270

Arolas JL, Aviles FX, Chang JY, Ventura S (2006) Folding of small disulfide-rich proteins: clarifying the puzzle. Trends Biochem Sci 31:292–301

Berkmen M (2012) Production of disulfide-bonded proteins in Escherichia Coli. Protein Expr Purif 82:240–251

Bulaj G, Olivera BM (2008) Folding of conotoxins: formation of the native disulfide bridges during chemical synthesis and biosynthesis of Conus peptides. Antioxid Redox Signal 10:141–155

Bulaj G, Buczek O, Goodsell I, Jimenez EC, Kranski J, Nielsen JS, Garrett JE, Olivera BM (2003) Efficient oxidative folding of conotoxins and the radiation of venomous cone snails. Proc Natl Acad Sci U S A 100 (Suppl 2):14562–14568

de Marco A (2009) Strategies for successful recombinant expression of disulfide bond-dependent proteins in Escherichia Coli. Microb Cell Factories 14:8–26

Ewbank JJ, Creighton TE (1993a) Pathway of disulfide-coupled unfolding and refolding of bovine α-lactalbumin. Biochemistry 32:3677–3693

Ewbank JJ, Creighton TE (1993b) Structural characterization of the disulfide folding intermediates of bovine α-lactalbumin. Biochemistry 32:3694–3707

Gilbert HF (1990) Molecular and cellular aspects of thiol–disulfide exchange. In: Meister A (ed) Advances in enzymology and related areas of molecular biology, volume 63. Wiley, Hoboken

Hidaka Y, Shimamoto S (2013) Folding of peptides and proteins: role of disulfide bonds, recent developments. Biomol Concepts 4:597–604

Hidaka Y, Shimono C, Ohno M, Okumura N, Adermann K, Forssmann WG, Shimonishi Y (2000) Dual function of the propeptide of prouroguanylin in the folding of the mature peptide: disulfide-coupled folding and dimerization. J Biol Chem 275:25155–25162

Hober S, Uhlen M, Nilsson B (1997) Disulfide exchange folding of disulfide mutants of insulin-like growth factor I in vitro. Biochemistry 36:4616–4622

Houry WA, Scheraga HA (1996) Nature of the unfolded state of ribonuclease A: effect of cis-trans X-Pro peptide bond isomerization. Biochemistry 35:11719–11733

Houry WA, Rothwarf DM, Scheraga HA (1994) A very fast phase in the refolding of disulfide-intact ribonuclease A: implications for the refolding and unfolding pathways. Biochemistry 33:2516–2530

Houry WA, Rothwarf DM, Scheraga HA (1995) The nature of the initial step in the conformational folding of disulphide-intact ribonuclease A. Nat Struct Biol 2:495–503

Iwaoka M, Juminaga D, Scheraga HA (1998) Regeneration of three-disulfide mutants of bovine pancreatic ribonuclease a missing the 65−72 disulfide bond: characterization of a minor folding pathway of ribonuclease A and kinetic roles of Cys65 and Cys72. Biochemistry 37:4490–4501

Kauzmann W (1959) Relative probabilities of isomers in cystine-containing randomly coiled polypeptides. In: Benesch R, Benesc RE, Boyer PD, Klotz IM, Middlebrook WR, Szent-Györgyi AG, Schwarz DR (eds) Symposium on sulfur in proteins. Academic Press, New York. Chapter II.2

Ke N, Berkmen M (2014) Production of disulfide-bonded proteins in Escherichia Coli. Curr Protoc Mol Biol 108:16. 1B.1–21

Kubo S, Chino N, Kimura T, Sakakibara S (1996) Oxidative folding of omega-conotoxin MVIIC: effects of temperature and salt. Biopolymers 38:733–744

Milner SJ, Carver JA, Ballard FJ, Francis GL (1999) Probing the disulfide folding pathway of insulin-like growth factor-I. Biotechnol Bioeng 62:693–703

Narayan M (2011) The case of oxidative folding of ribonuclease A: factors impacting fold maturation of ER-processed proteins: the case of oxidative folding of ribonuclease A. In: Chang RJY, Ventura S (eds) Folding of disulfide proteins, Protein reviews (Zouhair Atassi M). Springer. http://link.springer.com/book/10.1007%2F978-1-4419-7273-6#page-1

Narayan M, Welker E, Wedemeyer WJ, Scheraga HA (2000) Oxidative folding of proteins. Acc Chem Res 33:805–812

Narayan M, Welker E, Scheraga HA (2001) Development of a novel method to study the rate-determining step during protein regeneration: application to the oxidative folding of RNase A at low temperature reveals BPTI-like kinetic traps. J Am Chem Soc 123:2909–2910

Navon A, Ittah V, Landsman P, Scheraga HA, Haas E (2001) Distributions of intramolecular distances in the reduced and denatured states of bovine pancreatic ribonuclease A. Folding initiation structures in the C-terminal portions of the reduced protein. Biochemistry 40:105–118

Oas TG, Kim PS (1988) A peptide model of a protein folding intermediate. Nature 336:42–48

Pace CN, Creighton TE (1986) The disulphide folding pathway of ribonuclease T1. J Mol Biol 188:477–486

Pace CN, Grimsley GR, Thomson JA, Barnett BJ (1988) Conformational stability and activity of Ribonuclease T_1 with zero, one, and two intact disulfide bonds. J Biol Chem 263:11820–11825

Poland DC, Scheraga HA (1965) Statistical mechanics of noncovalent bonds in Polyamino acids. VIII covalent loops in proteins. Biopolymers 3:379–399

Radford SE, Dobson CM, Evans PA (1992) The folding of hen lysozyme involves partially structured intermediates and multiple pathways. Nature 358:302–307

Rothwarf DM, Scheraga HA (1993a) Regeneration of bovine pancreatic ribonuclease A. 1. Steady-state distribution. Biochemistry 32:2671–2679

Rothwarf DM, Scheraga HA (1993b) Regeneration of bovine pancreatic ribonuclease A. 2. Kinetics of regeneration. Biochemistry 32:2680–2689

Rothwarf DM, Scheraga HA (1993c) Regeneration of bovine pancreatic ribonuclease A. 3. Dependence on the nature of the redox reagent. Biochemistry 32:2690–2697. Erratum in: Biochemistry 1993 32:7064

Rothwarf DM, Scheraga HA (1993d) Regeneration of bovine pancreatic ribonuclease A. 4. Temperature dependence of the regeneration rate. Biochemistry 32:2698–2703

Rothwarf DM, Li YJ, Scheraga HA (1998a) Regeneration of bovine pancreatic ribonuclease A: identification of two nativelike three-disulfide intermediates involved in separate pathways. Biochemistry 37:3760–3766

Rothwarf DM, Li YJ, Scheraga HA (1998b) Regeneration of bovine pancreatic ribonuclease A: detailed kinetic analysis of two independent folding pathways. Biochemistry 37:3767–3776

Roux P, Ruoppolo M, Chaffotte A-F, Goldberg M (1999) Comparison of the kinetics of SS-bond, secondary structure, and active site formation during refolding of reduced denatured hen egg white lysozyme. Protein Sci 8:2751–2760

Stewart-Jones GB, Thomas PV, Chen M, Druz A, Joyce MG, Kong WP, Sastry M, Soto C, Yang Y, Zhang B, Chen L, Chuang GY, Georgiev IS, McLellan JS, Srivatsan S, Zhou T, Baxa U, Mascola JR, Graham

BS, Kwong PD (2015) A cysteine zipper stabilizes a pre-fusion F glycoprotein vaccine for respiratory syncytial virus. PLoS One 10:e0128779

Thornton JM (1981) Disulphide bridges in globular proteins. J Mol Biol 151:261–287

van den Berg B, Chung EW, Robinson CV, Mateo PL, Dobson CM (1999) The oxidative refolding of hen lysozyme and its catalysis by protein disulfide isomerase. EMBO J 18:4794–4803

Volles MJ, Xu X, Scheraga HA (1999) Distribution of disulfide bonds in the two-disulfide intermediates in the regeneration of bovine pancreatic ribonuclease A: further insights into the folding process. Biochemistry 38:7284–7293

Wedemeyer WJ, Welker E, Narayan M, Scheraga HA (2000) Disulfide bonds and protein folding. Biochemistry 39:4207–4216

Weissman JS, Kim PS (1995) A kinetic explanation for the rearrangement pathway of BPTI folding. Nat Struct Biol 2:1123–1130

Welker E, Narayan M, Volles MJ, Scheraga HA (1999) Two new structured intermediates in the oxidative folding of RNase A. FEBS Lett 460:477–479

Welker E, Narayan M, Wedemeyer WJ, Scheraga HA (2001a) Structural determinants of oxidative folding in proteins. Proc Natl Acad Sci U S A 98:2312–2316

Welker E, Wedemeyer WJ, Narayan M, Scheraga HA (2001b) Coupling of conformational folding and disulfide-bond reactions in oxidative folding of proteins. Biochemistry 40:9059–9064

Wlodawer A, Svensson LA, Sjölin L, Gilliland GL (1988) Structure of phosphate-free ribonuclease A refined at 1.26 A. Biochemistry 27:2705–2717

Xu X, Scheraga HA (1998) Kinetic folding pathway of a three-disulfide mutant of bovine pancreatic ribonuclease A missing the [40–95] disulfide bond. Biochemistry 37:7561–7571

Xu X, Rothwarf DM, Scheraga HA (1996) Nonrandom distribution of the one-disulfide intermediates in the regeneration of ribonuclease A. Biochemistry 35:6406–6417

Yang Y, Wu J, Watson JT (1999) Probing the folding pathways of long R(3) insulin-like growth factor-I (LR(3)IGF-I) and IGF-I via capture and identification of disulfide intermediates by cyanylation methodology and mass spectrometry. J Biol Chem 274:37598–37604

Yu MH, Weissman JS, Kim PS (1995) Contributions of individual side-chains to the stability of BPTI examined by alanine-scanning mutagenesis. J Mol Biol 249:388–397

Adv Exp Med Biol - Protein Reviews (2017) 2:181–202
DOI 10.1007/5584_2017_94

Published online: 9 September 2017

Polyspecificity of Anti-lipid A Antibodies and Its Relevance to the Development of Autoimmunity

Omid Haji-Ghassemi, Susannah M.L. Gagnon, Sven Müller-Loennies, and Stephen V. Evans

Abstract

The process of natural selection favours germ-line gene segments that encode CDRs that have the ability to recognize a range of structurally related antigens. This presents an immunological advantage to the host, as it can confer protection against a common pathogen and still cope with new or changing antigens. Cross-reactive and polyspecific antibodies also play a central role in autoimmune responses, and a link has been shown to exist between auto-reactive B cells and certain bacterial infections. Bacterial DNA, lipids, and carbohydrates have been implicated in the progression of autoimmune diseases such as systemic lupus erythematosus. As well, reports of anti-lipid A antibody polyspecificity towards single-stranded DNA together with the observed sequence homology amongst isolated auto- and anti-lipid A antibodies has prompted further study of this phenomenon. Though the lipid A epitope appears cryptic during Gram-negative bacterial infection, there have been several reported instances of lipid A-specific antibodies isolated from human sera, some of which have exhibited polyspecificity for single stranded DNA. In such cases, the breakdown of negative selection through polyspecificity can have the unfortunate consequence of autoimmune disease. This review

The atomic coordinates and structure factors for all structures discussed are available in the Protein Data Bank, Research Collaborators for Structural Bioinformatics, Rutgers University, New Brunswick, NJ (http://www.rcsb.org). See Table I.

O. Haji-Ghassemi
Department of Biochemistry and Molecular Biology, University of British Columbia, Vancouver, BC V6T 1Z3, Canada

S.M.L. Gagnon and S.V. Evans (✉)
Department of Biochemistry and Microbiology, University of Victoria, Victoria, BC V8P 3P6, Canada
e-mail: svevans@uvic.ca

S. Müller-Loennies (✉)
Research Center Borstel, Leibniz-Center for Medicine and Biosciences, Parkallee 22, Borstel D-23845, Germany
e-mail: sml@fz-borstel.de

summarizes current knowledge regarding such antibodies and emphasizes the features of S1-15, A6, and S55-5, anti-lipid A antibodies whose structures were recently determined by X-ray crystallography.

Keywords
Anti-carbohydrate antibodies • Autoimmune disease • Cross-reactivity • Polyspecificity • X-ray crystal structures

Abbreviations

ANA	anti-nuclear antibodies
APS	antiphospholipid syndrome
Fc	fragment crystallizable
FDC	follicular dendritic cells
Fv	fragment variable
MCTD	mixed connective tissue disease
MS	multiple sclerosis
RA	rheumatoid arthritis
SLE	systemic lupus erythematosus
V_H	variable domain of the heavy chain
V_L	variable domain of the light chain

1 Introduction

Paul Ehrlich was the first scientist to introduce the concept of immunological self/non-self discrimination, coining the term "Horror Autotoxicus" (Silverstein 2001), which he described as an organism's unwillingness to endanger itself by forming toxic self- or auto-antibodies (*i.e.* antibodies that bind host structures). Burnet expanded upon this idea, correctly predicting the mechanism through which the immune system distinguishes self- from non-self-antigens, when he proposed that self-reactive lymphocytes are removed before they can mature in a process called "clonal deletion" (Burnet 1959, 2007). This led to the notion that self-reactive lymphocytes might escape deletion and inactivation (anergy) in the periphery (Nossal 1996). Currently, according to the American Autoimmune Related Diseases Association Inc. (AARDA), at least 80 different autoimmune diseases afflict over 50 million US Americans (https://www.aarda.org/autoimmune-information/autoimmune-statistics), and the global incidence of these diseases is on the rise (Lerner et al. 2015).

A multi-disciplinary approach has advanced our understanding of the mechanisms underlying autoimmune disease (AD) pathogenesis. While some ADs have a clear genetic basis (*e.g.* autoimmune polyendocrinopathy syndrome type I), where a single gene can cause the disease phenotype, an external trigger is usually required for onset and progression (Su and Anderson 2009). All individuals are tolerant of their own potentially antigenic substances, and the breakdown of this tolerance is the fundamental cause of autoimmunity (Rioux and Abbas 2005; Ring and Lakkis 1999; Lleo et al. 2010). Several reviews describe in detail the mechanisms of self-tolerance (Murphy et al. 2012; Perniola 2012; Hogquist et al. 2005; Soyer et al. 2013; von Boehmer and Melchers 2010; Wing and Sakaguchi 2010).

Briefly, AD can develop when self-reactive lymphocytes escape tolerance and are activated either *via* genetic disposition or a combination of heritable genes, acquired environmental triggers (*e.g.* infections), and/or stochastic events (*e.g.* random mutations). Mutations that either promote or cause disease phenotypes involve all facets of the immune system, prominent examples being human leukocyte antigen (*HLA*) (Gough and Simmonds 2007), T cell receptor (*TCR*) genes (Dornmair et al. 2003), and B cell receptor (*BCR*) genes (Prak et al. 2011; Diamond and Scharff 1984). *BCR* genes are involved in many human autoimmune diseases, as evidenced by the successful treatment of patients suffering

from rheumatoid arthritis (RA) and systemic lupus erythematosus (SLE) with B cell-depleting therapies (Yildirim-Toruner and Diamond 2011; Edwards and Cambridge 2005). Clinicians have also detected autoantibodies in patients experiencing massive tissue damage (Fleming and Tsokos 2006; Gronwall et al. 2012), in patients with cancer (Patwa et al. 2009; Kupcinskas et al. 2016; Werner et al. 2016; Zaenker et al. 2016), and even in healthy individuals (Coutinho et al. 1995; Poletaev et al. 2008). Natural autoantibodies are thought to provide immediate protection against infection and prevent inflammation by facilitating the clearance of oxidized lipids, proteins, and apoptotic cells (Gronwall et al. 2012). Their role in the development of autoimmunity, however, remains uncertain.

1.1 Generation of the Primary Antibody Repertoire

The antibody repertoire stems from the formation of nascent B cell lymphocytes in the bone marrow. In each B cell, genes coding for one variable heavy (V_H) and one variable light (V_L) domain of the B cell receptor (Fig. 1A) are constructed from a limited number of inherited germ-line gene segments (Tonegawa 1983). These genes consist of *V* (variable), *D* (diversity), and *J* (joining) gene segments for the heavy chain and *V* and *J* segments for the light chain (Murphy et al. 2012; Dudley et al. 2005; Schroeder 2006). The *V* genes of the light chain are located on a separate chromosome and can be of either *kappa* or *lambda* type. *V*(*D*)*J* recombined genes encoding V_H and V_L domains are further paired with constant (C) gene segments that determine antibody isotype on the C-terminal portion of the antibody. The different isotypes and sub-isotypes alter the effector function of the antibodies and influence avidity (Dudley et al. 2005; Li et al. 2004). Soluble IgM molecules generated during the primary antibody response generally exhibit low affinities but form compensatory high avidity interactions due to their decavalency.

The five heavy chain isotypes α, δ, γ, ε, and μ, correspond to IgA, IgD, IgG, IgE, and IgM antibodies, respectively. The B cell receptor consists of a membrane-bound immunoglobulin (mIg) of one isotype and a signal transduction membrane protein, cluster of differentiation 79 (CD79) (Harwood and Batista 2010; Bankovich et al. 2007; Treanor 2012). The mIg is identical to the secreted form of bivalent antibodies (IgD, IgE, and IgG) with the exception of the integral membrane domain, and CD79 is a heterodimer consisting of Igα and Igβ chains.

Genetic recombination of germ-line genes generates substantial diversity, which allows the vertebrate immune system to recognize an astonishing number of antigens. IgM and IgD antibodies normally have low antigen-binding affinities, but T-helper cell co-stimulation induces migration (to germinal centres), proliferation, and differentiation of matured B cells into centroblast cells (LeBien and Tedder 2008) (Fig. 1B). During this stage, the centroblasts lose BCR receptor expression and undergo somatic hypermutation (SHM) of their immunoglobulin genes to produce mutant antibodies with potentially higher affinities. Centroblasts express large amounts of a B cell–specific activation-induced cytidine deaminase (AID) enzyme, which begins the process of affinity maturation (Muramatsu et al. 2000; Peled et al. 2008). AID is also involved in class switch recombination (CSR), a process that, in combination with a chemokine gradient derived from T-helper and stromal cells, results in the different antibody isotypes (Klein and Dalla-Favera 2008; Stavnezer et al. 2008).

In both humans and mice, IgG molecules are the main serum immunoglobulin components, with subclasses IgG1 through IgG4 in humans, and IgG1, IgG2a, IgG2b, and IgG3 in mice. Figure 1C depicts a generic plasma-soluble IgG1 molecule with the relative positions of the functional and structural domains indicated.

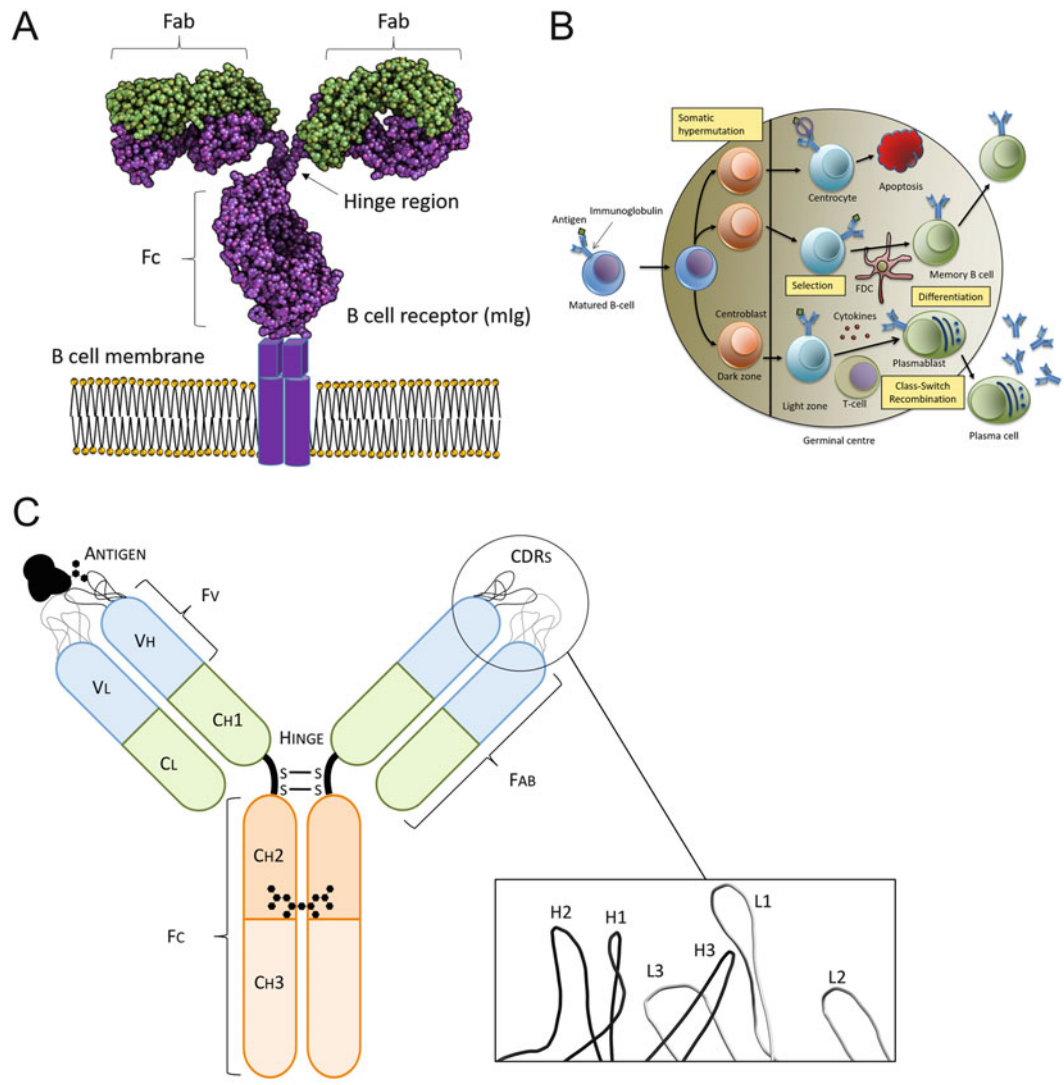

Fig. 1 (**A**) Schematic diagram of B cell receptor with the heavy chain in *purple* and the light chain in *green* (two domain dimers). Antigen binding can occur at two identical sites near the *N*-terminal portion of the B cell receptor. The associated CD79 co-receptor is not shown. With the exception of the integral membrane and an extra domain on the C-terminus, the membrane bound immunoglobulin (mIg) resembles that of an IgG antibody. Structure of the intact antibody belongs to PDB: 1IGT (Harris et al. 1998). (**B**) An activated B cell migrates to the dark zone of the germinal centre where the B cell undergoes differentiation into a centroblast cell. Centroblast cells lose expression of their surface mIgs and initiate cell division. During their expansion, centroblast undergo somatic hypermutation (SHM). The cells then proceed to the light zone where they re-express mutated Igs on their surface, at which point the cells become centrocytes. In the light zone, the centrocytes can have two different fates. With the help of follicular dendritic cells (FDC) and T helper cells, high affinity antibody-antigen contacts are selected and undergo further differentiation. A subset of selected centrocyte Igs undergo class switch recombination. Eventually the antigen-selected centrocytes differentiate into B memory cells and/or plasma cells. Low affinity Igs or unproductive antibodies produced because of SHM are not selected, which results in apoptotic cell death. (**C**) Schematic of a generic soluble IgG1 molecule, where dimerized heavy (V_H, C_H1, C_H2, C_H3) and light (V_L and C_L) chains form antigen-binding sites. The main chain trace of the six CDR loops (from S25-26, PDB: 4M7J, Haji-Ghassemi et al. 2014) of the N-terminal V_H and V_L domains is magnified in the inset. Black hexagons bridging the Fc domains represent *N*-glycans observed in the crystal structures of heavy chain fragments

1.2 Immunoglobulin Structure and Function

The general structure of antibodies was established by protein sequencing and crystallography in the 1970s, and fully elucidated through the work of McPherson and colleagues (Harris et al. 1998), who characterized structurally two complete IgG molecules. The IgG antibody features two identical heavy and light polypeptide chains that combine in a twelve-domain Y-shaped protein with two N-terminal antigen-binding sites (Fig. 1C).

Antibody specificity arises *via* complementarity-determining regions (CDRs). CDRs consist of six polypeptide loops of hypervariable sequence located in the antigen-binding fragment (Fab). There are three heavy chain (H1, H2 and H3) and three light chain (L1, L2 and L3) (Fig. 1C) CDRs, which together form a surface complementary to the antigen in shape, hydrophobicity, and charge. The CDRs typically form central pockets and grooves along the V_H-V_L interface (Kabat 1976). It is the combination of *J* and *D* genes in the heavy chain segments that generates divergent CDR H3 sequences and so, unsurprisingly, CDR H3 is highly involved in antigen recognition. Receptor editing mechanisms, which aim to limit or eliminate self-reactivity, include L chain rearrangement and V_H replacement (Prak et al. 2011). The latter often preserves a significant portion of CDR3 and so the H chain, particularly CDR3, provides a major contribution to autoantibody specificity and autoreactive B cell development (Prak et al. 2011; Rekvig and Nossent 2003; Eilat et al. 1988).

1.3 Generation of Autoreactive B Cells

The immune system normally eliminates autoreactive B cells at two major checkpoints: the bone marrow and the periphery. In the bone marrow polyreactive and autoreactive immature B cells are deleted, undergo receptor editing, or are rendered anergic before their exit (Kuraoka and Kelsoe 2011; Meffre 2011; Pillai et al. 2011; Wardemann et al. 2003). In the periphery autoreactive B cells are eliminated as immature B cells (Han et al. 2015; Suryani et al. 2010; Giltiay et al. 2012; Detanico et al. 2011). Dysregulation of these check points can occur in patients with ADs. Generally, pathogenic autoantibodies are of the IgG isotype (Fig. 1C) and have undergone somatic mutations, and so it follows that most autoreactive disease-causing B cells likely arise from the periphery and require T-cell help (Han et al. 2015; Giltiay et al. 2012; Herlands et al. 2008). However, in most cases, the exact autoreactive B cell epitope is unknown (Garabatos et al. 2014).

1.4 Autoreactive B Cell Antigens

Several reviews describe the range of antigens known to bind autoreactive B cells in connection with various ADs (Routsias et al. 2006; Suurmond and Diamond 2015; Riedhammer and Weissert 2015; Rekvig 2015). Autoantigen epitopes have been identified within large intracellular multiprotein complexes, which are usually non-covalently associated with single-stranded and double-stranded nucleic acids (*e.g.* histones and ribosomes), single proteins, cell-surface carbohydrates, glycoproteins, and phospholipids. Remarkably, ADs exhibit considerable overlap or similarity in their autoantigens, though they are diagnosed using distinct autoantibodies (Routsias et al. 2006; Suurmond and Diamond 2015; Riedhammer and Weissert 2015; Giles and Boackle 2013).

The well-known autoantigen cardiolipin (CL) is a mitochondrial phospholipid with a role in maintaining metabolism and membrane homeostasis (Houtkooper and Vaz 2008). CL is composed of disphosphatidylglycerol with four acyl chains and, exists as a dimer with a conical structure (Houtkooper and Vaz 2008). Anti-CL antibodies have been identified in many ADs: SLE (Ishii et al. 1990), antiphospholipid syndrome (APS) (Erkan et al. 2011; Asherson et al. 2003), Behçet's disease (Hull et al. 1984;

Table 1 Common autoantigens and the autoimmune disease(s) with which they are frequently associated

Autoantigen	Associated autoimmune disease(s)	Review of interest
ANA	SLE, drug-induced LE, MCTD, RA, Sjögren's syndrome	Routsias et al. (2006), Suurmond and Diamond (2015), Giles and Boackle (2013) and Castro and Gourley (2010)
dsDNA	SLE, MCTD, RA* (Abs found during RA patient treatment)	
β_2-Glycoprotein I (ApoH)	SLE, APS	
Histone	Drug-induced SLE	
Cardiolipin	SLE, APS, Behçet's disease, RA, Barth syndrome	Houtkooper and Vaz (2008)
Myelin binding protein	MS	Riedhammer and Weissert (2015)
Citrullinated proteins	RA	van Gaalen et al. (2005)

Zivkovic et al. 2011), and RA (Keane et al. 1987; Wolf et al. 1994) among others (Table 1).

Apolipoprotein H (APOH), also known as β2-glycoprotein I (β2GI), is another important class of autoantigen predominantly associated with APS (de Groot and Meijers 2011). APOH has an affinity for anionic phospholipids due to a basic stretch of six amino acids, four of which are lysine residues. This region is also thought to be involved in binding to lipopolysaccharide (LPS) (de Groot and Meijers 2011; Schwarzenbacher et al. 1999; Bouma et al. 1999).

Anti-nuclear antibodies (ANA) against double-stranded DNA (dsDNA), single-stranded DNA (ssDNA), and ribonucleoproteins (RNPs) are a hallmark of SLE (Routsias et al. 2006; Rekvig 2015; Isenberg et al. 1984). Anti-DNA antibodies were originally discovered in the sera of patients with bacterial infections (Winkenwerder et al. 1939; Sevag et al. 1938). Later experiments showed that bacterial DNA contains immunostimulatory sequences and acts as a trigger for the observed B-cell response (Krieg et al. 1995). In contrast, mammalian DNA is generally immunologically inert (Stollar 1986), and the origin of autoantibodies against mammalian DNA remains unknown (Rekvig 2015; Zouali et al. 1988). Several mechanisms have been proposed, most involving increased availability of extracellular DNA *via* necrotic and apoptotic events (Rekvig 2015; Giles and Boackle 2013; Su and Pisetsky 2009; Biermann et al. 2014; Fenton 2015). Given the inaccessibility of dsDNA base pairs, many anti-dsDNA antibodies are likely specific for epitopes involving the exposed polynucleotide phosphodiester backbone (Schwartz and Stollar 1985; Lafer et al. 1981). Notably, many of the anti-DNA autoantibodies identified in SLE patients have also shown specificity for other autoantigens, including phospholipids, cytoskeleton proteins, and platelets (Schwartz and Stollar 1985; Lafer et al. 1981).

Many antibodies directed against these antigens display some degree of cross-reactivity or polyspecificity. Testament to this phenomenon is the association of specific autoantigens with multiple ADs (Table 1), which has implications for the use of autoantigen- and autoantibody-detection assays in diagnosis and monitoring.

1.5 Polyspecificity and Cross-Reactivity of Antiphospholipid Antibodies

The terms polyspecificity and cross-reactivity are often used interchangeably, but there is an important distinction. Polyspecificity refers to

an antibody's capacity to bind chemically distinct antigens *via* identical or different paratopes and is likely an inherent property of some germline immunoglobulins (Chu et al. 2008; Wucherpfennig et al. 2007; Willis et al. 2013). In contrast, cross-reactivity describes antibody recognition of two or more distinct antigens that have identical or similar epitopes (Varga et al. 1973; Ternynck and Avrameas 1986; Nguyen et al. 2003; Blackler et al. 2012). Over time, selection of germ-line gene segments necessarily is biased towards their ability to encode CDRs that recognize a range of structurally related antigens. This affords an immunological advantage to the host, though cross-reactive and polyspecific antibodies are understood to have central roles in autoimmune responses (Jin et al. 2008; Oldstone 1998). Moreover, cross-reactivity and polyspecificity are especially prevalent in antibodies against phospholipids.

Antiphospholipid autoantibodies are of considerable clinical importance because of their association with thrombosis (Farmer-Boatwright and Roubey 2009), fetal growth restrictions or fetal loss (Hurtado et al. 2004; Esplin 2001), pre-eclampsia (Heilmann et al. 2011), and thrombocytopenia (Cuadrado et al. 1997), *i.e.* APS (Mcneil et al. 1991; Roubey 1994). These antibodies belong to four subtypes: anti-CL antibodies, lupus anticoagulants, anti-β2GP/prothrombin antibodies, and antibodies against bacterial phospholipids (Giannakopoulos and Krilis 2013). Ruff et al. recently implicated the fourth subtype, which has likely arisen from commensal bacteria (Ruff et al. 2015). The gut microbiome exerts profound effects on autoreactive T cells and autoantibodies that mediate autoimmunity in APS and SLE (Ruff et al. 2015; Mathis and Benoist 2011; Duan and Kasper 2011; Vieira et al. 2014). Many of these autoantigens share the features of other negatively-charged antigens, which include nucleic acids and carbohydrates. Indeed, antibodies capable of binding single-stranded or double stranded nucleic acids are often detected in AD patients, particularly those with APS and SLE (Han et al. 2015; Suurmond and Diamond 2015; Lafer et al. 1981; Massa et al. 1993; Zurgil et al. 1993; Hill and Nochy 2007; Ravirajan et al. 2001; Robertson and Pisetsky 1992; Kaburaki et al. 1992). Further, many research articles show that LPS plays a key role in the development of autoimmune disease (Ruff et al. 2015; Cavallo and Granholm 1991; Nogai et al. 2005; Yoshino et al. 2000; Helmerhorst et al. 1998; Sumazaki et al. 1986). Other reports show that immunization of mice with bacterial LPS yields mAbs with a polyspecific response to DNA (Sumazaki et al. 1986; Izui et al. 1977). Even mice with a genetic resistance to autoimmunity may develop ADs when given a high dose of LPS (Pullen et al. 1995; Lane et al. 1991).

1.6 Lipopolysaccharide Structure and Immunogenicity

The only absolute rule in biology seems to be that cell surfaces are decorated with carbohydrates (Gagneux and Varki 1999); in the case of Gram-negative bacteria, immunogenic LPS covers ~75% of the outer membrane surface (Nikaido 2003; Caroff and Karibian 2003; Kabanov and Prokhorenko 2010). Enterobacterial LPS consists of three components (Fig. 2A): lipid A, inner and outer core oligosaccharide, and O-polysaccharide (O-antigen). The lipid A anchor is an acylated glucosamine disaccharide (Fig. 2B) that is normally embedded in the bacterial outer membrane and is the Gram-negative endotoxin involved in triggering septic shock. Attached to the GlcN disaccharide of lipid A, is a relatively conserved inner core oligosaccharide, typically composed of 3-deoxy-D-*manno*-oct-2-ulosonic acid (Kdo) residues (Fig. 2B) and L-*glycero*-D-*manno*-heptose (Hep). The O-antigen, the outermost LPS region, consists of dozens to hundreds of repeating mono- or oligosaccharides and exhibits considerable variation both in length and composition among bacterial species and serovars (Rietschel et al. 1994; Abu-Lail and Camesano 2003; Strauss et al. 2009; Iguchi et al. 2014).

Infections from a wide range of Gram-positive and -negative bacteria induce septic shock in approximately one million people

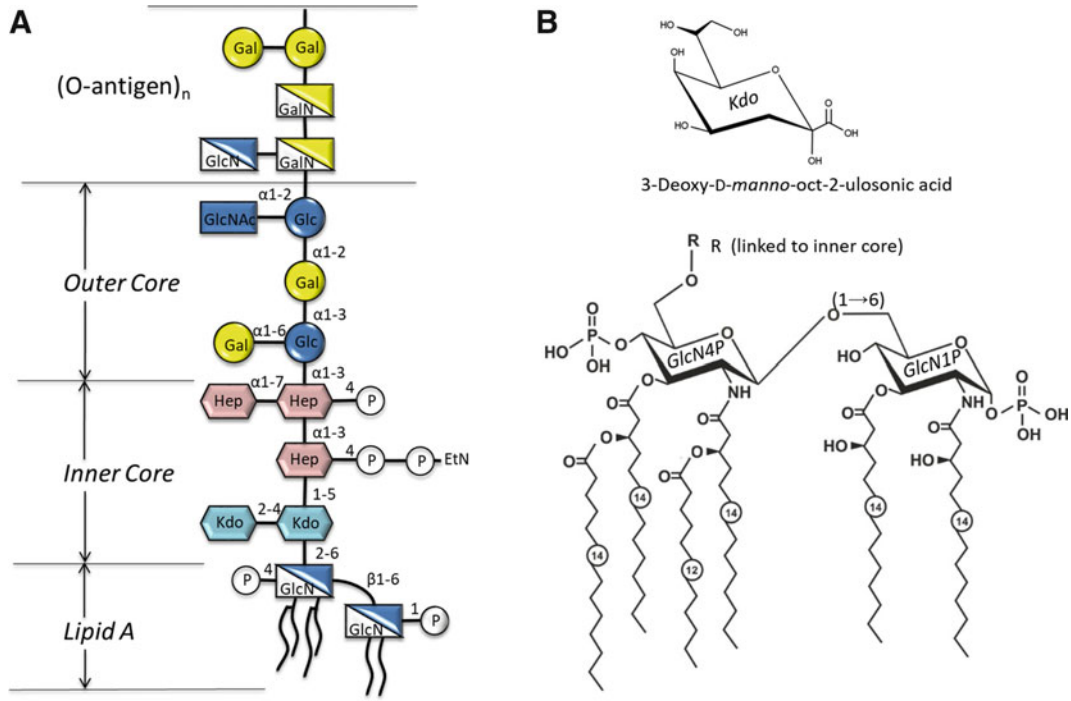

Fig. 2 (**A**) General LPS architecture found in *Salmonella* with the conserved linkages indicated for the inner and outer core oligosaccharide. (**B**) The inner core Kdo residue is anchored to the lipid A, the endotoxin principle of LPS, shown here with stereo chemical diagrams. The depicted lipid A structure is found in *E. coli* and *Salmonella*

annually in the United States with a mortality rate of 28–50% (Angus et al. 2001; Engel et al. 2007; Martin 2012). The inflammatory cascade, which leads to septic shock, is initiated by the formation of a signaling complex of LPS with Toll-like receptor 4 (TLR4) and the co-receptor myeloid differentiation factor 2 (Miller et al. 2005; Poltorak et al. 1998; Kim et al. 2007; Miyake 2007). One heavily investigated therapeutic route has focused on the potential for monoclonal antibodies (mAbs) to sequester LPS (Di Padova et al. 1993a, b; Gomery et al. 2012; Müller-Loennies et al. 2007) and prevent signaling complex formation. Treatment options are limited and mainly based on antibiotic therapy. Other methods of detoxification, such as LPS binding column-based therapies and irreversible chemical modification of LPS, have had contradictory or poor results in animal models and preliminary clinical trials (Buttenschoen et al. 2010; Lolis and Bucala 2003; Anspach 2001; Munford 2005; Vincent et al. 2002).

Although the lipid A structure is highly conserved among pathogenic species, none of the numerous reported antibodies purported to be specific for lipid A have had clinical success (Helmerhorst et al. 1998; Kuhn 1993; Kuhn et al. 1992; Fujihara et al. 1993a; Miller et al. 1996; Bhat et al. 1993; Yokota et al. 1996). Relative to lipid A, the greater accessibility or exposure of the conserved outer and inner core region enhances these structures' immunogenicity (Russo et al. 2007). This prompted several groups to generate cross-reactive, protective antibodies against the conserved core oligosaccharide antigens, which can include lipid A (Di Padova et al. 1993a; Müller-Loennies et al. 2007, 2003; Roche et al. 2011; Broecker et al. 2014; Rynkiewicz et al. 2012; Vulliez-Le Normand et al. 2008). However, the presence of

the O-antigen usually hinders antibody recognition of conserved epitopes and thus far, the only example of a cross-reactive antibody that binds the core region in the presence of an O-antigen is mAb WN1 222-5 (Di Padova et al. 1993a; Gomery et al. 2012; Müller-Loennies et al. 2003). Nevertheless, antibody therapy remains an attractive option for toxic shock treatment despite these challenges.

2 The Link Between Anti-lipid A Antibodies and Autoimmune Disease

Antibodies believed to be specific for lipid A were first observed after treating bacterial LPS with acid liberating the lipid A fragment to act as a neoantigen when embedded in erythrocytes or liposomes (Kuhn et al. 1992; Galanos et al. 1971). Other putative lipid A-specific antibodies were isolated from mice or human spleen cells following immunization with heat killed *Escherichia coli* J-5 cells (rough LPS phenotype) (Helmerhorst et al. 1998; Di Padova et al. 1993a; Appelmelk et al. 1988; Teng et al. 1985; Ziegler et al. 1982). Most notable among these, in terms of characterisation and polyspecific/cross-reactive potential, was the antibody Centoxin® (IgM), also known as H1-1A and nebacumab (Helmerhorst et al. 1998; Teng et al. 1985), and the A6 monoclonal antibody (IgG_{2b}) (Appelmelk et al. 1988).

2.1 Centoxin Binding Specificity and Polyspecific Potential

While most anti-lipid A antibodies bind the hydrophilic portion of lipid A (Helmerhorst et al. 1998; Kuhn 1993; Kuhn et al. 1992; Haji-Ghassemi et al. 2015a; Brade et al. 1993; Haji-Ghassemi et al. 2016), the human IgM antibody Centoxin was thought to bind the hydrophobic acyl chains (Helmerhorst et al. 1998). Centoxin was associated with increased survival and protection against Gram-negative bacteremia in murine and rabbit models (Teng et al. 1985) and, in contrast to its murine-derived antibody competitors (Greenberg et al. 1992), it appeared to produce no anti-drug antibodies (Fisher et al. 1990). However, subsequent studies in mice and canines had disparate results (Baumgartner et al. 1990; Quezado et al. 1993). Similarly, the first human clinical trials with Centoxin were promising, increasing the survival rate by 24% compared to placebo (Ziegler et al. 1991); however, a larger phase III clinical trial showed no significant difference between the placebo group and those receiving the drug (Mccloskey et al. 1994). Centoxin was eventually withdrawn due to safety, efficacy and commercial concerns (Marks 2012).

One of the major pitfalls of Centoxin was its lack of specificity; some researchers claimed it to be specific to lipid A (Fujihara et al. 1993a, b; Bogard et al. 1993), yet others observed that Centoxin also recognized i antigen found on cord erythrocytes, hydrophobic patches on partially denatured proteins, and anionic polymers, including ssDNA, chondroitin sulfate, and cardiolipin (Helmerhorst et al. 1998; Bhat et al. 1993; Bieber et al. 1995). This behaviour is commonly observed in IgM antibodies (Milner et al. 2005) and interestingly, occurs in other anti-lipid A antibodies (Bhat et al. 1993). E5, another lipid A-binding IgM obtained after *E. coli* J-5 immunization (Wood et al. 1992), also recognizes dsDNA (Fujihara et al. 1993a). Importantly, such polyspecificity or cross-reactivity may permit a scenario whereby patients induce 'self' antibodies in response to foreign antigen. Antibodies against DNA are noteworthy, since they are implicated in autoimmune diseases such as SLE (Ravirajan et al. 2001; Robertson and Pisetsky 1992; Spellerberg et al. 1995; Tillman et al. 1992), autoimmune thyroid disease (Pedro et al. 2006), and rheumatic disorders (Kaburaki et al. 1992; Miller et al. 1996) (Table 1). Notably, these autoantibodies commonly contain arginine and other basic amino acids in their heavy chain CDRs, conferring affinity toward negatively-charged single-stranded or double-stranded nucleic acid structures (Rekvig and Nossent 2003; Chang et al. 2009).

Further analysis of Centoxin revealed that the heavy chain sequence belonged to germ-line V(H)4.21 gene segment (Bieber et al. 1995), which is commonly utilized by anti-DNA antibodies isolated from SLE patients (Miller et al. 1996; Stevenson et al. 1993). A study by Spellerberg et al. (1995) also emphasized the involvement of V(H)4.21 germ-line in dual recognition of lipid A and host nucleic acids, demonstrating a possible link between systematic infection with Gram-negative bacteria and SLE development. Genes belonging to the V(H)4.21 also bind human B cells and cold agglutinins (Milner et al. 2005; Pascual et al. 1992; Kraj et al. 1995), both of which are recognized by Centoxin (Helmerhorst et al. 1998; Bieber et al. 1995). Ten Feizi first identified this bacterial link to autoantibodies, when she observed that human antibodies stimulated during infection with *Mycoplasma pneumoniae* seemed to be directed not against the bacteria, but against host red blood cells (Feizi and Taylor-Robinson 1967). Despite decades of progress, the molecular mechanism underlying this apparent polyspecificity is unknown, and there are no available experimentally-determined three-dimensional structures of anti-lipid A IgM antibodies or antibodies stimulated with *M. pneumoniae*.

2.2 Lipid A-Binding Antibodies A6, S1-15, and S55-3/S55-5

MAb A6 (IgG_{2b}) was isolated from mice immunized with heat-killed *E.coli* J-5 cells (Appelmelk et al. 1988; Haji-Ghassemi et al. 2015b), while S1-15 ($IgG_{2b,}$ also referred to as S1), S55-3 (IgG_{2b}), and S55-5 (IgG_1) were obtained *via* immunization of mice with BSA-lipid A glycoconjugate, (Kuhn et al. 1992; Haji-Ghassemi et al. 2016). Binding studies showed mAb A6 had a preference for the bisphosphorylated (*i.e.* native) glucosamine disaccharide with only weak binding to the monophosphorylated carbohydrate backbone (Kuhn et al. 1992). In contrast, S1-15 displayed high avidity for both the monophosphorylated and bisphosphorylated lipid A backbones (Kuhn et al. 1992; Brade et al. 1993). Similarly, mAbs S55-3 and S55-5 preferentially bound the bisphosphorylated lipid A, and showed only weak binding to the 4- monophosphorylated lipid A backbone (Haji-Ghassemi et al. 2016). None of these antibodies appeared to recognize intact LPS.

Brade et al. reported that such antibodies solely bind to the bisphosphorylated glucosamine disaccharide backbone lacking the acyl chains (Brade et al. 1993). Thus, apart from S1-15, A6, other lipid A binding Abs also likely recognize the carbohydrate backbone exclusively. Binding studies of the C6' methyl-capped disaccharide showed that neither S1-15 nor A6 mAbs could bind lipid A lacking a free hydroxyl at C6 on the β-glucosamine, which serves as the attachment point for LPS inner core residues (Brade et al. 1997). Recently, the Fab crystal structures of A6 and S1-15 were determined in complex with lipid A analog β-D-GlcN4*P*(1 → 6)α-D-GlcN1*P*, and refined to 2.15 Å and 1.95 Å resolutions respectively. The structures show that binding occurs largely through interactions among heavy chain CDR H3 residues and the 4*P* and 1*P* hydroxyl groups (Fig. 3A, B) (Haji-Ghassemi et al. 2015b). Similarly, structures of S55-3 and S55-5 in complex with lipid A show that most of the hydrogen bonds are directed to the lipid A 4*P* and 1*P* hydroxyls. The contacting residues stem from CDR H2 and H3 loops and single CDR L3 residue, Arg-96 (Fig. 3C) (Haji-Ghassemi et al. 2016). While the binding sites of S55-3 and S55-5 are almost identical in terms of antigen contacts (Haji-Ghassemi et al. 2016), these antibodies display a significantly different recognition strategy than S1-15 and A6. S1-15 and A6 form extended deep grooves, whereas S55-3 and S55-5 form a small cavity complementary to the lipid A backbone, as do antibodies raised against smaller antigens. Additionally, S1-15 and A6 do not utilize corresponding amino acid residues in lipid A-binding, despite their shared V_L chain genes (Haji-Ghassemi et al. 2015b). While A6 uses both light and heavy chain CDR residues, S1-15 binds lipid A exclusively through the heavy chain. This is an excellent example of how the humoral immune system has evolved

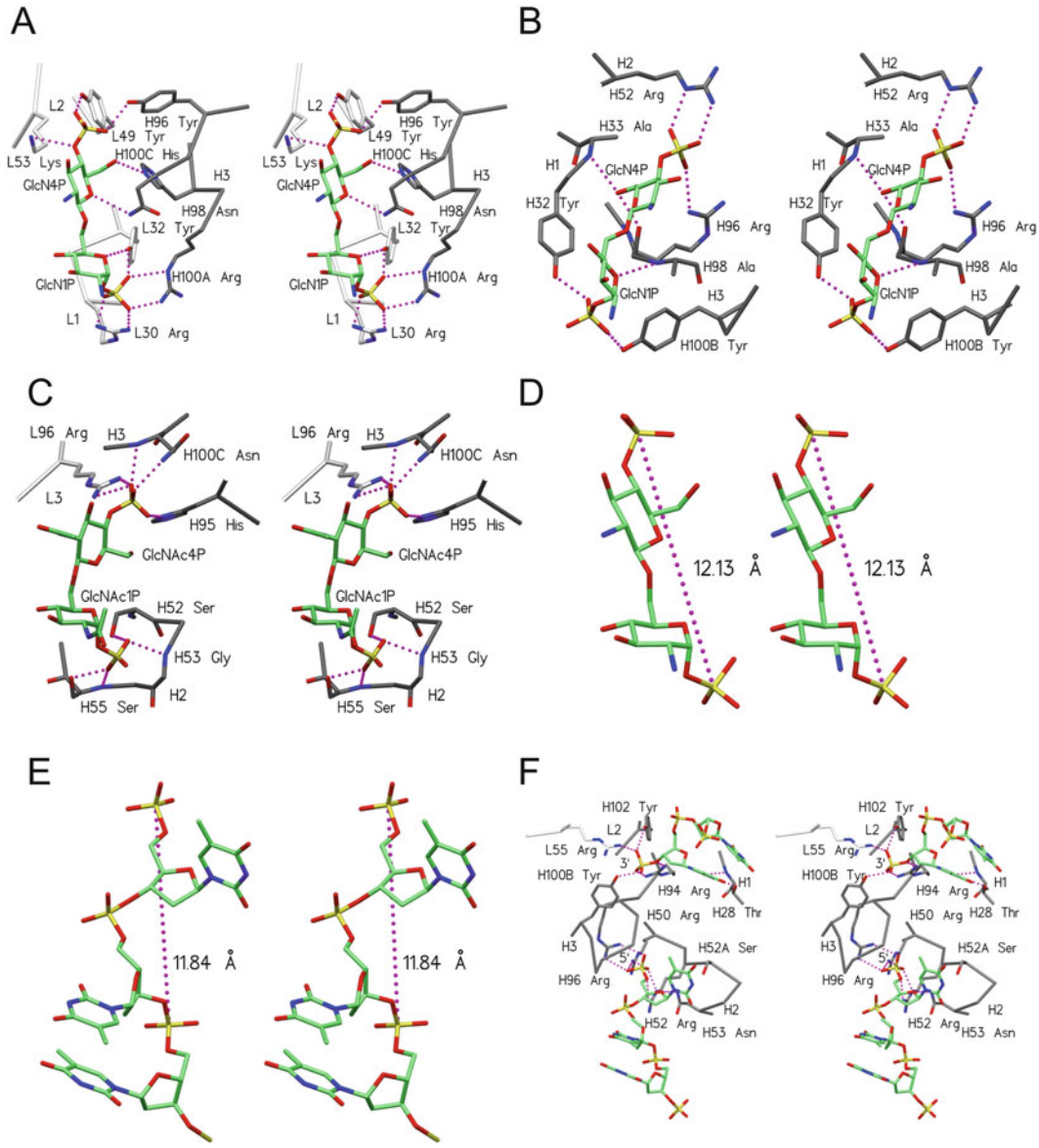

Fig. 3 Stereo diagrams of (**A**) A6 (PDB: 4ODV) and (**B**) S1-15 (PDB: 4ODT) in complex with lipid A analog β-D-GlcN4*P*(1 → 6)α-D-GlcN1*P* (Haji-Ghassemi et al. 2015b), (**C**) S55-5 (PDB: 5DQD) in complex with lipid A analog β-D-GlcNAc4*P*(1 → 6)α-D-GlcNAc1*P* (Haji-Ghassemi et al. 2016). Stereo view of A6-bound lipid A analog (**D**) and *p*5(dT)*p* ssDNA fragments (**E**) with the distance between each set of phosphates indicated with pink dashed spheres. Except for carbon, ligand atoms and CDR loop side chain atoms are colored by element with oxygen *red*, nitrogen *blue*, and phosphorous *yellow*. (**F**) Stereo view of S1-15 (PDB: 4ZSF) in complex with two *p*5(dT)*p* ssDNA fragments (Haji-Ghassemi et al. 2015b). Pink dashed spheres represent hydrogen bond interactions. For all complexes shown, carbon atoms are colored *white* and *gray* for light and heavy chain CDR loops, respectively, and carbon atoms are colored green for lipid A analogs and *p*5(dT)*p* ssDNA

redundant responses to a single epitope. As with S1-15 and A6, S55-3 and S55-5 do not bind the acyl chains of lipid A.

Unsurprisingly, the lysine and arginine residues within the CDRs of S1-15, A6, S55-3, and S55-5 allowed the formation of salt bridges

Table 2 Amino acid sequence comparisons of the CDR regions for mAbs S1-15 and A6, compared with V_L chain of anti-DNA antibodies 423 s.187 (GenBank: U55655)[1], 373p.77 (GenBank: U55595), 452 s.123 (GenBank: U55694), 73.23 (GenBank: U30238); and V_H chain of DNA binding antibodies BV04, A.1.11 (GenBank: AF006586), 64.9D (GenBank: AF006574), MRL-DNA4 (GenBank: M20829), 423 s.187 (GenBank: U55527), and the family V_H-gene 238 (GenBank: X17631). Residues underlined and in bold are involved in binding to the lipid A for A6 and S1-15, and ssDNA for S1-15. Arg(L)55 of S1-15 is only involved in recognition of ssDNA. Numbering is based on the Kabat scheme

Clone	**Variable Light (V_L) Chain CDR sequences**				**References**
	24	**50**	**88**	**A**	
S1-15	RASQDISNYLN	YTSRL**R**S	CQQGNTLP-WT		Haji-Ghassemi et al. (2015b)
423s.187	RASQDISNYLN	YTSRLHS	CQQGNTLP-WT		Krishnan et al. (1996)
373p.77	RASQDISNYLN	YTSRLHS	CQQGYTLP-LT		Krishnan et al. (1996)
452s.123	RASQDISNYLN	YTSRLHS	CQQGNTL--RT		Krishnan et al. (1996)
73.23	RASQDISNYLN	YTSRLHS	CQQGNTLP-WT		Ibrahim et al. (1995)
A6	RASQDI**R**N**Y**LS	**Y**TS**K**LHS	CQQGKTLPLYT		Haji-Ghassemi et al. (2015b)
	<**-CDR L1-**>	<**CDR L2**>	<**--CDR L3--**>		
Clone	**Variable Heavy (V_H) Chain CDR sequences**				**References**
	26	**50**	**ABC**	**93**	**ABCDEFGH**
S1-15	GFTFN**TYA**MN		**RIRS**KS**N**NYATYYADS	V**R**H**R**G**A**PLY**Y**GNGAWFA	Haji-Ghassemi et al. (2015b)
BV04	GFSFNTNAMN		RIRSKSNNYATYYADS	VRDQTGT------AWFA	Herron et al. (1991)
A.1.11	GFSFNTYAMN		RIRSKSNNYATYYADS	VRHG----------YLA	Weller et al. (1997)
64.9D	GFSFNTYAMN		RIRSKSNNYATYYADS	VRH----------YYFD	Weller et al. (1997)
MRL-DNA4	GFSFNTNAMN		RIRSKSNNYATYYADS	VRDAANWS----AWFA	Kofler et al. (1988)
A6	GFTFSSYYMS		AINS--NGGNTYYPDT	TRL**Y**G**N**Y**VRIH**TM---D	Haji-Ghassemi et al. (2015b)
VH238	GFTFSSYTMS		TISS—GGGNTYYPDS	AR----------	Shlomchik et al. (1990)
423 s.187	EFTFSNYGMS		ATISN-GGSYTYYPDS	ARPGNREGFVY----V	Krishnan et al. (1996)
	<−**CDR H1-**>		<−**----CDR H2----**>	<−**-----CDR H3-----**>	

[1]GenBank Accession numbers retrieved from the EMBL nucleotide database

to lipid A phosphates (Table 2). The Arg and Lys content within these CDRs may serve as the molecular basis for polyspecific/cross-reactive binding to other negatively-charged species. This is particularly relevant for DNA-binding antibodies, which display a high frequency of Arg/Lys in their CDRs (Chang et al. 2009; Krishnan et al. 1996).

2.3 Sequence Comparison of A6 and S1-15 mAbs with Anti-DNA Antibodies

The sequences of DNA-specific antibodies in mice generally belong to five subgroups of the J558 family: VH238 (IGHV5-9-03 or 01*),[1] 133.16VH (IGHV1–82-01*), VH31 (IGHV1S19–01*), 6G6VH (IGHV7–3- 04*), and pH 3–6a (IGVH9–1-02*) (Tillman et al. 1992; Krishnan et al. 1996; Shlomchik et al. 1990; Ibrahim et al. 1995). These genes also are utilized in antibodies to *p*-azophenylarsenate (Rathbun et al. 1988; Monestier et al. 1987), cardiolipin (Ibrahim et al. 1995), and a panel of other autoantigens (Monestier et al. 1987). Significantly, mAbs S1-15 and A6 share *V*-genes with several anti-DNA antibodies (Haji-

[1] The gene designations shown in parentheses are based on the IMGT/Vquest database (Monod et al. 2004; Brochet et al. 2008) and are used throughout this paper.

Ghassemi et al. 2015b). An alignment of the CDR sequences for a subset of these antibodies, which share either light or heavy chain genes with S1-15 and A6, is shown in Table 2.

The VL chains of S1–15 and A6 share over ~95% nucleotide and amino acid identity with four anti-DNA autoantibodies (Table 2), however their role in binding is unclear, since their bound or unbound structures are not available. Further, the CDR H3 residues of these antibodies are often incomplete. None of the four antibodies share VH genes with either S1-15 or A6 (Krishnan et al. 1996; Ibrahim et al. 1995). Nevertheless, some of the CDR residues contacting lipid A are conserved between VL chain residues of mAb A6 and these autoantibodies (Table 2). Notably, Tyr(L)50 (residues are identified as H or L to denote the heavy chain and light chains, respectively) and Lys(L)53 form hydrophobic interactions with the back face (hydrophobic face) of the second glucosamine as well as a salt bridge with the 4*P* of lipid A, respectively (Fig. 3A).

The VH of S1–15 shares ~90% nucleotide and >90% amino acid identity with four autoantibodies reported to bind DNA (Herron et al. 1991; Weller et al. 1997; Kofler et al. 1988). These antibodies have a significant number of lipid A-contacting residues in common, the most important being Arg(H)50, Arg(H)52, Arg(H)94, Arg(H)96, and Tyr(H)32. The arginine residues form salt bridges to the 1*P* and 4*P* hydroxyls of lipid A (Fig. 3B), while Tyr(H)32 acts in the same manner as Tyr(L)50 of A6 mAb. Although the VH chain of A6 is not involved in lipid A antigen recognition, its corresponding *V*-gene is closely related to an anti-DNA *V*-gene known as VH238 (Shlomchik et al. 1990), sharing 273/291 nucleotides and 85/98 amino acids.

2.4 Polyspecific/Cross-Reactive Potential of A6 and S1-15 mAbs

Based on the striking sequence similarities among A6, S1-15, and autoantibodies, and the fact that the binding sites of A6 and S1-15 could accommodate larger antigens, we sought to investigate whether these mAbs could bind other negatively-charged species, particularly phosphates and nucleic acids. S55-3 and S55-5 possess smaller binding sites compared to A6 and S1-15 and thus are unlikely to accommodate larger antigens other than the lipid A disaccharide.

Further, the clearly defined electron density corresponding to the CDRs and lipid A antigen, provided some insight into the potential polyspecific recognition of ssDNA by these antibodies. The distance between the two phosphates of the glucosamine disaccharide backbone is approximately 12.0 Å (Fig. 3D), nearly twice the distance between the two phosphates of adjacent nucleotides in a strand of nucleic acid (Fig. 3E), and also twice the distance between two phosphates of cardiolipin (not shown). Hence, we concluded that these antibodies cannot recognize the dsDNA when the helical turn of DNA disrupts the linear 12.0 Å epitope required for optimal binding. This would also suggests the minimum requirement of four nucleotides for recognition of ssDNA.

Further clues to the potential polyspecific behaviour of S1-15 came from the structure of BV04 autoantibody in complex with a trinucleotide (Herron et al. 1991). Interestingly, the 5'*P*-binding site of BV04 shares many interactions that correspond to the 4*P* hydroxyls of lipid A in the binding site of S1-15, marking its importance for dual recognition of ssDNA and lipid A (Haji-Ghassemi et al. 2015b).

An ELISA study (unpublished data) of mAbs A6 and S1-15 using five- and ten-oligo-T (thymine) nucleotides showed that these antibodies also bind ssDNA. Significant binding compared with a negative control were detected for both antibodies, though the avidity of A6 was lower than S1-15 by an order of magnitude. As the avidity of five and ten oligonucleotides were equivalent, crystallization trials in presence of different oligo-T fragments were carried out using S1-15 Fab. The high resolution (1.75 Å) structure of S1-15 was obtained in complex with two separate oligonucleotides (Haji-Ghassemi et al. 2015b) (Fig. 3F). Most of the hydrogens

bonds were directed toward the 3'*P* and 5'*P* hydroxyls and primarily involved CDR H3 residues (Fig. 3F). However, the binding of S1-15 to ssDNA did not occur in the same manner as observed for DNA-binding antibodies (where the oligonucleotide spanned the combining site). Instead S1-15 bound two separate oligonucleotides by their terminal 5′- and 3-′-phosphate groups (Fig. 3F). This arrangement was stabilized by base stacking between symmetry-related oligonucleotides (Haji-Ghassemi et al. 2015b). The binding site corresponding to the 1*P*-phosphate of lipid A was occupied by terminal 3′-*P*, while the 4*P* of lipid A pocket bound the 5′-*P* of the oligonucleotide. Importantly, structural overlap between S1-15 and BV04 showed that these antibodies share a phosphate-binding site for the 5′*P,* with many same residues involved in phosphate recognition. S1-15 also exhibited considerable flexibility in the phosphate-binding site.

Crystallization of S1-15 with an ssDNA oligomer lacking the 5′-terminal phosphate (PDB: 4Z95) resulted in the occupancy of only one phosphate-binding site, though the 3'*P* position shifted by 1.05 Å compared to the structure containing both terminal phosphates (PDB: 4Z8F) (Haji-Ghassemi et al. 2015b). Consequently, a hydrogen bond to Tyr(H)102 was replaced with Tyr(H)32.

A fundamental difference between published structures of antibodies in complex with nucleic acids and the S1-15-ssDNA complex involves the orientation of the backbone phosphates. These groups usually face away from the combining site, with Tyr/Trp residues in the CDRs forming stacking interactions with the hydrophobic bases (Tanner et al. 2001). This was not the case for S1-15, as there were few hydrogen bonds to the terminal bases.

Despite these differences, it is remarkable that S1–15 and A6 bind ssDNA at all; both have undergone affinity maturation toward the lipid A carbohydrate antigen, and the corresponding germ-line antibodies could exhibit alternative binding modes to ssDNA. Crucially, the higher avidity of decavalent IgM plays an important role in establishing polyspecificity toward single-stranded nucleic acids. Unfortunately, structures of A6 in complex with nucleic acids are not available at the time of writing.

2.5 Five-Residue Motif in CDR H2 Binds Negatively Charged Moieties

Though it is unlikely that the binding sites of S55-3 and S55-5 accommodate antigens other than lipid A, they nevertheless display features present in other antibodies that recognize negatively charged groups. The recognition of the 1*P* of the first glucosamine is mediated entirely *via* a short loop in CDR H2 of sequence Ser(H)52-Asn (H)52A/Arg(H)52A-Gly-Gly-Ser(H)55, for S55-3 and S55-5 respectively (Haji-Ghassemi et al. 2016). A survey of the Protein Data Bank (Herlands et al. 2008) shows that the sequence motif Xaa-Xaa-Gly-Gly-(Ser/Thr/Gly), where one of the Xaa residues is usually a serine or threonine, is involved in binding negatively-charged groups in antibodies of otherwise unrelated sequence and specificity. Examples include mAbs S25-26 (Haji-Ghassemi et al. 2014) and LPT-3 (Parker et al. 2014), which bind to bacterial LPS of *Chlamydiaceae* and *Neisseria meningitidis*, respectively. This motif is also present in antibodies against phosphopeptides and viral peptides (binding negatively- charged side chain of Asp or Glu) (Deng et al. 2013; Schulze-Gahmen et al. 1993; Shih et al. 2012; Koerber et al. 2013; Baek and Kim 2015).

The presence of this conserved sequence motif in CDR H2 of unrelated germ-lines is likely an evolved mechanism for recognition of negatively-charged moieties on antigens present on a variety of different pathogens. This motif could serve as a prediction tool for other antibodies with specificity toward charged antigens. For example, several DNA-binding antibodies (GenBank accession numbers AAB49122 and AAB49121, and AAB53403) possess the following CDR H2 sequence, Ser (H)-52-Ser-Gly-Gly-Ser(H)-55, which may form a pocket specific for a DNA backbone phosphate (Krishnan et al. 1996). Interestingly,

one of the antibodies from the same study (GenBank accession number: U55527) shares the V_L genes of S1-15 and A6 lipid A antibodies (Table 2) (Krishnan et al. 1996).

2.6 General Behaviour of Lipid A Binding Antibodies

Antibodies against lipid A have distinct properties that govern their polyspecific/cross-reactive behaviour, such as the dominating influence of arginine and lysine residues in phosphate binding, a common feature in antibodies against nucleic acids. Further, the distance between lipid A phosphates resembles that of single stranded nucleic acids (Fig. 3D, E). Finally, a common motif Xaa-Xaa-Gly-Gly-(Ser/Thr/Gly) on CDR H2 may facilitate binding to the phosphates of nucleic acids and other antigens.

Conflict of Interest None declared

References

Abu-Lail NI, Camesano TA (2003) Role of lipopolysaccharides in the adhesion, retention, and transport of *Escherichia coli* JM109. Environ Sci Technol 37:2173–2183

Angus DC, Linde-Zwirble WT, Lidicker J, Clermont G, Carcillo J, Pinsky MR (2001) Epidemiology of severe sepsis in the United States: analysis of incidence, outcome, and associated costs of care. Crit Care Med 29:1303–1310

Anspach FB (2001) Endotoxin removal by affinity sorbents. J Biochem Bioph Meth 49:665–681

Appelmelk BJ, Verweij-van Vught AM, Maaskant JJ, Schouten WF, De Jonge AJ, Thijs LG, Maclaren DM (1988) Production and characterisation of mouse monoclonal antibodies reacting with the lipopolysaccharide core region of gram-negative bacilli. J Med Microbiol 26:107–114

Asherson RA, Cervera R, de Groot PG, Erkan D, Boffa MC, Piette JC, Khamashta MA, Shoenfeld Y, Group, C. A. S. R. P (2003) Catastrophic antiphospholipid syndrome: international consensus statement on classification criteria and treatment guidelines. Lupus 12:530–534

Baek DS, Kim YS (2015) Humanization of a phosphothreonine peptide-specific chicken antibody by combinatorial library optimization of the phosphoepitope-binding motif. Biochem Bioph Res Co 463:414–420

Bankovich AJ, Raunser S, Juo ZS, Walz T, Davis MM, Garcia KC (2007) Structural insight into pre-B cell receptor function. Science 316:291–294

Baumgartner JD, Heumann D, Gerain J, Weinbreck P, Grau GE, Glauser MP (1990) Association between protective efficacy of anti-lipopolysaccharide (Lps) antibodies and suppression of Lps-induced tumor necrosis factor-alpha and interleukin-6. J Exp Med 171:889–896

Bhat NM, Bieber MM, Chapman CJ, Stevenson FK, Teng NN (1993) Human antilipid a monoclonal antibodies bind to human B cells and the I antigen on cord red blood cells. J Immunol 151:5011–5011

Bieber MM, Bhat NM, Teng NNH (1995) Antiendotoxin human monoclonal-antibody A6h4c5 (Ha-1a) utilizes the Vh4.21 gene. Clin Infect Dis 21:S186–S189

Biermann MH, Veissi S, Maueroder C, Chaurio R, Berens C, Herrmann M, Munoz LE (2014) The role of dead cell clearance in the etiology and pathogenesis of systemic lupus erythematosus: dendritic cells as potential targets. Expert Rev Clin Immunol 10:1151–1164

Blackler RJ, Müller-Loennies S, Brade L, Kosma P, Brade H, Evans SV (2012) Antibody recognition of *Chlamydia* LPS: structural insights of inherited immune responses. In: Kosma P, Müller-Loennies S (eds) Anticarbohydrate antibodies: from molecular basis to clinical application. Springer, Vienna, pp 75–120

Bogard WC, Siegel SA, Leone AO, Damiano E, Shealy DJ, Ely TM, Frederick B, Mascelli MA, Siegel RC, Machielse B, Naveh D, Kaplan PM, Daddona PE (1993) Human monoclonal-antibody ha-1a binds to endotoxin via an epitope in the lipid-a domain of lipopolysaccharide. J Immunol 150:4438–4449

Bouma B, de Groot PG, van den Elsen JM, Ravelli RB, Schouten A, Simmelink MJ, Derksen RH, Kroon J, Gros P (1999) Adhesion mechanism of human beta (2)-glycoprotein I to phospholipids based on its crystal structure. EMBO J 18:5166–5174

Brade L, Holst O, Brade H (1993) An artificial glycoconjugate containing the bisphosphorylated glucosamine disaccharide backbone of lipid-a binds lipid-a monoclonal antibodies. Infect Immun 61:4514–4517

Brade L, Engel R, Christ WJ, Rietschel ET (1997) A nonsubstituted primary hydroxyl group in position 6′ of free lipid a is required for binding of lipid a monoclonal antibodies. Infect Immun 65:3961–3965

Brochet X, Lefranc MP, Giudicelli V (2008) IMGT/V-QUEST: the highly customized and integrated system for IG and TR standardized V-J and V-D-J sequence analysis. Nucleic Acids Res 36:W503–W508

Broecker F, Aretz J, Yang Y, Hanske J, Guo XQ, Reinhardt A, Wahlbrink A, Rademacher C, Anish C, Seeberger PH (2014) Epitope recognition of antibodies against a *Yersinia pestis* lipopolysaccharide trisaccharide component. ACS Chem Biol 9:867–873

Burnet FM (1959) The clonal selection theory of acquired immunity. Cambridge University Press, Cambridge

Burnet FM (2007) A modification of Jerne's theory of antibody production using the concept of clonal

selection (reprinted from Australian journal of science, vol 20, 1957). Nat Immunol 8:1024–1026
Buttenschoen K, Radermacher P, Bracht H (2010) Endotoxin elimination in sepsis: physiology and therapeutic application. Langenbeck Arch Surg 395:597–605
Caroff M, Karibian D (2003) Structure of bacterial lipopolysaccharides. Carbohydr Res 338:2431–2447
Castro C, Gourley M (2010) Diagnostic testing and interpretation of tests for autoimmunity. J Allergy Clin Immun 125:S238–S247
Cavallo T, Granholm NA (1991) Bacterial lipopolysaccharide induces long-lasting Iga deficiency concurrently with features of polyclonal B-cell activation in normal and in lupus-prone mice. Clin Exp Immunol 84:134–138
Chang S, Yang L, Moon YM, Cho YG, Min SY, Kim TJ, Kim YJ, Patrick W, Kim HY, Mohan C (2009) Antinuclear antibody reactivity in lupus may be partly hard-wired into the primary B-cell repertoire. Mol Immunol 46:3420–3426
Chu Q, Ludtke JJ, Subbotin VM, Blockhin A, Sokoloff AV (2008) The acquisition of narrow binding specificity by polyspecific natural IgM antibodies in a semi-physiological environment. Mol Immunol 45:1501–1513
Coutinho A, Kazatchkine MD, Avrameas S (1995) Natural autoantibodies. Curr Opin Immunol 7:812–818
Cuadrado MJ, Mujic F, Munoz E, Khamashta MA, Hughes GRV (1997) Thrombocytopenia in the antiphospholipid syndrome. Ann Rheum Dis 56:194–196
de Groot PG, Meijers JCM (2011) β(2)-glycoprotein I: evolution, structure and function. J Thromb Haemost 9:1275–1284
Deng L, Zhong LL, Struble E, Duan HY, Ma L, Harman C, Yan HL, Virata-Theimer ML, Zhao Z, Feinstone S, Alter H, Zhang P (2013) Structural evidence for a bifurcated mode of action in the antibody-mediated neutralization of hepatitis C virus. P Natl Acad Sci USA 110:7418–7422
Detanico T, Heiser RA, Aviszus K, Bonorino C, Wysocki LJ (2011) Self-tolerance checkpoints in CD4 T cells specific for a peptide derived from the B cell antigen receptor. J Immunol 187:82–91
Di Padova FE, Brade H, Barclay GR, Poxton IR, Liehl E, Schuetze E, Kocher HP, Ramsay G, Schreier MH, Mcclelland DBL, Rietschel ET (1993a) A broadly cross-protective monoclonal-antibody binding to *Escherichia coli* and *Salmonella* lipopolysaccharides. Infect Immun 61:3863–3872
Di Padova FE, Gram H, Barclay R, Kleuser B, Liehl E, Rietschel ET (1993b) New anticore LPS monoclonal-antibodies with clinical potential. Int Congr Ser 1020:325–335
Diamond B, Scharff MD (1984) Somatic mutation of the T15 heavy-chain gives rise to an antibody with autoantibody specificity. Proc Natl Acad Sci U S A 81:5841–5844
Dornmair K, Goebels N, Weltzien HU, Wekerle H, Hohlfeld R (2003) T-cell-mediated autoimmunity - novel techniques to characterize autoreactive T-cell receptors. Am J Pathol 163:1215–1226
Duan JY, Kasper DL (2011) Regulation of T cells by gut commensal microbiota. Curr Opin Rheumatol 23:372–376
Dudley DD, Chaudhuri J, Bassing CH, Alt FW (2005) Mechanism and control of V(D)J recombination versus class switch recombination: similarities and differences. Adv Immunol 86:43–112
Edwards JCW, Cambridge G (2005) Prospects for B-cell-targeted therapy in autoimmune disease. Rheumatology 44:151–156
Eilat D, Webster DM, Rees AR (1988) V-region sequences of anti-DNA and anti-Rna autoantibodies from Nzb Nzw F1-mice. J Immunol 141:1745–1753
Engel C, Brunkhorst FM, Bone HG, Brunkhorst R, Gerlach H, Grond S, Gruendling M, Huhle G, Jaschinski U, John S, Mayer K, Oppert M, Olthoff D, Quintel M, Ragaller M et al (2007) Epidemiology of sepsis in Germany: results from a national prospective multicenter study. Intensive Care Med 33:606–618
Erkan D, Derksen R, Levy R, Machin S, Ortel T, Pierangeli S, Roubey R, Lockshin M (2011) Antiphospholipid syndrome clinical research task force report. Lupus 20:219–224
Esplin MS (2001) Management of antiphospholipid syndrome during pregnancy. Clin Obstet Gynecol 44:20–28
Farmer-Boatwright MK, Roubey RAS (2009) Venous thrombosis in the Antiphospholipid syndrome. Arterioscl Throm Vas 29:321–325
Feizi T, Taylor-Robinson D (1967) Cold agglutinin anti-i and *Mycoplasma Pneumoniae*. Immunology 13:405–409
Fenton K (2015) The effect of cell death in the initiation of lupus nephritis. Clin Exp Immunol 179:11–16
Fisher CJ, Zimmerman J, Khazaeli MB, Albertson TE, Dellinger RP, Panacek EA, Foulke GE, Dating C, Smith CR, Lobuglio AF (1990) Initial evaluation of human monoclonal anti-lipid-a antibody (ha-1a) in patients with sepsis syndrome. Crit Care Med 18:1311–1315
Fleming SD, Tsokos GC (2006) Complement, natural antibodies, autoantibodies and tissue injury. Autoimmun Rev 5:89–92
Fujihara Y, Bogard WC, Lei MG, Daddona PE, Morrison DC (1993a) Monoclonal anti-lipid A IgM antibodies HA-1A and E5 recognize distinct epitopes on lipopolysaccharide and lipid A. J Infect Dis 168:1429–1435
Fujihara Y, Lei MG, Morrison DC (1993b) Characterization of specific binding of a human immunoglobulin-M monoclonal-antibody to lipopolysaccharide and its lipid-a domain. Infect Immun 61:910–918
Gagneux P, Varki A (1999) Evolutionary considerations in relating oligosaccharide diversity to biological function. Glycobiology 9:747–755
Galanos C, Lüderitz O, Westphal O (1971) Preparation and properties of antisera against the lipid a

component of bacterial lipopolysaccharides. Eur J Biochem 24:116–122

Garabatos N, Alvarez R, Carrillo J, Carrascal J, Izquierdo C, Chapman HD, Presa M, Mora C, Serreze DV, Verdaguer J, Stratmann T (2014) In vivo detection of Peripherin-specific autoreactive B cells during type 1 diabetes pathogenesis. J Immunol 192:3080–3090

Giannakopoulos B, Krilis SA (2013) The pathogenesis of the Antiphospholipid syndrome. New Engl J Med 368:1033–1044

Giles BM, Boackle SA (2013) Linking complement and anti-dsDNA antibodies in the pathogenesis of systemic lupus erythematosus. Immunol Res 55:10–21

Giltiay NV, Chappell CP, Clark EA (2012) B-cell selection and the development of autoantibodies. Arthritis Res Ther 14:**S1**

Gomery K, Müller-Loennies S, Brooks CL, Brade L, Kosma P, Di Padova F, Brade H, Evans SV (2012) Antibody WN1 222-5 mimics toll-like receptor 4 binding in the recognition of LPS. Proc Natl Acad Sci U S A 109:20877–20882

Gough SCL, Simmonds MJ (2007) The HLA region and autoimmune disease: associations and mechanisms of action. Curr Genomics 8:453–465

Greenberg RN, Wilson KM, Kunz AY, Wedel NI, Gorelick KJ (1992) Observations using Antiendotoxin antibody (E5) as adjuvant therapy in humans with suspected, serious, gram-negative sepsis. Crit Care Med 20:730–735

Gronwall C, Vas J, Silverman GJ (2012) Protective roles of natural IgM antibodies. Front Immunol 3:66

Haji-Ghassemi O, Müller-Loennies S, Saldova R, Muniyappa M, Brade L, Rudd PM, Harvey DJ, Kosma P, Brade H, Evans SV (2014) Groove-type recognition of Chlamydiaceae-specific lipopolysaccharide antigen by a family of antibodies possessing an unusual variable heavy chain N-linked glycan. J Biol Chem 289:16644–16661

Haji-Ghassemi O, Blackler RJ, Martin Young N, Evans SV (2015a) Antibody recognition of carbohydrate epitopes. Glycobiology 25:920–952

Haji-Ghassemi O, Müller-Loennies S, Rodriguez T, Brade L, Kosma P, Brade H, Evans SV (2015b) Structural basis for antibody recognition of lipid a: insights to polyspecificity toward single stranded DNA. J Biol Chem 290:19629–19640

Haji-Ghassemi O, Muller-Loennies S, Rodriguez T, Brade L, Grimmecke HD, Brade H, Evans SV (2016) The combining sites of anti-lipid a antibodies reveal a widely-utilized motif specific for negatively charged groups. J biol chem 291:10104–10118

Han SH, Zhuang HY, Shumyak S, Yang LJ, Reeves WH (2015) Mechanisms of autoantibody production in systemic lupus erythematosus. Front Immunol 6:228

Harris LJ, Larson SB, Skaletsky E, McPherson A (1998) Comparison of the conformations of two intact monoclonal antibodies with hinges. Immunol Rev 163:35–43

Harwood NE, Batista FD (2010) Early events in B cell activation. Annu Rev Immunol 28:185–210

Heilmann L, Schorsch M, Hahn T, Fareed J (2011) Antiphospholipid syndrome and pre-eclampsia. Semin Thromb Hemost 37:141–145

Helmerhorst EJ, Maaskant JJ, Appelmelk BJ (1998) Anti-lipid a monoclonal antibody centoxin (HA-1A) binds to a wide variety of hydrophobic ligands. Infect Immun 66:870–873

Herlands RA, Christensen SR, Sweet RA, Hershberg U, Shlomchik MJ (2008) T cell-independent and toll-like receptor-dependent antigen-driven activation of autoreactive B cells. Immunity 29:249–260

Herron JN, He XM, Ballard DW, Blier PR, Pace PE, Bothwell ALM, Voss EW, Edmundson AB (1991) An autoantibody to single-stranded-DNA: comparison of the 3-dimensional structures of the unliganded fab and a deoxynucleotide fab complex. Proteins 11:159–175

Hill GS, Nochy D (2007) Antiphospholipid syndrome in systemic lupus erythematosus. J Am Soc Nephrol 18:2461–2464

Hogquist KA, Baldwin TA, Jameson SC (2005) Central tolerance: learning self-control in the thymus. Nat Rev Immunol 5:772–782

Houtkooper RH, Vaz FM (2008) Cardiolipin, the heart of mitochondrial metabolism. Cell Mol Life Sci 65:2493–2506

Hull RG, Harris EN, Gharavi AE, Tincani A, Asherson RA, Valesini G, Denman AM, Froude G, Hughes GRV (1984) Anticardiolipin antibodies: occurrence in Behçets syndrome. Ann Rheum Dis 43:746–748

Hurtado V, Montes R, Gris JC, Bertolaccini ML, Alonso A, Martinez-Gonzalez MA, Khamashta MA, Fukudome K, Lane DA, Hermida J (2004) Autoantibodies against EPCR are found in antiphospholipid syndrome and are a risk factor for fetal death. Blood 104:1369–1374

Ibrahim SM, Weigert M, Basu C, Erikson J, Radic MZ (1995) Light-chain contribution to specificity in anti-DNA antibodies. J Immunol 155:3223–3233

Iguchi A, Iyoda S, Kikuchi T, Ogura Y, Katsura K, Ohnishi M, Hayashi T, Thomson NR (2014) A complete view of the genetic diversity of the *Escherichia coli* O-antigen biosynthesis gene cluster. DNA research: an international journal for rapid publication of reports on genes and genomes, E-pub

Isenberg DA, Shoenfeld Y, Madaio MP, Rauch J, Reichlin M, Stollar BD, Schwartz RS (1984) Anti-DNA antibody idiotypes in systemic lupus erythematosus. Lancet 2:417–422

Ishii Y, Nagasawa K, Mayumi T, Niho Y (1990) Clinical importance of persistence of Anticardiolipin antibodies in systemic lupus-erythematosus. Ann Rheum Dis 49:387–390

Izui S, Kobayakawa T, Zryd MJ, Louis J, Lambert PH (1977) Mechanism for induction of anti-DNA antibodies by bacterial lipopolysaccharides in mice; II Correlation between anti-DNA induction and

polyclonal antibody formation by various polyclonal B lymphocyte activators. J Immunol 119:2157–2162
Jin C, Hantusch B, Hemmer W, Stadimann J, Altmann F (2008) Affinity of IgE and IgG against cross-reactive carbohydrate determinants on plant and insect glycoproteins. J Allergy Clin Immun 121:185–190.e2
Kabanov DS, Prokhorenko IR (2010) Structural analysis of lipopolysaccharides from gram-negative bacteria. Biochemistry (Mosc) 75:383–404
Kabat EA (1976) Structure of antibody combining sites. Ann Inst Pasteur Imm C127:239–252
Kaburaki J, Kuwana M, Ogasawara T, Takano M, Funatsu Y, Tojo T (1992) Specificity of antibodies to single-stranded (ss) DNA in SLE patients with anti-phospholipid syndrome. Keio J Med 41:10–15
Keane A, Woods R, Dowding V, Roden D, Barry C (1987) Anticardiolipin antibodies in rheumatoid-arthritis. Brit J Rheumatol 26:346–350
Kim HM, Park BS, Kim JI, Kim SE, Lee J, Oh SC, Enkhbayar P, Matsushima N, Lee H, Yoo OJ, Lee JO (2007) Crystal structure of the TLR4-MD-2 complex with bound endotoxin antagonist eritoran. Cell 130:906–917
Klein U, Dalla-Favera R (2008) Germinal centres: role in B cell physiology and malignancy. Nat Rev Immunol 8:22–33
Koerber JT, Thomsen ND, Hannigan BT, Degrado WF, Wells JA (2013) Nature-inspired design of motif-specific antibody scaffolds. Nat Biotechnol 31:916–921
Kofler R, Strohal R, Balderas RS, Johnson ME, Noonan DJ, Duchosal MA, Dixon FJ, Theofilopoulos AN (1988) Immunoglobulin-kappa light chain variable region gene-complex organization and immunoglobulin genes encoding anti-DNA autoantibodies in lupus mice. J Clin Invest 82:852–860
Kraj P, Friedman DF, Stevenson F, Silberstein LE (1995) Evidence for the overexpression of the Vh4-34 (Vh4.21) Ig gene segment in the normal adult human peripheral-blood B-cell repertoire. J Immunol 154:6406–6420
Krieg AM, Yi AK, Matson S, Waldschmidt TJ, Bishop GA, Teasdale R, Koretzky GA, Klinman DM (1995) CpG motifs in bacterial DNA trigger direct B-cell activation. Nature 374:546–549
Krishnan MR, Jou NT, Marion TN (1996) Correlation between the amino acid position of arginine in VH-CDR3 and specificity for native DNA among autoimmune antibodies. J Immunol 157:2430–2439
Kuhn HM (1993) Cross-reactivity of monoclonal antibodies and sera directed against lipid a and lipopolysaccharides. Infection 21:179–186
Kuhn HM, Brade L, Appelmelk BJ, Kusumoto S, Rietschel ET, Brade H (1992) Characterization of the epitope specificity of murine monoclonal antibodies directed against lipid A. Infect Immun 60:2201–2210
Kupcinskas J, Meistere I, Line A, Zayakin P, Pismennaja A, Jonaitis L, Kupcinskas L, Wu C, Leja M, Kalnina Z (2016) Cancer associated autoantibodies in gastric cancer. Helicobacter 21:127–127
Kuraoka M, Kelsoe G (2011) A novel role for activation-induced cytidine deaminase central B cell tolerance. Cell Cycle 10:3423–3424
Lafer EM, Rauch J, Andrzejewski C Jr, Mudd D, Furie B, Furie B, Schwartz RS, Stollar BD (1981) Polyspecific monoclonal lupus autoantibodies reactive with both polynucleotides and phospholipids. J Exp Med 153:897–909
Lane JR, Neumann DA, Lafondwalker A, Herskowitz A, Rose NR (1991) Lps promotes Cb3-induced myocarditis in resistant B10.A mice. Cell Immunol 136:219–233
LeBien TW, Tedder TF (2008) B lymphocytes: how they develop and function. Blood 112:1570–1580
Lerner A, Jeremias P, Matthias T (2015) The world incidence and prevalence of autoimmune diseases is increasing. Int J Celiac Dis 3:151–155
Li Z, Woo CJ, Iglesias-Ussel MD, Ronai D, Scharff MD (2004) The generation of antibody diversity through somatic hypermutation and class switch recombination. Genes Dev 18:1–11
Lleo A, Invernizzi P, Gao B, Podda M, Gershwin ME (2010) Definition of human autoimmunity - autoantibodies versus autoimmune disease. Autoimmun Rev 9:A259–A266
Lolis E, Bucala R (2003) Therapeutic approaches to innate immunity: severe sepsis and septic shock. Nat Rev Drug Discov 2:635–645
Marks L (2012) The birth pangs of monoclonal antibody therapeutics the failure and legacy of centoxin. Mabs-Austin 4:403–412
Martin GS (2012) Sepsis, severe sepsis and septic shock: changes in incidence, pathogens and outcomes. Expert Rev Anti-Infe 10:701–706
Massa M, Debenedetti F, Ravelli A, Martini A (1993) Anti-DNA antibodies in the primary Antiphospholipid syndrome. Brit J Rheumatol 32:1028–1028
Mathis D, Benoist C (2011) Microbiota and autoimmune disease: the hosted self. Cell Host Microbe 10:297–301
Mccloskey RV, Straube RC, Sanders C, Smith SM, Smith CR (1994) Treatment of septic shock with human monoclonal-antibody ha-1a - a randomized, double-blind, placebo-controlled trial. Ann Intern Med 121:1–5
Mcneil HP, Chesterman CN, Krilis SA (1991) Immunology and clinical importance of antiphospholipid antibodies. Adv Immunol 49:193–280
Meffre E (2011) The establishment of early B cell tolerance in humans: lessons from primary immunodeficiency diseases. Ann N Y Acad Sci 1246:1–10
Miller JJ, Bieber MM, Levinson JE, Zhu SL, Tsou E, Teng NNH (1996) V(H)4-34(V(H)4.21) gene expression in the chronic arthritides of childhood: studies of associations with anti-lipid a antibodies, HLA antigens, and clinical features. J Rheumatol 23:2132–2139

Miller SI, Ernst RK, Bader MW (2005) LPS, TLR4 and infectious disease diversity. Nat Rev Microbiol 3:36–46

Milner ECB, Anolik J, Cappione A, Sanz I (2005) Human innate B cells: a link between host defense and autoimmunity? Springer Semin Immun 26:433–452

Miyake K (2007) Innate immune sensing of pathogens and danger signals by cell surface toll-like receptors. Semin Immunol 19:3–10

Monestier M, Bonin B, Migliorini P, Dang H, Datta S, Kuppers R, Rose N, Maurer P, Talal N, Bona C (1987) Autoantibodies of various specificities encoded by genes from the Vh J558 family bind to foreign antigens and share Idiotopes of antibodies specific for self and foreign antigens. J Exp Med 166:1109–1124

Monod MY, Giudicelli V, Chaume D, Lefranc MP (2004) IMGT/junction analysis: the first tool for the analysis of the immunoglobulin and T cell receptor complex V-J and V-D-J JUNCTIONs. Bioinformatics 20:i379–i385

Müller-Loennies S, Brade L, MacKenzie CR, Di Padova FE, Brade H (2003) Identification of a cross-reactive epitope widely present in lipopolysaccharide from enterobacteria and recognized by the cross-protective monoclonal antibody WN1 222-5. J Biol Chem 278:25618–25627

Müller-Loennies S, Brade L, Brade H (2007) Neutralizing and cross-reactive antibodies against enterobacterial lipopolysaccharide. Int J Med Microbiol 297:321–340

Munford RS (2005) Detoxifying endotoxin: time, place and person. J Endotoxin Res 11:69–84

Muramatsu M, Kinoshita K, Fagarasan S, Yamada S, Shinkai Y, Honjo T (2000) Class switch recombination and hypermutation require activation-induced cytidine deaminase (AID), a potential RNA editing enzyme. Cell 102:553–563

Murphy K, Travers P, Walport M, Janeway C (2012) Janeway's immunobiology, 8th edn. Garland Science, New York, pp 290–326

Nguyen HP, Seto NOL, MacKenzie CR, Brade L, Kosma P, Brade H, Evans SV (2003) Germline antibody recognition of distinct carbohydrate epitopes. Nat Struct Biol 10:1019–1025

Nikaido H (2003) Molecular basis of bacterial outer membrane permeability revisited. Microbiol Mol Biol Rev 67:593–656

Nogai A, Siffrin V, Bonhagen K, Pfueller CF, Hohnstein T, Volkmer-Engert R, Bruck W, Stadelmann C, Kamradt T (2005) Lipopolysaccharide injection induces relapses of experimental autoimmune encephalomyelitis in nontransgenic mice via bystander activation of autoreactive CD4(+) cells. J Immunol 175:959–966

Nossal GJV (1996) Clonal anergy of B cells: a flexible, reversible, and quantitative concept. J Exp Med 183:1953–1956

Oldstone MBA (1998) Molecular mimicry and immune-mediated diseases. FASEB J 12:1255–1265

Parker MJ, Gomery K, Richard G, MacKenzie CR, Cox AD, Richards JC, Evans SV (2014) Structural basis for selective cross-reactivity in a bactericidal antibody against inner core lipooligosaccharide from *Neisseria meningitidis*. Glycobiology 24:442–449

Pascual V, Victor K, Spellerberg M, Hamblin TJ, Stevenson FK, Capra JD (1992) Vh restriction among human cold agglutinins. The Vh4-21 gene segment is required to encode anti-I and anti-I specificities. J Immunol 149:2337–2344

Patwa TH, Li C, Poisson LM, Kim HY, Pal M, Ghosh D, Simeone DM, Lubman DM (2009) The identification of phosphoglycerate kinase-1 and histone H4 autoantibodies in pancreatic cancer patient serum using a natural protein microarray. Electrophoresis 30:2215–2226

Pedro ABP, Romaldini JH, Americo C, Takei K (2006) Association of circulating antibodies against double-stranded and single-stranded DNA with thyroid autoantibodies in Graves' disease and Hashimoto's thyroiditis patients. Exp Clin Endocr Diab 114:35–38

Peled JU, Kuang FL, Iglesias-Ussel MD, Roa S, Kalis SL, Goodman ME, Scharff MD (2008) The biochemistry of somatic hypermutation. Annu Rev Immunol 26:481–511

Perniola R (2012) Expression of the autoimmune regulator gene and its relevance to the mechanisms of central and peripheral tolerance. Clin Dev Immunol 2012:1–12

Pillai S, Mattoo H, Cariappa A (2011) B cells and autoimmunity. Curr Opin Immunol 23:721–731

Poletaev AB, Stepanyuk VL, Gershwin ME (2008) Integrating immunity: the immunculus and self-reactivity. J Autoimmun 30:68–73

Poltorak A, He XL, Smirnova I, Liu MY, Van Huffel C, Du X, Birdwell D, Alejos E, Silva M, Galanos C, Freudenberg M, Ricciardi-Castagnoli P, Layton B, Beutler B (1998) Defective LPS signaling in C3H/HeJ and C57BL/10ScCr mice: mutations in Tlr4 gene. Science 282:2085–2088

Prak ETL, Monestier M, Eisenberg RA (2011) B cell receptor editing in tolerance and autoimmunity. Ann N Y Acad Sci 1217:96–121

Pullen LC, Park SH, Miller SD, Dalcanto MC, Kim BS (1995) Treatment with bacterial Lps renders genetically resistant C57bl/6 mice susceptible to Theilers virus-induced demyelinating disease. J Immunol 155:4497–4503

Quezado ZMN, Natanson C, Alling DW, Banks SM, Koev CA, Elin RJ, Hosseini JM, Bacher JD, Danner RL, Hoffman WD (1993) A controlled trial of ha-1a in a canine model of gram-negative septic shock. Jama-J Am Med Assoc 269:2221–2227

Rathbun GA, Otani F, Milner ECB, Capra JD, Tucker PW (1988) Molecular characterization of the a-J-J558 family of heavy-chain variable region gene segments. J Mol Biol 202:383–395

Ravirajan CT, Rowse L, MacGowan JR, Isenberg DA (2001) An analysis of clinical disease activity and

nephritis-associated serum autoantibody profiles in patients with systemic lupus erythematosus: a cross-sectional study. Rheumatology 40:1405–1412

Rekvig OP (2015) The anti-DNA antibody: origin and impact, dogmas and controversies. Nat Rev Rheumatol 11:530–540

Rekvig OP, Nossent JC (2003) Anti-double-stranded DNA antibodies, nucleosomes, and systemic lupus erythematosus: a time for new paradigms? Arthritis Rheum 48:300–312

Riedhammer C, Weissert R (2015) Antigen presentation, autoantigens, and immune regulation in multiple sclerosis and other autoimmune diseases. Front Immunol 6:322

Rietschel ET, Kirikae T, Schade FU, Mamat U, Schmidt G, Loppnow H, Ulmer AJ, Zahringer U, Seydel U, Dipadova F, Schreier M, Brade H (1994) Bacterial, endotoxin - molecular relationships of structure to activity and function. FASEB J 8:217–225

Ring GH, Lakkis FG (1999) Breakdown of self-tolerance and the pathogenesis of autoimmunity. Semin Nephrol 19:25–33

Rioux JD, Abbas AK (2005) Paths to understanding the genetic basis of autoimmune disease. Nature 435:584–589

Robertson CR, Pisetsky DS (1992) Specificity analysis of antibodies to single-stranded Micrococcal DNA in the sera of normal human-subjects and patients with systemic lupus-erythematosus. Clin Exp Rheumatol 10:589–594

Roche MI, Lu ZH, Hui JH, Sharon J (2011) Characterization of monoclonal antibodies to terminal and internal O-antigen epitopes of *Francisella tularensis* lipopolysaccharide. Hybridoma 30:19–28

Roubey RAS (1994) Autoantibodies to phospholipid-binding plasma-proteins - a new view of lupus anticoagulants and other Antiphospholipid autoantibodies. Blood 84:2854–2867

Routsias JG, Vlachoyiannopoulos PG, Tzioufas AG (2006) Autoantibodies to intracellular autoantigens and their B-cell epitopes: molecular probes to study the autoimmune response. Crit Rev Cl Lab Sci 43:203–248

Ruff WE, Vieira SM, Kriegel MA (2015) The role of the gut microbiota in the pathogenesis of Antiphospholipid syndrome. Curr Rheumatol Rep 17:472

Russo TA, Beanan JM, Olson R, Genagon SA, MacDonald U, Cope JJ, Davidson BA, Johnston B, Johnson JR (2007) A killed, genetically engineered derivative of a wild-type extraintestinal pathogenic *E. coli* strain is a vaccine candidate. Vaccine 25:3859–3870

Rynkiewicz MJ, Lu ZH, Hui JH, Sharon J, Seaton BA (2012) Structural analysis of a protective epitope of the *Francisella tularensis* O-polysaccharide. Biochemistry-US 51:5684–5694

Schroeder HW (2006) Similarity and divergence in the development and expression of the mouse and human antibody repertoires. Dev Comp Immunol 30:119–135

Schulze-Gahmen U, Rini JM, Wilson IA (1993) Detailed analysis of the free and bound conformations of an antibody. X-ray structures of fab 17/9 and 3 different fab-peptide complexes. J Mol Biol 234:1098–1118

Schwartz RS, Stollar BD (1985) Origins of anti-DNA autoantibodies. J Clin Invest 75:321–327

Schwarzenbacher R, Zeth K, Diederichs K, Gries A, Kostner GM, Laggner P, Prassl R (1999) Crystal structure of human beta2-glycoprotein I: implications for phospholipid binding and the antiphospholipid syndrome. EMBO J 18:6228–6239

Sevag MG, Lackman DB, Smolens J (1938) The isolation of the components of streptococcal nucleoproteins in serologically active form. J Biol Chem 124:425–436

Shih HH, Tu C, Cao W, Klein A, Ramsey R, Fennell BJ, Lambert M, Shuilleabhain DN, Autin B, Kouranova E, Laxmanan S, Braithwaite S, Wu L, Ait-Zahra M, Milici AJ et al (2012) An ultra-specific avian antibody to phosphorylated tau protein reveals a unique mechanism for phosphoepitope recognition. J Biol Chem 287:44425–44434

Shlomchik M, Mascelli M, Shan H, Radic MZ, Pisetsky D, Marshakrothstein A, Weigert M (1990) Anti-DNA antibodies from autoimmune mice Arise by clonal expansion and somatic mutation. J Exp Med 171:265–292

Silverstein AM (2001) Autoimmunity versus horror autotoxicus: the struggle for recognition. Nat Immunol 2:279–281

Soyer OU, Akdis M, Ring J, Behrendt H, Crameri R, Lauener R, Akdis CA (2013) Mechanisms of peripheral tolerance to allergens. Allergy 68:161–170

Spellerberg M, Chapman C, Hamblin T, Stevenson F (1995) Dual recognition of lipid a and DNA by human antibodies encoded by the V(H)4-21 gene - a possible link between infection and lupus. Ann N Y Acad Sci 764:427–432

Stavnezer J, Guikema JEJ, Schrader CE (2008) Mechanism and regulation of class switch recombination. Annu Rev Immunol 26:261–292

Stevenson FK, Longhurst C, Chapman CJ, Ehrenstein M, Spellerberg MB, Hamblin TJ, Ravirajan CT, Latchman D, Isenberg D (1993) Utilization of the V(H)4-21 gene segment by anti-DNA antibodies from patients with systemic lupus-erythematosus. J Autoimmun 6:809–825

Stollar BD (1986) Antibodies to DNA. CRC Crit Rev Biochem 20:1–36

Strauss J, Burnham NA, Camesano TA (2009) Atomic force microscopy study of the role of LPS O-antigen on adhesion of *E. coli*. J Mol Recognit 22:347–355

Su MA, Anderson MS (2009) Monogenic autoimmune diseases: insights into self-tolerance. Pediatr Res 65:20r–25r

Su KY, Pisetsky DS (2009) The role of extracellular DNA in autoimmunity in SLE. Scand J Immunol 70:175–183

Sumazaki R, Fujita T, Kabashima T, Nishikaku F, Koyama A, Shibasaki M, Takita H (1986) Monoclonal antibody against bacterial lipopolysaccharide cross-

reacts with DNA-histone. Clin Exp Immunol 66:103–110
Suryani S, Fulcher DA, Santner-Nanan B, Nanan R, Wong M, Shaw PJ, Gibson J, Williams A, Tangye SG (2010) Differential expression of CD21 identifies developmentally and functionally distinct subsets of human transitional B cells. Blood 115:519–529
Suurmond J, Diamond B (2015) Autoantibodies in systemic autoimmune diseases: specificity and pathogenicity. J Clin Invest 125:2194–2202
Tanner JJ, Komissarov AA, Deutscher SL (2001) Crystal structure of an antigen-binding fragment bound to single-stranded DNA. J Mol Biol 314:807–822
Teng NNH, Kaplan HS, Hebert JM, Moore C, Douglas H, Wunderlich A, Braude AI (1985) Protection against gram-negative bacteremia and Endotoxemia with human monoclonal Igm antibodies. P Natl Acad Sci USA 82:1790–1794
Ternynck T, Avrameas S (1986) Murine natural monoclonal autoantibodies - a study of their polyspecificities and their affinities. Immunol Rev 94:99–112
Tillman DM, Jou NT, Hill RJ, Marion TN (1992) Both Igm and igg anti-DNA antibodies are the products of clonally selective B-cell stimulation in (Nzb X Nzw)F (1) mice. J Exp Med 176:761–779
Tonegawa S (1983) Somatic generation of antibody diversity. Nature 302:575–581
Treanor B (2012) B-cell receptor: from resting state to activate. Immunology 136:21–27
van Gaalen F, Ioan-Facsinay A, Huizinga TWJ, Toes REM (2005) The devil in the details: the emerging role of anticitrulline autoimmunity in rheumatoid arthritis. J Immunol 175:5575–5580
Varga JM, Konigsbe W, Richards FF (1973) Antibodies with multiple binding functions - induction of single immunoglobin species by structurally dissimilar haptens. Proc Natl Acad Sci U S A 70:3269–3274
Vieira SM, Pagovich OE, Kriegel MA (2014) Diet, microbiota and autoimmune diseases. Lupus 23:518–526
Vincent JL, Sun QH, Dubois MJ (2002) Clinical trials of immunomodulatory therapies in severe sepsis and septic shock. Clin Infect Dis 34:1084–1093
von Boehmer H, Melchers F (2010) Checkpoints in lymphocyte development and autoimmune disease. Nat Immunol 11:14–20
Vulliez-Le Normand B, Saul FA, Phalipon A, Belot F, Guerreiro C, Mulard LA, Bentley GA (2008) Structures of synthetic O-antigen fragments from serotype 2a *Shigella flexneri* in complex with a protective monoclonal antibody. Proc Natl Acad Sci U S A 105:9976–9981
Wardemann H, Yurasov S, Schaefer A, Young JW, Meffre E, Nussenzweig MC (2003) Predominant autoantibody production by early human B cell precursors. Science 301:1374–1377
Weller S, Conde C, Knapp AM, Levallois H, Gilfillan S, Pasquali JL, Martin T (1997) Autoantibodies in mice lacking terminal deoxynucleotidyl transferase: evidence for a role of N region addition in the polyreactivity and in the affinities of anti-DNA antibodies. J Immunol 159:3890–3898
Werner S, Chen H, Butt J, Michel A, Knebel P, Holleczek B, Zornig I, Eichmuller SB, Jager D, Pawlita M, Waterboer T, Brenner H (2016) Evaluation of the diagnostic value of 64 simultaneously measured autoantibodies for early detection of gastric cancer. Sci Rep-Uk 6:25467
Willis JR, Briney BS, DeLuca SL, Crowe JE, Meiler J (2013) Human germline antibody gene segments encode polyspecific antibodies. PLoS Comput Biol 9:e1003045
Wing K, Sakaguchi S (2010) Regulatory T cells exert checks and balances on self tolerance and autoimmunity. Nat Immunol 11:7–13
Winkenwerder WL, Buell MV, Howard JE (1939) The sensitizing properties of the nucleic acids and their derivatives. Science 90:356
Wolf P, Gretler J, Aglas F, Auergrumbach P, Rainer F (1994) Anticardiolipin antibodies in rheumatoid-arthritis - their relation to rheumatoid nodules and cutaneous vascular manifestations. Brit J Dermatol 131:48–51
Wood DM, Parent JB, Gazzanosantoro H, Lim E, Pruyne PT, Watkins JM, Spoor ES, Reardan DT, Trown PW, Conlon PJ (1992) Reactivity of monoclonal-antibody E5® with endotoxin. I. Binding to lipid a and rough lipopolysaccharides. Circ Shock 38:55–62
Wucherpfennig KW, Allen PM, Celada F, Cohen IR, De Boer R, Garcia KC, Goldstein B, Greenspan R, Hafler D, Hodgkin P, Huseby ES, Krakauer DC, Nemazee D, Perelson AS, Pinilla C et al (2007) Polyspecificity of T cell and B cell receptor recognition. Semin Immunol 19:216–224
Yildirim-Toruner C, Diamond B (2011) Current and novel therapeutics in the treatment of systemic lupus erythematosus. J Allergy Clin Immun 127:303–312
Yokota S, Ohtsuka H, Kohzuki T, Noguchi H (1996) A polyreactive human anti-lipid a monoclonal antibody having cross reactivity to polysaccharide portions of *Pseudomonas aeruginosa* lipopolysaccharides. Fems Immunol Med Mic 14:31–38
Yoshino S, Sasatomi E, Ohsawa M (2000) Bacterial lipopolysaccharide acts as an adjuvant to induce autoimmune arthritisin mice. Immunology 99:607–614
Zaenker P, Gray ES, Ziman MR (2016) Autoantibody production in cancer-the humoral immune response toward autologous antigens in cancer patients. Autoimmun Rev 15:477–483
Ziegler EJ, Mccutchan JA, Fierer J, Glauser MP, Sadoff JC, Douglas H, Braude AI (1982) Treatment of gram-negative bacteremia and shock with human antiserum to a mutant Escherichia-Coli. New Engl J Med 307:1225–1230
Ziegler EJ, Fisher CJ, Sprung CL, Straube RC, Sadoff JC, Foulke GE, Wortel CH, Fink MP, Dellinger RP, Teng NNH, Allen IE, Berger HJ, Knatterud GL, Lobuglio AF, Smith CR (1991) Treatment of gram-negative

bacteremia and septic shock with ha-1a human monoclonal-antibody against endotoxin - a randomized, double-blind, placebo-controlled trial. New Engl J Med 324:429–436

Zivkovic M, Zlatanovic M, Zlatanovic G, Djordjevic-Jocic J, Cekic S (2011) Anticardiolipin antibodies in patients with Behcet's disease. Bosnian J Basic Med 11:58–61

Zouali M, Stollar BD, Schwartz RS (1988) Origin and diversification of anti-DNA antibodies. Immunol Rev 105:137–160

Zurgil N, Bakimer R, Tincani A, Faden D, Cohen J, Lorber M, Valesini G, Shoenfeld Y (1993) Detection of Antiphospholipid and anti-DNA antibodies and their Idiotypes in newborns of mothers with Antiphospholipid syndrome and Sle. Lupus 2:233–237

Adv Exp Med Biol - Protein Reviews (2017) 2: 203
DOI 10.1007/5584_2017

Index